SOLAR PHOTOCATALYSIS FOR THE REMOVAL OF TRACE ORGANIC POLLUTANTS IN WASTEWATER FROM A TYPICAL PETROCHEMICAL MANUFACTURING FACILITY

Thesis submitted to

Cochin University of Science and Technology

in partial fulfillment of the requirements

for the award of the degree of

Doctor of Philosophy

in

Environmental Chemistry

Under the faculty of Environmental Studies

By

Rajeev B.

(Reg. No. 4261)

SCHOOL OF ENVIRONMENTAL STUDIES

COCHIN UNIVERSITY OF SCIENCE AND TECHNOLOGY

KOCHI - 682 022

***May* 2018**

Solar photocatalysis for the removal of trace organic pollutants in wastewater from a typical petrochemical manufacturing facility

Ph.D. Thesis under the Faculty of Environmental Studies

Author

Rajeev B.
Research Scholar
School of Environmental Studies
Cochin University of Science and Technology
Kochi – 682 022
Kerala, India

Supervising Guide

Dr. E. P. Yesodharan
Professor (Emeritus)
School of Environmental Studies,
Cochin University of Science and Technology
Kochi – 682 022
Kerala, India

School of Environmental Studies
Cochin University of Science and Technology
Kochi, Kerala, India 682 022

May 2018

SCHOOL OF ENVIRONMENTAL STUDIES
COCHIN UNIVERSITY OF SCIENCE AND TECHNOLOGY
KOCHI - 682 022

Dr. E. P. Yesodharan
Professor (Emeritus)

Certificate

This is to certify that this thesis entitled **"Solar photocatalysis for the removal of trace organic pollutants in wastewater from a typical petrochemical manufacturing facility"** is an authentic record of the research work carried out by **Mr. Rajeev.B**, Research Scholar (Reg. No. 4261) under my guidance at the School of Environmental Studies, Cochin University of Science and Technology in partial fulfillment of the requirements for the award of the degree of Doctor of Philosophy in Environmental Chemistry and no part of this work has previously formed the basis for the award of any other degree, diploma, associateship, fellowship or any other similar title or recognition. All the relevant corrections and modifications suggested by the audience during the pre-synopsis seminar and recommended by the Doctoral committee have been incorporated in the thesis.

Kochi - 22
May 2018

Dr. E. P. Yesodharan
(Supervising Guide)

Declaration

I do hereby declare that the work presented in the thesis entitled **"Solar photocatalysis for the removal of trace organic pollutants in wastewater from a typical petrochemical manufacturing facility"** is based on the authentic record of the original work done by me, for my Doctoral Degree under the guidance of **Dr. E. P. Yesodharan**, Professor (Emeritus), School of Environmental Studies, Cochin University of Science and Technology in partial fulfillment of the requirements for the award of the degree of Doctor of Philosophy in Environmental Chemistry and no part of this work has previously formed the basis for the award of any other degree, diploma, associate ship, fellowship or any other similar title or recognition.

Kochi – 22 **Rajeev B.**
May 2018

Acknowledgements

I am extremely happy to acknowledge all those people who helped me a lot in one way or the other for successfully completing this work.

First of all I express my sincere thanks and heart-felt gratitude to my supervising guide Dr. E. P. Yesodharan, Professor (Emeritus), School of Environmental Studies (SES), Cochin University of Science and Technology (CUSAT) for his inspiring guidance, patience, unconditional support, timely advice and affection showered upon me throughout the research work. His in-depth knowledge, positive attitude, dedication and constant encouragement helped me a lot in accomplishing this work.

I am also indebted to Dr. Suguna Yesodharan, Professor (Emeritus), former Director (SES), (CUSAT), whose affection and encouragement helped me to enter into the world of Advanced Oxidation Processes. Her constant encouragement and advice helped me a lot in the successful completion of this work.

It is time to express my sincere gratitude and affection to the present Director SES, Dr. Rajathy Sivalingam as well as previous Directors, Prof. Suguna Yesodharan, Prof. Ammini Joseph and Dr. Harindranathan Nair for providing all the facilities of the school for the smooth conduct of the study. I also wish to express my deep sense of gratitude to Dr. Sivanandan Achari and Dr. M. Anand, faculty members of the school, for their support, suggestions, help and encouragement throughout the period of research. I also thank the non-teaching staff of the school for their help and assistance.

I would like to express my sincere and heartfelt gratitude to all the research scholars of our laboratory, Dr. Anju, Dr. Jyothi, Ms. Sindhu, Ms. Phonsy, Mr. Shibin, Mr. Hariprasad Narayanan, Ms. Veena, Ms. Gayathri, Ms. Vidya and Ms. Deepthi and all other research scholars and students of SES for their timely advice, help and affection.

I would like to extend my sincere gratitude to the management of M/s Hindustan Organic Chemicals Ltd (HOCL) for granting me permission to do

the research work and providing necessary support. I would like to express my gratitude to Mr. K. Rajan (former Executive Director, HOCL), Dr. K. N. Kutty (Executive Director, HOCL Kochi unit), Mr. K. K. Vijayakumar (former Unit In Charge of HOCL), Dr. P.V. Padmanabhan (former HOD, QC, HOCL), Mr. S. Sanil Kumar (GM, PSA, HOCL), Mr. A.V. Giri (HOD, QC, HOCL), Mr. P.O. Peter (former Assistant Manager, QC, HOCL) and all my colleagues for their constant encouragement throughout this work.

I recall with love and gratitude the sincere cooperation and encouragement, received from my friends Dr. J. D. Sudha, Miss. Prabha (NIIST Thiruvananthapuram) and Dr. Manoj P Rayaroth.

I also take this opportunity to express my love and gratitude to my parents, parents in-law, my wife Suja and our kids Vaishnav and Abhinav for their cooperation and support.

Above all, this piece of work is accomplished with the blessings and powers that work within me and also the people behind my life. I bow before GOD for all with a sense of humility and gratitude.....

Rajeev B.

Preface

Industry is one of the largest consumers of water. Majority of this water is discharged into the water bodies after conventional secondary treatment. This treated water may contain hazardous pollutants in trace quantities which can adversely affect the ecosystem in the long run as many of them have bioaccumulation potential. In order to reuse this water, these trace contaminants should be removed by suitable tertiary treatment techniques. Unfortunately, most of the tertiary treatment techniques are uneconomical and energy intensive at industrial level. Advanced Oxidation Processes (AOPs) can be effectively used as viable tertiary treatment methods for the complete degradation/mineralization of such hazardous/recalcitrant trace pollutants.

AOPs involve the generation and utilization of highly reactive •OH radicals, which are powerful oxidants. They can completely degrade/ mineralize the pollutants into harmless CO_2, H_2O and mineral salts. The most widely used AOPs include wet air oxidation, radiolysis, sono catalysis, photolysis, photocatalysis, Fenton oxidation, microwave catalysis and electrochemical oxidation. The present study is an investigation on the possibility of using ZnO mediated solar photocatalysis for the removal of pollutants such as Alpha methyl styrene (AMS), Acetophenone (ACP), Dimethyl phenylcarbenol (DMPC) and 2-Methyl benzofuran (2-MBF) in water both individually and in combination. These are the major pollutants in the effluent discharge from phenol manufacturing industry. The main objectives of the study are:

- Characterization of ZnO catalyst
- Optimization of various reaction parameters such as substrate concentration, catalyst loading, pH, presence of contaminants in water, O_2, oxidants such as H_2O_2 and persulphate etc., for the

degradation/mineralization of each pollutant individually and in combination.

- Identification of reaction intermediates and their effect on the degradation efficiency of the parent pollutant
- To understand the kinetics of the photocatalytic degradation of the four pollutants and propose suitable mechanisms
- To study the effect of natural contaminants such as dissolved salts and humic acid on the degradation efficiency of individual pollutants
- To study the effect of common oxidizing agents such as H_2O_2, KIO_3 and $K_2S_2O_8$ on the degradation of pollutants
- To study the effect of each pollutant on the degradation efficiency of the other in their combination
- To verify the viability of solar photocatalysis for the complete degradation and mineralization of a typical combination of the four pollutants in distilled water as well as in real industrial water matrix

The thesis provides a comprehensive report on the major findings of the study and a critical analysis of the observations. It is unequivocally concluded that ZnO mediated solar photocatalysis is an effective tool for the mineralization of many organic pollutants, even when they are present in traces in water. Part of the results are presented in various national/international conferences (Annexure II). Some of the findings are published as original research papers in three peer reviewed international journals as shown in Annexure III.

The thesis is presented in eight chapters and three annexures as given below:

Chapter1: Introduction: Background literature

Some reaction sequences and chemical equations are appearing repeatedly in different chapters in the thesis. However, every time when they are used (irrespective of the repetition), they are given new numbers for clarity and convenience of reading.

Contents

Chapter **2**

Chapter **3**

Chapter **6**

ZINC OXIDE MEDIATED SOLAR PHOTOCATALYTIC DEGRADATION OF 2-METHYL BENZOFURAN [2-MBF] IN WATER..... 287 - 338

Chapter **7**

ZINC OXIDE MEDIATED SOLAR PHOTOCATALYTIC DEGRADATION OF AMS, ACP, DMPC AND 2-MBF IN SYNTHETIC AND REAL INDUSTRIAL WASTEWATER..... 339 -379

List of Tables

List of Figures

.....ꕥ.....

Chapter 1

INTRODUCTION: BACKGROUND LITERATURE

Contents

1.1 General

Industry is the backbone of any civilized society. Industrial revolution made tremendous contribution to the development of the world. The development of science and technology during industrial revolution and the revolution itself indirectly resulted in the deterioration of the quality of the environment consisting of soil, water and air. The trend is continuing even today. Due to the unscientific waste disposal practices, the air, soil and water including ground water have become contaminated with a variety of hazardous/toxic chemicals such as solvents, volatile organics, pesticides, polychlorinated biphenyls (PCBs), dyes, phenols, heavy metals etc. These are adversely affecting the human health as well as the ecosystem.

Current world population which is approximately 6.5 billion is increasing at an alarming rate and is projected to be 9 million by 2050 [1]. This population explosion leads to a large scale deforestation and

decreased agricultural land which results in the need for extensive use of chemical fertilizers and persistent chemical pesticides to boost the agricultural production in order to meet the increasing demand for food. This adversely affects our ecosystem [2, 3]. Rapid industrialization leads to an increase in per capita consumption of natural resources especially water. Water is a fundamental requirement for life and it is essential for sustaining activities such as drinking, cooking, cleaning, agriculture, etc. Even though nature has its own mechanism for the recycling of water in order to provide us with the required quantity of fresh water for ever, this mechanism is disrupted and made inefficient by human activities which ultimately leads to shortage of potable water.

It was estimated that 700 million people across the globe face water scarcity and this figure may touch 1.8 billion by 2025 [4]. According to a World Health Organization (WHO) report, water borne diseases kill nearly 12 million people every year [5]. About 90% of all diseases occurring in developing countries are related to the consumption of impure water leading to nearly 4 billion reported cases of diseases contracted from water [6].

Industrial sector is one of the largest consumers of water. Water is required for various industry related activities and during the process, it may get contaminated with toxic/hazardous chemicals. The effluent water from such industries is discharged after treatment to the water bodies in accordance with the norms of the pollution control agencies. This water still contains trace quantities of pollutants which may contaminate the surface water/ground water due to the accumulation of these trace pollutants. Eventually, this will affect the flora and fauna. The annual

water consumption by Indian industry is about 40 billion cubic meters and the annual waste water discharge is approximately 30.7 billion cubic meters. This means that for every cubic meter of water consumed, 0.77cubic meters of waste water is discharged. It was estimated that only 10 % of the waste water generated is treated and the rest is discharged as such into the water bodies [7]. The water productivity of some of the G20 countries is shown in figure 1.1.

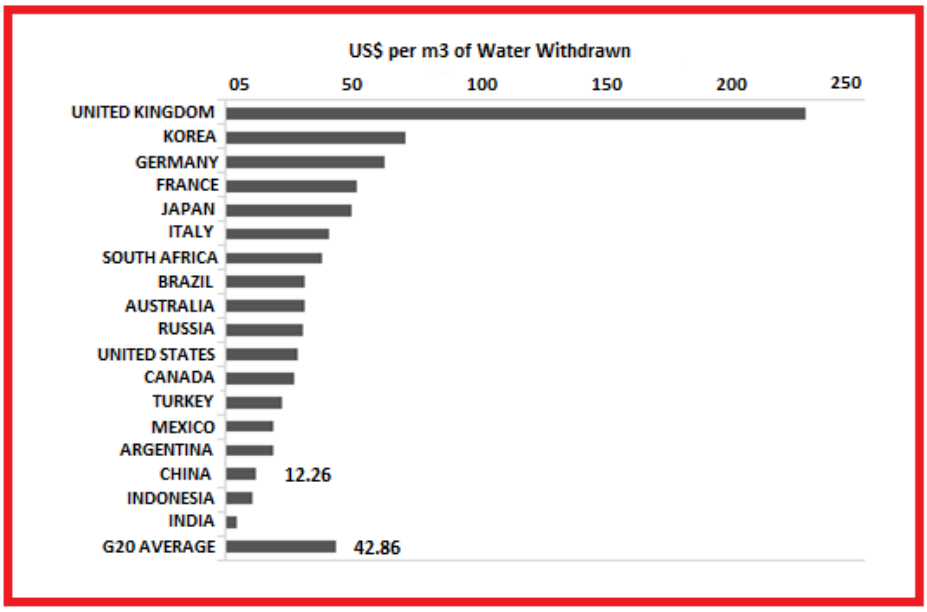

Fig. 1.1: Water productivity of G20 countries [8]

As seen from the figure the most inefficient water productivity is in India, compared to other nations. Most of the industries are not reusing the treated water as the quality is not adequate for the purpose even after the secondary treatment. A tertiary treatment method is therefore necessary for further polishing of the treated water. Unfortunately, most of the

conventional tertiary treatment methods currently used in wastewater treatment plants such as ultrafiltration, microfiltration, reverse osmosis, activated carbon adsorption and sand filtration etc., are ineffective and expensive. Traces of persistent pollutants such as phenols, pesticides, dyes, solvents etc., are still detected in the treated water [9, 10]. Hence, it is important to develop advanced technologies for the removal of such pollutants in order to achieve the twin objectives of water recycling and pollution abatement. Advanced Oxidation Process [AOP] has now emerged as a viable technology for the removal of recalcitrant/toxic pollutants from industrial effluents.

Part A

Advanced Oxidation Processes (AOP)

The concept of "advanced oxidation process" was initially proposed by Glaze et al. in 1987 [11] and is defined as the "process at near ambient temperature and pressure which involves the generation of highly reactive hydroxyl radicals ($^{\bullet}OH$) in sufficient quantity to effect water purification". AOP is considered as the "treatment process of the 21st century" as it can reduce the contaminant concentration from several hundred ppm to less than 5 ppb, when applied appropriately. AOPs are based on the chemistry of hydroxyl radicals ($^{\bullet}OH$), which are non-selective reactive species, able to oxidize pollutants into mineral end-products, yielding CO_2, H_2O and inorganic ions [12]. AOPs can be effectively used for the removal of organic contaminants such as halogenated hydrocarbons (e.g. trichloroethane, trichloroethylene), aromatics (e.g. Benzene, toluene and

xylene), pentachlorophenol (PCP), nitrophenol, detergents, pesticides, dyes, pharmaceuticals etc. This method can also be applied for the oxidation of inorganic contaminants such as cyanides, sulfides and nitrites [13].

1.A.1 General mechanism of AOP

The mechanism of AOP involves the generation of highly reactive free radicals ($^{\bullet}OH$), which can effectively destroy the organic molecules because of their electrophilic character. Some of the characteristic features of $^{\bullet}OH$ radicals are shown in figure 1.2.

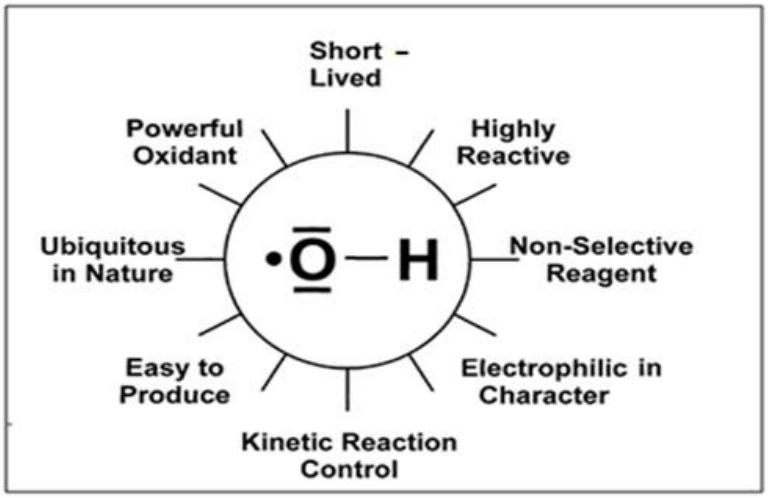

Fig. 1.2: Characteristic features of $^{\bullet}OH$ radicals [14]

Because of the higher oxidation potential (2.8 eV), $^{\bullet}OH$ radicals exhibit faster rate of oxidation compared to the conventional oxidizing agents such as H_2O_2, $KMnO_4$ etc. Hydroxyl radicals are known to be the second strongest oxidants after fluorine. Comparison of the oxidation potentials of some of the commonly used oxidants is shown in table 1.1.

Table 1.1: Oxidation potentials of some common oxidants

Sl. No.	Oxidation species	Oxidation potential (eV)
1	Fluorine	3.06
2	Hydroxyl radical	2.8
3	Sulphate radical	2.6
4	Atomic oxygen	2.42
5	Nascent oxygen	2.42
6	Ozone	2.07
7	Persulphate	2.01
8	Hydrogen peroxide	1.77
9	Perhydroxyl radical	1.70
10	Permanganate	1.68
11	Hypobromous acid	1.59
12	Hypochlorous acid	1.49
13	Hypochlorite	1.49
14	Hypoiodous acid	1.45
15	Chlorine	1.36
16	Chlorine dioxide	1.27
17	Oxygen(molecular)	1.23
18	Bromine	1.09
19	Iodine	0.54

Because of their high reactivity, $^{\bullet}OH$ radicals must be generated continuously insitu through chemical or photochemical reactions. They attack most part of organic molecules with rate constants usually of the order of 10^6-10^9 $M^{-1}s^{-1}$. Once generated, the hydroxyl radical can attack the pollutant organic molecule by radical addition, hydrogen abstraction and electron transfer (equation 1-3).

$R + {}^{\bullet}OH \rightarrow ROH$: Addition (1)

$R + {}^{\bullet}OH \rightarrow R^{\bullet} + H_2O$: Abstraction (2)

$R + {}^{\bullet}OH \rightarrow R^{+} + OH^{-}$: Electron transfer (3)

Where R = Organic molecule

Various steps involved in AOPs are:

1) Formation of strong oxidants (e.g. hydroxyl radical)
2) Reaction of the oxidants with organic pollutants in water and formation of bio-degradable intermediates
3) Reaction of bio-degradable intermediate with oxidants and their conversion to carbon dioxide, water and inorganic salts (mineralization)

These steps are schematically represented in figure 1.3.

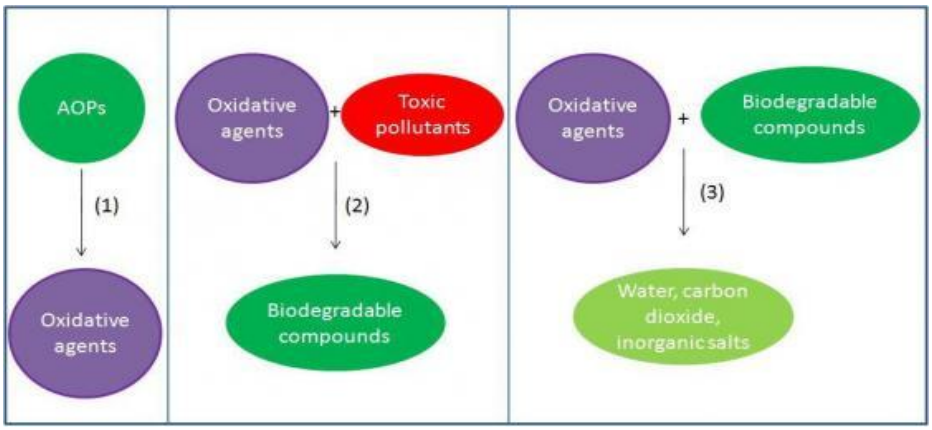

Fig. 1.3: Various steps involved in AOP

1.A.2 Advantages of AOPs

The main advantages of AOPs are [15]:

- They can destroy toxic organic compounds without transferring the pollution to another phase
- Very efficient technique to treat many organic pollutants as well as some toxic metals
- Can be used for water disinfection
- Installation is relatively less expensive

- Suitable for small scale application
- High rate of pollutant oxidation
- Flexibility concerning water quality variations and dimensions of equipments

1.A.3 Disadvantages of AOPs

The main disadvantages of AOPs are [16]:

- Special safety requirement because of the use of reactive chemicals [ozone, hydrogen peroxide] and energy input [UV lamp, electron beams, radioactive sources]
- Possible formation of potentially toxic intermediates from the parent compound
- Skilled professionals are required for the design and operation
- Still an emerging technology and requires more research for improving the efficiency

1.A.4 Classification of AOPs

Based on the mode of generation of $^{\bullet}OH$ radical, AOPs can be classified as photochemical and non-photochemical as listed in table 1.2.

Table 1.2: Non photochemical and photochemical AOP systems.

Non-photochemical	Photochemical
O_3/ $^{\bullet}OH$	H_2O_2/UV
O_3/H_2O_2	O_3/UV
O_3/US	O_3/H_2O_2/UV
O_3 /GAC*	Fe^{2+}/H_2O_2 /UV(Fenton system)
Electro-Fenton	UV/TiO_2, ZnO/UV
Electron beam irradiation	O_2/TiO_2/UV
Ultrasound(US)	UV/US
H_2O_2/US	

GAC*-Granulated Activated Carbon

Photochemical AOPs generally use a combination of strong oxidizing agents (e.g. H_2O_2, O_3) with catalysts (e.g. transition metal ions) and irradiation (e.g. ultraviolet, visible). This method can be effectively used for the decontamination of water containing recalcitrant organic pollutants. The main advantages of this method are high pollutant oxidation rate, flexibility concerning water quality parameters and small dimensions of equipments. However, relatively higher treatment costs, need for special safety requirement (because of the use of reactive chemicals such as ozone, H_2O_2 etc.,) and high energy sources like UV lamp, electron beams etc., are considered as their inherent limitations.

AOPs can also be classified based on the medium in which the processes take place viz, Homogeneous or Heterogeneous AOPs as shown in figure 1.4.

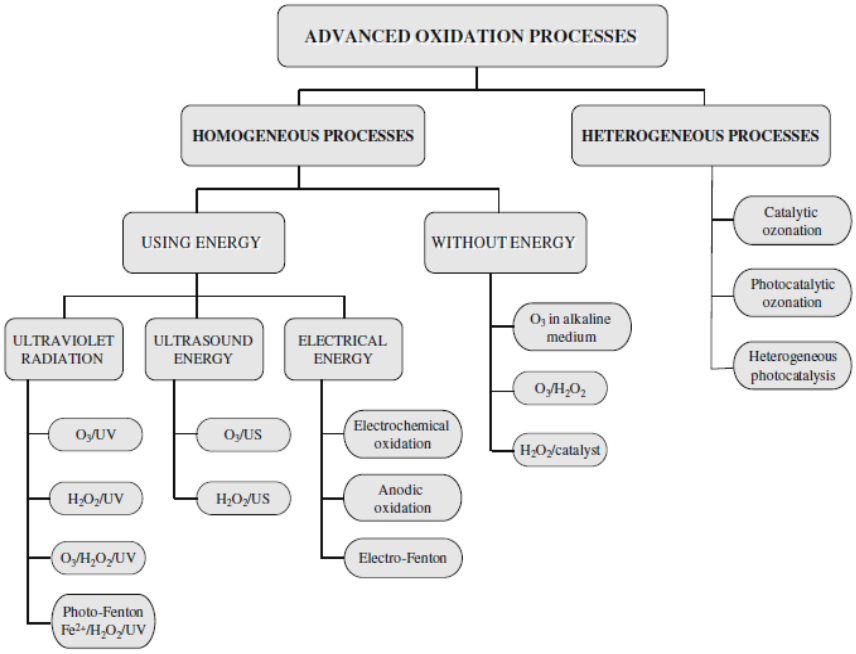

Fig. 1.4: Classification of AOPs [17]

1.A.5 Homogeneous AOPs

Homogeneous AOPs may or may not use energy. UV radiation is the most commonly used energy source. Typical homogeneous AOPs include O_3/UV, H_2O_2/UV, O_3/H_2O_2/UV, photo-Fenton etc., (which are often classified under homogeneous photocatalysis).

1.A.6 Heterogeneous AOPs

Heterogeneous AOPs generally involve the use of a catalyst for the degradation of the organic compound. Here the contaminants are present in the aqueous phase and the catalyst in the solid phase and hence the name heterogeneous AOP. The advantage of heterogeneous AOP over homogeneous AOP is the greater ease in the separation of the catalyst.

1.A.7 Photocatalysis

A photocatalyst is defined as a substance which is activated by absorption of a photon and is capable of accelerating a reaction without being consumed [18]. Photocatalysis can be defined as a chemical reaction induced by photon absorption by the catalyst, which remains unchanged during the reaction. Photocatalysis is now widely employed as a powerful AOP for the complete mineralization of organic molecules into nontoxic CO_2 and water under atmospheric conditions. Photocatalysis, which uses light as the energy source for activation, can be either homogeneous or heterogeneous.

1.A.7.1 Homogeneous photocatalysis

In homogeneous photocatalysis, the reactant and the photocatalyst exist in the same phase. Some of the commonly employed homogeneous

photocatalytic processes include O_3/UV, H_2O_2/UV, O_3/H_2O_2/UV and photo-Fenton. The use of solar irradiation in homogeneous aqueous system cannot lead to the mineralization as it can bring only primary structural changes in the molecule. However, the use of UV light in homogeneous photocatalysis can result in the degradation of the pollutants due to the generation of hydroxyl radical in the system. Even though the oxidizing strength of H_2O_2 as such is very low, the UV light irradiation enhances the rate and strength of its oxidation through the production of a large amount of reactive hydroxyl radicals in the system.

1.A.7.1.1 *UV/Hydrogen peroxide (UV/H_2O_2)*

This process involves the generation of hydroxyl radicals by the photolysis of H_2O_2, if the wave length of the photon is shorter than 370 nm. These radicals can oxidize organic compounds containing an alkyl group R. The rate of photolysis of aqueous H_2O_2 has been found to be pH dependent and increases under alkaline conditions. This may be due to the higher molar absorption coefficient of the peroxide anion (240 $M^{-1}cm^{-1}$) [19].

$$H_2O_2 + h\nu \rightarrow 2\ {}^{\bullet}OH \qquad (4)$$

The mechanism of the reaction of the hydroxyl radical generated in presence of the organic substrate can be described as

Hydrogen abstraction

$${}^{\bullet}OH + RH \rightarrow R^{\bullet} + H_2O \qquad (5)$$

Electrophilic addition

$${}^{\bullet}OH + PhX^{-} \rightarrow HOPhX^{-} \qquad (6)$$

Electron transfer

$$^{\bullet}OH + RX \rightarrow RX^{\bullet +} + HO^{-} \quad (7)$$

Radical-radical recombination

$$2\ ^{\bullet}OH \rightarrow H_2O_2 \quad (8)$$

The sequence of reactions during the process is shown in figure 1.5.

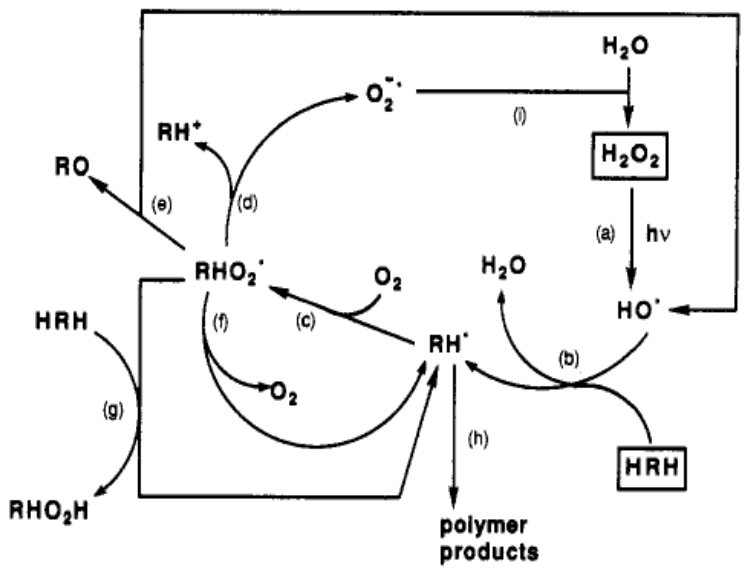

Fig. 1.5: Reaction sequence for the UV/H_2O_2 process [20]

Hydroxyl radicals generated by hydrogen peroxide photolysis as in reaction (a) react with organic compounds (HRH) primarily by hydrogen abstraction to produce an organic radical **(**$RH^{\bullet}$**)** as in reaction (b). This radical reacts quickly with dissolved oxygen to yield an organic peroxyl radical ($RHO_2^{\bullet}$) as in reaction (c) initiating subsequent thermal oxidation reactions. Peyton [21] proposed three different reaction paths for either peroxyl radicals or their tetra oxide dimers: (1) heterolysis and generation of organic cations as well as superoxide anion as in reaction (d), (2) l,-3

hydrogen shift and homolysis into hydroxyl radicals and carbonyl compounds as in reaction (e), and **(**3**)** back reaction to $RH^{\bullet}$ and O_2 as in reaction (f). In aqueous systems, cations will further react by solvolysis and superoxide anion will readily disproportionate to yield H_2O_2 as in reaction (i) [19].

Advantages of UV/ H_2O_2 process are:

1) Commercial availability and the infinite solubility of the oxidant (H_2O_2)
2) Formation of two hydroxyl radicals from each molecule of H_2O_2
3) H_2O_2 is readily available in the solution form that can be diluted to give desired concentrations
4) It can be stored safely onsite
5) No mass transfer problem associated with gases
6) Formation of photolysed peroxyl radical by the attack of $^{\bullet}OH$ radical on the organic substrate leading to subsequent thermal oxidation reactions
7) Minimal capital investment and simple operation
8) Does not lead to air emissions

The disadvantages are:

1) Presence of residual H_2O_2 in the treated water can promote biological growth in the distribution system
2) Low molar extinction coefficient in the near UV-region and small absorption cross section at 254 nm

1.A.7.1.2 *UV/Ozone (UV/O_3)*

The UV/O_3 process is an advanced water treatment method for the effective oxidation and removal of toxic and refractory organics, bacteria and viruses in water. The light induced decomposition of O_3 in aqueous solution involves a two-step process; the light induced homolysis of O_3 and the subsequent production of $^{\bullet}OH$ radicals by the reaction of O (^1D) with water [19].

$$O_3 + h\nu \rightarrow O_2 + O\,(^1D) \quad (9)$$

$$O\,(^1D) + H_2O \rightarrow {}^{\bullet}OH + {}^{\bullet}OH \quad (10)$$

However, it has been observed that photolysis of O_3 dissolved in water leads to the production of H_2O_2 (11) in a sequence of reactions, where hydroxyl radicals, if at all formed, do not escape from the solvent cage.

$$O_3 + H_2O + h\nu \rightarrow O_2 + H_2O_2 \quad (11)$$

Advantages of UV/O_3 process are:

1) More efficient in generating hydroxyl radicals, because of its high molar extinction coefficient at 254 nm
2) Destruction of toxic refractory organics and microbial populations
3) Higher rates of degradation compared to using UV or Ozone alone
4) Higher amount of hydroxyl radical is generated during this process

Disadvantages are:

1) Low solubility of O_3 in water compared to H_2O_2
2) O_3 does not absorb at wavelengths > 300 nm
3) Potential secondary reactions of the oxidative intermediates
4) Less energy efficient

1.A.7.1.3 *UV/Ozone and Hydrogen peroxide (UV/O_3/H_2O_2)*

The efficiency of the UV/O_3 process is enhanced by the addition of H_2O_2 due to the increased production of hydroxyl radicals. Hence UV/O_3/H_2O_2 process is a very powerful method for the fast and total mineralization of pollutants. The reaction pathways leading to the formation of hydroxyl radicals are summarized below [19]:

$$H_2O_2 + H_2O \leftrightarrow H_3O^+ + HO_2^- \quad (12)$$

$$O_3 + H_2O_2 \rightarrow O_2 + {}^{\bullet}OH + HO_2^{\bullet} \text{ (very slow)} \quad (13)$$

$$O_3 + HO_2^- \rightarrow {}^{\bullet}OH + O_2^{-\bullet} + O_2 \quad (14)$$

$$O_3 + O_2^{-\bullet} \rightarrow O_3^{-\bullet} + O_2 \quad (15)$$

$$O_3^{-\bullet} + H_2O \rightarrow {}^{\bullet}OH + HO^- + O_2 \quad (16)$$

The schematic representation of the reaction pathways in UV/ozone and ozone/H_2O_2 system is presented in figure 1.6.

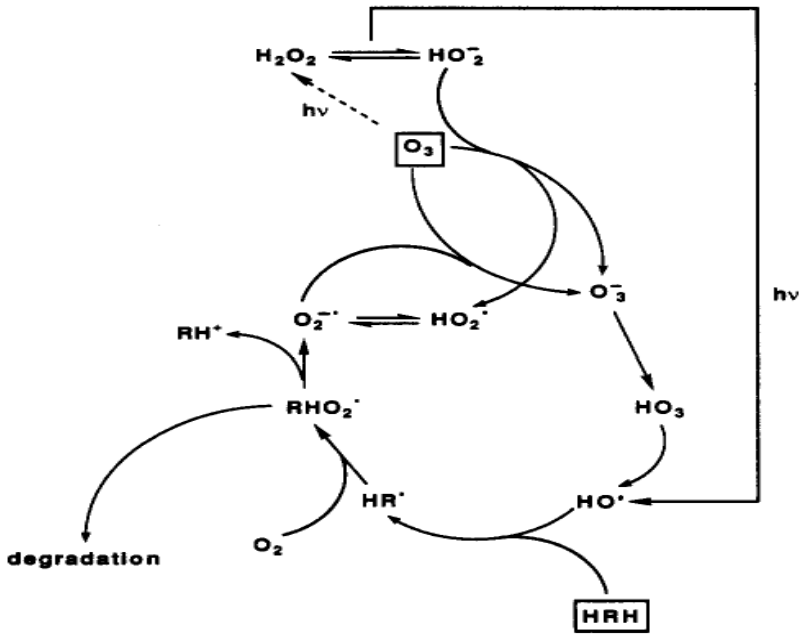

Fig. 1.6: Reaction pathways in the UV/ozone and UV/ozone/H_2O_2 systems

1.A.7.1.4 *Fenton's reaction*

Fenton's reagent, a mixture of ferrous iron (catalyst) and H_2O_2 (oxidizing agent) is a powerful oxidant for organic contaminants. The mechanism of Fenton process is as shown below [22, 23]:

$$Fe^{2+} + H_2O_2 \rightarrow Fe^{3+} + OH^- + {}^{\bullet}OH \quad (17)$$

$$Fe^{2+} + {}^{\bullet}OH \rightarrow Fe^{3+} + OH^- \quad (18)$$

$${}^{\bullet}OH + RH \rightarrow H_2O + R\bullet \quad (19)$$

$$R\bullet + Fe^{3+} \rightarrow R + Fe^{2+} \quad (20)$$

In dark condition, the reaction stops when the Fe^{2+} is completely converted to Fe^{3+}

The photo Fenton process ($H_2O_2/Fe^{2+}/UV$) involves the ${}^{\bullet}OH$ formation through photolysis of hydrogen peroxide (H_2O_2/UV) and Fenton reaction (H_2O_2/Fe^{2+}). In the presence of UV irradiation, the ferric ions (Fe^{3+}) produced in equation 17 are photocatalytically converted to ferrous ions (Fe^{2+}), with the formation of an additional equivalent of hydroxyl radical (equation 21) [24].

$$Fe^{3+} + H_2O \rightarrow Fe^{2+} + H^+ + {}^{\bullet}OH \quad (21)$$

The hydroxyl radicals formed react with organic species, promoting their oxidation.

Typical photo-Fenton-type system is shown in figure 1.7.

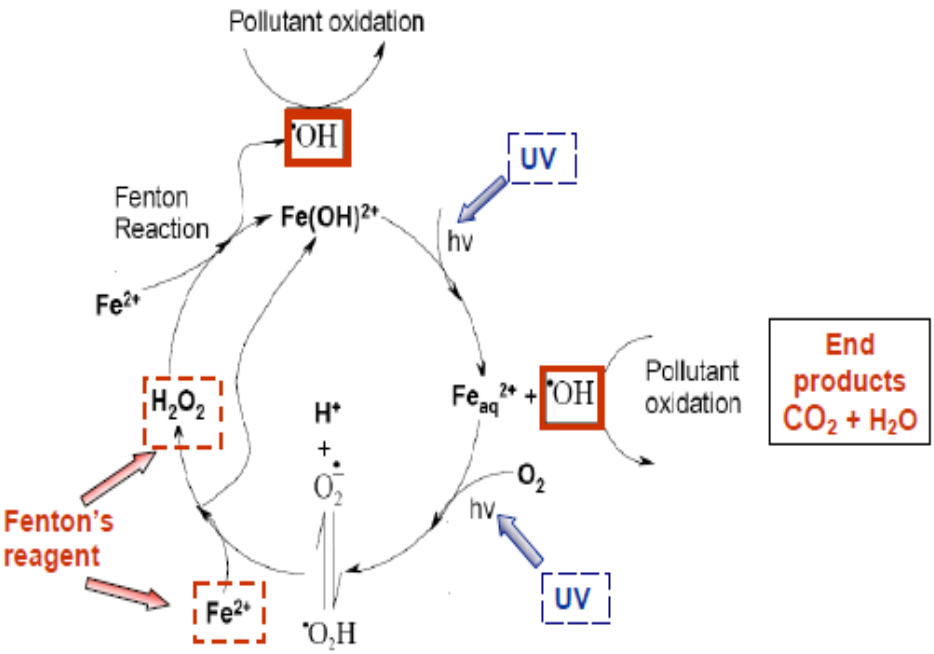

Fig. 1.7: Reaction processes in UV/H_2O_2 and UV/Fenton systems [25]

Advantages of Fenton process are;

1) Complete mineralization of organic matter
2) Very fast reaction

Disadvantages are:

3) Requirement of low pH
4) Formation of ferric oxide sludge, which requires continuous removal

1.A.7.2 Heterogeneous photocatalysis

In heterogeneous photocatalysis, the catalyst and the reactants exist in different phases and the reaction can be carried out in different media, namely gas phase, pure organic liquid phase as well as in aqueous solution.

Heterogeneous photocatalysis is now widely accepted as an alternative technology to traditional biological, chemical and physical decontamination technologies due to their characteristics such as non-selectivity, non-toxicity, total removal of pollutants and byproducts and cost effectiveness [26-29]. The five basic steps involved in heterogeneous photocatalytic process are:

1) Transfer of reactants in the fluid phase
2) Adsorption of reactants on the surface of the catalyst
3) Reaction in the adsorbed phase, which include
   - Absorption of photon by the solid
   - Creation of photo-induced electrons and holes
   - Electron transfer reaction (ionosorption, charge neutralization, radical formation, surface reactions)
4) Desorption of the final products
5) Removal of final products in the fluid phase

Transition metal oxides and semiconductors are the most commonly used photocatalysts due to their unique characteristics.

1.A.7.3 Semiconductor photocatalysis

According to the band theory of solids, during the formation of a crystal from a large number of atoms or molecules, the electron orbitals of comparable energy levels combine together to form energy bands. The energy levels of the electron orbital in a band are assumed to be continuous and the electron can move within the band easily if the band is not fully occupied. However, atomic or molecular orbitals with different

energy level form different energy bands. The orbitals of the valence electrons (the highest filled orbits) form the valence band (VB), and the lowest unoccupied orbitals of atoms form the conduction band (CB). The energy difference between the valence and conduction band is called the band gap energy (Eg). In metals, the bands are so closely spaced that there is practically a continuum of energy levels so that the electron can move freely within the band, which account for its good thermal and electrical conductivity. Hence they are called conductors. In insulators, there exists a wide band gap between the valence and conduction band so that the transfer of electron from valence band to conduction band is not possible. In semiconductors, there exists a small band gap between the valence and conduction band, so that by supplying sufficient energy, electrons can be promoted from valence band to conduction band. The band structures of insulators, conductors and semiconductors are shown in figure 1.8.

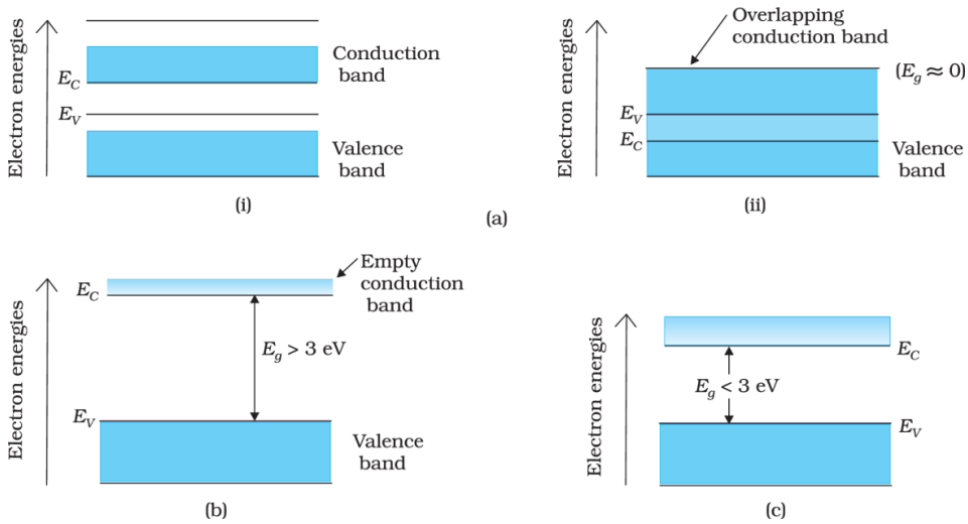

Fig. 1.8: Difference between energy bands in (a) metals, (b) insulators and (c) semiconductors [30]

Semiconductors are electronic conductors with electric resistivity in the range of 10^{-2} to 10^{9} ohm-cm at room temperature, intermediate between conductors (10^{-6} ohm-cm) and insulators (10^{14} to 10^{22} ohm-cm.). Perfect crystals of most semiconductors will be insulators at absolute zero temperature. Semiconductors can be classified into intrinsic and extrinsic semiconductors. In intrinsic semiconductors, electrons can be excited to the conduction band leaving the same number of holes in the valence band. In order to promote conductivity of extrinsic semiconductors, they must be doped with adequate number of impurities, such as metal oxides or sulfur compounds. Depending on the nature of impurities introduced, the extrinsic semiconductors can be divided into n-type (in which majority charge carriers are electrons) and p-type (in which majority charge carriers are holes).

In semiconductors, mobile charge carriers can be generated by three different mechanisms

1) Thermal excitation: Thermal excitation can promote electron from valence band to conduction band provided that the band gap energy of the semiconductor is sufficiently small (< ½ eV)

2) Photo excitation: Here the electron can be promoted from the valence band to the conduction band of the semiconductor by the absorption of the photon of light, provided that the energy of the photon is greater than or equal to the band gap energy.

3) Doping: It is a process of introducing a new level into the band gap. There are two types of doping for semiconductors. For n-type doping (with group III elements such as B, Al, Ga and In), occupied donor levels are created near the conduction band

edge, where the conduction is mainly due to the negative charge carriers. Similarly p-type doping (with group V elements like P, As, Sb, and Bi) leads to the formation of empty acceptor levels, creating positive charge carriers where the conduction is mainly due to positive charges. The surface defects and impurities in n-type and p-type semiconductors are responsible for the change in the band gap of the semiconductor.

1.A.7.4 Photocatalytic semiconductor materials

Metal oxides, sulphides and their various combinations represent a large class of semiconductor materials suitable for photocatalysis as they have band-gap energies sufficient for promoting or catalyzing a wide range of chemical reactions of environmental interest (e.g. TiO_2, ZnO, Fe_2O_3, WO_3, CdS, and ZnS).

The characteristics of a good photocatalyst are:

1) Photoactivity
2) Biological and chemical inertness
3) Stability towards photocorrosion
4) Absorption of visible or near UV light
5) Low cost and
6) Lack of toxicity

For a material to act as a good photocatalyst, redox potential of valence band hole and conduction band electron must be positive and negative respectively to generate hydroxyl and superoxide radicals. The energy level of some typical semiconducting materials used for photocatalytic reactions are shown in figure 1.9.

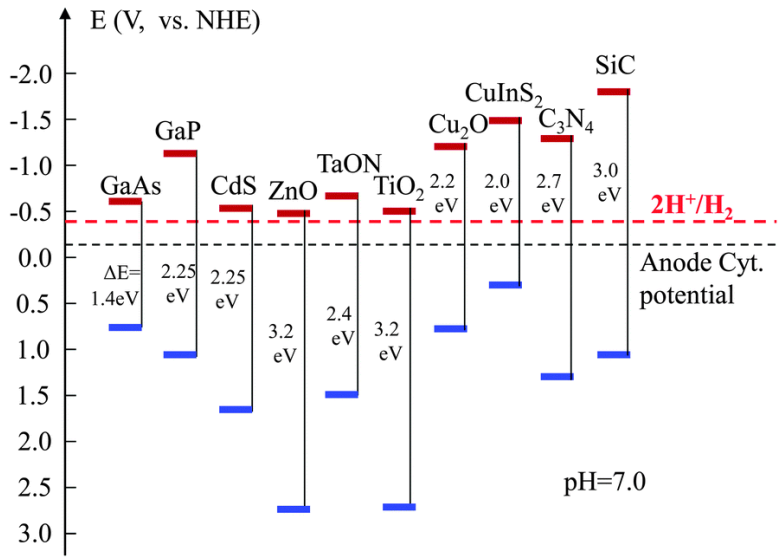

Fig. 1.9: Energy level diagram of some semiconducting materials

Even though metal oxides are usually less active as catalysts than noble metals, they are widely used as catalysts because of their resistance to poisoning. Combination of two or more metal oxide catalysts can improve non-selectivity and catalytic activity. Among the various semiconductor materials, TiO_2 is extensively used as a photocatalyst for environmental applications such as water purification, wastewater treatment, hazardous waste control, air purification, and water disinfection, because of its high photoactivity, desirable physical and chemical properties, low cost and easy availability. Of the three TiO_2 crystalline forms namely rutile, anatase and brookite, anatase shows greater efficiency as photocatalyst. The metal sulfide semiconductors are unsuitable as they readily undergo photo anodic corrosion. The iron oxide polymorphs, in spite of their high band gap energies and low cost, are unsuitable as photocatalysts because they readily undergo photo cathodic corrosion.

1.A.7.5 ZnO as a semiconductor photocatalyst

ZnO is also widely studied as a suitable alternative to TiO_2 as photocatalyst as it has same band gap energy as TiO_2 and follows a similar reaction mechanism**.** In fact ZnO is considered as a promising catalyst for water detoxification as it produces H_2O_2 efficiently and shows high reaction and mineralization rate. ZnO is proved to be a superior photocatalyst compared to TiO_2 due to its higher absorption efficiency of solar radiation [31]. ZnO is also nontoxic and is "generally recognized as safe (GRAS)" substance by the U.S. Food and Drug Administration. ZnO is also used as a common food additive and a component in sun screens and cosmetics [32]. Hence it is safe to use ZnO as a photocatalyst for environmental remediation as well as in water purification.

The main disadvantage of ZnO is that it can undergo photocorrosion through self-oxidation and is unstable in extremely acidic and alkaline conditions due to dissolution (equations 22, 23, 24) [33].

$$ZnO + 2h^+ \rightarrow Zn^{2+} + 1/2O_2 \quad (22)$$

$$ZnO + 2H^+ \rightarrow Zn^{2+} + H_2O \quad (23)$$

$$ZnO + H_2O + 2OH^- \rightarrow Zn(OH)_4^{2-} \quad (24)$$

1.A.7.6 Advantages of semiconductor photocatalysis

The main advantages of semiconductor photocatalysis in waste water treatment include:

1) Availability of highly active and inexpensive catalysts suitable for specially designed reactor systems
2) Complete oxidation of organic pollutants within few hours

3) No formation of polycyclic products
4) Oxidation of pollutants in ppb range
5) A good substitute for the energy-intensive conventional treatment methods with the capacity for using renewable and pollution-free solar energy
6) Unlike conventional treatment measures, which transfer pollutants from one medium to another, photocatalysis leads to the formation of innocuous products
7) Can be used to destroy a variety of hazardous compounds in different wastewater streams
8) The reaction conditions for photocatalysis are mild, the reaction time is modest, and less chemical input is required
9) Secondary waste generation is minimal
10) The option for recovery can also be explored for metals, which are converted to their less-toxic/nontoxic metallic states [34]

1.A.7.7 General mechanism of semiconductor photocatalysis

When a semiconductor material is illuminated with light of energy equal to or greater than its band gap energy, the electrons from the valence band are excited to the conduction band leaving holes in the valence band and electrons in the conduction band. If the excited electron-hole pairs recombine either in the bulk or at the surface, the energy is released as heat without any chemical effect. But if the electron-hole recombination is prevented they can migrate to the surface of the semiconductor and participate in various oxidation and reduction

reactions with adsorbed species such as water, oxygen and other organic or inorganic species. The positive hole can either oxidize the pollutant directly or react with water molecule to produce highly reactive $^{\bullet}OH$ radical whereas the electron in the conduction band reduces the oxygen adsorbed on the catalyst to form a superoxide radical anion ($O_2^{-\bullet}$). A schematic diagram representing the principle of semiconductor photocatalysis is shown in figure 1.10.

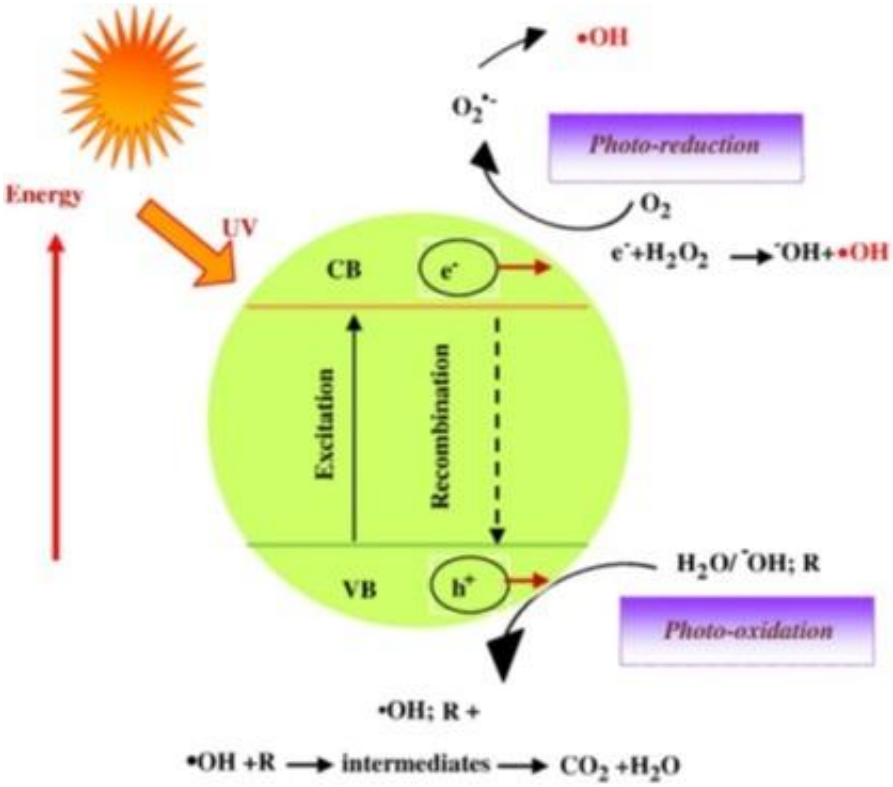

Fig. 1.10: Schematic diagram of principle of semiconductor photocatalysis [35]

Various steps involved in semiconductor photocatalysis are:

$$h\nu + \text{Semiconductor} \rightarrow e_{cb}^{-} + h_{vb}^{+} \quad (25)$$

$$H_2O + h^{+} \rightarrow H^{+} + {}^{\bullet}OH \quad (26)$$

$$2H_2O + 2h^{+} \rightarrow 2H^{+} + H_2O_2 \quad (27)$$

$$H_2O_2 \rightarrow {}^{\bullet}OH + {}^{\bullet}OH \quad (28)$$

$$(O_2)\ ads + e^{-} \rightarrow O_2^{-\bullet} \quad (29)$$

$$H_2O \rightarrow OH^{-} + H^{+} \quad (30)$$

$$O_2^{-\bullet} + H^{+} \rightarrow HOO^{\bullet} \quad (31)$$

$$HOO^{\bullet} + e^{-} \rightarrow HOO^{-} \quad (32)$$

$$HOO^{-} + H^{+} \rightarrow H_2O_2 \quad (33)$$

$$H_2O_2 + e^{-} \rightarrow OH^{-} + {}^{\bullet}OH \quad (34)$$

The hydroxyl radicals (${}^{\bullet}OH$) generated in both reactions (26 and 34) are powerful oxidants with an oxidation potential of 2.8 eV vs NHE. ${}^{\bullet}OH$ rapidly attacks pollutants at the surface as well as in solution and mineralizes them into CO_2, H_2O etc.

Hydroxyl radical (${}^{\bullet}OH$) and superoxide radical anion ($O_2^{-\bullet}$) are the primary oxidizing species in the photocatalytic oxidation processes. They cause the degradation of the organic (RH) pollutants by oxidation via successive attack by ${}^{\bullet}OH$ radicals.

$$RH + {}^{\bullet}OH \rightarrow R^{\cdot} + H_2O \quad (35)$$

$$R + h^{+} \rightarrow R^{\cdot +} \rightarrow \text{degradation intermediates} \rightarrow \rightarrow \text{mineralized products} \quad (36)$$

1.A.8 Use of sunlight as energy source in photocatalysis

Most of the photocatalytic degradation studies of organic pollutants use UV as the energy source. But the use of UV is harmful and

uneconomical for large scale applications. Sunlight can be effectively used as an energy source for photocatalysis by using suitable catalysts which can absorb a large fraction of solar spectrum. India being a tropical country (8° 4' -36° 6' N latitude), high level of solar UV radiation is available for almost 10 months a year. UV radiation represents 3.5 to 8% of the total solar spectrum, fluctuating with the presence of clouds and increasing with altitude and this can be effectively harvested for large scale photocatalytic degradation processes. The ultraviolet spectrum on the surface of the earth is shown in figure 1.11.

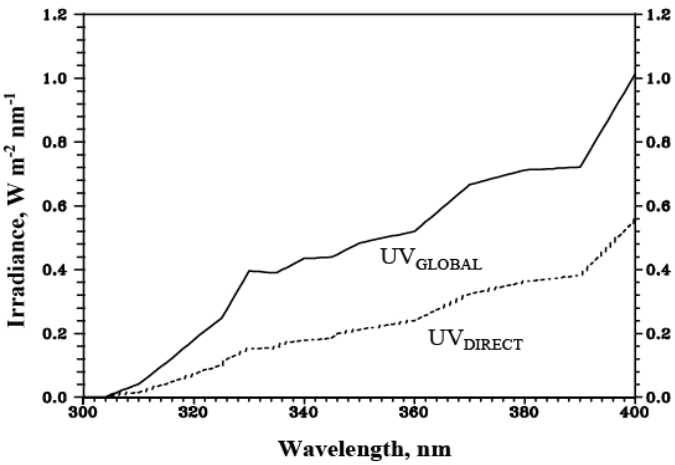

Fig. 1.11: Ultraviolet spectrum on the earth surface

1.A.9 Some typical photocatalytic degradation studies

Most of the studies on the application of photocatalysis in water treatment have been summarized in excellent reviews [19, 36-43]. The review articles that appear at regular intervals in highly rated journals speak of the volume of research being carried out on this topic around the world. Some such studies of immediate relevance to the current investigation are summarized here.

Qamar et al. [44] compared the photocatalytic activity of TiO_2 and ZnO under UV irradiation for the degradation of vanillin under different pH, catalyst and substrate concentrations and in presence of electron acceptors such as H_2O_2. Degussa P25 was more efficient as a photocatalyst compared to other photocatalysts, Hombikat UV100 and ZnO.

Baruah et al. [45] studied the photocatalytic activity of ZnO nanorods which were grown on a paper support prepared from soft wood pulp using Methylene Blue and Methyl Orange as the test pollutants under visible light irradiation for 120 min. About 93% degradation for Methylene Blue and 35% degradation for Methyl Orange were reported under identical conditions. Antibacterial test showed that the photocatalytic paper inhibited the growth of *Escherichia coli* under room lighting conditions.

Patil et al. [46] investigated the photocatalytic activity of both TiO_2 and ZnO catalysts under UV illumination for the treatment of coloured wastewater from the textile dyeing and printing industry under various reaction conditions. ZnO was found to be more effective compared to TiO_2 under the operating parameters used.

Dhanavel et al. [47] studied the photocatalytic activity of Chitosan encapsulated zinc oxide (ZnO) hybrid nanocomposite which was prepared by chemical precipitation method. The composite showed high photocatalytic activity for the degradation of Methylene Blue. Over 80% degradation of the dye was achieved under UV irradiation within 4hr.

Sharma et al. [48] studied the photocatalytic degradation of copper soap prepared from the neem seed oil by the direct metathesis method

using ZnO catalyst under visible light irradiation. The method is found to be effective and rapid for the degradation of such non-biodegradable molecules. The effect of various parameters such as concentration of soap, amount of semiconductor, effect of light intensity, effect of polarity of the solvent etc., on the rate of photocatalytic degradation was investigated in detail. The degradation is maximum at a light intensity of 34 $mWcm^{-2}$. Polar solvent such as methanol inhibits the rate of degradation.

Mashkour et al. [49] investigated the photocatalytic decolorization of aqueous solutions of Reactive Red 2 dye in the presence of ZnO and artificial UV-A light sources. The effects of various parameters, such as time of irradiation, photocatalyst amount, pH, addition of H_2O_2 and temperature on the degradation were investigated. The decolorization was found to increase significantly with time of irradiation. Under optimal conditions, the extent of decolorization was 100% after 30 min of irradiation. Oxidizing agents such as oxygen and H_2O_2 enhance the decolorization rate. However, excess H_2O_2 inhibits the decolorization rate. The decolorization process of the dye follows pseudo-first order kinetics.

Nirmala et al. [50] studied the photocatalytic efficiency of ZnO nanoparticles synthesized by DC thermal plasma using the degradation of Methylene Blue (MB) in water under UV irradiation as the test reaction. ZnO nanopowder resisted the growth of bacteria such as *Escherichia coli* and *Klebsiella pneumoniae*. The study proved the potential of ZnO in reducing the environmental toxicity as well as in biomedical applications.

Jayamadhava et al. [51] investigated the photocatalytic activity of ZnO nano particles prepared by solution combustion method using Brilliant

Red dye as the test pollutant. The degradation efficiency was found to increase with increase in pH, with maximum at pH 9.

Mohabansi et al. [52] carried out a comparative study of the efficiency of TiO_2 and ZnO photocatalysts for the photodegradation of Methylene Blue (MB) dye effluent under UV radiation. Their study shows that ZnO is a very effective and suitable alternative to TiO_2 in terms of percentage degradation of MB.

He et al. [53] prepared Co and Mn doped ZnO nanoparticles with upto 5 atom % doping level using a mechanochemical method. The photocatalytic activity is studied using Rhodamine B as the probe molecule. It was found that Co doping strongly reduced the photocatalytic activity, while Mn doping increased the same at low doping levels but reduced the activity at high doping levels. A possible explanation for this phenomenon is that the Mn at low-doping level increased the photo-response in visible light range which led to the increase in overall photocatalytic activity under the entire simulated sunlight spectrum. As for the high-doping level of Mn, the cause of the reduction in photocatalytic property may be attributed to the physical defects and increased oxidation state of Mn ions, which may act as trapping sites for photo-generated charges and promote the recombination of electrons and holes. This also decreases the generation of reactive species such as •OH and $O_2^{-\bullet}$.

Kim et al [54] studied the photocatalytic activity of ZnO/Fly ash composite prepared by hydrothermal process using Methylene Blue as the test molecule. Fly ash particles (FAPs, the inorganic residue generated in the combustion of coal) consist of fine powdery particles having a spherical

shape and substantial granular components of silicon dioxide (SiO_2), alumina (Al_2O_3), calcium oxide (CaO), magnesium oxide (MgO) and titanium dioxide (TiO_2). The characterization of the ZnO/FAP composite was done using Field Emission Scanning Electron Microscopy (FE-SEM), Energy Dispersive Spectroscopy (EDS), Transmission Electron Microscopy (TEM), X-ray Diffraction (XRD), Fourier Transform Infrared Spectroscopy (FT-IR), and Photoluminescence Spectroscopy (PL) etc. The study revealed that ZnO/FAP composite shows greater efficiency towards the photodegradation of MB under constant UV irradiation than pristine ZnO and the photocatalytic efficiency increases with increase in the amount of FAP. The superior photocatalytic activity of the composite was related to the greater deposition of ZnO on the surface of FAPs and the electron transfer between the conduction bands of light-activated ZnO and light-activated FAPs.

Borker et al. [55] compared the photocatalytic activity of ZnO, N-doped ZnO and iron ore rejects using Methylene Blue [MB] as the model pollutant and sunlight as the energy source. Zinc oxalate and hydrazinated zinc oxalate were used as the precursors for ZnO and N-doped ZnO [$ZnO_{(1-x)}N_x$] respectively. The study shows that iron ore reject shows greater catalytic activity followed by $ZnO_{(1-x)}N_x$ and ZnO. $ZnO_{(1-x)}N_x$ absorbs in visible region as it has a lower band gap energy (2.48eV) compared to ZnO (3.19 eV). Here more electron-hole pairs formed in nitrogen are likely to donate some electrons to Zn, which also enhances the generation of hydroxyl radicals. This increases the efficiency of $ZnO_{(1-x)}N_x$ compared to ZnO. During the degradation, the ore reject forms hydroxyl ion radicals similar to Fenton reagent. Chain reaction during the process supplies hydroxyl ions continuously due to

formation of Fe^{3+}/Fe^{2+}. Hence efficacy of the ore reject is best amongst the three.

Fu et al. [56] prepared C_{60}-hybridized ZnO photocatalyst [C_{60} molecules with monomolecular layer state dispersed on the surface of ZnO] and showed that it has better photocatalytic activity as well as corrosion resistance. The photocorrosion inhibition of ZnO by C_{60} molecule (fullerene containing a closed-shell configuration consisting of 30 bonding molecular orbitals with 60 π-electrons) could be attributed to the reduced activation of surface oxygen atom. The enhanced photocatalytic activity for C_{60}-hybridized ZnO was due to the high migration efficiency of photo induced electrons at the interface of C_{60} and ZnO, which was produced by the interaction of C_{60} and ZnO with a conjugative π-system.

Lv et al. [57] prepared ZnO with surface oxygen vacancies by vacuum deoxidation. This ZnO has significantly enhanced UV light photocatalytic activity and distinct visible light activity compared to normal ZnO for the degradation of Methylene Blue [MB]. The UV photocatalytic activity of vacuum-treated ZnO was found to increase with the increase in vacuum temperature or time. The visible light photocatalytic activity also shows the same trend. The enhancement of UV activity is attributed to the high separation efficiency of photogenerated electron-hole pairs caused by the broadening of VB width induced by surface oxygen-vacancies. The generation of visible light activity originates from the reduced energy band gap due to the rise of valence band maximum.

Catano et al. [58] prepared ZnO nanostructured thin films by electro-deposition at constant potential from zinc nitrate solutions. It was

found that by changing the precursor concentration and the electro-deposition time, different morphologies which evolve from nano needles and nano rods to thin films can be created. The photocatalytic activity of different nanostructures was tested using Methyl Orange as the test molecule under UV illumination. Results show that the surface area, the exposed crystalline planes, the morphology and the band gap of the ZnO nanostructured thin films play important role in this activity.

Zhang et al. [59] studied the photocatalytic activity of Nd doped ZnO nanoparticles with varying Nd content prepared by sol-gel method. The study shows that Nd doped ZnO shows better photocatalytic activity than the undoped ZnO for the photodegradation of the dye Congo Red [CR]. For the Nd doped ZnO, more lattice defects are introduced by Nd located at substitutional positions of Zn site, the more the singly ionized oxygen vacancy (Vo^{+}) defects the higher the photocatalytic efficiency. More oxygen vacancies promote the adsorption of O_2 and there is a strong interaction between photo induced electrons bound by oxygen vacancies and adsorbed O_2 producing $O_2^{-\bullet}$. This oxygen species is active in promoting the oxidation of organic substances. Moreover, large number of oxygen vacancies can produce a strong adsorption of OH^{-} ions on the surface of ZnO. These OH^{-} ions are assumed to serve as surface bound traps for the photogenerated holes, which prevent electron-hole recombination. Nd doped ZnO nanoparticles, (Nd3z) can also work as electron scavengers and prevent the electron-hole recombination. Therefore, Nd doped ZnO nanoparticles have higher photocatalytic activity than ZnO nanoparticles.

Ghaneian et al. [60] investigated the photocatalytic degradation of Humic Acid [HA] using Ag/ZnO nanoparticles under UV illumination. The maximum efficiency for the humic acid removal was observed at pH=7. Reaction kinetics of humic acid degradation by Ag/ZnO photocatalyst in the presence of UV is well described by a pseudo-first-order reaction.

Hiremath et al. [61] prepared ZnO nano particles by green synthesis using zinc nitrate precursor and *Euphorbia tirucalli (Pencil Cactus)* stem extract. The photocatalytic activity of the biosynthesized ZnO was tested using Rhodamine B as the test pollutant. The effect of various parameters such as photocatalyst concentration, pH and Hydrogen peroxide addition was studied. The ZnO nano particles were found to be very effective for degrading Rhodamine B.

Tian et al. [62] prepared ZnO catalyst by the calcination of zinc acetate at different calcination temperatures and their catalytic efficiencies were tested using Methyl Orange as the pollutant under UV light. The catalyst prepared at different temperatures shows varying activity due to the difference in their crystallinity and the BET surface area. The prepared ZnO was found to have excellent photocatalytic activity compared to Degussa P25 TiO_2.

Mohamed et al. [63] prepared ZnO/SiO_2 nanoparticle by sol-gel technique. The synthesized material was further modified by incorporating nano sized Pt from H_2PtCl_6 solution through photo assisted deposition (PAD) and impregnation (img) routes. The photocatalytic activity of the Pt-ZnO/SiO_2 was evaluated by the degradation of phenol in synthetic wastewater under UV-irradiation. Results revealed that the surface area and the photocatalytic activity of the prepared samples increased in the

order ZnO/SiO_2 < PAD: Pt-ZnO/SiO_2 < img: Pt-ZnO/SiO_2. The surface area decreased from 480 to 460 and 450 m^2/g, while the efficiency of phenol degradation increased from 80 to 85 and 100%, with the ZnO/SiO_2, Img: Pt-ZnO-SiO_2, and PAD: Pt-ZnO-SiO_2 samples, respectively. The smallest particle size and lowest band gap of the PAD: Pt-ZnO-SiO_2 sample resulted in a high increase in the surface area and pore volume and consequently the best photoactivity for Phenol degradation.

Yogendra et al. [64] compared the photocatalytic decolorization efficiencies of two ZnO composites, ZnO composite-1 (synthesized using zinc chloride and hydrazine hydrate) and ZnO composite-II (synthesized by solution combustion method using zinc nitrate and hydrazine hydrate) using Coralene Red F3BS dye in aqueous solution with sunlight as the energy source. ZnO composite-II was more efficient by achieving 98% decolorization of the dye solution in 45 min at pH 12.9. The photodecolorization is dependent on the pH of the dye solution and catalyst dosage.

Sudha and Rajarajan [65] synthesized bare and PVP (poly vinyl pyrrolidone) capped ZnO nanoparticles through precipitation method and their photocatalytic activity was evaluated by monitoring the photo bleaching of the aqueous solutions of RhB dye under UV irradiation. The study showed that PVP capped ZnO nanoparticles have reduced photocatalytic activity compared to bare ZnO nanoparticles. An indirect outcome of the study is the observation that the reduced photocatalytic activity of PVP capped ZnO nanoparticles can enhance their performance as durable, safe and non-reactive UV blockers in cosmetics.

Karthikeyan et al. [66] compared the photocatalytic degradation efficiency of coupled ZnO/Ag/CuO nano photocatalyst prepared by thermal decomposition method annealed at three different temperatures 300, 400 and 500°C with separately synthesized ZnO, Ag, and CuO using Methylene Blue dye as the test molecule under UV illumination. They found that the coupled photocatalyst annealed at 400°C exhibited higher efficiency and that at 300°C showed the least efficiency among the prepared catalysts. The higher efficiency of the catalyst at 400°C was attributed to the reduced band gap (revealed by the UV-Vis diffused reflectance spectroscopy) and also to comparatively uniform distribution of spherically shaped smaller particles [revealed by the FESEM (Field Emission Scanning Electron Microscopy) micrographs]. The lower efficiency of the catalyst annealed at 300°C is explained as due to the presence of Cu metal phase, in the nanorod form. Larger spherically shaped particles and intense agglomeration in ZnO/Ag/CuO catalyst annealed at 500°C contributed to its reduced photocatalytic activity.

Shanthi and Kuzhalosai [67] investigated the photocatalytic degradation of the dye Acid Red 27 using nano ZnO under UV illumination. The degradation kinetics follows Langmuir-Hinshelwood model. The study reveals that the addition of oxidizing agents such as H_2O_2, $K_2S_2O_8$ and $KBrO_3$ increases the rate of degradation upto certain concentration. The enhancement in degradation by H_2O_2 is attributed to the increase in the hydroxyl radical generation, both by the decomposition of H_2O_2 as well as its reaction with superoxide anion. The enhancement obtained with $K_2S_2O_8$ was explained as due to the inhibition of electron-hole recombination by

the formation of sulphate radical anion ($SO_4^{-\bullet}$), which itself is a strong oxidant and also generates hydroxyl radicals by reacting with photo generated electrons. The enhancement with $KBrO_3$ at lower concentration was attributed to the reaction between conduction band electron and BrO_3^-, which prevents the electron-hole recombination. The decrease in degradation rate at higher $KBrO_3$ concentration is due to the adsorption effect of Br^- ion on ZnO with reduction in its catalytic activity.

Muneer et al. [68] investigated the solar photocatalytic degradation of 2, 4-dichlorophenol in aqueous solution with ZnO catalyst prepared by sol-gel method. Over 98% degradation was achieved within 1 hr with a catalyst loading of 2 g/L. The photocatalytic activity was sustained upto two cycles for the degradation of 2, 4-dichlorophenol.

Tang [69] prepared ZnO with different morphologies, rod-like (designated as ZnO (I)), rice-like (designated as ZnO (II)) and granular-like (designated as ZnO (III)) from different zinc sources as precursors and their photocatalytic activities were compared using Methyl Orange (MO) as the model molecule under UV irradiation. The effective surface areas of the granular-like ZnO and the rice-like ZnO nanostructures are larger than that of the rod-like ZnO. After 60 min UV irradiation, approximately 40% of the MO is degraded over the rod-like ZnO catalyst while the rice-like and granular-like ZnO catalysts showed 96% and 99% degradation respectively under the same conditions. The high photocatalytic activity of the granular-like ZnO and the rice-like ZnO nanostructures can be ascribed to their small size, which leads to an increase in both the band gap energy and its surface-to-volume (S/V)

ratio. Moreover, the granular-like and rice-like nanostructures favor the movement or transfer of electrons and holes generated inside the crystal to the surface which enhances the photocatalytic activity.

Tabatabaee and Mirrahimi [70] prepared Ag/ZnO heterostructure nanocatalyst and studied the photocatalytic degradation of the textile dye Reactive Blue 49 (RB49) using UV irradiation. Under optimized conditions, they obtained more than 90% degradation of the dye in presence of H_2O_2 within 30 min. The degradation rate increased with increasing H_2O_2 concentration upto 12 mmol/L, above which the degradation rate decreased. The enhancement is due to the formation of more hydroxyl radicals from H_2O_2 and the decrease in degradation rate is attributed to the scavenging of hydroxyl radicals by H_2O_2. The degradation was found to follow first order kinetics with a rate constant (k) of 0.57 min^{-1}.

Hong et al. [71] prepared ZnO nanoparticles by precipitation method and the surface was modified, by grafting polystyrene to improve the dispersion of the particles and to reduce their photocatalytic activity. The characterization of the bare and modified ZnO catalyst was done by FTIR, XRD, and TEM. The photocatalytic activity was compared using Methyl Orange under UV irradiation. The bare ZnO nanoparticles which are hydrophilic showed higher photocatalytic activity exhibiting 80% degradation after 4 hr while the hydrophobic polystyrene capped ZnO showed little photocatalytic activity. This can be explained by the fact that the long polymer chain on the ZnO surface prevents the adsorption of dye molecule and the contact with air. Moreover, the UV absorption of ZnO nanoparticles may be reduced due to surface modification. Even if

electron-hole pairs are formed in the interior of ZnO by UV illumination, they cannot reach the surface of the modified particles. The particles cannot adsorb enough Methyl Orange molecules which also lead to the retardation of photocatalytic degradation.

Elamin and Elsanousi [72] compared the photocatalytic activity of ZnO nanostructured materials (nanotubes and nanosheets) synthesized by hydrothermal method using the degradation of Methyl Orange (MO) as the test reaction. The study revealed that ZnO nanosheets are more effective than the nanotubes, probably due to their high surface area.

Kulkarni and Thakur [73] investigated the photocatalytic degradation of the reactive azo dye Navy blue HE2R 1 (NB) with nanoparticles of P-25 TiO_2, Merck ZnO and Merck TiO_2 under 8W low-pressure mercury vapor lamp irradiation. The study revealed that under optimum conditions, complete decolorization and substantial mineralization of the dye is achieved as proven by the decrease in chemical oxygen demand (COD) and total organic carbon (TOC) of the dye solution. The Merck ZnO was found to be the best in terms of percentage decolorization of the dye while P-25 TiO_2 was the best photocatalyst in terms of mineralization. The order of photocatalytic efficiency was:

P-25 TiO_2 > Merck ZnO > Merck TiO_2.

Abdollahi and Abdullah [74] carried out the photodegradation of m-cresol with ZnO catalyst under visible light irradiation and optimized various reaction parameters. The optimum concentration of m-cresol and ZnO were found to be 25 ppm and 1.5 g/L respectively. The optimum

pH range for the degradation was found to be 6-9. The intermediates detected were 2-methyl-1,4-benzodiol, 2-methyl-para-benzoquinone, 3,5-dihydroxytoluene and 2,5-dihydroxy benzaldehyde. The ZnO catalyst can be reused at least five times without any significant reduction in the efficiency.

Parida et al [75] prepared ZnO catalyst by different methods such as sol-gel method from $Zn(CH_3COO)_2$ and precipitation method from various precursors. The prepared catalysts were characterized by XRD, BET-surface area, surface acidity and crystallite size. ZnO prepared from $Zn(CH_3COO)_2$ by precipitation method possesses highest surface area and surface acidity. This catalyst also showed greater photocatalytic activity towards the degradation of 4-nitrophenol and reduction of Cr(VI) under solar irradiation in a batch reactor. This catalyst is subjected to microwave irradiation (upto 30 min) and subsequently calcined at different temperatures and tested for its activity for the same reaction. The ZnO catalyst irradiated for 15 min under microwave and calcined at 300^oC possesses highest surface area and acid sites and shows highest degradation and reduction efficiencies for 4-nitrophenol (92%) and Cr(VI) (98%) respectively. During microwave irradiation, heat energy is produced by the particle-particle vibration and it is transferred in the particles by dipole rotation and ionic conduction. During the application of high frequency voltage to a material, the molecules with permanent or induced diploe moment change their orientation in the direction opposite to that of the applied field. The generation of heat by the synchronized agitation of the molecules may be responsible for the improved activity of the ZnO catalyst.

Lee et al. [76] prepared zinc oxide (ZnO) nano-particles from different precursors such as zinc acetate, zinc nitrate, and zinc chloride by matrix assisted method, using activated carbon as the matrix. The morphology, particle size and surface area of the synthesized ZnO was found to vary with the precursor used. The activity of the catalyst was investigated for the removal of very low concentration of sulfur compounds (H_2S, COS) present in fuel gas. Zinc acetate was found to be the best precursor for the formation of the ZnO nano-particles in this study, where the size of the particle was in the range of 10-30 nm and surface area was about 40.7 m^2/g. The study revealed that the activity of the ZnO nanoparticles was higher when the particles were smaller and the surface areas larger.

Daneshvar et al. [77] studied the photocatalytic efficiency of ZnO nanoparticles prepared by precipitation method for the degradation of the insecticide diazinon under UV irradiation. The study of the degradation of the insecticide (20 ppm) in real water (Carbonate hardness: 88 mg/L $CaCO_3$, Sulphate concentration: 172.8 mg/L) showed that in presence of carbonate, bicarbonate and sulphate ions, the percentage degradation decreases. This is explained as due to the scavenging effect of the ions for hydroxyl radicals.

Swati and Meena [78] studied the photocatalytic decolorization of Direct Red 23, a reactive textile azo dye under UV irradiation using Methylene Blue immobilized resin dowex-11(MBIR-11) as photocatalyst. The decolorization efficiency increases with increase in dye concentration to a certain level. Further increase in the dye concentration leads to decrease

in the degradation rate. This can be explained by the fact that at high dye concentrations the generation of $^{\bullet}OH$ radicals on the surface of the catalyst is reduced since the active sites are covered by dye ions. The major portion of degradation occurs in the region near the irradiated side (termed as reaction zone) where the irradiation intensity is much higher than on the other side. Thus at higher dye concentrations, decolorization decreases at sufficiently long distance from the light source or the reaction zone due to the retardation in the penetration of light. The rate of degradation was found to be very low at high acidic pH range (lower than pH 3.5). When the pH increases, the rate of degradation also increases and high degradation was obtained in the pH range 7.5 to 9. The increase in rate of photocatalytic degradation at this pH may be due to the availability of more OH^- ions.

Sun et al. [79] prepared a new photocatalyst, CuPp–ZnO by impregnating copper (II) 5- mono-[4-(2-ethyl-p-hydroxybenzoate) ethoxyl]-10, 15, 20-triphenylporphyrin (CuPp) on the surface of ZnO and characterized the same by a series of instrumentation techniques. The catalytic activity of the CuPp-ZnO was tested both under UV and visible light ($\geq$ 420 nm) irradiation using Rhodamine B (RhB) as the test substrate. CuPp-ZnO has higher photodegradation efficiency than bare ZnO, due to the improved separation of photogenerated electrons and holes. The catalyst was found to be active even after five catalytic cycles and showed good stability for the photodegradation of RhB both under UV and visible light.

Banerjee et al. [80] prepared ZnO particles by the ultrasonication of aqueous-alcohol (5% methanol, ethanol and isopropanol each separately)

solution of zinc acetate in the absence of alkali. The characterization of the prepared catalysts by XRD, AFM, FESEM etc. showed that the size and other characteristics of the catalyst varied with the solvent used. The catalyst obtained with isopropanol as solvent showed more crystalline nature. The activity of the nano particles was tested for the photocatalytic reduction of hexavalent chromium in aqueous medium. The prepared ZnO catalyst showed double reduction efficiency compared to the commercial ZnO, even though the photocatalytic efficiency of catalyst prepared using different solvents was different. This difference is attributed to the difference in morphology of synthesized ZnO crystallites.

Giwa et al. [81] investigated the photocatalytic decolorization and degradation of two reactive dyes, Reactive Yellow 81 (RY81) and Reactive Violet 1 (RV1) in aqueous solution with TiO_2-P25 (Degussa) as photocatalyst in slurry form, using sunlight as the energy source. Comparison of the decolorization of the dye using TiO_2-P25, ZnO, and TiO_2 (anatase) showed that the most effective catalyst was TiO_2-P25, which showed 92% for Reactive Yellow 81 (50 mg/L) and 85% for Reactive Violet 1 (50 mg/L) in 20 min. The order of activity of the photocatalysts is TiO_2-P25 > ZnO > TiO_2 anatase. The high photo reactivity of TiO_2-P25 was explained as due to the slow recombination of electron-hole pairs as well as its large surface area.

Kansal and Chopra [82] studied the photocatalytic degradation of 2, 6-Dichlorophenol (2, 6-DCP) in aqueous solution by Titania (PC-105) photocatalyst under UV irradiation. Maximum degradation was obtained with a catalyst loading of 1.25 g/L. The optimum pH was found to be 4,

which was explained based on the PZC (Point of Zero Charge) of TiO_2 and the charge of chlorophenol. Low pH values facilitate the adsorption of chlorophenols promoting their photocatalytic degradation. The reaction was found to be of first order with a rate constant of $4.78 \times 10^{-4}\ s^{-1}$.

Mangalampalli et al. [83] synthesized improvised porous silica (E-Si) material support for TiO_2 using acrylic acid emulsion. The prepared catalyst was tested for the photocatalytic degradation efficiency of the herbicide isoproturon (N, N-dimethyl-N-[4-(1-methylethyl) phenyl] urea), with sunlight as the energy source. The adsorption study shows that E-Si acts only as a support and that the TiO_2 loading over E-Si support affects the photocatalytic activity for isoproturon degradation. Maximum degradation of the herbicide was obtained with 5 wt % TiO_2 over E-Si. Comparison of the degradation with that in presence of bare TiO_2 shows that TiO_2 supported system shows higher rate of degradation. This is explained as due to the synergistic effect resulting from adsorption of isoproturon over porous support material, facilitating the degradation without adversely affecting the photocatalytic properties of TiO_2. The better dispersion of photoactive TiO_2 leads to the presence of more number of active sites near the adsorbed isoproturon molecules resulting in faster degradation rates. The catalyst recycling study shows that both the adsorption and degradation activity are decreasing compared to the first cycle. This is attributed to the adsorption of the intermediates of the pesticide on the surface/cavities of the photocatalyst resulting in lower adsorption/degradation. This is reconfirmed by the fact that the catalyst after 3rd recycle regained its original adsorption as well as activity after calcination at 300°C.

Pozan and Kambur [84] prepared alkaline earth oxide (MgO, CaO, SrO) doped TiO_2 catalysts by impregnation method in order to study the effects of these alkaline earth basic oxides on the structural and surface properties of TiO_2 and the photocatalytic activities. The prepared catalyst was used for the degradation of 4-chlorophenol (4-CP) under UV irradiation. The highest percentage of 4-CP degradation (100%) and highest reaction rate (0.82 mg L^{-1} min^{-1}) in 1hr was shown in presence of 10 wt% MgO/TiO_2. Its catalytic activity was higher than that of nano TiO_2 and P-25 photocatalysts. The increased activity of alkaline earth oxide doped TiO_2 is explained based on the entry of Mg^{2+} into the lattice of nano TiO_2 and high dispersion. The alkaline earth metal oxide effectively decreases the band gap of TiO_2. The increased adsorption of 4-CP over the catalyst surface and decrease in particle size as a result of Mg^{2+} loading is responsible for the higher activity of the catalyst.

Qamar et al. [85] investigated the photocatalytic degradation of two dye derivatives Chromotrope 2B (1) and Amido Black 10B (2), in aqueous suspensions of titanium dioxide under UV illumination. Comparison of the degradation of the dyes with Titanium dioxide Degussa P25, Hombikat UV100 and PC500 showed that Degussa P25 is a better catalyst than the other two. Degussa P25 owes its high photo reactivity to slow recombination between electrons and holes whereas Sachtleben Hombikat UV100 has a high photo reactivity due to fast interfacial electron transfer rate. The degradation rate for both dyes increases with increase in pH with highest efficiency observed at pH=9. The study of the effect of electron acceptors such as hydrogen peroxide (H_2O_2), potassium bromate ($KBrO_3$) and ammonium persulphate $(NH_4)_2S_2O_8$ shows that all the additives showed

beneficial effect on the degradation. These additives enhance the hydroxyl radical formation as well as inhibit the electron-hole recombination.

Aarthi and Madras [86] compared the photocatalytic activities of commercial Degussa P-25 and TiO_2 synthesized by the combustion solution method (CS TiO_2) for the degradation of Rhodamine dyes with different functional groups such as Rhodamine B ($C_{28}H_{31}ClN_2O_3$), Rhodamine 6G ($C_{28}H_{31}ClN_2O_3$), Rhodamine Blue ($C_{28}H_{32}N_2O_3$), and Rhodamine 6G perchlorate ($C_{28}H_{31}ClN_2O_7$). The photocatalytic activity of CS TiO_2 was considerably higher than that of Degussa P-25 in degrading Rhodamine B and Rhodamine 6G. But in the case of Rhodamine Blue and Rhodamine 6G perchlorate, faster degradation was obtained with Degussa P25. The study of the effect of organic solvents (ethanol and acetonitrile) and metal ions ($Cu^{2+,}$ Fe^{3+}, Zn^{2+}, and Al^{3+}) on the photodegradation of Rhodamine B shows that the presence of solvents and metal ions significantly reduced the degradation rate.

The above short review of photocatalysis clearly demonstrates that this technique can be effectively used for the degradation/mineralization of a variety of water pollutants. Inspired by these reports, present study is an investigation on the application of photocatalysis for the tertiary treatment of effluent water from a phenol manufacturing industry. The chemical process followed and the water treatment techniques used in the industry are briefly discussed in Part-B.

Part -B

Process description of a typical phenol manufacturing industry

A typical phenol manufacturing unit consists of the following sections:

1. Propylene Recovery Unit (PRU)
2. Cumene production plant
3. Oxidation section
4. Cleavage section
5. Direct Neutralization and Effluent Treatment (DNET)section
6. Fractionation section

1.B.1 Propylene Recovery Unit

The process flow is schematically presented in figure 1.12.

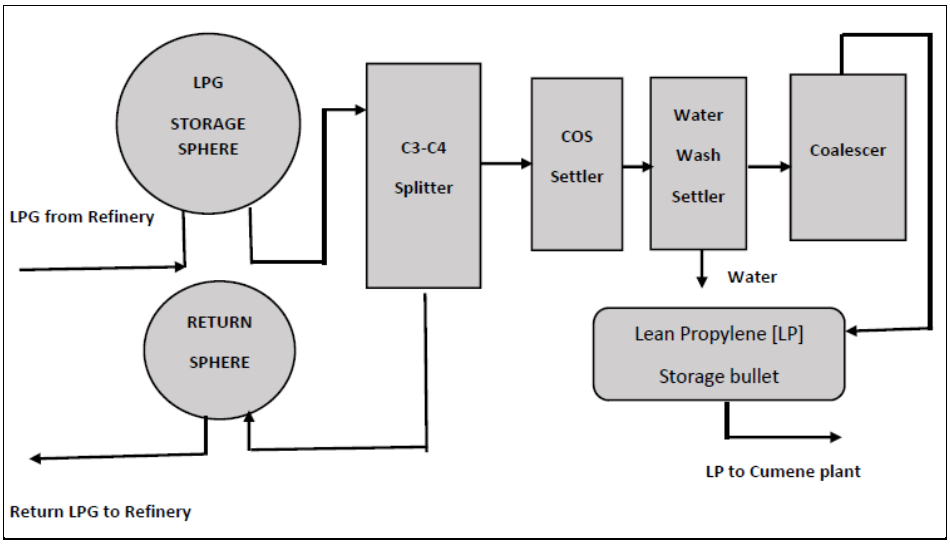

Fig. 1.12: Flow diagram of Propylene Recovery Unit (PRU)

This unit produces propylene of 75% purity which is used for the production of cumene. Propylene is recovered from cracked LPG which is a mixture of propene, propane, butanes and butenes. The process scheme

consists of a fractionating column (C_3-C_4 splitter), where the LPG feed is fractionally distilled using low pressure steam. The column overhead which contains 75% propylene and 25% propane (Lean Propylene) is passed through caustic/ Mono ethanol amine (MEA) /water wash system for the removal of carbonyl sulphide (COS) and hydrogen sulphide (H_2S). Any carry over caustic MEA solution in lean propylene is separated in water washing vessel where it is dispersed into a water column. The lean propylene then flows to a coalescer for removal of water and ultimately to storage bullets.

1.B.2 Cumene Production

Cumene synthesis is based on catalytic condensation process. The process flow diagram is given in figure 1.13. Lean propylene obtained from the PRU is treated with benzene over solid phosphoric acid (SPA) catalyst [$Si_3(PO_4)_4$] to get high purity isopropyl benzene commonly known as cumene (reaction 37). The overall process flow consists of combining benzene with propylene in presence of propane and trace amount of moisture. The propane is used as a heat sink for the exothermic alkylation reaction. The combined feed of propene, propane and benzene in the ratio 1:2:8 together with 150-200 ppm of water is heated and routed to the reactor which consists of four beds of SPA catalyst where the exothermic alkylation takes place. The reactor effluent containing cumene, unreacted benzene, propane and byproducts are then passed through a series of fractionating columns. The high boiling fractions are rejected in the cumene column bottom. The unreacted propane and benzene are recycled. Pure cumene (>99.85%) is obtained at the top of the cumene column and is stored in cumene storage tanks.

(37)

Benzene Propylene Cumene

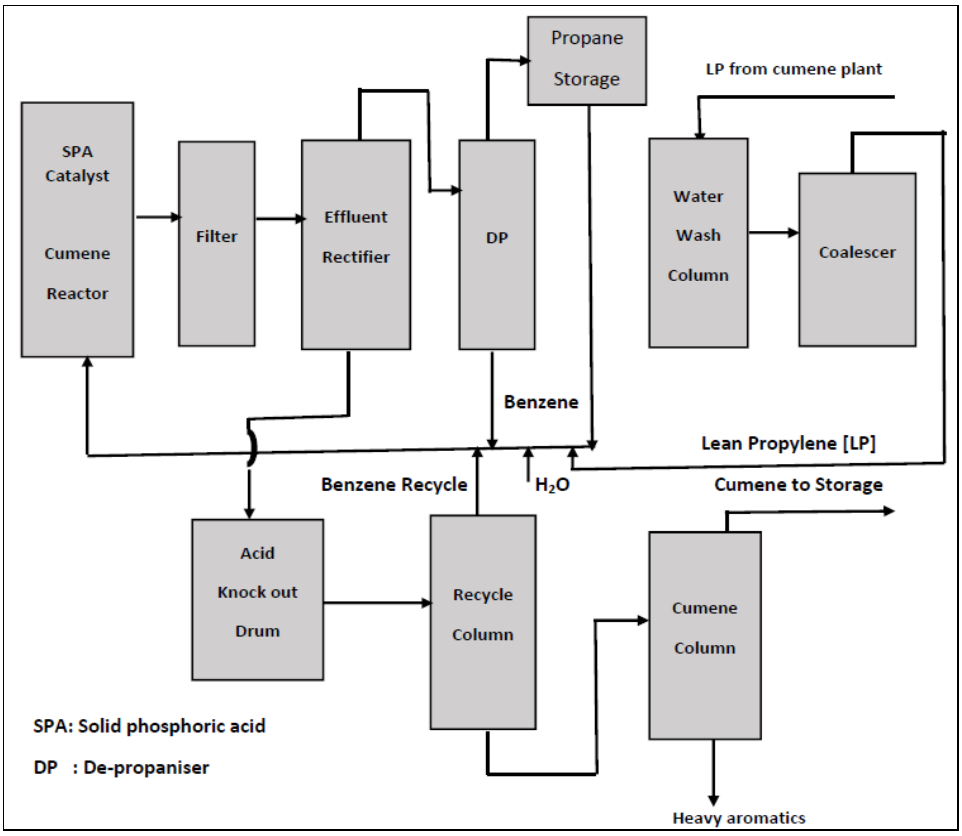

Fig. 1.13: Flow diagram of Cumene plant

1.B.3 Oxidation/Evaporation

In this section cumene is oxidized to cumenehydroperoxide (CHP). The process flow diagram is given in figure1.14. Cumene and oxygen are made to react at pH 8 to 10 at a temperature around 90°C in presence of CHP itself as an initiator. Since the oxidation is highly exothermic, there

is every possibility that the reaction may turn violent and result in explosion. Hence the oxidation is usually carried out in two steps with intermittent cooling of the product. In the first step, cumene is oxidized to get 15% CHP. It is then cooled and routed to the second oxidizer where the CHP concentration is increased to 25%. Small quantities of Dimethyl phenylcarbenol (DMPC) and Acetophenone (ACP) are also formed as byproducts (reaction 38).

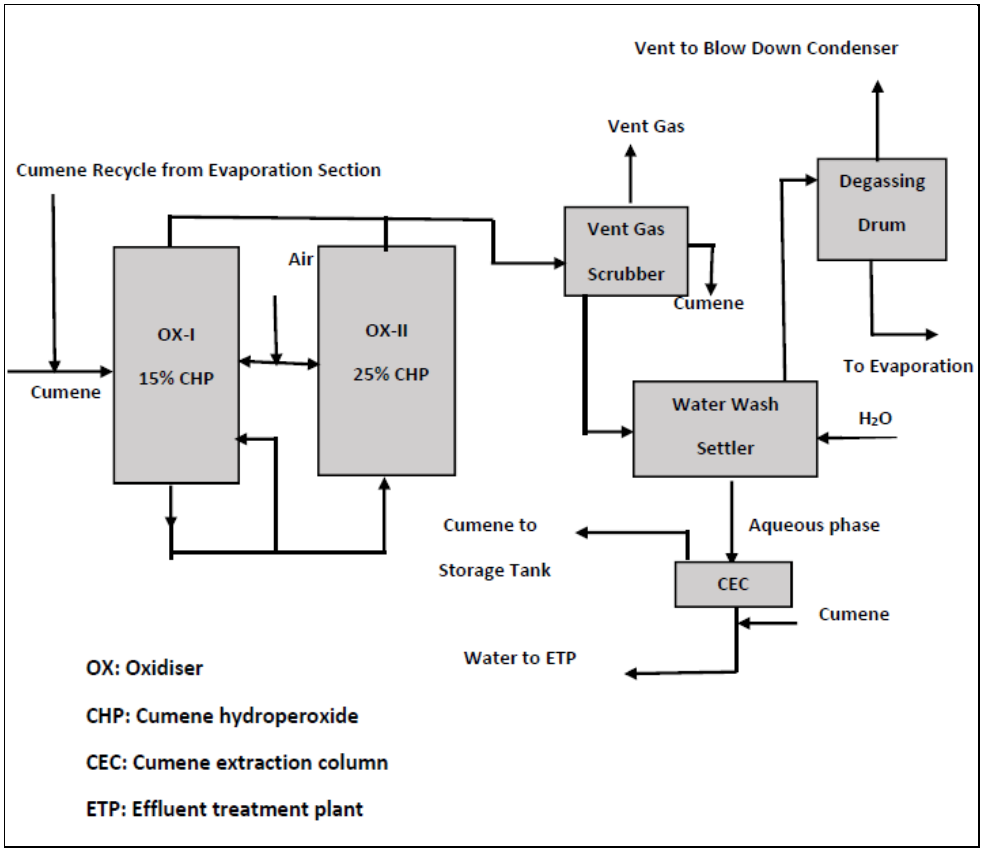

Fig. 1.14: Flow diagram of Oxidation section

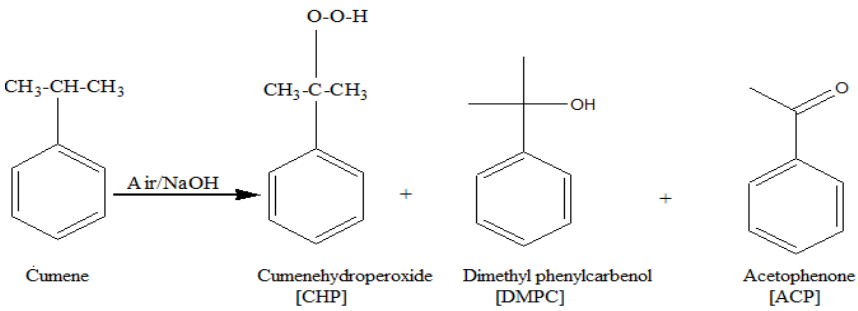

(38)

CHP is further concentrated to 80% by evaporating cumene in two steps. In the first step, CHP is concentrated approximately to 40% in the evaporator pre-flash drum and in the next step, the product from pre-flash drum flows through a parallel set of thin film evaporators where 80% CHP is produced (figure 1.15).

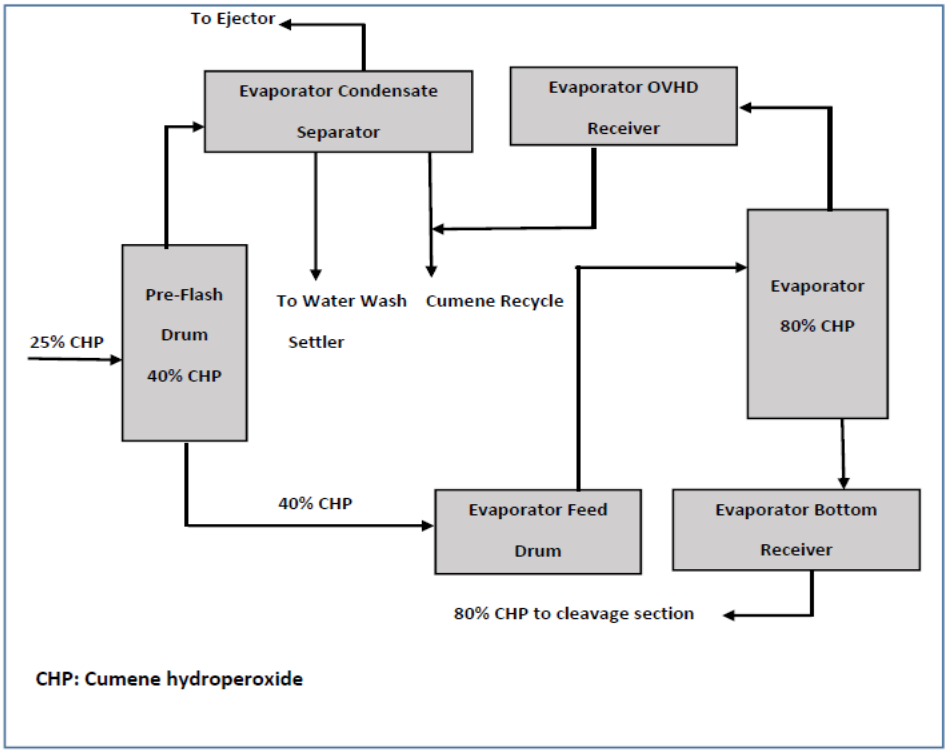

Fig. 1.15: Simplified flow diagram of Evaporation section

1.B.4 Cleavage

Concentrated CHP [80%] obtained from the oxidation section is subjected to cleavage using H_2SO_4 (98.5 wt. %). A mixture of phenol and acetone is kept under circulation in a cleavage loop which acts as the heat sink for the exothermic cleavage reaction. Concentrated CHP is fed into this mixture and heated to 56°C. Concentrated H_2SO_4 is injected into the loop with the help of a needle pump. CHP gets cleaved to give phenol and acetone (reaction 39). The DPMC formed in the oxidation section is dehydrated to form Alpha methyl styrene (AMS) as shown in reaction 40. Usually an excess of H_2SO_4 (less than 0.10 wt. %) is maintained in the reaction mixture to ensure the complete cleavage of CHP. A simplified diagram of the cleavage section is shown in figure 1.16.

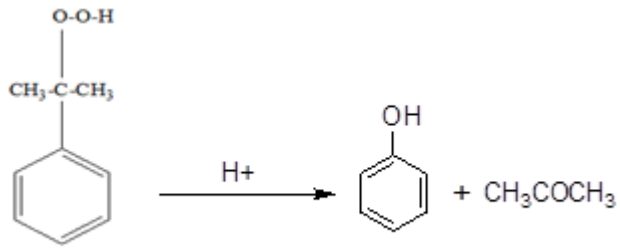

(39)

CHP Phenol Acetone

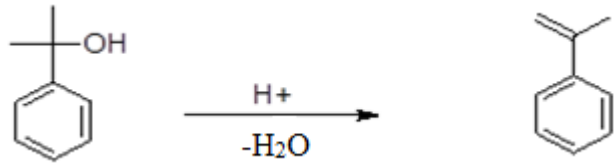

(40)

DMPC Alpha methyl styrene

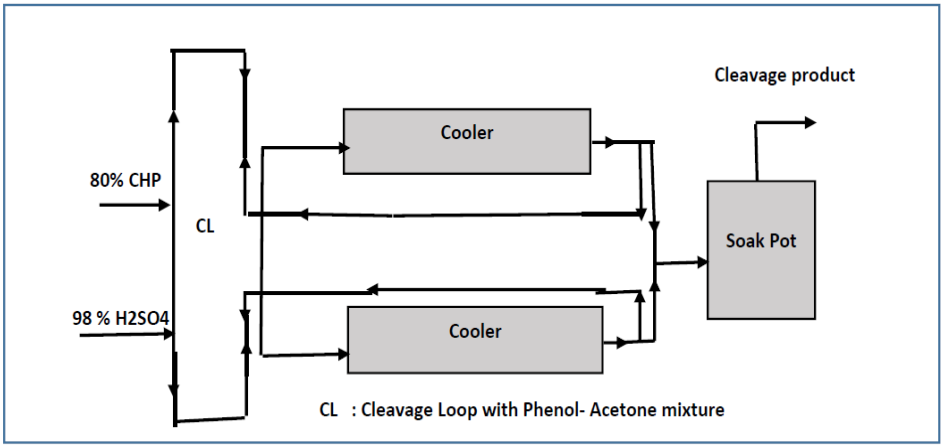

Fig. 1.16: Flow diagram of Cleavage section

1.B.5 Direct Neutralization and Effluent Treatment [DNET]

In this section (see figure 1.17) the excess acid present in the cleavage product is neutralized. If NaOH is used for neutralization, Na_2SO_4 and H_2O are obtained. If sodium phenate is used for neutralization, phenol and Na_2SO_4 are obtained. The Na_2SO_4 formed is removed by water washing and the trace amount of phenol present in the aqueous phase is removed by extraction with cumene in the oil extraction column (OEC) and then sent to Effluent Treatment Plant (ETP) for further treatment. The organic phase after water washing, known as DNET product containing mainly phenol and acetone along with some tarry material, ACP, DMPC, AMS, cumene, water etc., is sent to the fractionation section.

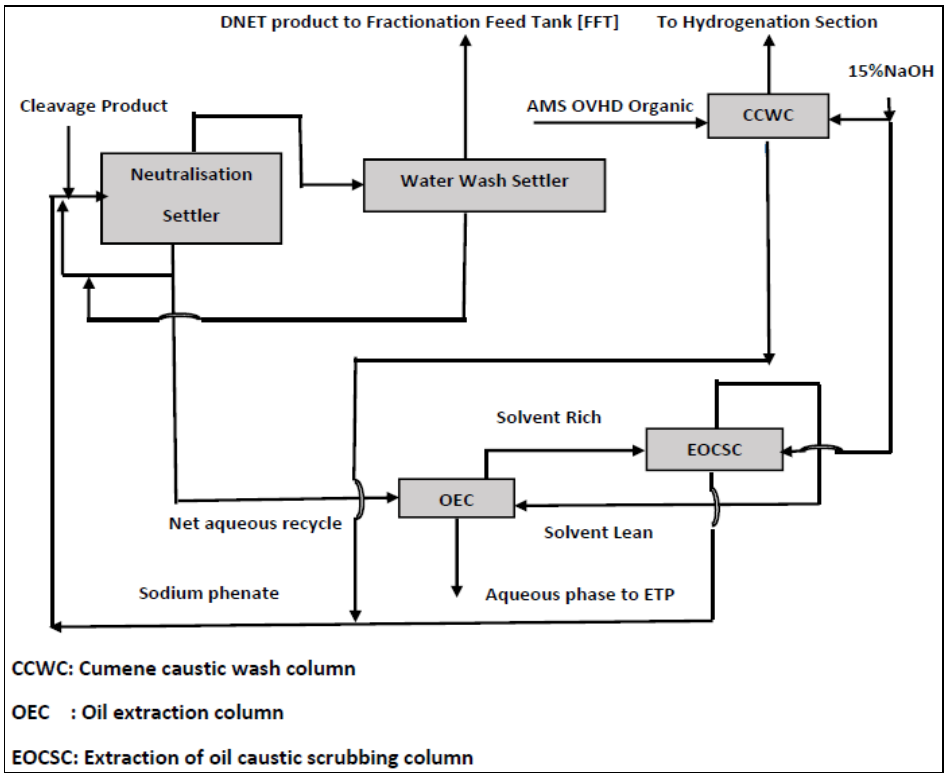

Fig. 1.17: Flow diagram of DNET section

1.B.6 Fractionation section

This section separates phenol and acetone from other byproducts by using a series of fractionating columns (figure 1.18). In the first stage, the DNET product (Fractionation feed) is fractionally distilled in the Crude Acetone Column (CAC) to separate acetone and water. The acetone is further purified in the Finished Acetone Column (FAC). The rest of the material containing phenol and other impurities after the removal of water and acetone (CAC bottom) is sent to the Tar Column (TC) to remove tarry materials. The crude phenol from the TC overhead is sent to AMS Column (AMSC) to remove AMS and cumene and the TC bottom material is sent to the tar cracking section.

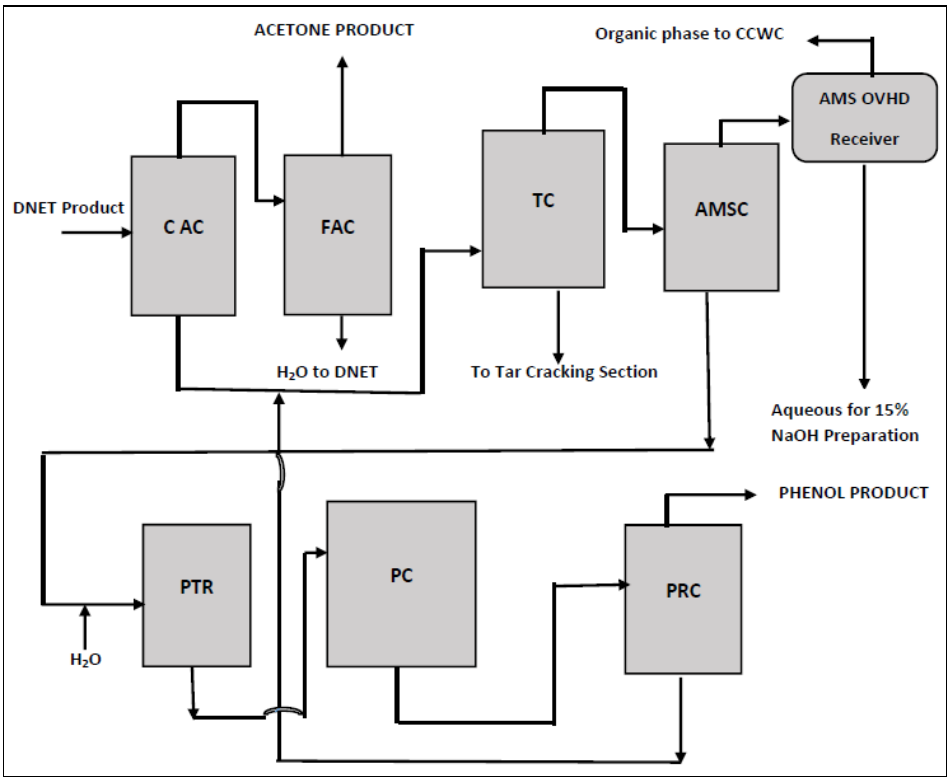

Fig. 1.18: Simplified flow diagram of Fractionation section

The organic stream from AMS overhead after phenol removal is sent to the hydrogenation section, where it is hydrogenated to cumene by hydrogen in presence of pre-reduced sulphided palladium catalyst with alumina as support material (reaction 41). The cumene thus obtained is recycled to the oxidation section.

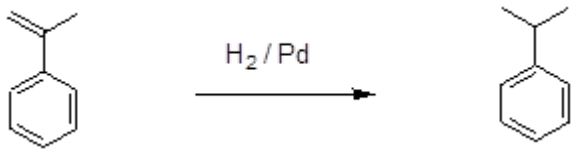

AMS Cumene (41)

The bottom material from the AMS column is sent to the Phenol Treating Reactor (PTR). The main function of the PTR is to convert some of the impurities in the crude phenol, which will otherwise contaminate the final product into compounds which are removable by distillation. Thus Mesityl oxide (MEO) is converted to acetone (reaction 42), and hydroxyacetone is converted to 2-methylbenzofuran (2-MBF) in presence of PTR catalyst (90% silica and 10% alumina) (reaction 43).

$$(CH_3)_2C{=}CH\text{-}CO\text{-}CH_3 + H_2O \xrightarrow{\text{Catalyst}} 2\ CH_3COCH_3 \qquad (42)$$

Mesityl oxide [MEO] Acetone

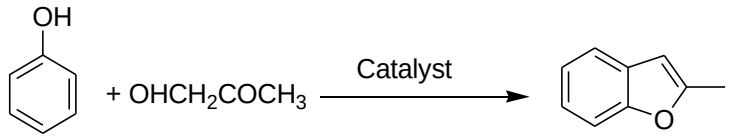

(43)

Phenol Hydroxy acetone 2-MBF

The effluent from PTR is sent to Phenol Column (PC), where the lighter materials are removed. The bottom material from the PC goes to Phenol Rectification Column (PRC), where pure phenol is distilled out as overhead product and the PRC bottom material is sent to the Tar Column (TC). The products, acetone from FAC and phenol from PRC are collected and stored in respective storage tanks.

1.B.7 Effluent Treatment Plant

The phenol production process as explained above, generates different types of pollutants which can cause water, air and soil pollution. The air pollution is minimized by adopting appropriate technologies such

as scrubbing the organic vapours with chilled water before releasing the air into the atmosphere. Continuous monitoring of the stack emissions ensures that the discharge conforms to relevant specifications. The discharge from pressure vessels are connected to the flare system to prevent the accidental release of organic vapour into the atmosphere in the event of popping of safety valves. The possible source of soil pollution is from the solid catalyst such as SPA, Hydrogenation catalyst, PTR catalyst and the possible leakage of liquid effluent from the plant area. The spent catalyst is either recycled or sent for safe disposal to authorized agencies. All the vessels in this unit are provided with closed drains which are routed to the Effluent Treatment Plant. The floor washings are also directed to the ETP, thereby ensuring that all the contaminants are treated properly within the battery limit of this unit before discharged to the environment. Hence soil pollution is not a major problem in the phenol manufacturing unit. However, contamination of water by different organic compounds is a major pollution hazard. The unit is using large quantities of water for various activities and the water can get contaminated with various organic and inorganic pollutants. Moreover, there may be draining of various vessels, pumps, heat exchangers etc., during shutdown and startup operations. The floor washings and rain water coming out of the unit may also get contaminated with various pollutants. Therefore it is necessary to remove these pollutants from the effluent water before it is discharged into the water bodies.

1.B.7.1 Present treatment methods

The treatment methods being used in the industry can be broadly classified into:

1. Physical Treatment
2. Chemical and Physicochemical Treatment
3. Sedimentation

} Primary treatment

4. Biological Treatment or secondary treatment

Typical flow diagram of the Effluent Treatment Plant (ETP) is shown in figure 1.19.

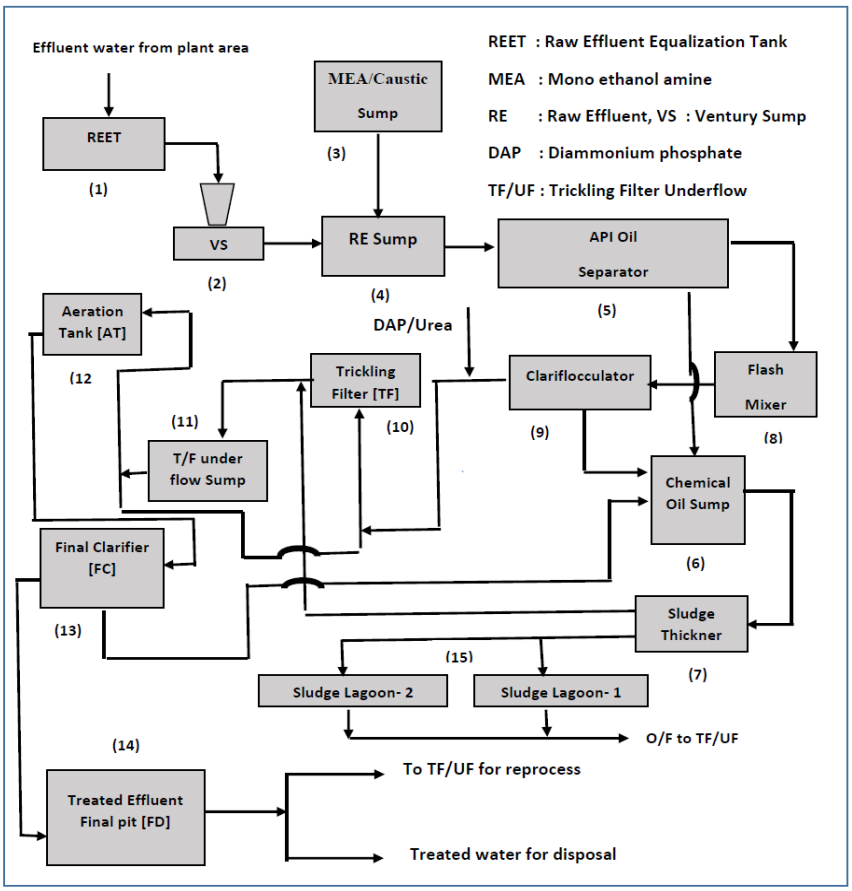

Fig. 1.19: Simplified flow diagram of the Effluent Treatment Plant for the phenol manufacturing unit

1.B.7.2 *Physical Treatment*

The effluent water generated from a phenol plant may contain suspended solids (oil and grease, settleable solids), colloidal solids (emulsified oil and fine solids), organic compounds such as phenol, cumene, AMS, DMPC, ACP, 2-MBF etc. The purpose of the physical treatment is to remove free oils in the effluent. The free or floated oil on the surface is skimmed with the help of wooden skimming arms and the removed oil is collected in the chemical oil sump. The settled sludge at the bottom of the oil separator is desludged frequently and is collected in the sludge sump. After the oil removal, the effluent is sent for chemical treatment (1-7 in figure 1.19).

1.B.7.3 *Chemical treatment*

Contaminants such as acids, alkalies, sulphides, colloidal solids, oil-water emulsions etc can be economically removed by chemical treatment. After oil removal the effluent is mixed with chlorinated copperas [$FeSO_4.7H_2O$] and NaOH in a flash mixer (8 in figure 1.19), where the components are thoroughly mixed with an agitator, for the removal of sulphides and any emulsified oil which may be present in the effluent. The effluent from the flash mixer is sent to the clariflocculator. The sulphides are precipitated in the clariflocculator. The floc formed due to $Fe(OH)_3$ helps in the flocculation and coagulation of emulsified oil and colloidal particles. The basic chemical reactions involved are:

$$6FeSO_4.7H_2O + 3Cl_2 \rightarrow 2\ Fe_2(SO_4)_3 + 2\ FeCl_3 + 42\ H_2O \qquad (44)$$

$$Fe_2(SO_4)_3 + 3Na_2S \rightarrow 2FeS + S + 3Na_2SO_4 \qquad (45)$$

$$FeCl_3 + 3NaOH \rightarrow Fe(OH)_3 + 3NaCl \qquad (46)$$

The overall reaction can be written as

$$6\ FeSO_4.7H_2O + 3Cl_2 + 3Na_2S + 3NaOH \rightarrow 2FeS + Fe(OH)_3 + 3Na_2SO_4 + 42\ H_2O + 3NaCl \quad (47)$$

1.B.7.4 *Sedimentation*

The purpose of the sedimentation is to ensure that the suspended solid concentration in the effluent is within the specified limit before discharge. The clariflocculator provides enough residence time for the coagulated particles to settle down at the bottom. The settled sludge is collected in the sludge pit from where it is sent to the sludge sump. The clarified effluent free from sulphide and emulsified oil is sent for biological treatment. (10-12 in figure 1.18).

1.B.7.5 *Biological Treatment [Secondary treatment]*

Soluble organics in the effluent water, which cannot be removed by normal physical or physicochemical method are removed by biological treatment. The method involves the use of microorganisms such as bacteria and protozoa which consume the organic pollutants as food. They metabolize the biodegradable organics, converting them to carbon dioxide, water, and energy for their growth and reproduction. This natural aerobic process requires oxygen.

The aerobic biological oxidation can be generally represented as

$$\text{Organic matter} + \text{Bacteria} + O_2 \rightarrow \text{New bacteria} + H_2O + CO_2 + N_2 + NH_3 \quad (48)$$

The conventional methods of water treatment as above may be sufficient to decontaminate the water in order to meet the statutory requirements. However, there are many limitations as follows:

1.B.7.6 *Limitations of the present methods*

1) The method is very expensive in terms of energy consumption, cost of operation and maintenance
2) The biological process is subjected to shock loads of toxic and organic materials and requires strict control over the operating parameters for better efficiency
3) The biological treatment methods generate excessive sludge, which often cause sludge bulking and sludge removal problems. Under certain conditions in an activated sludge treatment plant, filamentous or stringy bacteria grows prolifically in the aeration tank, making the sludge very fluffy and light. This problem called 'Sludge bulking" leads to slow settling. Hence a clear supernatant is not formed in the clarifier and much of the sludge flows out with the effluent
4) Another problem is that even after this treatment, small quantities of the pollutant may still remain in water, which will get accumulated over time. Being highly toxic, these chemical pollutants will be harmful to the ecosystem and all types of living organisms in a variety of ways. Hence the removal of such micro quantities of pollutants is essential for the long-term safety of the environment. A tertiary treatment is necessary for further polishing of the water so that it can be reused/disposed off to water bodies without any adverse effect on the environment. But most of the conventional tertiary treatment systems such as microfiltration, ultrafiltration, chemical oxidation, reverse

osmosis, activated carbon adsorption, sand filters etc., are found to be ineffective/expensive for the tertiary treatment of effluent water from this industry. It is in this context that AOPs such as photocatalysis, sonocatalysis, Fenton process, microwave catalysis, wet-air oxidation etc., and their combinations become important.

The present study is an attempt to develop a suitable photocatalytic process for the removal of last traces of the major chemical pollutants present in the effluent water. Typical pollutants chosen for the study are Alpha methyl styrene (AMS), Acetophenone (ACP), Dimethyl phenyl carbenol (DMPC) and 2-Methyl benzofuran (2-MBF). Sunlight is used as the source of activation, with the objective of minimizing the cost of operation and developing a convenient model of solar energy harvesting. Basic principles involved in photocatalysis as well as brief review of relevant literature in the field was provided in Part-A of this chapter.

.....ꕥ.....

Chapter 2

OBJECTIVES OF THE STUDY, MATERIALS USED AND PLAN OF THE THESIS

Contents

2.1 Objectives

As discussed in Chapter 1, the industrial waste water even after the conventional secondary treatment methods, is still found to contain trace quantities of hazardous pollutants. Further polishing of this water is very expensive as well as energy intensive. Advanced Oxidation Processes (AOPs) are nowadays widely discussed as alternative methods for the complete mineralization of such trace pollutants. AOPs such as semiconductor mediated photocatalysis have been gaining much attention in this regard. However, most of photocatalytic studies use TiO_2 as the photocatalyst under UV irradiation. They may not be economical for the large scale industrial waste water treatment owing to the high energy requirement. Even though ZnO is an effective alternative to TiO_2 in many respects, its potential as a photocatalyst is not fully exploited. ZnO is expected to be a better solar catalyst as it can absorb wider wavelengths of solar spectrum. India, being a tropical country, receives large quantities

of sunlight and hence solar based process for waste water treatment will be viable technologically and economically.

The main objective of the present study is to examine the possibility of using ZnO mediated photocatalysis for the removal of trace quantities of organic pollutants from the effluent water after secondary treatment from a petrochemical industry. Since industrial effluent will contain multiple pollutants, the influence of the components on the degradation of each other is important. The use of sunlight as the energy source can reduce the operating cost of this tertiary treatment method compared to the conventional methods such as ultrafiltration, adsorption etc.

The applicability of commercial ZnO as solar photocatalyst for the removal of four typical organic pollutants from the petrochemical industry, namely, Alpha methyl styrene (AMS), Acetophenone (ACP), 2-methyl benzofuran (2-MBF), Dimethyl phenyl carbenol (DMPC) and their combinations is examined in this study.

The specific aims of the study under this broad objective are as follows:

1) Characterization of the ZnO to be used as the catalyst
2) Identification of major reaction parameters for efficient photocatalytic degradation of the pollutants
3) Optimization of the catalyst dosage for the efficient mineralization of each of the pollutants
4) Optimization of other reaction parameters such as pH, pollutant concentration, reaction time etc., for the mineralization/ degradation of each of the pollutants

5) To understand the kinetics of the photocatalytic degradation of the four pollutants and propose suitable mechanism

6) To study the effect of natural and added contaminants such as humic acid and dissolved salts on the degradation efficiency of each of these pollutants

7) To evaluate the effect of common oxidizing agents such as, H_2O_2, KIO_3 and $K_2S_2O_8$ on the photocatalytic degradation of individual pollutants and identify the most efficient oxidant

8) To identify the photocatalytic reaction intermediates formed from each of the pollutants

9) To study the effect of each pollutant on the degradation efficiency of others in their combined presence in water

10) To verify the applicability of the optimized process parameters for the complete mineralization of the pollutants in a real industrial effluent water matrix

2.2 Materials

The photocatalyst used in the study is commercial ZnO from Merck India Ltd.

2.2.1 Zinc Oxide (ZnO)

ZnO is present as the mineral zincite in the earth's crust. ZnO has three types of crystal structures namely wurtzite, zinc blende and rock salt. Among these, wurtzite is the most thermodynamically stable phase at

room temperature. The wurtzite structure is composed of hexagonal unit cell as shown in figure 2.1.

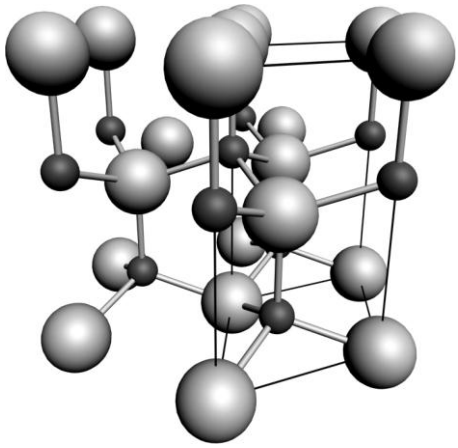

Fig. 2.1: Wurtzite structure of ZnO

The large spheres represent 'O' atoms and small black spheres represent the Zn atoms. The hexagonal lattice of ZnO is characterized by two interconnecting Zn^{2+} and O^{2-} sub lattices in such a manner that each Zn ion is surrounded by a tetrahedra of O ions, and vice-versa. The polar symmetry along the hexagonal axis is due to the tetrahedral coordination and is responsible for many properties of ZnO such as piezoelectricity and spontaneous polarization. The Zn-O bond possesses very strong ionic character even though the tetrahedral coordination of ZnO indicates sp^3 covalent bonding.

The cubic zinc blende and rock salt (NaCl) structures of a single unit cell of ZnO are shown in figure 2.2. The zinc blende ZnO is stable only by growth on cubic structures [87-89] while the rock salt structure is a high pressure metastable phase, which is formed at ~10 GPa [90].

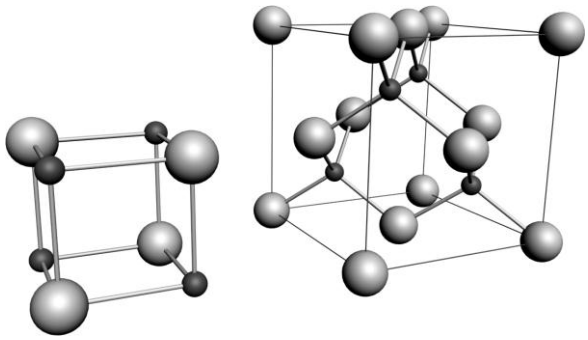

Fig. 2.2: The cubic zinc blende and rock salt (NaCl) structures of a single unit cell of ZnO

ZnO is considered as one of the 'future materials' by the scientific community because of its wide range of applications in many fields.

Uses:

More than 45% of the world production of ZnO is used in the rubber industry to control the vulcanization process and as additive [91]. Other uses are:

1) In the methanol synthetic process, ZnO is part of the Cu-ZnO-Al_2O_3 catalyst.
2) In the pharmaceutical industry, ZnO is applied in ointments because of its antiseptic properties [92].
3) The optical properties make ZnO suitable for many applications, such as pigment in paints, as UV filter in products for sun protection and for the production of LEDs and Thin Film Transistors (TFTs) [93].
4) Because ZnO can absorb the UV part of solar light, it has been widely used as an excellent UV absorber in outdoor textile and cosmetic products [94,95].

5) Ultrafine ZnO particles show a high degree of transparency due to their negligible light scattering power [96, 97] making ZnO useful in sunscreen, paints, varnishes and plastics applications.

ZnO is a wide gap semiconductor with a band gap of E_g= 3.4 eV at low temperature and 3.37 eV at room temperature with large free-exciton binding energy (60 meV at room temperature). Hence, excitonic emission processes can persist at or even above room temperature. ZnO can be considered as a suitable alternative to TiO_2 as solar photocatalyst because it can absorb relatively larger fraction of solar spectrum. Moreover, ZnO has similar band gap and follows the same mechanism of photocatalysis as in the case of TiO_2. Some of the properties of ZnO are listed in table 2.1.

Table 2.1: Properties of Zinc oxide

Property	**Value**
Crystal Structure	Wurtzite
Molecular mass	81.34g/mol
Melting point	1975 ^oC
Boiling point	2360 ^oC
Density	5.606 g/cm^3
Solubility in water	0.16mg/100 mL(20^oC)
Energy gap	3.4 eV, direct
Exciton binding energy	60meV
Photoluminescence	375 nm
High electron mobility	>100cm^2/(V.s)
Hole effective mass	0.59
Static dielectric constant	8.656

Crystalline ZnO changes its colour from white to yellow on heating and the original colour is regained on cooling in air (thermochromic). This colour change is due to the formation of non-stoichiometric, $Zn_{(1+x)}O$, where, x = 0.00007 at 800°C, caused by the small loss of

oxygen atoms at high temperature. ZnO is amphoteric and is insoluble in water but soluble in acid. Zinc oxide undergoes photocorrosion both under acidic and alkaline conditions, as shown in the following equations.

$$ZnO + 2\ HCl \rightarrow ZnCl_2 + H_2O \quad (49)$$

$$ZnO + 2\ NaOH + H_2O \rightarrow Na_2\,[Zn\,(OH)_4] \quad (50)$$

2.2.2 Alpha methyl styrene [AMS]

The AMS used in the study is from Merck India Ltd., and of purity 99.90%. Alpha Methylstyrene (AMS) is mainly obtained as a byproduct in the phenol production process. It is an intermediate used in the manufacturing of plasticizers, resins, and in many polymer production processes. It is a colourless liquid with strong aromatic odour.

The characteristics of AMS are listed in table 2.2.

Table 2.2: Characteristics of AMS

Chemical Name	Alpha Methylstyrene
Synonyms:	Alpha-Methyl styrene; Isopropenyl benzene; Benzene, (1-Methylethenyl); 1- Methyl-1-phenyl ethylene; 2-Phenylpropene; and AMS
Molecular structure	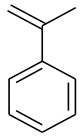
Molecular formula	C_9H_{10}
Molecular weight	118.18
Freezing point	-24°C
Boiling point	165 to 169°C
Specific gravity	0.909 (Water = 1)
Vapor density	4.1 (Air = 1)
Vapor pressure	2.1 (5.2) mm Hg @ 20°C (37.7°C)
Solubility	Insoluble in cold water
Refractive Index at 20°C	1.5386
Dielectric Constant 25°C	21.45

Uses:

- AMS is used to improve the impact and heat resistant properties of certain polymers, including speciality grades of plastic, rubber, and adhesives
- Production of para-cumylphenol, a speciality intermediate for thermoplastics and polycarbonate resins

Health effects:

- Short term exposure to AMS may cause irritation to eye, nose and respiratory system. Inhalation of high concentration of AMS vapour can cause depression of Central Nervous System (CNS), headache, dizziness, drowsiness and unconsciousness
- Prolonged skin contact with the liquid can cause defatting of the skin
- It is moderately toxic to aquatic organisms such as fishes, invertebrates and algae. It is not readily biodegradable and is reported to have moderate bioaccumulation potential. AMS is harmful to aquatic life even at a very low concentration.

2.2.3 Acetophenone [ACP]

The ACP used in the study is from Merck India Ltd, and its purity is 98%. Acetophenone is a colourless to yellow-tinted liquid with a sweet strong odour. Acetophenone comes mainly as a byproduct of the phenol-acetone synthesis in the cumene oxidation process to cumene hydroperoxide. Different methods of manufacturing Acetophenone are:

- Oxidation of cumene
- Oxidation of ethyl benzene
- Reaction of benzene and acetyl chloride in presence of aluminum chloride
- Catalytic reaction of acetic and benzoic acids
- Reaction of benzene and acetic anhydride
- By-product in the Hock phenol synthesis

Uses

- In perfumery to impart an orange-blossom-like odor
- Catalyst for the polymerization of olefins
- In organic syntheses, as photosensitizer
- Speciality solvent for plastics and resins
- Chemical intermediate for ethyl-methyl phenylglycidate (odorant), 2-chloro acetophenone and 2-bromo acetophenone (riot control agent), 3-nitro acetophenone (for pharmaceuticals and dyes) etc.
- Flavoring agent in non-alcoholic beverages, ice cream, candy, baked goods, gelatins and puddings, chewing gum, tobacco etc.
- Fragrance ingredient in soaps, detergents, creams, lotions, perfumes etc.
- Solvent for synthesis of pharmaceuticals, rubber, chemicals, dyestuffs and corrosion inhibitors

Health effects:

Eye: May cause transient corneal injury. Causes severe eye irritation and possible injury

Skin: May cause skin irritation.

Ingestion: May cause gastrointestinal irritation with nausea, vomiting and diarrhea, central nervous system depression, characterized by excitement followed by headache, dizziness, drowsiness, and nausea. Advanced stages may cause collapse, unconsciousness, coma and possible death due to respiratory failure. May be harmful if swallowed.

Inhalation: Inhalation of high concentrations may cause central nervous system effects characterized by nausea, headache, dizziness, unconsciousness.

The characteristics of ACP are listed in table 2.3.

Table 2.3: Characteristics of ACP

Chemical Name:	**Acetophenone**
Synonyms:	Methyl phenyl ketone; Phenyl methyl ketone; Acetyl Benzene
Molecular structure	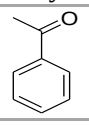
Molecular formula	C_8H_8O
Molecular weight	120.16 g/mole
Melting point	19.7^{o}C
Boiling point	201.7^{o}C
Specific gravity	1.0296 @ 20°C
Density	1.028 g/cm^3
Vapor pressure	0.33 mm Hg @ 20°C
Solubility in water	5.5 g/L @ 25°C
Viscosity	1.62 cP @25°C

2.2.4 Dimethyl phenyl carbenol [DMPC]

The DMPC used in the study is from Aldrich India Ltd, and the purity was 99.7%. DMPC is a low melting solid. It is obtained as a byproduct during phenol-acetone manufacture by cumene oxidation process. The production as well as use of DMPC as a floatation frother results in its release into the environment. It has been identified in drinking water as well as in ground, surface and waste water. It is a fragrance ingredient used in many products such as decorative cosmetics, shampoos, toilet soaps, household cleaners and detergents [98]. The characteristics of DMPC are listed in table 2.4.

Table 2.4: Characteristics of DMPC

Chemical Name:	**Dimethyl phenyl carbenol**
Synonyms:	2-Phenyl-2-propanol, alpha-Cumyl Alcohol, 2-Phenylisopropanol; α, α-Dimethyl benzyl alcohol
Molecular structure	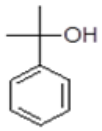
Molecular formula	$C_9H_{12}O$
Molecular weight	136.19 g/mol
Melting point	32 to 34°C
Boiling point	202 to 215°C
Specific gravity	0.9735 (Water = 1)
Refractive index	1.5325
Vapor pressure	0.0468 mm Hg @ 25°C
Solubility in water	6113mg/L @25°C

Uses

- Intermediate for the production of Alpha Methylstyrene (AMS)
- Used as a fragrance ingredient in many compounds such as shampoos, toilet soaps, house hold cleaners and detergents

Health effects:

- DMPC is severely irritating to the lungs, mucous membranes, and respiratory tract
- Over exposure may lead to headache, dizziness, nausea and vomiting

2.2.5 2-Methyl benzofuran [2-MBF]

The 2-MBF used in the study is from Aldrich India Ltd, and of purity 97.0%. It is a colourless liquid and is obtained as a byproduct during the phenol-acetone manufacturing by cumene oxidation process.

The characteristics of 2-MBF are listed in table.2.5

Table 2.5: Characteristics of 2-MBF

Chemical Name:	**2-Methylbenzofuran**
Synonyms:	2-MBF, 2-methyl-1-benzofuran, 2-methyl cumarone, 2-methyl benzo[b]furan, methyl benzoxole
Molecular structure	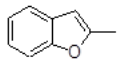
Molecular formula	C_9H_8O
Molecular weight	132.16g/mole
Boiling point	197.3-197.8°C
Vapor pressure	0.6 ± 0.4 mmHg @ 25°C
Solubility in water	Insoluble
Density	1.1 ± 0.1 g/cm^3
Refractive index	1.587

Uses:

- Used as VPC (Vapour Phase Calibration) and UV standard in the analysis of commercial phenol streams
- Used as a flavoring agent

Health effects:

It can degrease the skin and can cause non-allergic skin reactions. There has been greater concern that this compound can cause cancer or mutation.

2.2.6 Humic acid [HA]

The HA used in the study is from Himedia and the purity was 90%.

Humic substances, which are the major organic constituents of soils and sediments are widely distributed over the earth's surface and are present in all aquatic and terrestrial environments [99]. It is the characteristic component of the dissolved organic carbon (DOC) pool in freshwater and marine system [100]. Humic substances are formed by the microbial degradation of dead plant matter such as lignin and charcoal. These are heterogeneous biomolecules with varying but definite molecular weight and are biologically recalcitrant. Humic substances are not a well-defined class of organic compounds and their distinction is based on the difference in solubility in aqueous solutions at different pH levels. The major humic fractions include humic acid, fulvic acid and humin.

Humic acids consist of a mixture of weak aliphatic and aromatic organic acids, which are insoluble in water under acidic conditions but soluble in alkaline conditions. Humic acid consists of that fraction of

humic substances that are precipitated from aqueous solution, when the pH is decreased below 2. They are considered as polydisperse due to their variable chemical features. Structure of a typical humic acid with phenolic and carboxylic substituents is shown in figure 2.3.

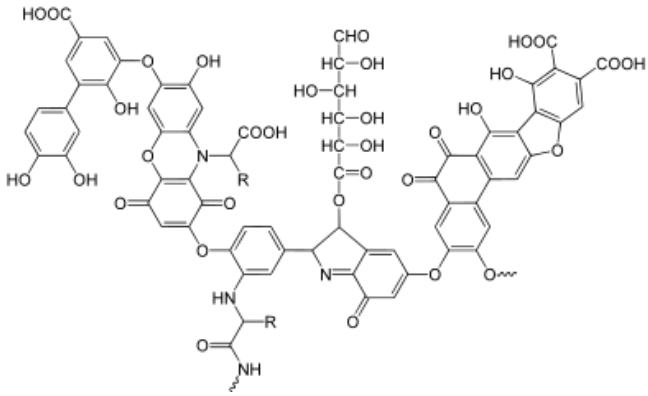

Fig. 2.3: Structure of a typical humic acid

The three dimensional structure of this compound is considered to be a flexible linear polymer that exists as random coils with cross linked bonds. About 35% of the humic acid molecules are aromatic, while the remaining are aliphatic in nature and their molecular weight ranges from 10,000 to 100,000. The humic acids have important role in aquatic systems. They can complex heavy metals and organic pollutants such as pesticides. The reaction between chlorine and humic acid in water treatment generates carcinogenic substances such as trihalomethanes (THMs) and haloaceticacids (HAAs). Hence it is necessary to remove humic acid before water chlorination. The significance of humic acid in the present study is that most of the industrial waste waters may contain humic acid which can affect the photocatalytic degradation of the pollutants.

2.2.7 Hydrogen peroxide (H_2O_2)

The H_2O_2 used in the present study is from M/s HOCL (India) and the purity was 50%. Hydrogen Peroxide is a clear, colourless, slightly viscous liquid with a pungent acid odour and miscible in all proportions with water. It is mainly manufactured using the anthraquinone process. Hydrogen Peroxide has strong oxidizing properties; products of decomposition are oxygen and water, which are harmless. The structure of H_2O_2 is shown in figure 2.4.

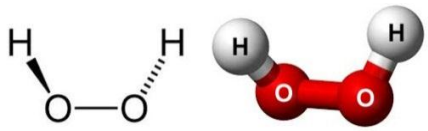

Fig. 2.4: Structure of H_2O_2

The characteristics of H_2O_2 are shown in table.2.6

Table 2.6: Characteristics of H_2O_2

Chemical name	**H_2O_2**
Molecular mass	34.0147 g/mol
Density	1.1 g/cm^3
Melting point	-0.43 ^oC
Boiling point	150.2 ^oC
Viscosity	1.245 cP
Dipole moment	2.26 D
Acidity(pKa)	11.75
Solubility in water	Miscible

Uses

- In textile and paper industry as a bleaching agent
- Its most significant use is in environmental remediation where it is used for the treatment of domestic waste and industrial effluents
- It is used as hair bleach and also as a mild disinfectant.

2.2.8 Phenol

The phenol used in the present study is from M/s HOCL (India) and the purity was 99.80%. Phenol and its derivatives are highly toxic and bio-calcitrant in nature. As per the Environment Protection Rules of Central Pollution Control Board, India (1992), the maximum discharge limit of phenols in inland water is 1 mg/L. The health effects of phenol include respiratory irritation, headache and burning eyes. Severe exposure to high amount of phenol causes skin burns, liver damage, irregular heartbeat and even death.

The characteristics of phenol are shown in table 2.7

Table 2.7: Characteristics of phenol

Chemical name	**Phenol**
Appearance	Transparent crystalline solid
Molecular structure	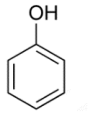
Molecular formula	C_6H_5OH
Molar mass	94.11g/ mol
Stability	Stable, flammable
Odour	Sweet and tarry
Density	1.07 g/cm^3
Melting point	40.5^{o}C
Boiling point	181.7^{o}C
Solubility in water	8.3 g/ 100 mL
Dipole moment	1.224 D
Acidity (pKa)	9.95 (in water)

Uses:

- For the manufacture of epoxy and polycarbonate resins
- In the study and extraction of bio-molecules.
- In cosmetic industry for the manufacturing of sunscreens, skin lightening creams and hair coloring solutions
- In manufacturing pesticides and insecticides and also in the pharmaceutical industry.

2.2.9 Miscellaneous materials

Details of various other materials used in the study are provided in respective chapters.

2.3 The experimental set up

The experimental set up and procedures are discussed in respective chapters.

2.4 Analytical procedures

The various analytical procedures used in this study include Gas chromatography, LC/MS, Spectroscopy, Wet analysis etc.

2.4.1 Analysis of phenol

Trace amounts of phenol formed as intermediate during the photocatalytic degradation of ACP, DMPC and 2-MBF is determined by spectrophotometry. The sample taken from the reactor at regular intervals is filtered and the phenol formed is determined. The determination is based on the reaction of phenol with 4-amino antipyrene at pH 10 ±0.2 in

presence of potassium ferricyanide to form a coloured antipyrene dye. The absorbance of this coloured complex is measured at 500 nm using a spectrophotometer (Perkin-Elmer UV/VIS spectrometer-Lambda 20). The spectrophotometer is initially calibrated with a series of known concentrations of phenol at ranges comparable to the amount formed to get the calibration factor. A similar reaction system kept in the dark under exactly identical conditions but without sunlight irradiation was used as the reference.

2.4.2 Analysis of H_2O_2

H_2O_2 was analysed by standard iodometric method. The oxidation of iodide ions by H_2O_2 was carried out in 1 N sulphuric acid in presence of five drops of saturated ammonium molybdate solution, which acts as the catalyst for the reaction. The reaction was allowed to go to completion (5 min) in the dark. The liberated iodine was then titrated against standard sodium thiosulphate solution, (2×10^{-3} N prepared freshly from 10^{-1} N stock solution). Freshly prepared starch solution was used as the indicator.

2.4.3 Determination of COD

COD analysis is carried out by open reflux method [101]. The sample is refluxed with known amount of excess acidified $K_2Cr_2O_7$ solution whereby the organic matter is destroyed, and the excess dichromate is titrated with ferrous ammonium sulphate (FAS). The reacted $K_2Cr_2O_7$ is then converted into oxygen equivalent to get the COD value.

10 mL of the sample is pipetted out in to 250 mL Erlenmeyer flask and 20 mL $K_2Cr_2O_7$ solution (0.10 N) is added to it. 30 mL of

concentrated H_2SO_4 is slowly added to the flask which is fitted with a condenser provided with cooling water circulation. The content of the flask is refluxed for 2 hr. It is then allowed to cool to room temperature and the condenser is washed down with distilled water. The excess $K_2Cr_2O_7$ in the flask is titrated against standard ferrous ammonium sulphate solution (0.1 N) using Ferroin indicator (3 drops). The end point is the first sharp colour change from blue green to reddish brown. A blank experiment is also conducted with 10 mL distilled water instead of the sample in the same manner as described above. The COD is calculated using the equation

$$\text{COD (mg/L)} = (A-B) \times N \times 8000 / \text{Sample volume (mL)} \qquad (51)$$

Where:

A = mL of FAS used for blank

B = mL of FAS used for the sample

N = normality of FAS and

8 = equivalent weight of oxygen

2.4.4 Adsorption

A fixed amount (0.1 g) of the catalyst was suspended in 100 mL of the adsorbate solution in a 250 mL reaction flask and the pH was adjusted as required. The suspension was agitated continuously at a constant temperature of 29 ± 1^0C for 2 hr to achieve equilibrium and then kept undisturbed for 2 hr. It was then centrifuged at 3000 rpm for10 min. After centrifugation, the concentration of adsorbate in the supernatant was determined using gas chromatography.

The adsorbate uptake was calculated from the relation

$$q_e = (C_0 - C_e)\ V / W \qquad (52)$$

Where C_0 is the initial adsorbate concentration (mg/L), C_e is the equilibrium adsorbate concentration in solution (mg/L), V is the volume of the solution in litre, W is the mass of the adsorbent in gram and q_e is the amount adsorbed in mg per gram of the adsorbent.

2.4.5 Analysis of phosphate

The analysis of phosphate was done using Vanadomolybdophosphoric acid colorimetric method [96]. In a dilute orthophosphoric acid solution ammonium molybdate reacts under acidic condition to form molybdophosphoric acid (a heteropoly acid). In presence of vanadium, yellow vanadomolybdophosphoric acid is formed. The intensity of the yellow colour is proportional to the phosphate concentration.

50 mL of the sample is mixed with 5 mL 1:3 nitric acid and digested for 30 min. The sample is cooled and mixed with 10 mL phosphate reagent (containing ammonium molybdate and ammonium metavanadate). The solution is made up to 100 mL and the absorbance of the sample is measured at 420 nm using a spectrophotometer (Perkin-Elmer UV/VIS spectrometer-Lambda 20). The instrument was previously calibrated with a series of standard phosphate solutions of comparable concentration and the calibration factor so obtained is used for the determination of phosphate concentration in the sample. 50 mL distilled water treated in the same way as that of sample is used as the reference.

2.4.6 LC/MS Analysis

The identification of some of the photocatalytic reaction intermediates is done by LC/MS using Waters Xevo G2 Q-TOF. In a Q-TOF instrument, the sample is introduced through the interface, and ions are focused using the hexapole ion bridge into the quadrupole MS. Here, the precursor ion is selected for later fragmentation and analysis with a mass window of approximately 3 mass units, which is a typical window to preserve the isotope envelopes in the product ion spectra. The ions are ejected into the hexapole collision cell, where argon is used for fragmentation. From this point, the ions are collected into the TOF region of the MS/MS.

2.4.7 FT-IR spectrum

FT-IR analysis was done using Thermo Nicolet, Avatar 360 with KBr beam splitter and DTGS (Deuterated triglycine sulfate) detector. The details of sample preparation are given in the respective sections/subsections.

2.4.8 pH determination

The pH measurements were carried out using pH meter (Systronics µ pH System 361), initially calibrated with standard buffer solutions.

2.4.9 SEM (Scanning Electron Microscopy) analysis

The SEM image of ZnO catalyst was obtained using JOEL Model JSM-6390 LV.

2.4.10 TEM (Transmission Electron Microscopy) analysis

TEM analysis was performed using Joel JEM 2100.

2.4.11 XRD (X-ray Diffraction)

XRD measurements were made using Rigaku X-ray diffractometer with Cu-Kα radiation

Various other analytical procedures used in the present study are described in respective chapters.

2.5 Plan of the thesis

The current thesis is divided into eight chapters. Each chapter has its own specific objectives, experimental procedures, results, discussion and conclusions.

Chapter 1 entitled "**Introduction: Background literature**" gives an overview of various Advanced Oxidation Processes with their merits and limitations with special emphasis on photocatalysis. It also gives an outline of various unit operations involved in the phenol manufacturing process and the formation of pollutants selected for the present study. A description of the conventional Effluent Treatment Plant (ETP) for the phenol manufacturing unit with its inherent limitations is also provided.

Chapter 2 entitled "**Objectives of the study, Materials used and Plan of the thesis"** gives a detailed description of the main objectives of the present study and the specific activities undertaken to achieve the objectives. Various materials and analytical procedures used in the study as well as the plan of the thesis are presented.

Chapter 3 entitled "**ZnO mediated solar photocatalytic degradation of Alpha Methylstyrene [AMS] in water"** deals with the characterization

of the ZnO catalyst and detailed investigation on the photocatalytic degradation of AMS under solar irradiation. The effect of various reaction parameters on the degradation efficiency of AMS and details on the detection and identification of reaction intermediates are presented. The effect of common anions/oxidants on AMS degradation is investigated in detail. Oscillation in the concentration of insitu formed H_2O_2, role of dissolved oxygen in photocatalysis, detection of hydroxyl radical, and reusability study of the catalysts etc. are also discussed.

Parts of major findings reported in this chapter were published as original research papers in peer reviewed journals as follows:

Paper 1. "Zinc oxide photocatalysis using solar energy for the removal of trace amounts of Alpha-methylstyrene, Diquat and Indigo Carmine from water", ***J. Adv. Oxid. Technol.*** *Vol. 17, No. 2, (2014*) 297-30

Paper 2. "Application of solar energy in wastewater treatment: Photocatalytic degradation of α-methyl styrene in water in presence of ZnO", **Journal of Water Process Engineering.** 8 (2015) 108-118

Chapter 4 entitled **"ZnO mediated solar photocatalytic degradation of Acetophenone [ACP] in water"** deals with the detailed investigation on the solar photocatalytic degradation of ACP in water. Various reaction intermediates formed during the degradation were detected and identified. The effect of various reaction parameters, externally added reaction intermediates, anions, oxidants etc., on the degradation is presented and discussed in this chapter.

Some of the findings reported in this chapter were published in the following peer reviewed journal as original research paper.

Paper 3. "Sunlight activated ZnO mediated photocatalytic degradation of acetophenone in water" ***IOSR Journal of Applied Chemistry (IOSR-JAC)*** e-ISSN2278- 5736. (2016)55-70.

Chapter 5 entitled **"ZnO mediated solar photocatalytic degradation of Dimethyl phenyl carbenol [DMPC] in water"** presents the investigations on the solar photocatalytic degradation of DMPC under various reaction conditions. Various reaction intermediates were identified and the effect of some of them on the degradation is investigated in detail. The effect of common anions/oxidants on the degradation is investigated and the possible reasons for the findings are discussed. A possible mechanism for DMPC degradation is also proposed.

Chapter 6 entitled **"ZnO mediated solar photocatalytic degradation of 2-Methyl benzofuran [2-MBF] in water"** presents the results of the study on the solar photocatalytic degradation of 2-MBF and the effect of various reaction parameters influencing the degradation efficiency. Various reaction intermediates were identified and a possible mechanism for the degradation is proposed. Reusability study of the catalyst as well as the corrosion study of ZnO at different pH is made and the results are discussed.

Chapter 7 entitled **"ZnO mediated solar Photocatalytic degradation of combination of AMS, ACP, DMPC and 2-MBF in synthetic and real industrial wastewater"** presents the results of detailed investigation on the effect of each pollutant on the degradation /mineralization efficiency

of the other in a system containing multiple pollutants. The applicability of solar photocatalysis for the degradation of the combination of pollutants in real industrial waste water matrix is investigated in detail. The role played by the phosphate anion and turbidity in inhibiting the photocatalytic mineralization of the combination of pollutants in the effluent water matrix is established. The study clearly shows that both these factors have to be removed from the effluent water by suitable techniques in order to ensure the efficiency of solar photocatalytic mineralization.

Chapter 8 entitled **"Summary and conclusion"** summarizes the findings of the study and highlights the conclusions.

Annexure I lists the abbreviations used in the thesis. Expansions of respective abbreviations are shown in the text also in the first place where they appear in the thesis.

Annexure II provides the list of original research papers based on the results of this study published in peer reviewed journals and/or presented in conferences.

Annexure III compiles the reprints of the papers already published.

.....ꕥ.....

Chapter 3

ZINC OXIDE MEDIATED SOLAR PHOTOCATALYTIC DEGRADATION OF ALPHA METHYL STYRENE [AMS] IN WATER

Contents

3.1 Introduction

Alpha methyl styrene (AMS) is a major intermediate/byproduct in phenol manufacturing industry. Small amounts of AMS is hence seen in the effluent water from many related petrochemical industries. The effluent water containing small amounts of AMS is usually treated by conventional secondary treatment methods including biological methods. But these methods are ineffective in removing the last traces of AMS from water before recycling/safe disposal. Since photocatalysis has been proven to be an effective AOP capable of removing the last traces of many toxic organic pollutants from water [37, 102-106], the possibility of using the same for the complete removal of AMS is investigated using ZnO as the photocatalyst and sunlight as the energy source.

Photocatalytic oxidation of AMS over TiO_2 supported on zeolites was reported earlier [107]. Addition of acidic zeolites decreases the photocatalytic oxidation rate though the selectivity towards acetophenone

(ACP) is enhanced [108]. It has also been reported recently that the rate of photocatalytic oligomerization of AMS can be enhanced by effective metal-to-ligand charge-transfer localization on the bridging ligand [109]. However, no detailed studies on the sunlight induced photocatalytic degradation/mineralization of trace amounts of AMS in water are reported so far. The efficiency of one of the most widely investigated semiconductor oxide photocatalysts i.e., ZnO, also has not been tested in this context. In this chapter, ZnO mediated photocatalytic degradation and mineralization of trace amounts of AMS in water is investigated using sunlight as the energy source. The influence of various reaction parameters such as catalyst dosage, initial concentration of AMS, pH, insitu formed intermediates, humic acid, H_2O_2, electrolytes etc., on the rate of degradation is investigated in detail.

The chemical structure and the physico-chemical characteristics of AMS are given in Chapter 2.

3.2 Experimental Details

3.2.1 Materials

AMS (99.9%) and Zinc oxide (~99.70%, BET surface area ~4 m^2/g) were obtained from Merck India and used as such without further purification. LR grade H_2O_2 and HCl were from Nice chemicals, India. Millipore water was used for the preparation of standard solutions. Other chemicals such as NaF, NaCl, NaBr, Na_2CO_3, $NaNO_3$, Na_2HPO_4, CH_3COONa, $K_2S_2O_8$ etc., were of 'Reagent grade' or equivalent and used as such without further purification.

3.2.2 Analytical Procedures

Perkin Elmer Auto System XL Gas Chromatograph was used for the analysis of AMS and its degradation products in water using flame ionization detector and Elite 1301 column with hydrogen as the carrier gas. The calibration graph is obtained by multiple level calibration method, in which different known concentrations of AMS solution (5, 10, 15, 20 and 25 mg/L) are prepared and each solution is injected into the GC [1.0 µL). The procedure is repeated several times to get the average calibration value corresponding to the respective concentration so that the error can be minimized.

GC parameters used for the analysis are:

(a) Oven Temperature

The temperature programme for the GC analysis of AMS is given in table 3.1

Table 3.1: Oven Temperature programme for AMS analysis by GC

Oven Ramp	Rate (^{0}C/min)	Temperature[^{0}C]	Hold [min]
Initial	0.0	60.0	3.0
1	3.0	130.0	5.0

(b) Detector [FID]

Temperature = 225°C

(c) Injector

Programmable split/splitless injector with temperature =225°C

Carrier gas = H_2 [1.50 psi]; Flow rate = 2.0 mL/min

The calibration graph prepared for the analysis is shown in figure 3.1.

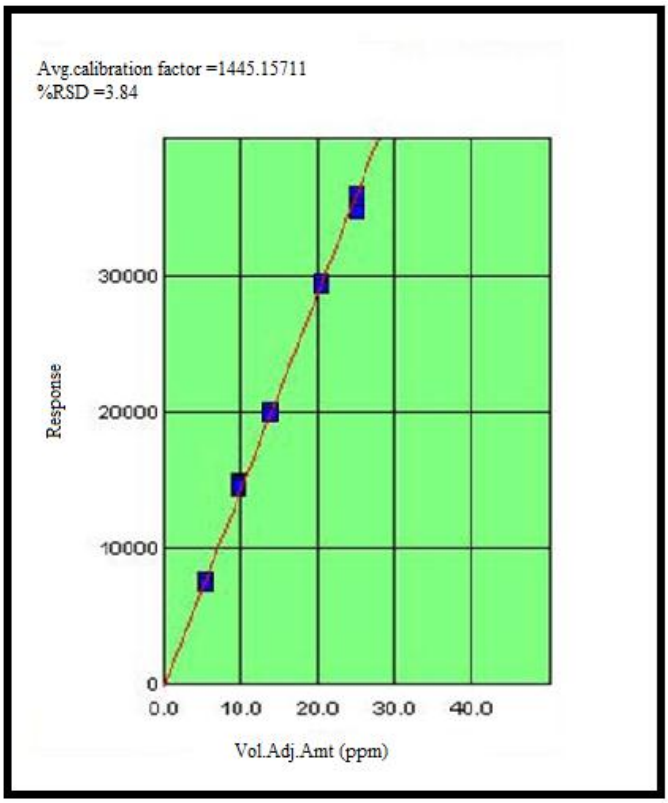

Fig. 3.1: Calibration graph for AMS analysis

'Vol Adj Amt' refers to known concentrations of AMS used for calibration and the response corresponds to the peak area for each concentration. From the peak area of the experimental sample injection, the concentration of AMS remaining in the system can be computed using the calibration graph.

For the estimation of AMS in the reaction system, 5 mL of the sample from the reactor is withdrawn at regular time intervals and centrifuged at 3000 rpm for 5 min to remove the catalyst particles. The

clear sample (1 µL) injected into the GC to get the concentration of AMS remaining in the solution (in mg/L). The major intermediate formed from AMS is identified as acetophenone (ACP). Ultimately ACP also gets mineralized as seen from the analysis by GC.

3.2.3 Characterization of the catalyst

Surface area of the ZnO catalyst was measured by BET method using TriStar 3000.V6.07A. The X-ray diffraction (XRD) measurements were made using Rigaku X-ray diffractometer with Cu-Kα radiation. Scanning Electron Microscopy (SEM) measurements were performed using JEOL Model JSM-6390 LV. TEM analysis was performed using Joel JEM 2100.

3.2.4 Photocatalytic Experimental set up

The photocatalytic degradation study of AMS in water was performed in a jacketed pyrex reactor [figure 3.2 (a) and (b)]. Required volume of AMS solution prepared in double-distilled water together with weighed amount of ZnO catalyst was taken in the inner compartment of the reactor. Cooling water from a thermostat (29 ± 1^0C) was constantly circulated through the outer jacket. The solar experiments were performed by placing the reactor system on the roof top of our laboratory at Kochi, Kerala, India (9°57'51"N, 76°16' 59 " E) during sunny days in April-May, August-December 2012, January-May, August-December 2013, January-May, August-December 2014, January-May, August-December 2015, January-May, August-December 2016 and January-May, August-December 2017. The suspension was constantly stirred to ensure uniform mixing.

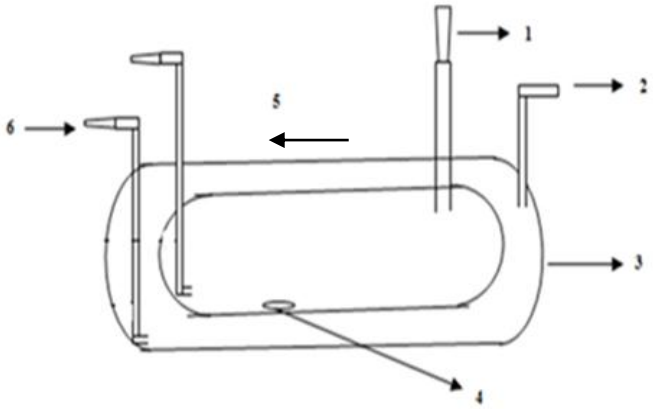

Fig. 3.2 (a): Schematic diagram of the photocatalytic reactor used for the study (1. Sample inlet, 2. Water outlet, 3.Outerjacket, 4.Magnetic pellet, 5.Gas purging tube, 6.Water inlet)

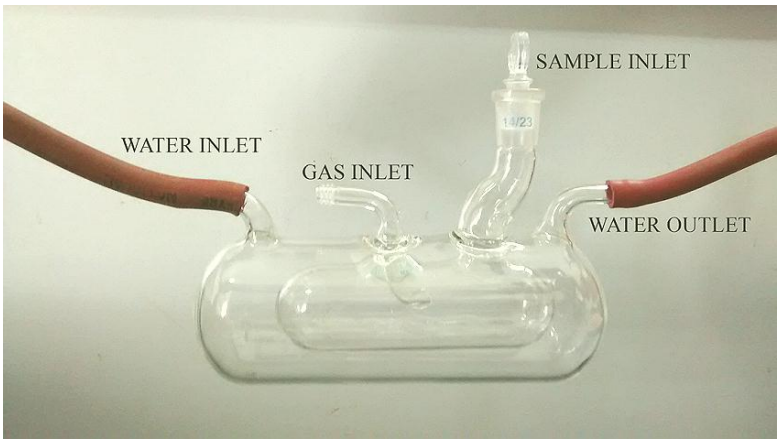

Fig. 3.2 (b): Photo reactor used in the study

Average solar light intensity during the experiments was 1.25×10^5 Lux, as calculated from the measurements using LT-Lutron LX-101A Digital Lux meter. To ensure the consistency and reliability of the results, the standardized reference experiment under optimized reaction condition was conducted every time when a new parameter is tested. Samples from

the reactor were drawn periodically, filtered through 0.45 µm filter and analysed for the remaining AMS as well as the insitu formed intermediates by Gas Chromatography. For eliminating the contribution from adsorption and dark reaction, if any, towards the reduction in the AMS concentration, suspension kept under identical condition in the dark is used as the reference.

3.3 Results and Discussion

3.3.1 Characterization of ZnO

The ZnO catalyst used in the study is characterized by surface area, particle size analysis, pore size distribution, adsorption, X-Ray Diffraction (XRD), Scanning Electron Microscopy (SEM) and Transmission Electron Microscopy (TEM). The pore size distribution is shown in figure 3.3(a).

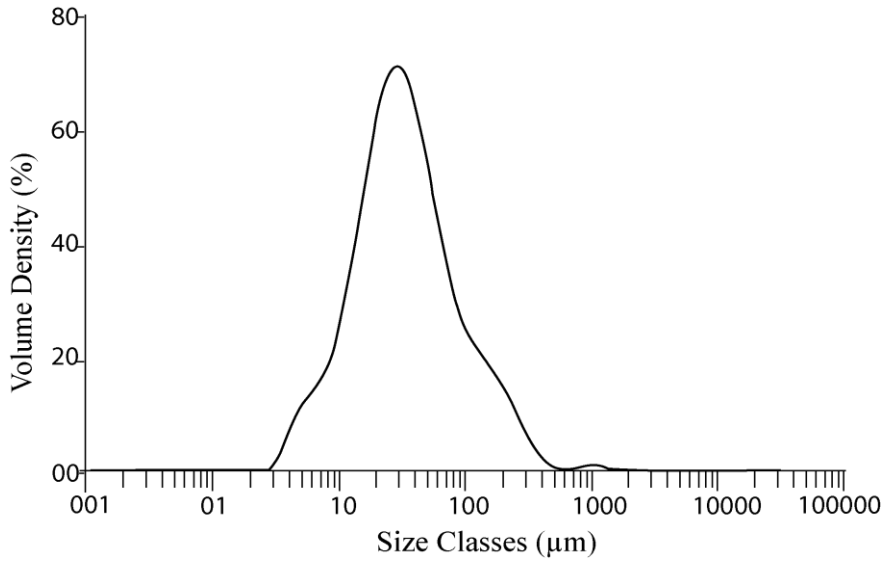

Fig. 3.3(a): Pore size distribution of ZnO

Pore size distribution is also measured using Micrometrics Tristar surface area and porosity analyzer which showed that more than 70% of the pores in ZnO were <250 Å. The average pore width is 123 A^0 and size distribution is approximately; < 250 Å (70.1%), 250-500 Å (11.3%) and >500 Å (17.8%).

The XRD pattern of ZnO catalyst presented in figure 3.3(b) shows three sharp peaks with very high intensity from 30 to 40 (2θ), which correspond to the phases (100), (002) and (101) respectively. The surface area of ZnO determined by the BET method is approximately 4 m^2/g. The SEM image of ZnO catalyst is shown in figure 3.3(c). The average particle size of ZnO was approximately in the range 0.1 to 0.40 µm. The average particle size as analysed using Malvern Mastersizer 3000 is 0.32 µm.

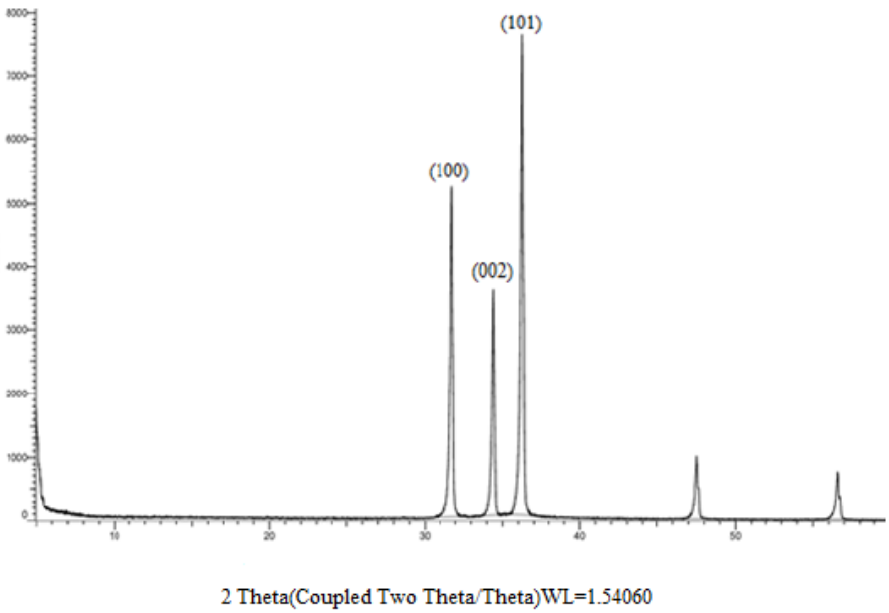

Fig. 3.3(b): XRD pattern of ZnO

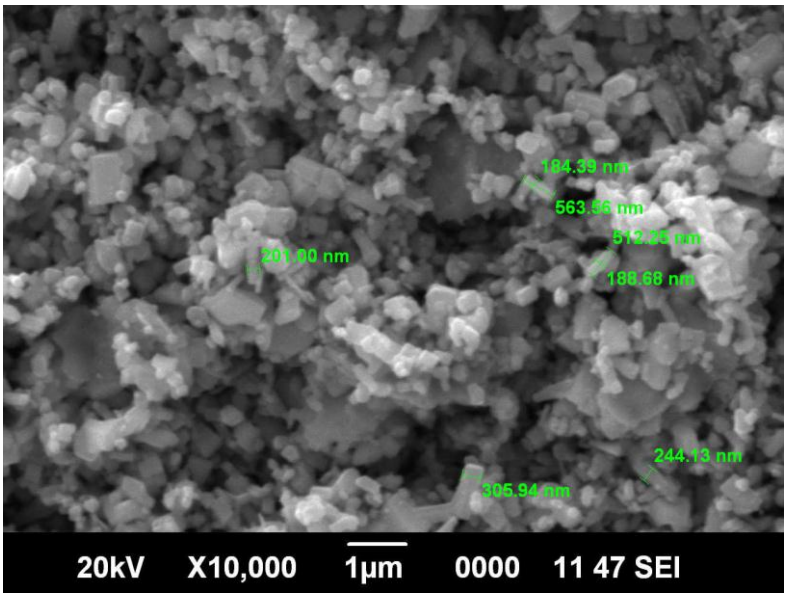

Fig. 3.3(c): SEM image of ZnO

The TEM image [figure 3.3 (d)] shows that most of the ZnO particles are of rod shape with average particle size of 0.09-0.2 μm.

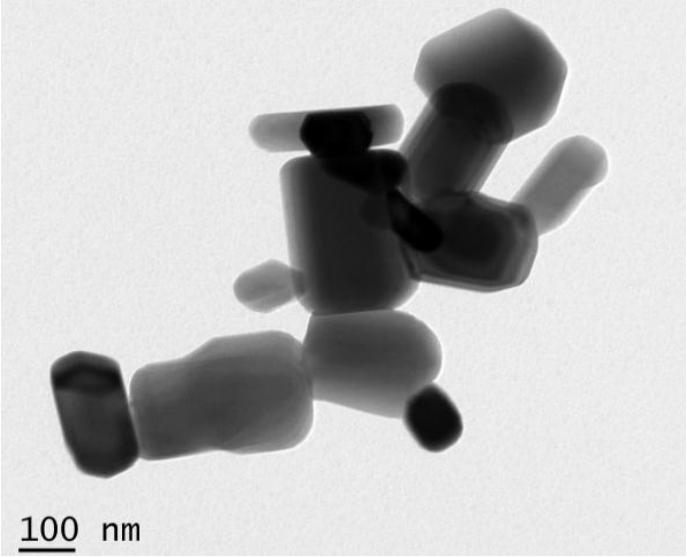

Fig. 3.3(d): TEM image of ZnO

3.3.2 Preliminary experiments

Preliminary results on the photocatalytic degradation of AMS (25 mg/L) using ZnO catalyst (80 mg/L) under sunlight is shown in figure 3.4. Approx. 80% degradation took place within 3 hr of irradiation. No degradation was observed in parallel experiments under identical conditions in the absence of either light or catalyst. This indicates that both light and catalyst are required for the degradation of AMS. Acetophenone (ACP) is identified as the major intermediate in the degradation reaction which also gets degraded fast on continued irradiation. The initial decrease in the AMS concentration in dark in presence of ZnO catalyst can be attributed to the adsorption which finally gets equilibrated and stabilized after the surface is fully covered. Under the given experimental conditions, the maximum adsorption of AMS is only 62 mg/g of ZnO. This adsorption is actually the preferred condition for effective photocatalytic degradation of AMS even though small amount of AMS in the bulk solution can also get degraded by the interaction with the surface generated reactive free radicals, which find their way into the bulk. Turchi and Ollis [110] have demonstrated that though photocatalytic degradation depends on the adsorptive properties of organic compounds on the surface, it is not a requirement for the reaction because the reactive $^{\bullet}OH$ radicals and other oxidizing species can diffuse into the bulk solution to react with the organic pollutant.

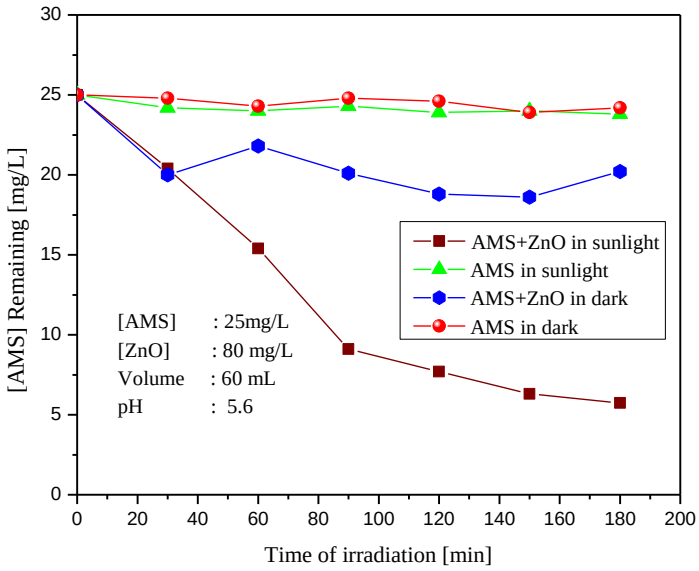

Fig. 3.4: Photocatalytic degradation of Alpha Methyl Styrene (AMS) on ZnO

The decrease in concentration of AMS after 3 hr of irradiation is at least four times more than that in the dark. This clearly shows that the faster decrease in AMS concentration in presence of light and catalyst is mainly due to continuous degradation of the species adsorbed on the surface. This degradation and subsequent desorption of the products liberate the surface sites which can adsorb more fresh molecules and the process continues.

The degradation decreases with time. Probable reasons for this may be the decrease in the relative concentration of AMS in the system and the competition between various reaction intermediates and the AMS molecules for the surface sites as well as for the reactive free radicals. ACP is the only intermediate detected by GC during the photocatalytic degradation of AMS which also gets degraded and mineralized as seen from the complete disappearance of AMS and ACP after long irradiation (8 hr)

[figure 3.5]. The COD value is also 'nil' at this stage thereby confirming the complete mineralization.

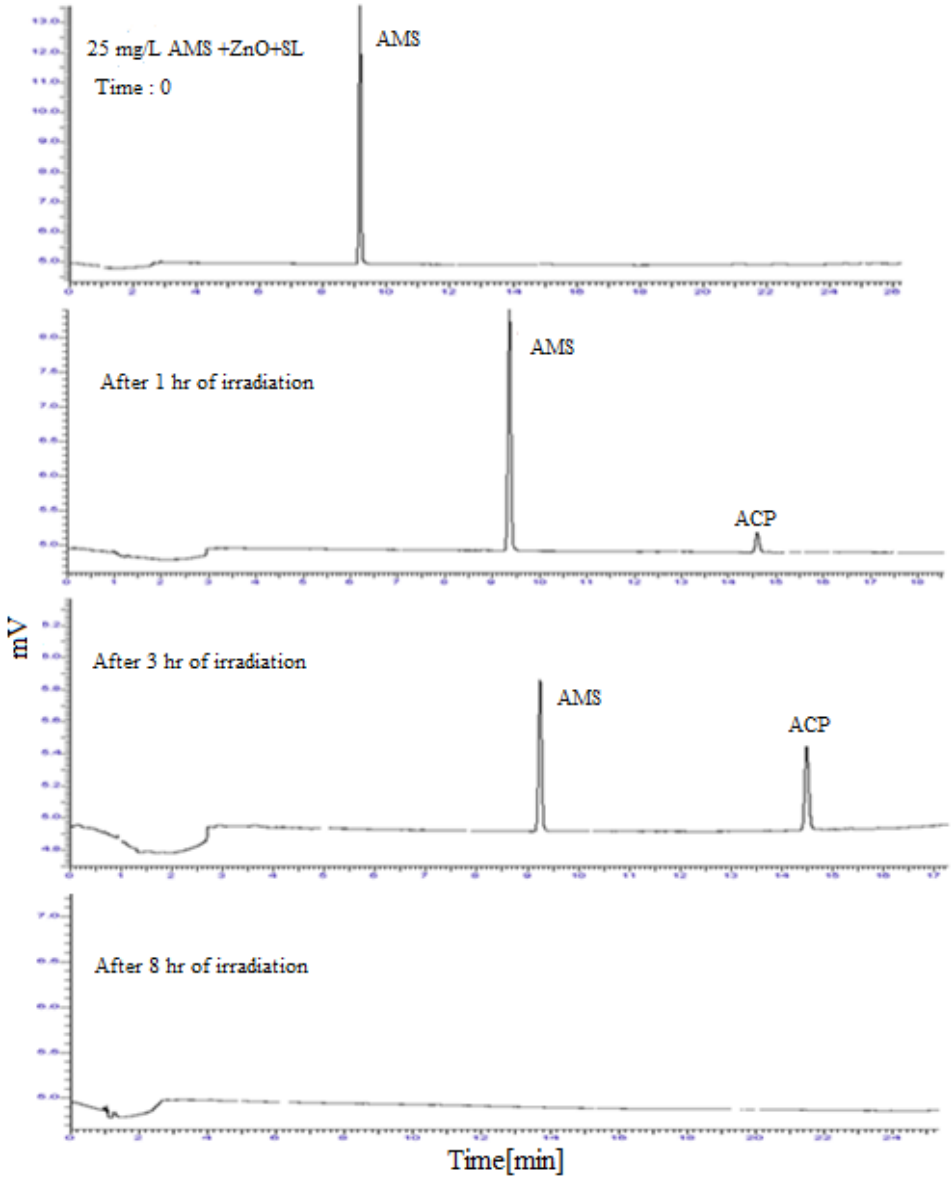

Fig. 3.5: Chromatogram showing solar photocatalytic degradation of AMS, formation of ACP and eventual disappearance of both AMS and ACP, [ZnO] = 80 mg/L

LC/MS analysis of the reaction system at the stage of 50% degradation (of AMS) showed the presence of more intermediates as in table 3.2.

Table 3.2: LC/MS analysis of intermediates formed during the solar photocatalytic degradation of AMS over ZnO

SL No	Mass	Proposed structure
1	119	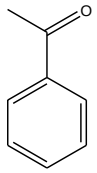
2	107	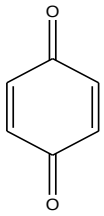
3	135	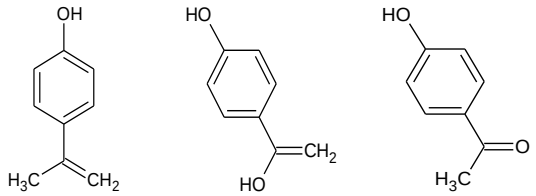
4	137	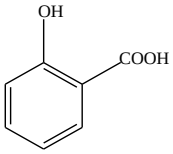
5	149	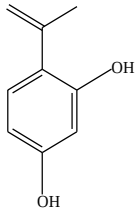

5	151	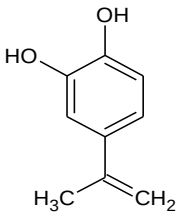
6	167	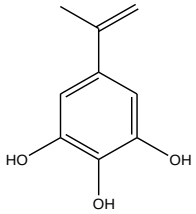
7	236	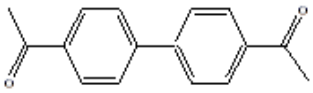
8	251	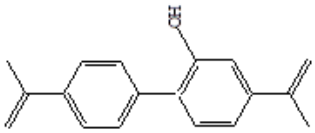
6	271	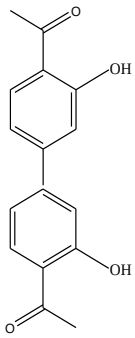
8	331	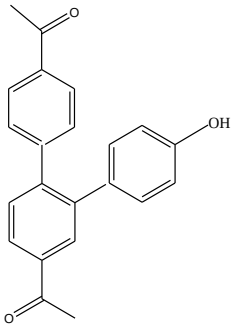

However, the presence of these intermediates during the reaction is inconsistent and often in amounts not detectable by GC, probably because they also get degraded and mineralized as fast as or even faster than AMS.

The effect of various reaction parameters on the degradation of AMS is investigated systematically as follows:

3.3.3 Effect of catalyst dosage

In photocatalytic degradation studies, optimization of the catalyst concentration is very important for the economic use of the catalyst, maximum photon absorption and efficiency of the process. The effect of catalyst loading on the photocatalytic degradation of AMS is investigated by varying the amount of ZnO from 20 to 120 mg/L, keeping other parameters identical. The results are given in figure 3. 6.

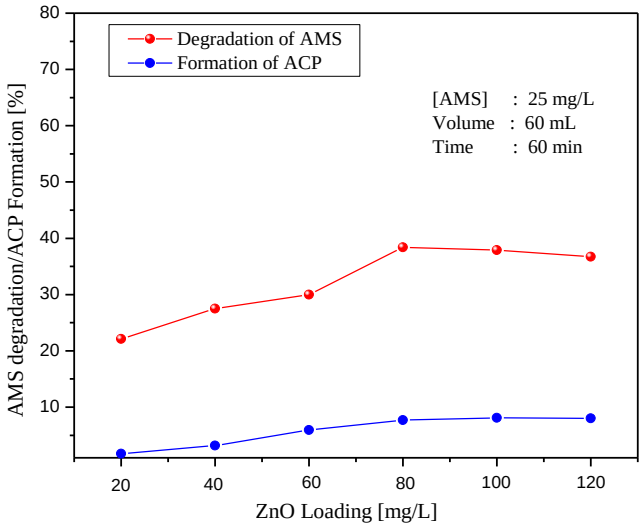

Fig. 3.6: Effect of catalyst dosage on the solar photocatalytic degradation of AMS

The degradation of AMS increases slowly with increase in ZnO loading upto 80 mg/L and stabilizes/decreases thereafter. The concentration of the intermediate ACP also increases slowly, reaches an optimum and then stabilizes/decreases. The stabilization of AMS degradation and ACP formation occurs at identical catalyst loading, which is a clear indication of the relation between the two processes. The observed increase in degradation at higher catalyst loadings may be due to the increased number of adsorption and interaction sites for AMS and/or the intermediates and more effective absorption of light. This in turn leads to the formation of more number of reactive hydroxyl and other radicals which interact with the pollutant. However, further increase in the catalyst loading beyond the optimum can only lead to the scattering and reduced passage of light through the suspension medium. Also at higher catalyst loading there is possible aggregation of catalyst particles causing a decrease in the number of available active surface sites. The particles cannot be effectively and fully suspended above a particular loading in a particular reactor which also leads to suboptimal penetration of light and reduced adsorption of substrate on the catalytic surface. It is also possible that at higher catalyst loading, part of originally activated ZnO is deactivated through collision with ground state catalyst as follows [111]:

$$MO^* + MO \rightarrow MO\# + MO \qquad (53)$$

MO is semiconductor oxide ZnO, MO* is activated ZnO and MO# is its deactivated form.

The optimum catalyst loading will depend on the size, shape and geometry of the reaction assembly as well as other reaction parameters.

Hence, for each reactor configuration the optimization has to be done separately. In the present case the optimum loading of ZnO is 80 mg/L. Hence all further studies were carried out with this loading.

3.3.4 Effect of initial concentration of AMS

It is important to study the dependence of photocatalytic degradation rate on the concentration of the pollutant both from the mechanistic and application point of view. The effect of initial concentration of AMS on its solar photodegradation using ZnO catalyst is investigated in the concentration range 10-30 mg/L in increments of 5 mg/L. The degradation profile is inconsistent and widely varying above this concentration range, probably due to poor solubility of AMS in water. The result shows that the percentage degradation of AMS decreases sharply as the AMS concentration is increased (figure 3.7A).

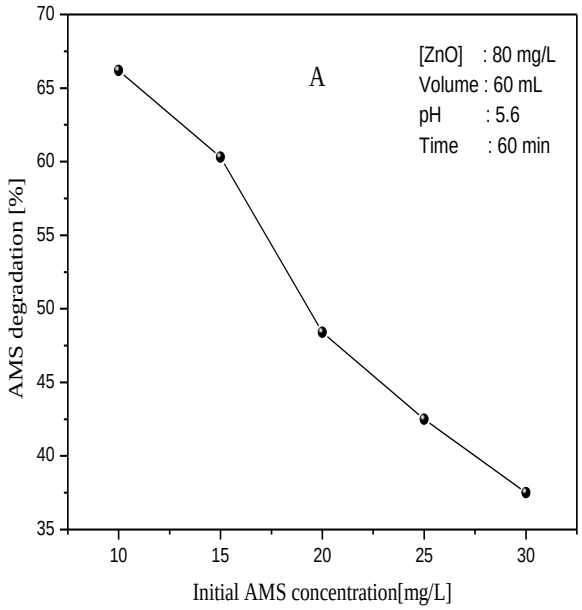

Fig. 3.7A: Effect of concentration of AMS on its percentage degradation

However, the rate of removal of AMS steadily increases with increase in the initial AMS concentration and stabilizes eventually (figure 3.7.B). As is clear from the graph, the reaction follows first order kinetics upto 20 mg/L of AMS. The optimum rate of 1.8×10^{-1} mg/L/min was obtained at 25 mg/L of AMS. This is followed by almost constant degradation rate implying zero order kinetics.

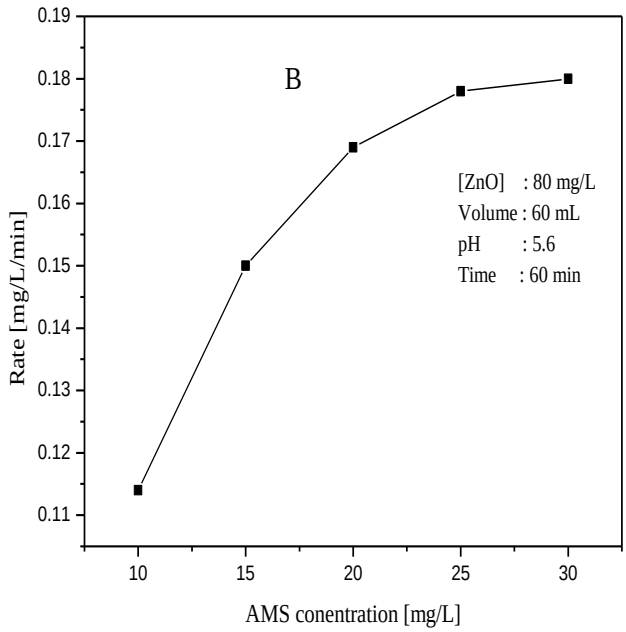

Fig. 3.7B: Effect of concentration of AMS on its rate of degradation

The photocatalytic degradation of many pollutants follows pseudo first order kinetics [112-114]. In the present study, the increase in degradation with increase in AMS concentration upto 25 mg/L may be attributed to the increase in adsorption of AMS on ZnO which will continue until the catalyst surface is fully covered and all the active sites are fully occupied. Also, at higher concentration, more AMS molecules

will be available in the bulk as well as in the proximity of the surface which can actively interact with the surface-generated active free radicals and other Reactive Oxygen Species (ROS) such as $^{\bullet}OH$ and H_2O_2. However, at higher concentrations of AMS beyond the optimum, there is a possibility that at least a part of the incident light may be blocked and/or absorbed by AMS and the intermediates formed from it. Thus the photons available for the activation of the catalyst are reduced. Another possible reason may be that major portion of the reaction occurs in the region (reaction zone) close to the irradiated side where the irradiation intensity is much higher than the other side. This retardation in the penetration of light at longer distance from the light source will be more at higher concentration of the substrate and it results in decreased degradation [115]. With increase in the initial concentration of AMS, the catalyst surface required for maintaining consistent degradation rate also increases. Since the illumination intensity and catalyst concentration are constant, the relative number of ROS available for interacting with the increased number of AMS molecules at higher concentration also presumably decreases. This also leads to stabilized/decreased rate of degradation.

Once the concentration of the substrate is enough to interact with all the optimum available ROS and other reactive free radicals, any further increase cannot result in increased reaction and the AMS removal becomes independent of concentration. It is also possible that at higher substrate concentration, some of the reaction intermediates may get adsorbed on the surface or remain in the bulk for relatively longer period

which results in less frequent interaction between fresh AMS molecules and the insitu generated ROS.

The domination of the reaction system by the reactant/intermediates/ products can also result in the suppression of the generation of surface initiated reactive free radicals. At any point of time, there will be an optimum for the number of substrate molecules which can interact with the reactive free radicals generated by the surface. This optimum in turn will depend on a number of parameters such as initial concentration of the substrate, wavelength of light, intensity of illumination, mass and type of photocatalyst, type and geometry of the photo reactor etc. Hence the measurement and calculations apply only to specific reaction conditions and cannot be generalized.

According to the Langmuir-Hinshelwood (L-H) model, modified to accommodate reactions occurring at solid-liquid interface [116, 117], the simplest way to represent the photocatalytic degradation of the substrate, assuming that there is no competition with reaction byproducts/ intermediates, is

$$r_0 = -dC/dt = k_r K C_0 / (1 + K C_0) \quad (54)$$

Where, r_0 is the rate of disappearance of AMS (mg L^{-1} min^{-1}), C_0 (mg L^{-1}) is the initial concentration, K is the equilibrium adsorption coefficient and k_r is the reaction rate constant at maximum surface coverage. Equation 54 can be rewritten as

$$1/r_0 = 1/k_r + 1/k_r K \times 1/C_0 \quad (55)$$

Plot of $1/r_0$ against $1/C_0$ yields straight line in the concentration range 10-25 mg/L indicating first order kinetics and L-H mechanism (figure 3.7.C). Further, integration of equation 54 yields:

$$\ln (C_0 /C) + k(C_0 - C) = k_r Kt \quad (56)$$

When C_0 is very small, above equation becomes

$$\ln (C_0/ C) = k_r Kt = k't \quad (57)$$

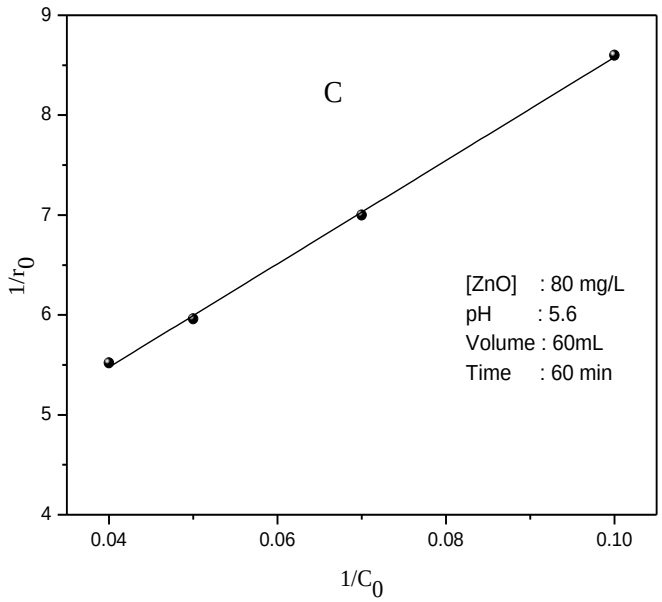

Fig. 3.7C: Reciprocal plot of initial rate of degradation of AMS versus its initial concentration

The plot of $\ln (C_0/C)$ versus irradiation time (t) for the concentration range 10-25 mg/L yields straight lines (figure 3.7D) thereby reconfirming pseudo first order kinetics. The slope of each line is the apparent rate constant of degradation k' at the corresponding concentration of the substrate. The results thus computed are presented in table 3.3.

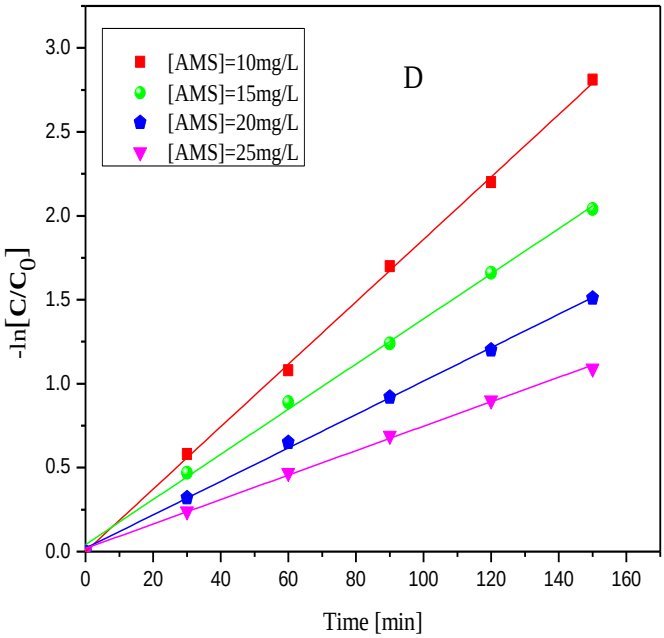

Fig. 3.7 D: Logarithmic plot of pseudo first order kinetics for the degradation of AMS

Table 3.3: Pseudo first order rate constants for the photocatalytic degradation of AMS over ZnO.

Sl No	[ZnO], mg/L	[AMS], mg/L	k_r x 10^{-3} (min^{-1})
1	80	10	18.7
2	80	15	13.6
3	80	20	10
4	80	25	7.2

The rate constant decreases with the increase in concentration of AMS, the decrease being steeper in the lower concentration range. This may be explained as follows:

For a fixed amount of catalyst and hence finite number of surface-generated active species available for interaction, the number of substrate

molecules is excessive at higher concentrations. This reduces the relative percentage fraction of substrate which can successfully interact with the ROS, leading to a decrease in the apparent rate constant. Obviously at higher concentration range of the substrate, the increase in the rate of degradation with concentration will be lower, compared to that at lower concentration range. However, the above rate constants apply only under the current experimental conditions including reactor size, shape, geometry etc and are not absolute.

Decrease in the rate of photocatalytic degradation and hence in the order of the reaction at higher concentrations of the substrate has been reported earlier [114,116,118]. Varying kinetics depending on the concentration of the substrate has been reported in the case of semiconductor mediated sono photocatalytic reactions also [113].

3.3.5 Effect of pH

The effect of pH on the photocatalytic degradation reactions has been studied extensively [119,120]. pH affects the charge on the catalyst particle, size of the aggregates and the position of the conduction and valence bands [121]. The properties of solid-electrolyte interface, i.e. the electrical double layer, can get modified as the pH of the medium changes. Consequently, the effectiveness of the adsorption-desorption process and the separation of the photogenerated electron-hole pair are also substantially affected [122]. The pH of the reaction medium has significant effect on the aqueous phase photocatalytic degradation process, since the surface characteristics of the catalyst and the chemical nature of the substrate and species derived from them change with the pH. The pH at which the

surface of an oxide is uncharged is known as the Point of Zero Charge (PZC). The PZC of ZnO is approx. 9.3. At pH values above 9.3, the catalyst surface is negatively charged and below 9.3, the surface is positively charged. There can be electrostatic attraction or repulsion taking place depending upon the ionic form of the organic compound, i.e., anionic, neutral or cationic. Accordingly, the photodegradation rate can be enhanced or inhibited.

The effect of pH on the photocatalytic degradation of AMS is studied by changing the pH of the medium from 2 to 12, keeping all other parameters constant. The results are presented in figure 3.8.

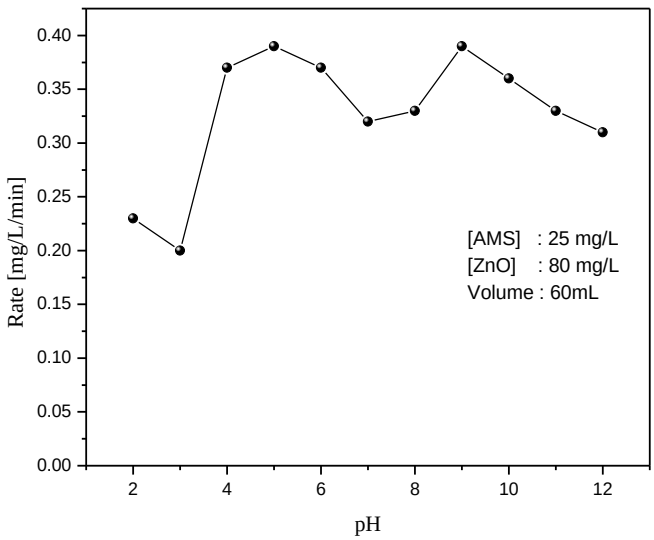

Fig. 3.8: Effect of pH on the rate of photocatalytic degradation of AMS on ZnO

It is observed that the degradation of AMS is slow at pH 2 and 3, which may be attributed to the corrosion of ZnO at lower pH and consequent decrease in the availability of enough active surface sites.

Poulios et al. [123] also reported similar observations. As the pH of the medium increases, the degradation increases, reaches maximum at pH ~5-6. Thereafter it starts decreasing slowly until around pH 7-8, increases again up to pH 9 and then decreases slowly. Since ZnO surface is positively charged below pH 9.3 and AMS is a non-polar hydrocarbon, it can remain adsorbed onto the surface or be in close proximity to the surface. Hence the degradation is relatively more in the pH range of 4-9. The slight decrease in the rate of degradation of AMS from pH > 9 may be attributed to a decrease in the adsorption as well as decrease a in the number of catalytically active sites due to the alkaline dissolution of ZnO as follows [33]:

$$ZnO + H_2O + 2OH^- \rightarrow [Zn(OH)_4]^{2-} \quad (58)$$

However, the concentration of OH^- ions and hence of reactive $^{\bullet}OH$ radicals will be relatively more in this pH range. Hence there will be effective interaction of $^{\bullet}OH$ with the substrate in the bulk too and consequently, there is reasonable amount of degradation, inspite of poor adsorption.

The effect of pH on the photocatalytic efficiency of ZnO is often inconsistent and depends on the complex relation among many factors, i.e., chemistry of the surface, extent and mode of adsorption (of AMS as well as ACP and/or other minor unidentified intermediates in this case), concentration of reactive free radicals such as $^{\bullet}OH$ etc. The adsorption of the substrates is more in the acidic range while the concentration of the $^{\bullet}OH$ radical is more in the alkaline region as explained earlier. Thus the effect of pH on these two factors, i.e., adsorption of substrate on ZnO and concentration of reactive $^{\bullet}OH$ radicals, which are important for the

degradation of AMS, is different and opposite. As a consequence, the combined net effect need not necessarily be exactly the same quantitatively at any pH at different times. Hence moderate variation in the extent of degradation of the substrate is possible even at the same pH in different experiments. This may be the reason, at least partly, for the minor zigzag behaviour in the pH range of 4-10. However, the variation is not much significant and the degradation may be considered as fairly the same in this pH range.

Correlation of the effect of pH on the degradation of AMS with the PZC of ZnO is not fully applicable in the present context since the degradation does not follow a consistent pattern above or below the PZC. Hence PZC may not be the only factor that determines the adsorption or degradation in the case of a neutral molecule like AMS. Lack of direct correlation between the PZC and the adsorption/degradation rate can also be due to the fact that the PZC itself depends on a number of factors including the size and nature of dispersion of the particles, chemistry of substrates and the intermediates and the type of catalyst itself. Similar observations are reported by other workers also [28, 33, 124].

3.3.6 Corrosion of ZnO under solar photocatalysis at different pH

The corrosion of ZnO catalyst under extreme acidic and alkaline conditions as well as photo-corrosion under the experimental conditions was tested by weight-loss method at different pH. 60 mL of AMS solution (25 mg/L) was taken in different 250 mL beakers and the pH was adjusted as required. ZnO (80 mg/L) is added to each of these beakers and mixed well. The suspensions were kept for specific period of time (1 and 4 hr).

The suspension in each beaker is centrifuged and the clear supernatant solution was transferred to previously weighed (weight: A) dry 250 mL beakers. The clear AMS solution in each beaker was evaporated at 100°C. The weight of the dry beaker was determined, when the evaporation was complete. It was then dried again for 1 hr and weighed. The process was repeated until the weight became constant (weight: B).

(B-A) corresponds to the ZnO dissolved in water. If W is the weight of ZnO suspended in water initially,

The % corrosion is: $(B-A) \times 100 / W$ (59)

The same experiments were repeated with the suspension subjected to solar irradiation. From the weight difference, the percentage corrosion of ZnO was calculated. The results are presented in figure 3.9.

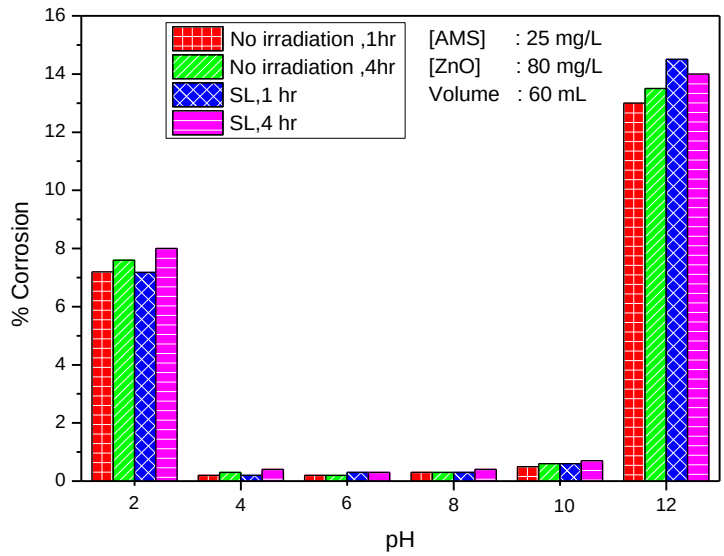

Fig. 3.9: Corrosion of ZnO at different pH in the presence and absence of solar irradiation

The corrosion is found to be negligible in the pH range of 4 to 10. Irradiation by sunlight has no influence on the corrosion, at all pH. Similarly, there is no significant change in the corrosion after 1and 4 hr of irradiation at pH below 12. The corrosion is ~8% at pH 2 and ~15% at pH 12 after 4 hr. Since the investigation of the photocatalytic degradation of AMS is carried out at pH~5.6, corrosion can be considered as negligible under the condition of the study.

3.3.7 Effect of Acetophenone

Acetophenone (ACP) is detected as the major reaction intermediate in the photocatalytic degradation of AMS. Maximum amount of ACP detected at any point of time was less than 10% of the amount expected from AMS degradation thus showing that the former is also degrading fast (figure 3.10). In the early stages of the reaction the degradation of AMS proceeds smoothly. It was found that when sufficient concentration of ACP is built up in the system, the degradation of AMS slows down. The increasing competition from the ACP for surface sites and ROS and decrease in concentration of AMS may be responsible for this decrease in degradation. The fact that the concentration of insitu formed ACP increases very slowly or levels off even when the degradation of AMS continues, indicates the facile degradation of ACP.

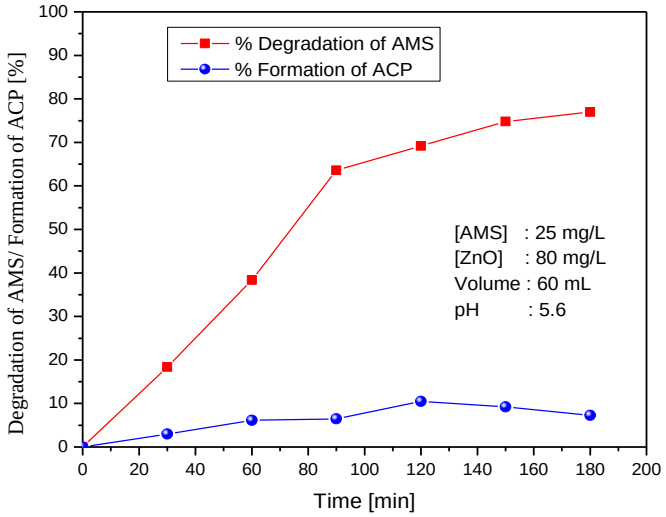

Fig. 3.10: Photocatalytic degradation of AMS and the concurrent formation of ACP on ZnO.

This is further verified by extra addition of ACP in the reaction system. The effect of externally added ACP on the photocatalytic degradation of AMS is shown in figure 3.11.

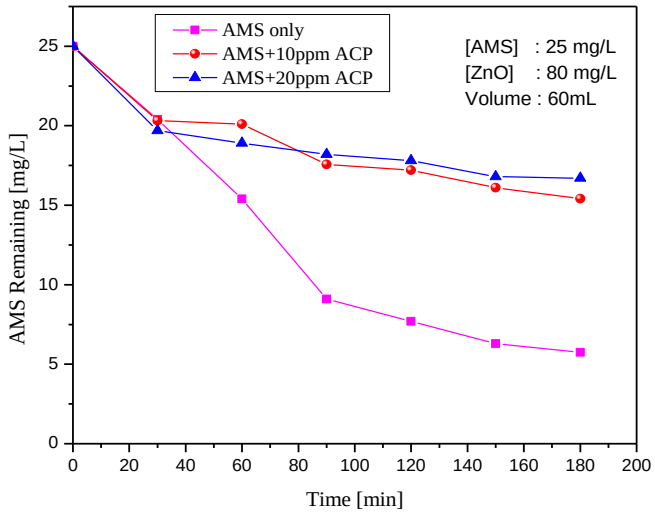

Fig. 3.11: Effect of ACP on the photocatalytic degradation of AMS on ZnO

In the presence of added ACP, the degradation of AMS decreases from 38 to 25% in first 60 min and from 70 to 30% in 120 min. At the same time, the extent of inhibition does not increase corresponding to the increase in added ACP concentration. At both concentrations of added ACP the pattern of inhibition remains more or less the same (with minor variations). The ACP formed insitu from AMS degradation also will be adding to its net concentration in the system. Thus even at relatively lower concentration, ACP is capable of inhibiting the degradation of AMS which is a clear indication of the competition between the two species for accessing the surface sites and/or interaction with the ROS. According to Xu and Langford [125], ACP undergoes facile degradation yielding dihydroxy acetophenone isomers as intermediates during photocatalysis. These intermediates get degraded faster as indicated by the fact that their concentration does not increase with time of irradiation. The intermediates being carbonyl compounds having negatively charged oxygen atom on the carbonyl group can get adsorbed on the positively charged ZnO surface at the acidic pH even in presence of higher concentration of strongly adsorbing species such as AMS. The optimum AMS degradation also happens in the acidic pH range as shown earlier. Thus there is strong competition between AMS, ACP and various intermediates for the surface sites of ZnO. But ACP is competitively better placed for adsorption because of its structural advantage which is responsible for its higher degradation. This also accounts for the significant reduction in AMS degradation in presence of ACP.

Further verification of this effect was done by investigating the photocatalytic degradation of ACP in presence of added AMS. The results are shown in figure 3.12.

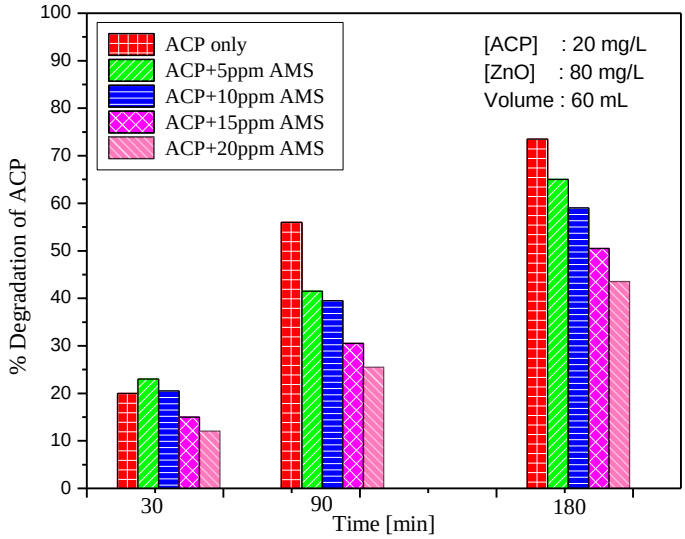

Fig. 3.12: Effect of AMS on the photocatalytic degradation of ACP on ZnO

It was found that at lower concentration of added AMS, in the early periods of irradiation the effect is negligible or appear slightly positive, possibly due to the insitu formation of ACP. As the AMS concentration is increased, the inhibition of ACP degradation also increases with time. This study reconfirms the competition between AMS and ACP for the adsorption sites and ROS. The mutual inhibition of the photocatalytic degradation of AMS and ACP by one another depends primarily on their relative concentration. Thus in the AMS/ZnO/sunlight system, initially ACP formation is less and hence inhibition also is less. As the irradiation continues, more ACP is formed and its rate of degradation also increases. Correspondingly the degradation of AMS decreases (as seen from figure 3.11). Comparison of the figures 3.11 and 3.12 shows that ACP inhibits the degradation of AMS more than the inhibition of the degradation of ACP by AMS. However, this conclusion need not be very precise since

the insitu formation of ACP from AMS during the photocatalytic degradation of the latter also needs to be taken into account.

The relative adsorption of AMS and ACP individually as well as in the presence of one another is experimentally verified and the results are presented in table 3.4.

Table 3.4: Adsorption of AMS and ACP over ZnO individually as well as in the presence of one another.

TIME [min]	20 mg/L AMS+ ZnO	20mg/L AMS+ 5ppm ACP+ ZnO	20mg/L ACP + ZnO	20mg/L ACP+ 5ppm AMS+ ZnO
	% Adsorption of AMS	% Adsorption of AMS	% Adsorption of ACP	% Adsorption of ACP
0	0	0	0	0
30	43.0	38.4	2.0	2.0
60	43.0	36.0	3.5	2.0
90	44.0	38.5	4.0	1.5
120	45.2	37.5	4.5	2.0
150	48.0	35.5	4.0	2.5
180	48.5	38.5	3.5	3.0

AMS shows considerable adsorption over ZnO catalyst compared to ACP, even though the chemical structure as explained earlier was expected to favour the latter. Hence it is possible that under light irradiation when the catalyst surface as well as substrate molecules are activated, the nature of adsorption and/or interaction can be different. It is also possible that the processes in the reaction bulk may be favoring ACP more than AMS. Hence irrespective of the poor adsorption in the dark, the degradation of ACP (or the dihydroxy intermediates formed from it) is comparable to that of AMS and the former inhibits the degradation of the latter more than the other way.

The adsorption of both AMS and ACP decreases moderately in presence of one another. Hence it is quite probable that the mutual inhibitive effect on the photocatalytic degradation of either component is at least partly a surface based process. The inhibition may be attributed to the competition between the components for surface sites, photons as well as the ROS. Consequently the interactions of each component with the ROS is less in presence of one another in the bulk as well as on the surface and the degradation is inhibited correspondingly.

3.3.8 Formation and fate of H_2O_2

H_2O_2 is detected as a co-product in the photocatalytic degradation of AMS, ACP as well as many other organic compounds [37, 38, 103, 111,114,119]. However, its concentration does not increase corresponding to the degradation of the pollutant and is stabilized or even decreases before the pollutant degradation is complete [figure 3.13].

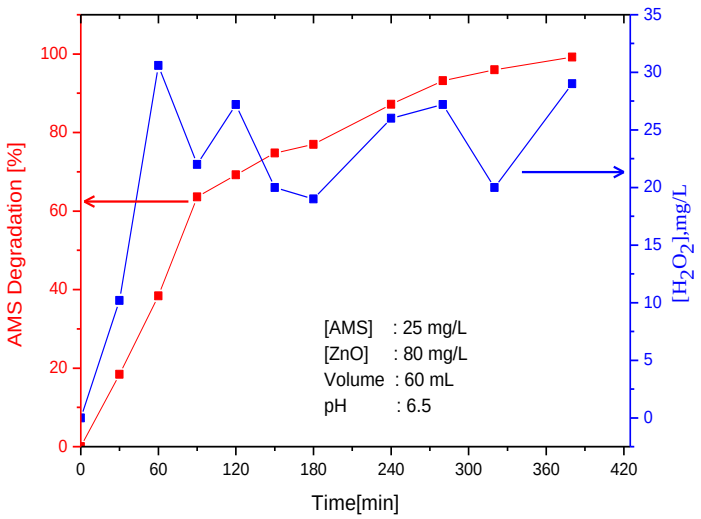

Fig. 3.13: Formation and fate of H_2O_2 during the photocatalytic degradation of AMS on ZnO

There is no direct correlation between the concentration of the pollutant degraded and the quantity of H_2O_2 detected. Earlier studies have attributed this to the concurrent formation and decomposition of H_2O_2 which results in stabilization/periodic increase and decrease in the concentration, i.e., oscillation [113, 126]. Depending on the domination of formation or decomposition rate, the net concentration of H_2O_2 at any point of time varies resulting in periodic crests and troughs (figure 3.13).

Various steps leading to the concurrent formation (equations 60-66) and decomposition (equations 67-73) of H_2O_2 may be summarized as follows [113, 126-130]:

$$ZnO + h\nu \rightarrow Zn\,(e^-) + Zn\,(h^+) \quad (60)$$

$$O_2 + e^- \rightarrow O_2^{-\bullet} \quad (61)$$

$$O_2^{-\bullet} + H^+ \rightarrow HO_2^{\bullet} \quad (62)$$

$$2HO_2 \rightarrow H_2O_2 + O_2 \quad (63)$$

$$O_2^{-\bullet} + HO_2\bullet \rightarrow O_2 + HO_2^{-\bullet} \quad (64)$$

$$HO_2^- + H^+ \rightarrow H_2O_2 \quad (65)$$

$$^{\bullet}OH + {}^{\bullet}OH \rightarrow H_2O_2 \quad (66)$$

$$H_2O_2 + h\nu \rightarrow 2{}^{\bullet}OH \quad (67)$$

$$H_2O_2 + O_2^{-\bullet} \rightarrow {}^{\bullet}OH + OH^- + O_2 \quad (68)$$

$$H_2O_2 + e^- \rightarrow {}^{\bullet}OH + OH^- \quad (69)$$

$$2OH^- + h^+ \rightarrow {}^{\bullet}OH + OH^- \quad (70)$$

$$H_2O_2 + 2\,h^+_{vb} \rightarrow O_2 + 2H^+ \quad (71)$$

$$H_2O_2 + OH/h^+ \rightarrow HO_2\bullet + H_2O/H^+ \quad (72)$$

$$HO_2\bullet + {}^{\bullet}OH \rightarrow H_2O + O_2 \quad (73)$$

Repeated attacks by the $O_2^{-\bullet}$/$^{\bullet}OH$ /$HO_2\bullet$ radicals on the pollutant nuclei ultimately lead to the mineralization producing mainly CO_2 and water. This is further confirmed by the progressive decrease and eventual disappearance of chemical oxygen demand (COD) as the reaction progresses.

3.3.9 Mineralization of AMS in presence of ZnO/sunlight

One of the advantages of semiconductor mediated photocatalysis is the possibility of complete mineralization of the pollutant. In the case of AMS degradation, the mineralization is confirmed by the progressive decrease and eventual disappearance of the chemical oxygen demand (COD) as the reaction proceeds, as shown in figure 3.14.

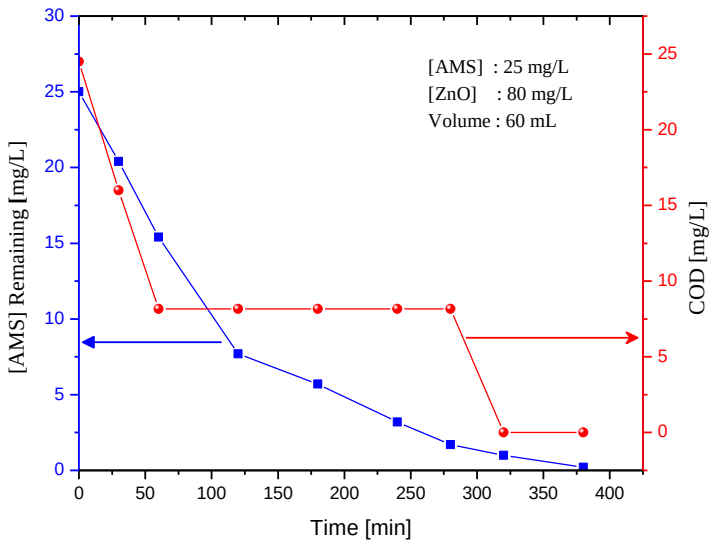

Fig. 3.14: Mineralization of AMS in solar photocatalytic degradation of AMS

As can be seen from the figure, the COD remains steady over a long time of irradiation indicating that the intermediates formed during the

degradation are more stable under photocatalysis. Further degradation of the intermediates leading to eventual mineralization occurs after ~5hr only and it is much faster thereafter. It is possible that the degradation may be yielding another set of less stable intermediates and these are not detected due to the limitation of the analytical method used. The study shows that sunlight induced zinc oxide mediated photocatalysis can be used as an effective method for the removal and mineralization of trace amounts of AMS from industrial effluent.

3.3.10 Effect of added H_2O_2

The effect of externally added H_2O_2 on the photocatalytic degradation of AMS and the formation of ACP is investigated at two different concentrations, i.e. 10 and 20 mg/L of H_2O_2. The results are shown in figure 3.15.

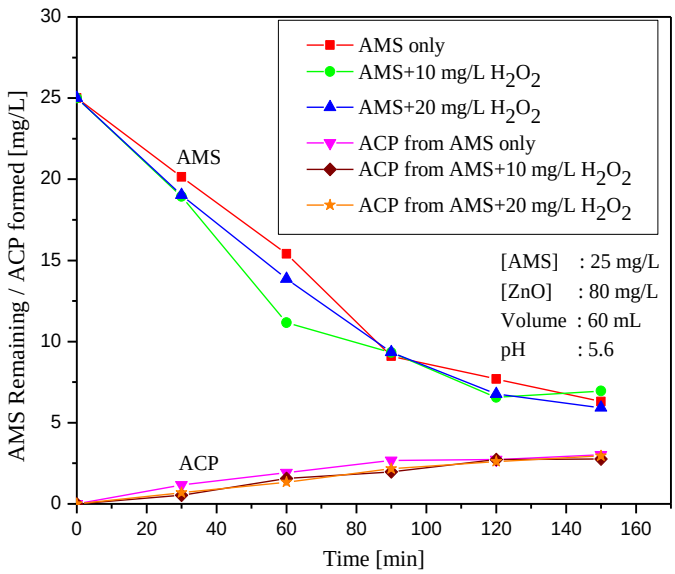

Fig. 3.15: Effect of H_2O_2 on the photocatalytic degradation of AMS and formation of ACP

Even though the added H_2O_2 slightly enhances the degradation of AMS initially, the enhancement is steady or slightly less at higher concentration (20 mg/L) of H_2O_2. The rate of enhancement gradually decreases and eventually the rate of degradation becomes comparable to that without added H_2O_2. This can be explained by the fact that there is an optimum concentration upto which H_2O_2 can act as a promoter of AMS degradation and together with the insitu formed H_2O_2 the concentration may have reached that critical level towards the later stages of reaction. Beyond this optimum, H_2O_2 plays the role of an inhibitor which is responsible for the slightly lower degradation of AMS. Once the insitu formed H_2O_2 is sufficient for the optimum, the effect of added H_2O_2 becomes superfluous and indistinguishable. Similarly, the formation of ACP also is slightly inhibited initially and stabilized later on. The dual role of H_2O_2 as a promoter as well as an inhibitor of photocatalytic degradation has been reported by others also and it depends on the concentration of reactants, reaction conditions and the nature of interactions [118, 130].

The enhancement in the photodegradation of AMS by H_2O_2 can be explained based on its role as an electron acceptor and consequent inhibition of the recombination of photogenerated electrons and holes. H_2O_2 can also produce reactive $^{\bullet}OH$ radicals as in equations 67-69 which enhance the degradation of the pollutant**.** But, at higher concentrations of H_2O_2, which is either formed insitu in the system or by external addition, it acts more as a hole scavenger as well as an $^{\bullet}OH$ scavenger as shown in equations 71 and 72. Under this condition, H_2O_2 becomes a major competitor to the substrate for available ROS on the surface of the catalyst as well as in the bulk of the solution, leading to its self decomposition as well as the reduction in AMS

degradation. This inhibition by H_2O_2 at higher concentration as a result of its competition with organic pollutants for the ROS has also been reported earlier [129]. It was found experimentally that the adsorption of H_2O_2 on ZnO is negligible [127]. Hence most of the H_2O_2 will be in solution. This is also responsible for its competition with the substrate for ROS in the bulk of the suspension. The adsorption of H_2O_2 on the surface of another semiconductor oxide, i.e., TiO_2 has also been proven to be negligible [131].

3.3.11 Effect of humic acid

Humic substances are ubiquitous and are defined as a category of naturally occurring biogenic heterogeneous organic substances that can be generally characterized as being yellow-brown in colour and having high molecular weights [132]. These are also defined as the fraction of filtered water that adsorb on XAD-8 resin (non-ionic polymeric adsorbent) at pH 2 [99]. Humic substances are the main constituents of the dissolved organic carbon (DOC) pool in surface and ground waters, and commonly impart a yellowish-brown colour to the water system [133]. Their size, molecular weight, structure, elemental composition and the number as well as the position of functional group may vary depending on the origin and age. The concentration of the humic substances also vary from place to place [134]. They are known to affect the behavior of the pollutants such as trace metal speciation, toxicity [135,136], solubilization, adsorption [137,138] as well as the aqueous photochemistry [139] in natural environments.

Humic substances are known to influence the efficiency of photocatalytic degradation of water pollutants. Hence the effect is tested on ZnO mediated photodegradation of AMS. The result is presented in figure 3.16.

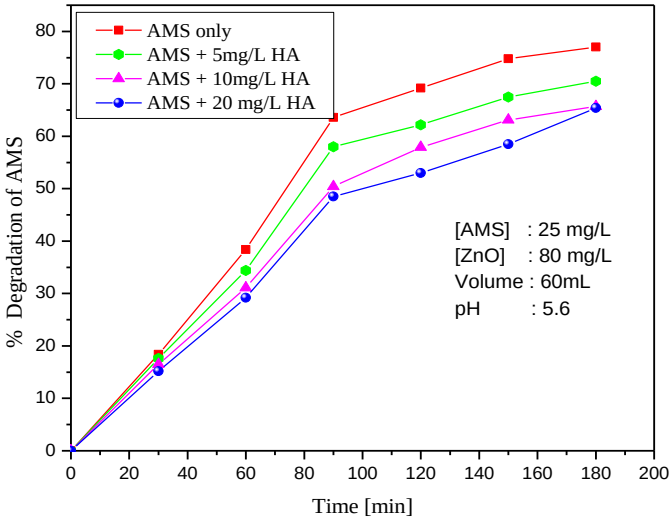

Fig. 3.16: Effect of Humic acid [HA] on the photocatalytic degradation of AMS on ZnO

In the early stages of the reaction, the effect of HA on the degradation of AMS is negligible in the concentration range 5-20 mg/L. But towards the later stages of the reaction, when the concentration of the AMS was significantly reduced, the HA inhibits the degradation. Both inhibition as well as slight enhancement in the degradation of organic pollutants in presence of HA is reported [140]. In the case of N, N-diethyl-m-toluidine (DEET), the degradation is inhibited by natural lignite HA while synthetic HA which is aromatic rich enhances the degradation slightly.

Natural organic matter might affect the photocatalytic process through different mechanisms. The organic matter may absorb light thereby reducing the quantum of light available for the catalyst activation. Since the formation of free radicals such as $^{\bullet}OH$ and the reactive H_2O_2 responsible for the degradation are generated by the light activated surface, the fraction of light intensity available for the surface is important. Humic material also

is an effective free radical scavenger which can consume ROS such as $^{\bullet}OH$ / $HO_2^{\bullet}/O_2^{-\bullet}$ as follows [141]:

$$HA + h\nu \rightarrow HA* \quad (74)$$

$$^{\bullet}OH, HO_2^{\bullet}, O_2^{-\bullet} etc. + HA* \rightarrow \text{Intermediates} \rightarrow \text{Oxidized products} \quad (75)$$

The excited HA (HA∗) will decompose/oxidize eventually. In the present study, the concentration of added HA is kept small to be comparable to that in natural waters in local streams and ponds. In this range HA does not affect AMS degradation significantly. However, at higher concentrations, HA can inhibit the degradation of AMS, as seen in figure 3.17. The accelerated inhibition at later stages of reaction when the concentration of AMS is quite low compared to HA also confirms this.

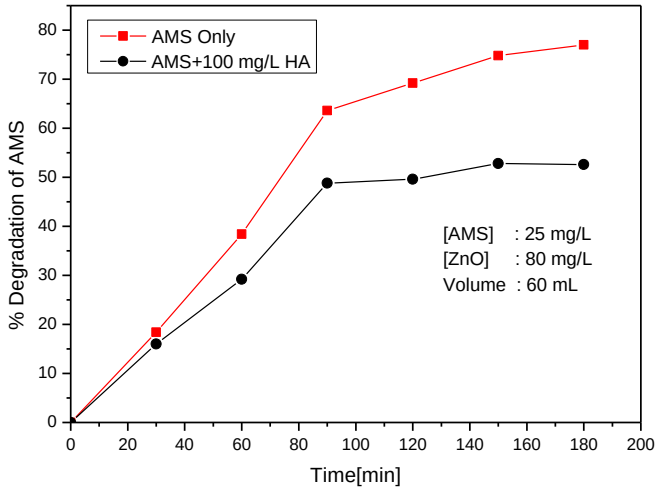

Fig. 3.17: Inhibition of AMS degradation at higher concentration of HA

3.3.12 Effect of oxygen

Oxygen plays an important role in the photocatalytic degradation reactions in aqueous solutions by scavenging the electrons generated

during the photo excitation of ZnO catalyst thereby preventing the possible electron-hole recombination. Thus both electrons and holes will be available for the subsequent generation of free radicals and their interaction with the pollutant. The photogenerated electron is picked up by the O_2 molecules to produce superoxide radical anion and other reactive species. Hirakawa et al. [142] demonstrated the role of dissolved O_2 and superoxide ion in TiO_2 photocatalysis and even developed a method to follow photocatalytic reactions by measuring the consumption of dissolved oxygen. In order to study the effect of O_2 on the photocatalytic degradation AMS, the reaction system is deaerated with N_2 for 2 min and the experiments were carried out under otherwise identical conditions. The deaeration was done only for this limited period to avoid any possibility of evaporation loss of the pollutant. The results are shown in figure 3.18.

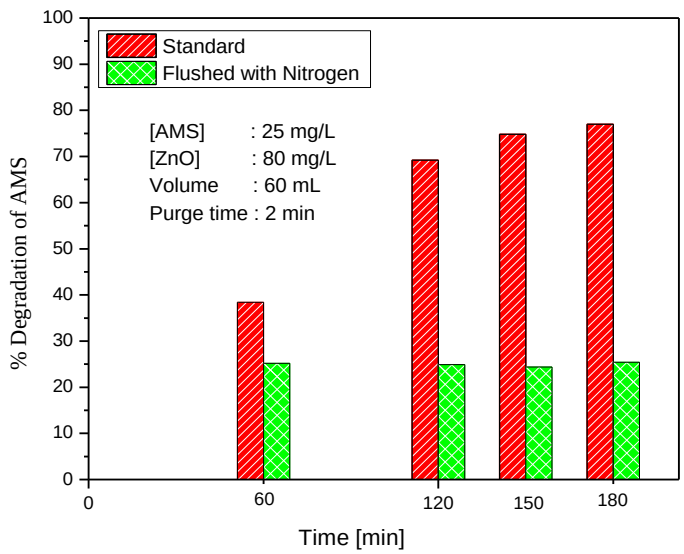

Fig. 3.18: Effect of O_2 on the photocatalytic degradation of AMS on ZnO

The results clearly show that O_2 plays an important role in the photocatalytic degradation of organic pollutants. Since the deaeration was done only for a short duration, it is possible that the adsorbed O_2 and part of dissolved O_2 may not have been fully removed from the system. Hence there is reasonable amount of degradation even in the N_2 flushed reaction system until this O_2 is consumed. Once the O_2 is completely consumed, there is no further increase in the degradation. This is evident from the steady degradation of AMS in the deaerated system at all time periods of irradiation from 60 to 180 min.

3.3.13 Effect of anions

Industrial effluents invariably contain different types of electrolytes which can influence the photocatalytic degradation of pollutants either positively or negatively. The anions/electrolytes present in the effluent water can compete with the pollutant molecules or the intermediates for the active sites on the catalyst surface. They can also interact with various ROS and deactivate them. These ions can reduce the amount of light quanta reaching the catalyst surface and can also lead to the formation of undesirable byproducts in the system. All these processes can affect the photocatalytic degradation and mineralization efficiency. Hence the effect of some commonly occurring anions in the industrial wastewater on the photocatalytic degradation efficiency of AMS is investigated. The anions studied are fluoride, chloride, bromide, iodide, carbonate, bicarbonate, sulphate, nitrate, acetate, oxalate and phosphate at varying concentrations and at different reaction times. The cation is kept the same (Na^+). The effect of concentration of the anions and the reaction time

on the degradation is investigated and the results are shown in figures 3.19 and 3.20.

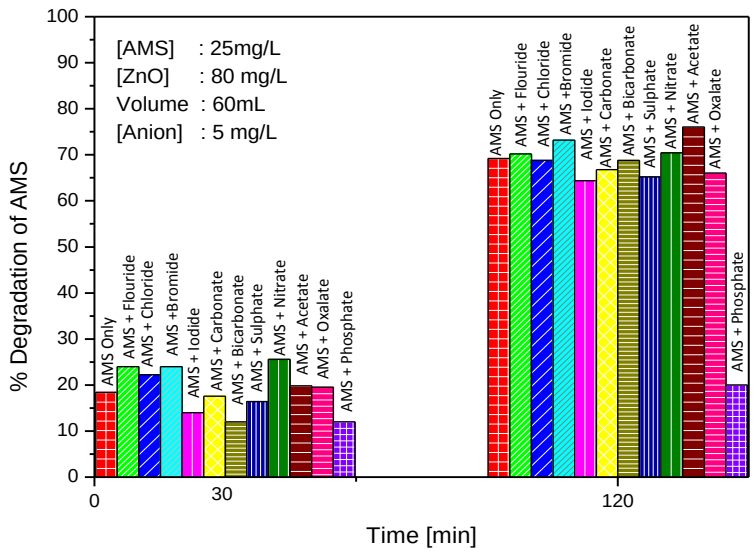

Fig. 3.19: Effect of anions on the degradation of AMS after 30 and 120 min of irradiation.

At lower concentration of anions (5 mg/L) and in the early stages the degradation reaction (30 min), fluoride, chloride, bromide, and nitrate ions enhance the degradation while iodide, bicarbonate, sulphate, and phosphate ions inhibit the degradation. Carbonate, oxalate and acetate ions have practically 'no effect'.

The effect of anions (5 mg/L) on the degradation of AMS after 30 min of reaction may be summarized as:

Inhibition: $PO_4^{3-} \approx HCO_3^- > I^- > SO_4^{2-}$(mild inhibition)

No effect: CO_3^{2-}, $C_2O_4^{2-}$, CH_3COO^-

Enhancement: $NO_3^- > F^- \approx Br^- > Cl^-$

However, after extended irradiation/reaction time (120 min) the effect does not follow the same trend. In this case, PO_4^{3-} continues to be a strong inhibitor, while the effect of I^- changes from strong inhibition to mild inhibition. Effect of HCO_3^- changes from 'inhibition' to 'no effect'. Similarly the strong enhancement by F^- and NO_3^- changes to 'no effect' while CH_3COO^- becomes a mild enhancer.

The effect of anions at 5 mg/L concentration, after 120 min of reaction may be summarized as:

Inhibition: $PO_4^{3-} > I^-$ (mild In) $\approx SO_4^{2-} \approx C_2O_4^{2-} \approx CO_3^{2-}$
No effect: F^-, Cl^-, HCO_3^-, NO_3^-
Enhancement: $CH_3COO^- > Br^-$

The effect of concentration of the anions on the degradation is investigated at 5 and 15 mg/L and the results after 30 min of irradiation are plotted in figure 3.20.

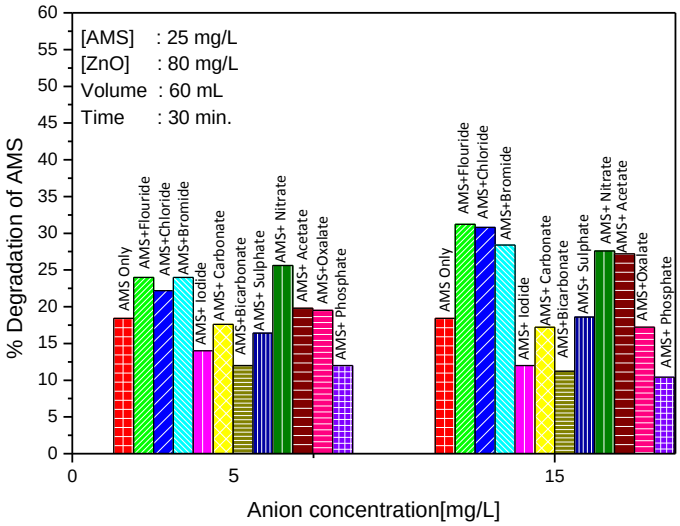

Fig. 3.20: Effect of various anions at different concentrations on the degradation of AMS

At 5 mg/L concentration, NO_3^- is the best enhancer while at 15 mg/L concentration, F^- and Cl^- are the best enhancers. CH_3COO^- and Br^- also remain as enhancers at 15 mg/L. PO_4^{3-}, HCO_3^- and I^- remain as strong inhibitors at both concentrations.

The effect of anions at the two different concentrations after 30 min of irradiation can be summarized as:

5 mg/L:

Inhibition: $PO_4^{3-} \approx HCO_3^- > I^- > SO_4^{2-}$

No effect: CO_3^{2-}, $C_2O_4^{2-}$, CH_3COO^-

Enhancement: $NO_3^- > F^- \approx Br^- > Cl^-$

15 mg/L:

Inhibition: $PO_4^{3-} \approx HCO_3^- \approx I^- > CO_3^{2-}$ (mild inhibition) $\approx C_2O_4^{2-}$

No effect: SO_4^{2-}

Enhancement: $F^- \approx Cl^- > Br^- > NO_3^- \approx CH_3COO^-$

The results show that the effect of anion is not consistent and varies with concentration as well as the duration of the reaction. This indicates that the intermediates formed during the degradation may be interfering with the anion effect. The nature and concentration of the intermediates will vary with reaction time and there will be multitude of complex interactions as the reaction progresses. This makes the prediction of anion effect difficult based on any single parameter. It is also possible that ‘mild enhancement’ and ‘mild inhibition’ and ‘no effect’ can be treated as more or less same, i.e., ‘no effect’.

Since the concentration of the anion and the reaction time are observed to be influencing the rate of degradation of AMS, detailed investigation is made on the effect of these two parameters for each anion and the results are plotted in figures 3.21-3.31.

a) Effect of F^-

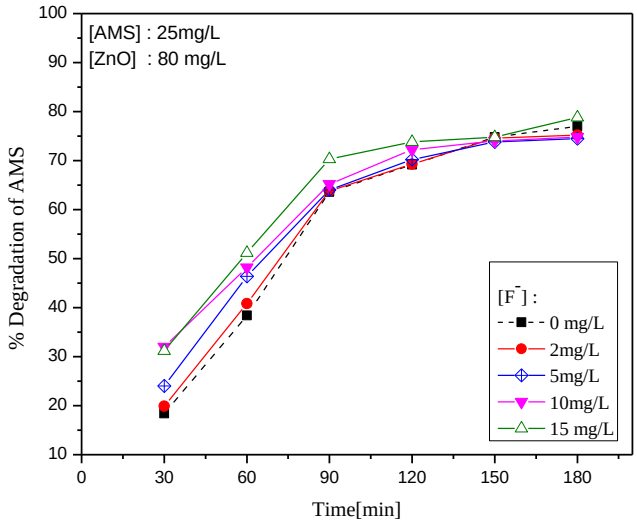

Fig. 3.21: Effect of concentration of F^- and reaction time on the photocatalytic degradation of AMS

Generally F^- is an enhancer at all concentrations and extended reaction times (except at 2 mg/L after 30 min.). However eventually, the 'enhancing' effect becomes 'no effect' towards later stages of reaction (>150 min).

b) Effect of Cl^-

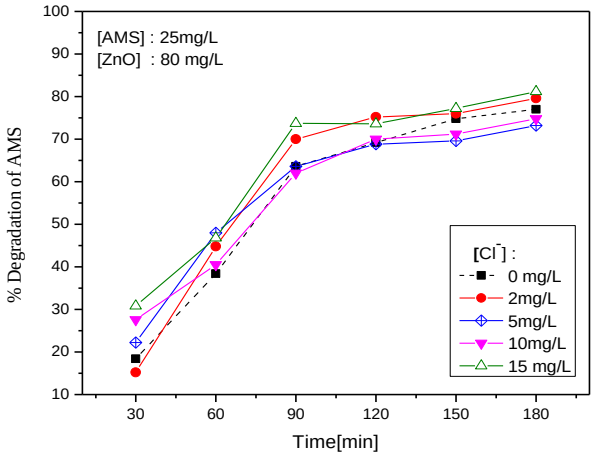

Fig. 3.22: Effect of concentration of Cl^- and reaction time on the photocatalytic degradation of AMS

Cl^- is also an enhancer throughout. However, towards the later stage of the reaction, when most of the substrate has disappeared, Cl^- effect can be termed as 'no effect' or mild inhibition.

c) Effect of Br^-

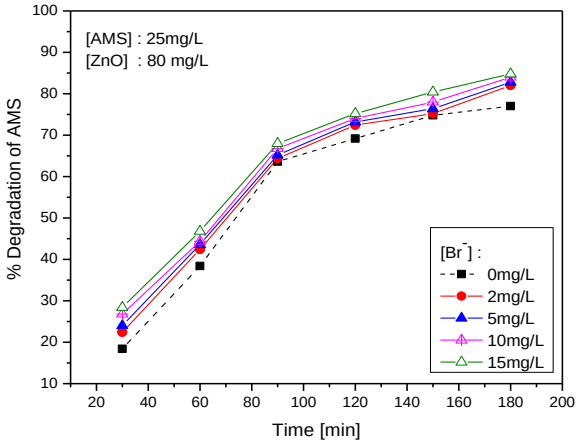

Fig. 3.23: Effect of concentration of Br^- and reaction time on the photocatalytic degradation of AMS

Br^- is an enhancer throughout at all concentrations and reaction times.

d) Effect of I^-

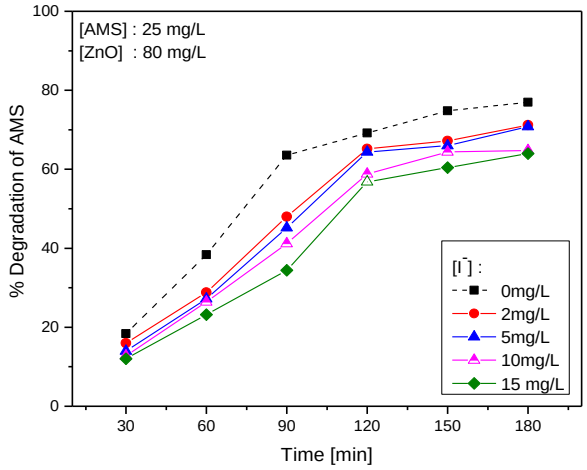

Fig. 3.24: Effect of concentration of I^- and reaction time on the photocatalytic degradation of AMS

I^- is a strong inhibitor of the degradation at all concentrations and all reaction times.

e) Effect of CO_3^{2-}

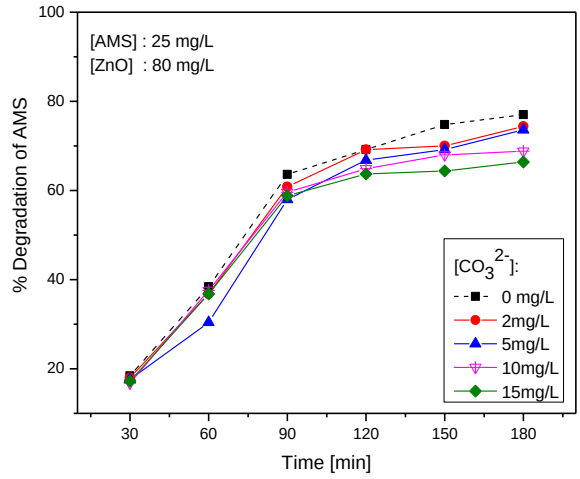

Fig. 3.25: Effect of concentration of CO_3^{2-} and reaction time on the photocatalytic degradation of AMS

CO_3^{2-} is generally an inhibitor. However, in the early stages of the reaction, the effect can be termed as 'no effect'.

f) Effect of HCO_3^-

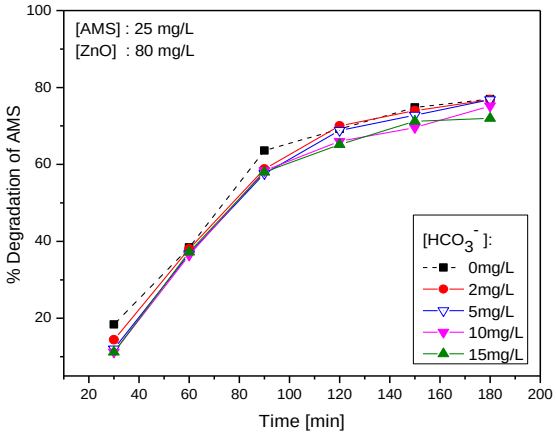

Fig. 3.26: Effect of concentration of HCO_3^- and reaction time on the photocatalytic degradation of AMS

HCO_3^- is a mild inhibitor. However, in most cases of concentration and reaction time variation, this anion has practically 'no effect'.

g) Effect of SO_4^{2-}

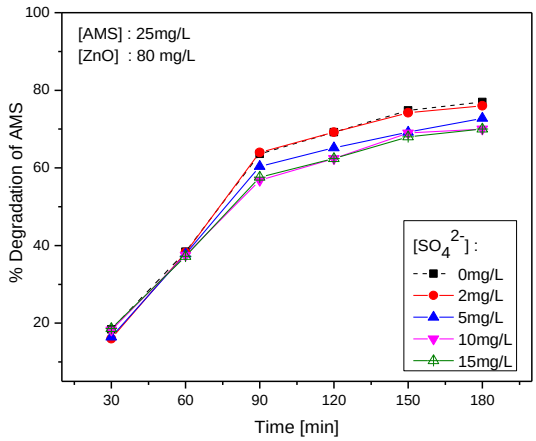

Fig. 3.27: Effect of concentration of SO_4^{2-} and reaction time on the photocatalytic degradation of AMS

The effect of SO_4^{2-} varies from 'no effect' to 'mild inhibition'. In the early stages of the reaction when the concentration of substrate is significant, SO_4^{2-} ion has practically 'no effect'.

h) Effect of NO_3^-

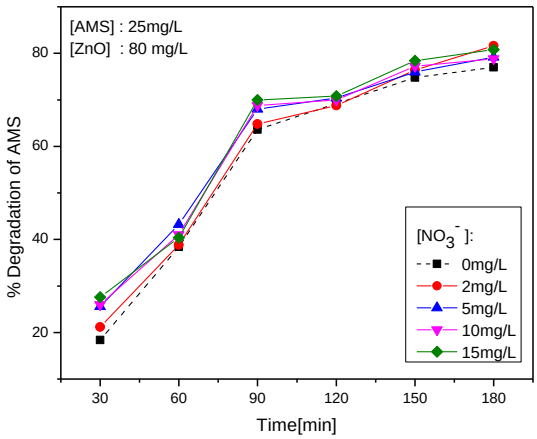

Fig. 3.28: Effect of concentration of NO_3^- and reaction time on the photocatalytic degradation of AMS

NO_3^- is a mild enhancer at all concentrations and reaction times.

i) Effect of CH_3COO^-

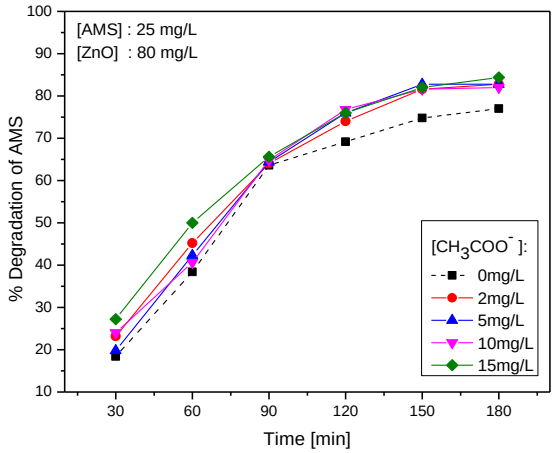

Fig. 3.29: Effect of concentration of CH_3COO^- and reaction time on the photocatalytic degradation of AMS

CH_3COO^- ion is an enhancer at all concentrations and reaction times. At very low concentration and early reaction time the enhancing effect is mild enough to be termed as 'no effect'

j) Effect of $C_2O_4^{2-}$

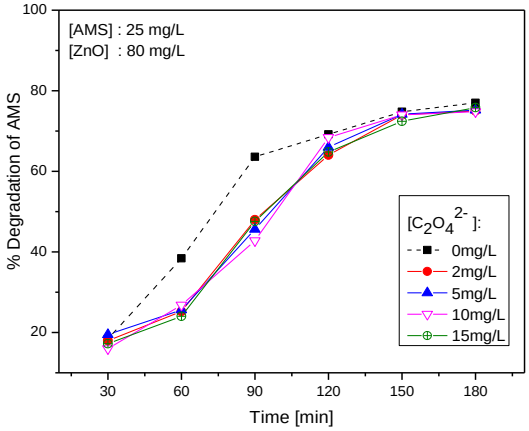

Fig. 3.30: Effect of concentration of $C_2O_4^{2-}$ and reaction time on the photocatalytic degradation of AMS

Oxalate is a clear inhibitor. Towards the later stages of the reaction, the inhibition becomes 'no effect'. However, concentration of the anion does not have any influence on the effect.

k) Effect of PO_4^{3-}

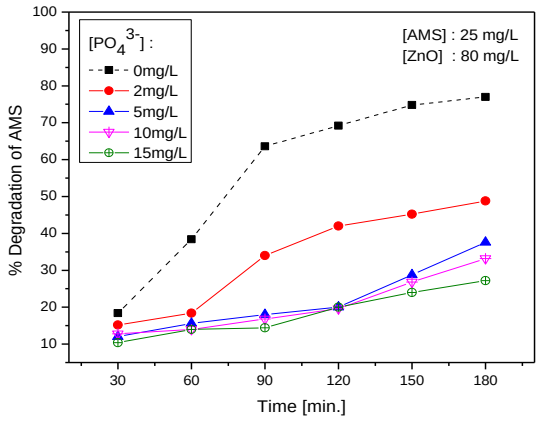

Fig. 3.31: Effect of concentration of PO_4^{3-} and reaction time on the photocatalytic degradation of AMS

PO_4^{3-} is a strong inhibitor of the degradation at all concentrations and reaction times.

The results show that iodide, carbonate, bicarbonate, oxalate, sulphate and phosphate ions inhibit the degradation of AMS, though by varying degrees. Fluoride ion shows enhancement at lower reaction time of 30 and 60 min at almost all concentrations. The enhancement increases with increase in concentration and maximum enhancement was obtained with 15 mg/L of fluoride ion. Similar results are observed in the case of Cl^- and Br^- ions. In the case of CH_3COO^- and NO_3^-, the degradation is enhanced at all concentrations and all reaction times. In the case of the enhancers, the enhancement effect is not much and the effect may even be termed as 'practically no effect', within the limit of experimental error. In any case, the presence of these anions does not adversely affect the degradation of the pollutant in water. PO_4^{3-} as expected, remains as strong inhibitor. I^- also inhibits the degradation. In both cases, the inhibition increases with increase in concentration of the anions. SO_4^{2-} also is a mild inhibitor, while $C_2O_4^{2-}$ is a strong inhibitor in the early stages of the reaction. The inconsistency with time of reaction and varying concentration of anions may be due to a number of complex interactions among the anions, ROS, the substrate and the intermediates on the surface as well as in the bulk. The study clearly illustrates that the anion effect is very complex and unpredictable and each case has to be individually evaluated. The comparative effect of the anions at various concentrations and reaction times is summarized in table 3.5. Since the effect is not significant in many cases, the comparison is only qualitative and applicable only under the reaction conditions used here.

Table 3.5: Qualitative comparison of the effect of anions at various concentrations and reaction times on the photocatalytic degradation of AMS.
[AMS] =25 mg/L, [ZnO] = 80 mg/L)

Time of Reaction, min.	[Anion],* mg/L	Comparative effect
30	2	Enhancement: $CH_3COO^- > Br^- > NO_3^-$ No effect: CO_3^{2-}, $C_2O_4^{2-}$, F^-, Cl^-, SO_4^{2-} Inhibition: $HCO_3^- > PO_4^{3-} > I^-$
	5	Enhancement: $NO_3^- > F^- = Br^- > Cl^-$ No effect: CO_3^{2-}(mild inh), CH_3COO^-(mild en) , $C_2O_4^{2-}$ Inhibition: $PO_4^{3-} \approx HCO_3^- > I^- > SO_4^{2-}$
	10	Enhancement: $F^- > Cl^- \approx Br^- > NO_3^- > CH_3COO^-$ No effect: SO_4^{2-} Inhibition: $HCO_3^- > PO_4^{3-} > I^- > C_2O_4^{2-} > CO_3^{2-}$
	15	Enhancement: $F^- \geq Cl^- > Br^- > NO_3^- \geq CH_3COO^-$ No effect: SO_4^{2-} Inhibition: $PO_4^{3-} \geq HCO_3^- \geq I^- > C_2O_4^{2-} = CO_3^{2-}$
60	2	Enhancement: $CH_3COO^- > Cl^- > Br^- > F^-$ No effect: $HCO_3^- \approx SO_4^{2-} \approx NO_3^-$ Inhibition: $PO_4^{3-} > C_2O_4^{2-} > I^- > CO_3^{2-}$
	5	Enhancement: $Cl^- > F^- > Br^- > NO_3^- > CH_3COO^-$ No effect: HCO_3^-, SO_4^{2-} Inhibition: $PO_4^{3-} > C_2O_4^{2-} > I^- > CO_3^{2-}$
	10	Enhancement: $F^- > Cl^- > Br^- > NO_3^- > CH_3COO^-$ No effect: CO_3^{2-}, SO_4^{2-}, HCO_3^- Inhibition: $PO_4^{3-} > I^- > C_2O_4^{2-}$
	15	Enhancement: $F^- > CH_3COO^- > Cl^- = Br^-$ No effect: CO_3^{2-}, HCO_3^-, NO_3^-, SO_4^{2-} Inhibition: $PO_4^{3-} > I^- > C_2O_4^{2-}$
	2	Enhancement: Cl^- No effect: F^-, Br^-, SO_4^{2-}, NO_3^- , CH_3COO^- Inhibition: : $PO_4^{3-} > C_2O_4^{2-} > I^- > HCO_3^- > CO_3^{2-}$

90	5	Enhancement: NO_3^- No effect: F^-, Cl^-, Br^-, CH_3COO^-, SO_4^{2-} Inhibition: $PO_4^{3-} > I^- > C_2O_4^{2-} > HCO_3^- > CO_3^{2-}$
	10	Enhancement: $NO_3 > Br^-$ No effect: F^-, Cl^-, CH_3COO^- Inhibition: $PO_4^{3-} > I^- > C_2O_4^{2-} > SO_4^{2-} > HCO_3^- > CO_3^{2-}$
	15	Enhancement: $Br^- > Cl^- > F^- \approx NO_3^-$ No effect: CH_3COO^- Inhibition: $PO_4^{3-} > I^- > C_2O_4^{2-} > SO_4^{2-} > HCO_3^- > CO_3^{2-}$
120	2	Enhancement: $Cl^- > CH_3COO^- > Br^-$ No effect: F^-, $CO_3^{2-} \approx HCO_3^- \approx SO_4^{2-} \approx NO_3^-$ Inhibition: $PO_4^{3-} > C_2O_4^{2-} > I^-$
	5	Enhancement: $CH_3COO^- > Br^-$ No effect: F^-, Cl^-, HCO_3^-, NO_3^- Inhibition: $PO_4^{3-} > I^- \geq SO_4^{2-} \geq CO_3^{2-} \approx C_2O_4^{2-}$
	10	Enhancement: $CH_3COO^- > Br^-$ No effect: F^-, Cl^-, HCO_3^-, NO_3^-, $C_2O_4^{2-}$ Inhibition: $PO_4^{3-} > I^- > SO_4^{2-} > CO_3^{2-}$
	15	Enhancement: $Br^- > CH_3COO^- > F^- \approx Cl^-$ No effect: NO_3^- Inhibition: $PO_4^{3-} > I^- > SO_4^{2-} > CO_3^{2-} > C_2O_4^{2-} > HCO_3^-$
150	2	Enhancement: CH_3COO^- No effect: F^-, Cl^-, Br^-, HCO_3^-, SO_4^{2-}, NO_3^-, $C_2O_4^{2-}$ Inhibition: $PO_4^{3-} > I^- > CO_3^{2-}$
	5	Enhancement: CH_3COO^- No effect: F^-, Br^-, HCO_3^-, $C_2O_4^{2-}$, NO_3^- Inhibition: $PO_4^{3-} > I^- \approx SO_4^{2-} > CO_3^{2-} > Cl^-$
	10	Enhancement: CH_3COO^- No effect: F^-, Cl^-, Br^-, NO_3^-, $C_2O_4^{2-}$ Inhibition: $PO_4^{3-} > I^- > CO_3^{2-} > SO_4^{2-} > HCO_3^-$
	15	Enhancement: $Br^- > CH_3COO^- > NO_3^-$ No effect: F^-, Cl^-, $C_2O_4^{2-}$ Inhibition: $PO_4^{3-} > I^- > CO_3^- > SO_4^{2-} > HCO_3^-$

180	2	Enhancement: CH_3COO^- > Br^- > NO_3^- > Cl^- No effect: F^-, HCO_3^-, SO_4^{2-}, $C_2O_4^{2-}$ Inhibition : PO_4^{3-} > I^- > CO_3^{2-}
	5	Enhancement: Br^- = CH_3COO^- No effect: F^-, Cl^-, CO_3^{2-}, HCO_3^-, $C_2O_4^{2-}$, NO_3^- Inhibition : PO_4^{3-} >I^- > SO_4^{2-}
	10	Enhancement: CH_3COO^-, Cl^-, Br^-, NO_3^- No effect: F^-, HCO_3^-, $C_2O_4^{2-}$ Inhibition : PO_4^{3-} > I^- > CO_3^{2-} > SO_4^{2-}
	15	Enhancement: CH_3COO^- > Br^- >Cl^- No effect: F^-, NO_3^-, $C_2O_4^{2-}$ Inhibition: PO_4^{3-} > I^- > CO_3^{2-} > SO_4^{2-} > HCO_3^-

* For most of the anions, the effect at very low concentration of 2 mg/L is different from other concentrations. May be at this concentration, the effect is not much significant and is subject to inconsistency in interpretation.

The results show that it is difficult to make any general conclusion on the anion effect quantitatively and comparatively, at least in the range of parameters investigated here. However, qualitatively it may be concluded that ions such as CH_3COO^-, NO_3^-, Br^- and to a certain extent F^- are enhancers at almost all concentrations. SO_4^{2-} has generally 'no effect'. PO_4^{3-}, I^-, CO_3^{2-} and to a great extent HCO_3^- function as inhibitors. Hence it will be more appropriate to consider the effect of each anion under specific reaction conditions. Surface characteristics of ZnO, chemistry of the substrate and the intermediates, interaction of these species and the anions with various ROS etc., have to be taken into account while evaluating the anion effect. The inconsistency and unpredictability of anion effect in AOPs have been reported by other workers also [143]. Some of the parameters which can influence the anion effect are briefly discussed below.

3.3.14 Adsorption effect

Competition between the pollutant molecule and the anions for the active sites on the catalyst surface is an important factor in photocatalytic degradation of AMS, as the latter shows considerable adsorption over ZnO catalyst, especially in the acidic pH. The Point of Zero Charge (PZC) of ZnO is ~9±0.3 [144]. The ZnO surface is positively charged when the pH is lower than this value and negatively charged when the pH is higher. Hence the ionization state of the ZnO surface is affected by the pH of the solution as,

$$---Zn - OH + H^{+} \leftrightarrow [Zn\ (OH)_{2}]^{+} \quad (76)$$

$$-- Zn - OH + OH^{-} \leftrightarrow Zn\text{-}O^{-} + H_2O \quad (77)$$

AMS being a neutral molecule, its adsorption pattern is not greatly affected by the pH. However, at the natural pH of the reaction solution, i.e., 5.6, AMS can get adsorbed on the ZnO surface or be in close proximity to the surface. Under acidic pH the anions can get adsorbed strongly on the positively charged surface thereby depriving the AMS molecules from the surface sites. In this context, the adsorption of one of the strongest inhibitors of the degradation, i.e., PO_4^{3-} on ZnO surface under reaction conditions is tested by IR spectroscopy. The results are presented in figure 3.32. The spectra of pure PO_4^{3-}, pure ZnO and ZnO treated with PO_4^{3-} solution at room temperature (adsorption) are recorded. Comparison of the spectral pattern shows that PO_4^{3-} gets adsorbed on the surface.

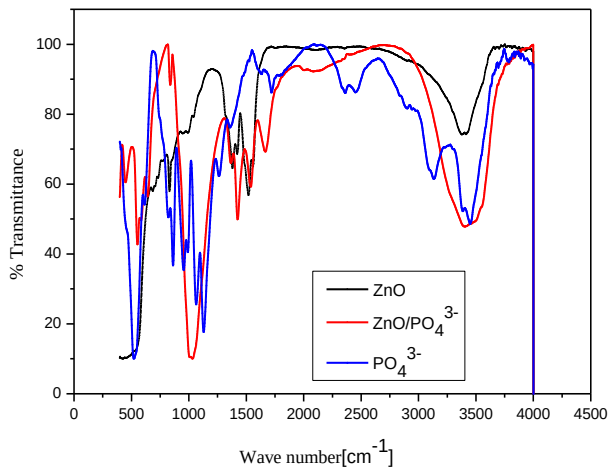

Fig. 3.32: FTIR spectrum of ZnO, PO_4^{3-}, ZnO/PO_4^{3-}

Stronger adsorption of phosphate on semiconductor oxides, such as TiO_2 have been reported earlier [145]. However, all anions which can get adsorbed on the surface do not cause inhibition. Some of the ions such as nitrate, bromide and acetate show enhancement of AMS degradation in spite of their adsorption on ZnO surface. The adsorption of AMS in presence of various anions is measured and the results are presented in table 3.6.

Table 3.6: Adsorption of AMS over ZnO in presence of anion
[AMS] =25 mg/L, [ZnO] =80 mg/L, Volume=60 mL,
[Anion] =10 mg/L Time = 2 hr

Anion	% Adsorption of AMS
No anion	40.0
F^-	30.2
Cl^-	29.4
Br^-	29.0
I^-	31.8
CO_3^{2-}	30.2
HCO_3^-	29.5
SO_4^{2-}	29.5
NO_3^-	30.5
PO_4^{3-}	32.4
CH_3COO^-	28.9
$C_2O_4^{2-}$	30.2

The adsorption is generally inhibited in presence of all the anions. In order to verify whether the preferential adsorption of these anions on the surface of the catalyst and the resultant decrease in the adsorption of the substrate is responsible for the inhibition/enhancement of the degradation of AMS, ZnO is pre-adsorbed with two typical anions, i.e., NO_3^- (enhancer) and PO_4^{3-} (inhibitor) individually and used as the catalyst. The experiment is performed as follows:

1) 1 g of ZnO catalyst is dispersed in 100 mL of each anion solution (30 mg/L) and stirred for 2 hr. The suspension is kept overnight, filtered and dried at room temperature (≈ 30°C) to get anion- pre-adsorbed ZnO.
2) The photocatalytic degradation of AMS is carried out with normal ZnO as well as the anion-pre-adsorbed ZnO as catalyst. The results are shown in figure 3.33

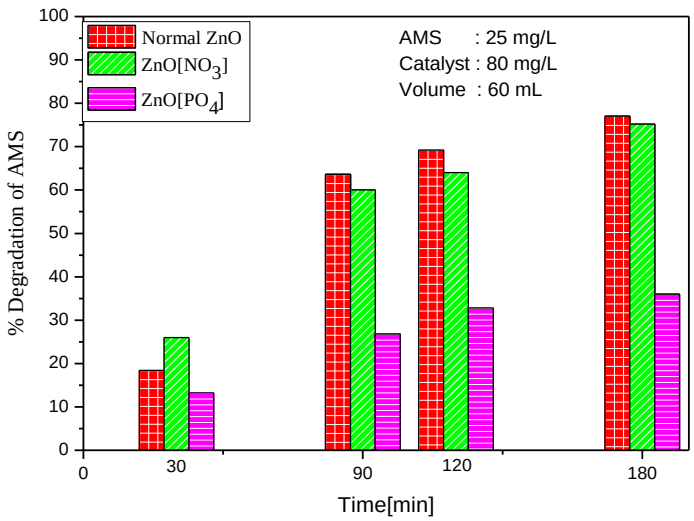

Fig. 3.33: Degradation of AMS in presence of anion pre-adsorbed ZnO catalyst.

The study shows that the degradation of AMS is enhanced initially by the NO_3^- pre-adsorbed ZnO while it is inhibited by the PO_4^{3-} pre-adsorbed catalysts. The initial enhancement by NO_3^- is due to the formation of radical anion on the surface as well as in the bulk and their interaction with the substrate as explained later in this chapter (section 3.3.15). Once the adsorbed NO_3^- is consumed and deactivated by the reactions cited, the NO_3^- pre-adsorbed ZnO behaves similar to pure ZnO. Figure 3.34, which shows the FTIR spectra of ZnO, $NaNO_3$ and ZnO-pre adsorbed with $NaNO_3$ confirms that the adsorption of NO_3^- on ZnO is weak.

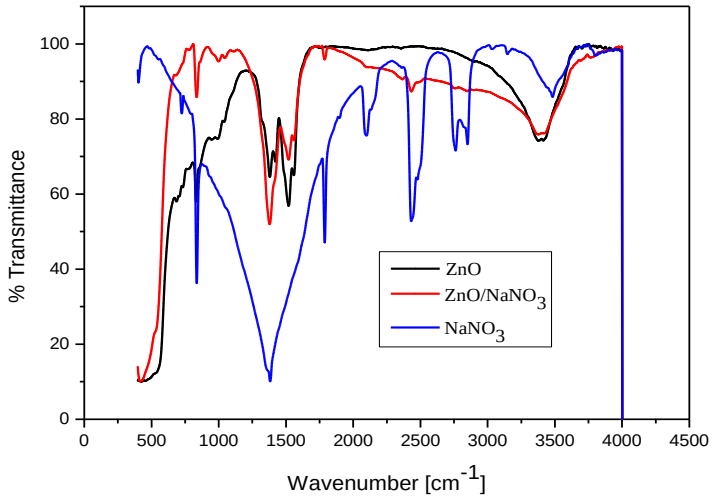

Fig. 3.34: FTIR spectrum of ZnO, NO_3^- , ZnO/ NO_3^-

However, PO_4^{3-} is strongly adsorbed on the surface as shown earlier and consequently PO_4^{3-} pre-adsorbed ZnO functions as inhibitor throughout due to reasons explained earlier.

The study however shows that the adsorption of anions on ZnO cannot be strictly correlated with the enhancement/inhibition of the degradation of AMS. Hence it is not the surface processes alone that are

responsible for the anion effect, even though the inhibition can be partially attributed to the competition between the anions and the substrate.

In order to reconfirm the effect of anions on the photocatalytic degradation of AMS, further experiments were conducted in presence of these two typical anions, NO_3^- and PO_4^{3-}, the former an enhancer and the latter an inhibitor.

1) In the first experiment, AMS degradation in the absence of anion is studied at regular intervals
2) In the second experiment, the degradation of AMS was conducted without any anions upto 60 min and then 5 mg/L of nitrate is added to the system and the degradation is followed at regular intervals
3) In the third experiment, the degradation of AMS was conducted without any anion upto 60 min then 5 mg/L of phosphate is added to the system and the degradation is followed at regular intervals. The results are plotted in figure 3.35.

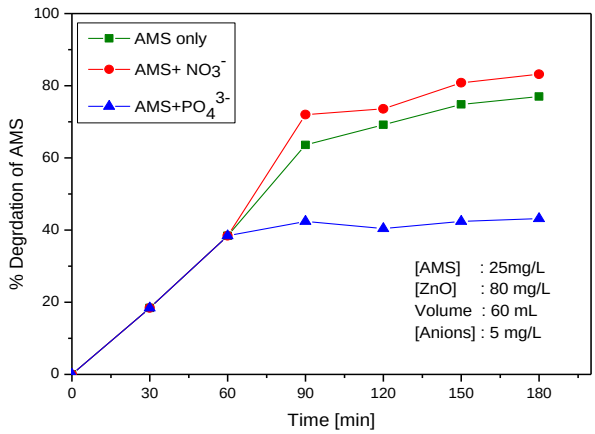

Fig. 3.35: Effect of in-between addition of nitrate and phosphate ions on the photocatalytic degradation of AMS

As expected, nitrate ion enhances the degradation of AMS while phosphate ion acts as a strong inhibitor from the point of addition (60 min).

3.3.15 Scavenging effect of anions

Another mode of evaluating the effect of various anions on the photocatalytic degradation of a substrate is on the basis of their ability to scavenge the insitu formed reactive $^{\bullet}OH$ radicals. The scavenging rate constants of $^{\bullet}OH$ by some of the anions tested here are summarized in table 3.7 [146-148].

Table 3.7: Scavenging rate constants of $^{\bullet}OH$ by various anions

Anions	Scavenging Rate constants ($mol^{-1}s^{-1}$)
NO_3^-	1.4×10^8
Cl^-	4.3×10^9
CO_3^{2-}	3.9×10^8
SO_4^{2-}	1×10^{10}
$H_2PO_4^-$	2×10^4
Ac^-	7.0×10^7
HCO_3^-	8.5×10^6
Br^-	1.06×10^8
I^-	1.1×10^{10}

Fluoride ions having higher oxidation potential than $^{\bullet}OH$ radical is an exception to other halide ions as it cannot be oxidized by the valence band holes or the $^{\bullet}OH$ radicals [149].

Comparison of the effect of various anions, which act as ‘enhancers’, ‘inhibitors’ or having ‘no effect’ with the scavenging rate constant values shows that there is no direct correlation between them. The stronger

inhibitor PO_4^{3-} has very low scavenging rate constant while NO_3^-, which is an enhancer has a higher scavenging rate constant. The scavenging rate constant of other anions also indicate the lack of correlation of this parameter with their effect.

Scavenging of the $^{\bullet}OH$ radical by an ion generates the corresponding radical anion species as follows:

$$^{\bullet}OH + NO_3^- \rightarrow OH^- + NO_3^{-}\bullet \quad (78)$$

$$^{\bullet}OH + SO_4^{2-} \rightarrow OH^- + SO_4^{-}\bullet \quad (79)$$

$$^{\bullet}OH + HCO_3^- \rightarrow H_2O + CO_3^{-}\bullet \quad (80)$$

$$^{\bullet}OH + CO_3^{2-} \rightarrow OH^- + CO_3^{-}\bullet \quad (81)$$

$$CH_3COO^- + {}^{\bullet}OH \rightarrow OH^- + CH_3COO^{\bullet} \rightarrow CH_3^{\bullet} + CO_2 \quad (82)$$

$$^{\bullet}OH + Cl^-/Br^-/I^- \rightarrow OH^- + Cl\bullet / Br\bullet / I\bullet \quad (83)$$

$$Cl\bullet + Cl^- \rightarrow Cl_2^{-}\bullet \quad (84)$$

$$Br\bullet^{\cdot} + Br^- \rightarrow Br_2^{-}\bullet \quad (85)$$

$$I\bullet + I^- \rightarrow I_2^{-}\bullet \quad (86)$$

These radical anion species can also react with and oxidize the organic compound even though less efficiently than $^{\bullet}OH$ [146]. These radical anion species such as $CO_3^{-}\bullet$, $NO_3^{-}\bullet$, $Cl_2^{-}\bullet$, $CH_3^{\bullet}$ etc., undergo radical-radical recombination or deactivation at much lower rate compared to $^{\bullet}OH$. They are therefore more readily available in the system for longer time to react with the substrate and effect the degradation for longer time compared to the $^{\bullet}OH$ radicals. Hence, the relatively low

reactivity of the radical anion species is compensated by their better and sustained availability for the substrate. In the absence of any reaction with the anions, some of the $^{\bullet}OH$ would get deactivated by recombination. Hence, it can be assumed that the enhancement of the degradation of AMS in presence of anions is possible only when the reaction rate between anions and $^{\bullet}OH$, which results in the formation of radical anions is higher compared to that between substrate and $^{\bullet}OH$. The more frequent interaction of the readily available radical anion with the substrate, compared to the $^{\bullet}OH$ radical which takes part in a number of interactions including self-destroying recombination, can be a reason for the enhancement by the anions. However, when the anions do not form reactive radical anions and interfere with the surface processes as explained earlier, enhancement is not possible and instead inhibition can result.

In view of the complexity of the anion effect, it may not be appropriate to draw general conclusions or commonly applicable explanations. For example, in the case of NO_3^- ion the enhancement can also be linked to direct and indirect formation of $^{\bullet}OH$ radical as follows [150].

$$NO_3^- + h\nu \rightarrow NO_2^- + O \quad (87)$$

$$NO_3^- + H_2O + h\nu \rightarrow NO_2^- + OH^- + {}^{\bullet}OH \quad (88)$$

$$O + H_2O \rightarrow 2{}^{\bullet}OH \quad (89)$$

Presence of salts is known to diminish the colloidal stability. This is followed by surface charge neutralization which increases the mass transfer limitation and reduces the contact of the pollutants with the

catalyst. Screening of the UV light, competitive adsorption at the surface sites, competition for photons, surface layer formation and deposition of elemental metals, radical and hole scavenging etc., can influence the photocatalytic degradation.

3.3.16 Anion effect on pH

The possibility of variation in the pH of the system in presence of anions and consequent changes in the surface and bulk processes is also examined. The pH of the system in presence of anions is measured and tabulated in table 3.8.

Table 3.8: pH of AMS solution with ZnO in presence of various anions
[AMS] = 25 mg/L, [ZnO] = 80 mg/L, [Anion] =10 mg/L, Time= 2 hr

Anion	pH
No anion	5.6
F^-	7.35
Cl^-	7.33
Br^-	7.39
I^-	7.42
CO_3^{2-}	8.06
HCO_3^-	7.80
SO_4^{2-}	7.50
NO_3^-	7.57
CH_3COO^-	7.57
$C_2O_4^{2-}$	7.86
PO_4^{3-}	7.85

The pH increases marginally to ~7.5 in presence of all the anions. The study of pH effect has shown that (section 3.3.5) the degradation is marginally less in the pH range 6-8. Hence the decrease in degradation in presence of anions can be partially attributed to their effect on pH.

However, some anions such as NO_3^-, CH_3COO^- etc., which function as enhancers also exhibit same effect on pH. Hence this conclusion may not be applicable generally and has to be evaluated along with other factors.

3.3.17 Steric effect

The size of the anion may be an important factor that influences its effect on the photocatalytic activity of ZnO and degradation of organic pollutants, especially when surface initiated process is important. Bigger ions may block more surface sites on the catalyst even at lower concentration, which prevents the access of the substrate molecule to the catalyst surface and may inhibit the degradation of the pollutant molecule. In order to verify this, the case of halide ions is considered. The size of the anions is in the order $I^- > Br^- > Cl^- > F^-$ as shown in table 3.9.

Table 3.9: Size of halide ions

Halide ion	Ionic radius (nm)
F^-	0.136
Cl^-	0.181
Br^-	0.195
I^-	0.216

Accordingly the inhibition/slowdown of enhancement must be in the order

$I^- > Br^- > Cl^- > F^-$

This order is followed only in the case of I^-, which is a strong inhibitor. The strong inhibition by I^- has been reported by other workers also recently [151]. This is explained based on the ability of I^- to act as scavenger of both holes and $^{\bullet}OH$ radicals. Other halides also have similar

scavenging function. However, they function as 'enhancers' or have 'no effect'. It is also possible that the smaller ions can occupy surface sites more effectively especially at higher concentration and influence the surface processes. This can explain the varying concentration effect by Cl^- and F^-, which functions as enhancers at low concentrations and have 'no effect' later on. The consistently higher 'enhancing effect' by Br^- needs to be investigated further so that it can be utilized for the enhanced photocatalytic degradation of organic pollutants. However, as in the case of many earlier studies, in this case also no consistent conclusions on the correlation of anion effect with any single parameter is possible.

3.3.18 Solubility of anions and layer formation

Another possible reason for the inhibitory effect of anions towards the photocatalytic degradation of pollutants is the formation of an inorganic layer on the surface of the catalyst. The efficiency of the inorganic layer formation is reported to depend on the solubility of the salts [145]. Salts with higher solubility show lower layer formation. The solubility of some of the salts (in mg/g of water at 20^0C) used in the study is in the order:

NaI (191) > NaBr (98.4) > $NaNO_3$ (94.9) > CH_3COONa (54.6) > Na_2SO_4 (40.8) ≥ Na_2CO_3 (39.7) > NaCl (36.1) > Na_3PO_4 (16.3) > $NaHCO_3$ (11.1) > NaF (4.22) > $Na_2C_2O_4$ (3.81)

The layer formation will be in the reverse order, i.e.

$C_2O_4^{2-}$ >F^- > HCO_3^- > PO_4^{3-} > Cl^- > CO_3^{2-} > SO_4^{2-} > CH_3COO^- > NO_3^- >Br^->I^-

If the layer formation by the anions is a cause of inhibition, the inhibition will be in the order,

$C_2O_4^{2-} > F^- > HCO_3^- > PO_4^{3-} > Cl^- > CO_3^{2-} > SO_4^{2-} > CH_3COO^- > NO_3^- > Br^- > I^-$

Alternatively, in the case of enhancement, effect of anions must be in the reverse order, i.

$I^- > Br^- > NO_3^- > CH_3COO^- > SO_4^{2-} > CO_3^{2-} > Cl^- > PO_4^{3-} > HCO_3^- > F^- > C_2O_4^{2-}$

Based on this, $C_2O_4^{2-}$ ion with highest tendency for layer formation is expected to show maximum inhibition towards AMS degradation. Similarly NO_3^- ions with the least layer formation is expected to show the least inhibition. Even though there is no strict correlation between the layer formation and inhibition, it may be inferred that generally the inhibition by PO_4^{3-}, $HCO3^-$ and $C_2O_4^{2-}$ can be correlated at least partially with the layer formation. Similarly, the least inhibition (in this case even enhancement) in the case of NO_3^-, CH_3COO^- and Br^- can be at least partially due to the high solubility and consequently poor layer formation. It is also possible that more soluble anions can influence the processes in the liquid bulk thereby generating more (or less) reactive species which may enhance or inhibit the degradation as the case may be.

In general, it may be concluded that the 'anion effect' depends on a number of parameters and their complex interactions in the reaction system. Hence it is not possible to draw any general conclusion on the

effect of anions on the photocatalytic degradation of organic pollutants in water. For every pollutant/catalyst system, the effect of each anion has to be evaluated individually.

3.3.19 Effect of Oxidants

The effect of H_2O_2, which is an important oxidant in AOPs on the photocatalytic degradation of AMS has been experimentally verified in detail and reported under section.3.3.10 of this chapter. The effect of two other major oxidants, i.e., KIO_3 and $K_2S_2O_8$ is also investigated. The results presented in figures 3.36 and 3.37 show that the effect depends on both the concentration of the oxidants and the irradiation time.

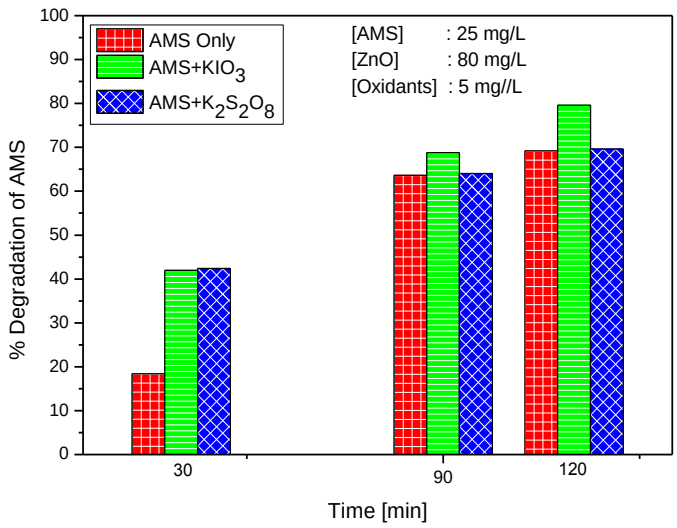

Fig. 3.36: Effect of KIO_3 and $K_2S_2O_8$ on the degradation of AMS at different reaction times

At lower concentration of oxidants (5 mg/L) and at lower reaction time (30 min) the oxidants enhance the degradation. But at higher

reaction time of 90 and 120 min the effect is negligible with slight enhancement in presence of KIO_3.

The effect of concentration of the oxidant on the photocatalytic degradation of AMS is shown in figure 3.37.

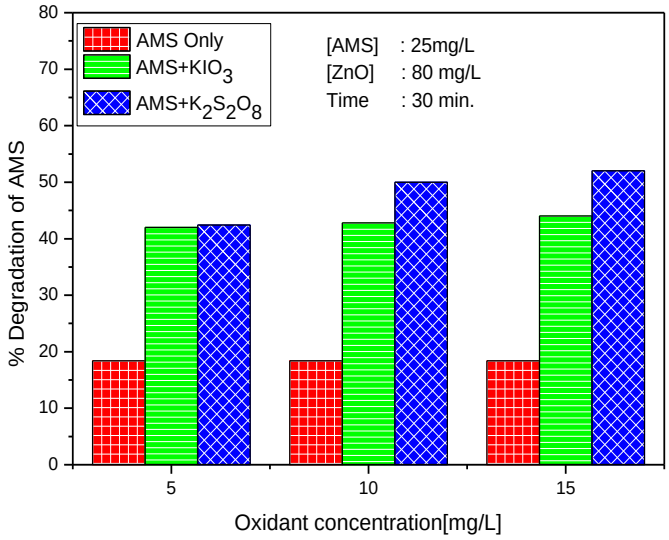

Fig. 3.37: Effect of KIO_3 and $K_2S_2O_8$ at different concentrations on the degradation of AMS

As the concentration of the oxidant is increased, the enhancement also increases initially and is then stabilized. The degree of enhancement decreases with time probably because, the net concentration of the pollutant remaining in the system and consequently the number of interactions with the oxidant or oxidant-derived ROS also diminishes. Results of detailed investigation of the two oxidants at different concentrations and reaction times are presented in table 3.10.

Table 3.10: Effect of oxidant concentration and reaction time on the photocatalytic degradation of AMS.

Oxidants	[Oxidant], mg/L	% Degradation of AMS after				
		30 min	60 min	90 min	120 min	150 min
Nil	0	18.4	38.4	63.6	69.2	74.8
KIO_3	5	42.0	47.2	68.8	79.6	82.4
	10	42.8	52.0	71.6	81.6	82.8
	15	44.0	55.2	72.8	84.8	86.0
$K_2S_2O_8$	5	42.4	48.4	64.0	69.6	79.2
	10	50.0	54.8	64.8	71.2	78.8
	15	52.0	56.8	66.4	75.2	82.4

The mechanism of enhancement by the oxidant may be explained as follows:

In aqueous solution, under irradiation by light, $S_2O_8^{2-}$ can generate highly active sulphate radical anion ($SO_4^{-\bullet}$) both thermally and photo chemically.

$$S_2O_8^{2-} + h\nu \rightarrow 2SO_4^{-\bullet} \quad (90)$$

The sulphate radical anion can also be formed by the trapping of electron by $S_2O_8^{2-}$

$$S_2O_8^{2-} + e- \rightarrow SO_4^{2-} + SO_4^{-\bullet} \quad (91)$$

SO_4^{2-} formed get adsorbed on the surface and can interact with the photogenerated holes forming reactive sulphate radical

$$h^+ + SO_4^{2-} \rightarrow SO_4^{-\bullet} \quad (92)$$

As S is a strong oxidizing agent, the sulphate radical (reduction potential of $SO_4^{-\bullet}$ = 2.6 eV) can accelerate the degradation according to the reaction,

$$SO_4^{-\bullet} + H_2O \rightarrow SO_4^{2-} + {}^{\bullet}OH + H^+ \quad (93)$$

$$SO_4^{-\bullet} + AMS \rightarrow SO_4^{2-} + \text{Intermediate} \rightarrow SO_4^{2-} + CO_2 + \text{Salts} \quad (94)$$

Both $SO_4^{-\bullet}$ and ${}^{\bullet}OH$ are highly reactive radical species which can oxidize the organics. At the same time, SO_4^{2-} ions are also generated which act as inhibitors. Hence as more SO_4^{2-} is built up in the system slowly, $S_2O_8^{2-}$ induced enhancement slows down and ends up with no effect.

In the case of IO_3^-, the oxyanion can trap the conduction band electrons on the surface of the semiconductor oxide as in the case of $S_2O_8^{2-}$ (reaction 91) thereby reducing the recombination of the charge carriers, i.e., electrons and holes [152]. The oxidants thus increase the quantum efficiency. Consequently, the formation of ${}^{\bullet}OH$ as well as the oxidation of AMS will be promoted by the valence band holes.

The IO_3^- can also accelerate the photocatalytic process through thermal and photochemical oxidations in the bulk solution. The relevant reactions and the reduction potentials are:

$$IO_3^- + 2H^+ + e^- \rightarrow IO_2^- + H_2O, \text{ Reduction potential, } E^0g=1.15 \text{ eV} \quad (95)$$

$$IO_3^- + 6H^+ + 6e^- \rightarrow I^- + 3H_2O, E^0g=1.44 \text{ eV} \quad (96)$$

The formation of I^-, which is an inhibitor can eventually compensate for the enhancing effect of IO_3^- thereby reaching a state of stabilization.

It is possible that IO_3^- can scavenge the reactive oxygen species such as $O_2^{-\bullet}$, $HO_2^\bullet$, $^\bullet OH$, H_2O_2 etc. However, there is kinetic limitation to this [153,154]. In the case of the most reactive oxygen species, i.e., $^\bullet OH$, the possible reaction is:

$$^\bullet OH + IO_3^- \rightarrow OH^- + IO_3^\bullet \quad (97)$$

$$(IO_3^- / IO_3^\bullet \approx 2.1 \text{ eV})$$

Since the degradation is not inhibited and is only enhanced in presence of IO_3^- , the deactivation of the $^\bullet OH$ radical is not taking place, thereby confirming the kinetic limitation.

The effect of combination of the three oxidants is tested and the results are shown in figure 3.38.

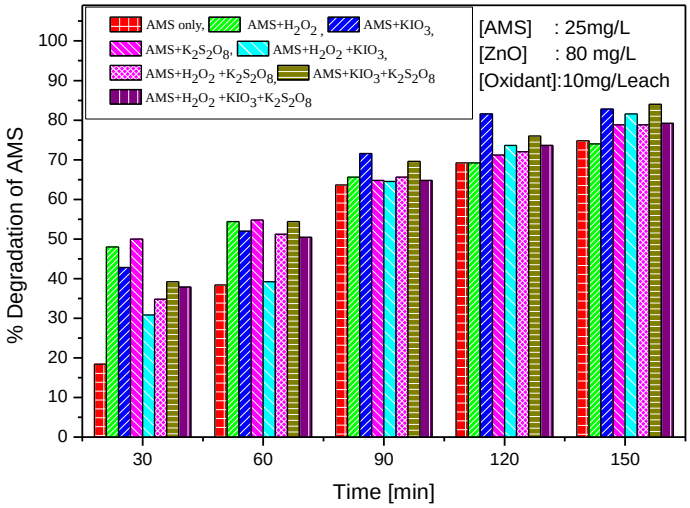

Fig. 3.38: Effect of combination of H_2O_2, $K_2S_2O_8$ and KIO_3 on AMS degradation

Maximum enhancement in AMS degradation was observed in presence of KIO_3 only, towards the later stages of the reaction. The

combination of oxidants has no additive effect of enhancement and even reduces the enhancement of degradation effected by individual oxidants, especially in the early stages of the reaction. This may be due to the multitude of interactions and consequent deactivation of the reactive free radicals formed from individual oxidants. As the degradation progresses and the concentration of the substrate decreases, the enhancing effect of oxidant, whether individually or in combination also diminishes. The study clearly shows that the use of any of this combination of oxidants has no special advantage over the individual oxidants for the photocatalytic degradation of AMS. In any case, the use of these oxidants beyond a particular concentration for water purification may not be desirable due to the negative effect of accumulation of I or S in water.

3.3.20 Recycling of the catalyst

For the efficient and economic application of photocatalysis for pollution abatement and water purification, the catalyst must be recycled as many times as possible without any considerable loss in the efficiency**.** In the present study the possibility of recycling the used ZnO catalyst is tested by separating the catalyst from the reaction system by centrifugation, followed by air drying at room temperature (~30^0C) and then reusing as such for the photocatalytic degradation of AMS. The results are presented in figure 3.39 which show that the catalyst remains active for at least 3 recycles before the activity decreases. This is an important factor for scaling up the process and its eventual commercialization.

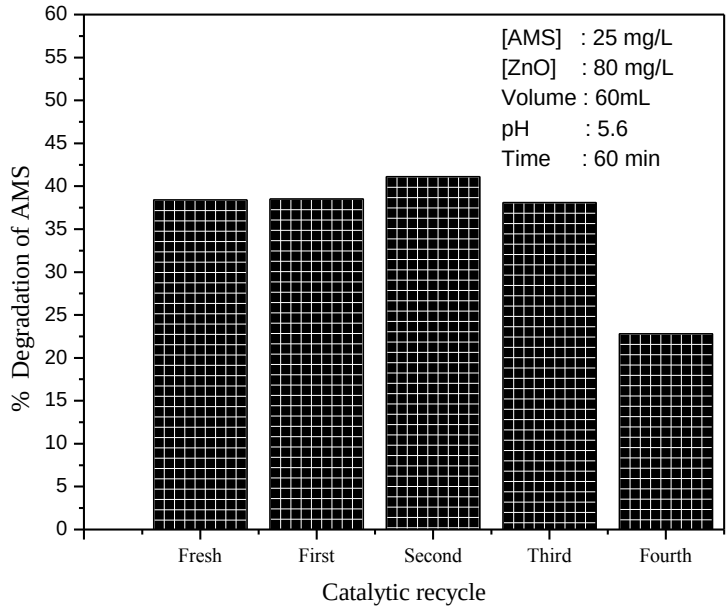

Fig. 3.39: Recycling of ZnO for the photocatalytic degradation of AMS

Possible reasons for decrease in the photocatalytic activity of ZnO at the fourth recycling after being steady for the first three recycles were explored by examining the physical characteristics of the used catalyst. The BET surface area of the catalyst remains more or less the same (~4 m^2/g) even after the fourth recycling. The adsorption of AMS on ZnO also remained fairly same upto three recycles, i.e., 21.8, 21.6, 21.2 and 18.8% on fresh, once used (before first recycling), twice used (before second recycling) and thrice used (before third recycling) catalyst respectively (table 3.11).Thereafter, it showed steep decrease in adsorption, i.e., 10% after the fourth use (before being used for the fourth recycle). With increasing number of recycles at least some of the substrate and/or the intermediate molecules might be remaining strongly adsorbed or

getting trapped in the cavities on ZnO, resulting in lower adsorption of fresh substrate molecules and hence decreased photocatalytic degradation. Formation of small amounts of photo-insensitive hydroxides (fouling) has also been reported on the surface of repeatedly used ZnO photocatalyst [112]. However, this can affect the photocatalytic activity of ZnO only when a certain critical concentration, adequate to reduce the light absorption, is reached. In the current instance, this critical concentration together with significant reduction in adsorption may be attained after the third recycling. However, the significant reduction in the adsorption of substrate and increase in the concentration of photo-insensitive hydroxides on the surface to reach critical level may not necessarily be taking place precisely after third recycling, as in the present case, in all experiments.

The number of possible recycles before the sharp decline in activity may vary depending on the reaction conditions, chemistry of the substrate and the intermediates, reactor size and geometry etc. In any case, it may be inferred that decrease in adsorption of the substrate and formation of surface hydroxides are two major factors leading to decreased activity of continuously recycled ZnO, even though other factors also cannot be ruled out. The adsorption of AMS on the fifth recycled ZnO was fully restored and even enhanced (from 8.8 to 27.8%) by washing three times with distilled water followed by calcination at 250^0C for 2 hr (table 3.11). This treatment is known to convert the surface hydroxides to the oxides again. Experiments showed that the photocatalytic activity for AMS degradation is also fully restored (~40–44% in 60 min) after this

treatment. Hence it may be concluded that by proper washing and calcination treatment, the photocatalytic activity of ZnO can be fully restored and it can be recycled many times for the degradation of AMS. Similar results were reported earlier in the case of ZnO, TiO_2 and impregnated ZnO catalysts [112, 155,156].

Table 3.11: Adsorption study of recycled catalyst

Catalyst cycle	% Adsorption of AMS after 60 min	% Degradation of AMS after 60 min
Fresh	21.8	38.4
First recycling	21.6	38.5
Second recycling	21.2	41.1
Third recycling	18.8	38.1
Fourth recycling	10.0	22.80
Fifth recycling	8.8	20.0
Catalyst washed, dried and calcined at 250^0C for 2 hr		
Sixth recycling	27.8	44.0
Seventh recycling	24..6	40.0
Eight recycling	14.0	32.8

There are no significant changes in the physico-chemical characteristics of the used ZnO catalyst as is evident from its XRD, BET, pore size and pore volume analyses (figures 3.40-3.41 and table 3.12). The pore volume and pore size are more for the used catalyst though the increase is not significant enough to cause any change in activity.

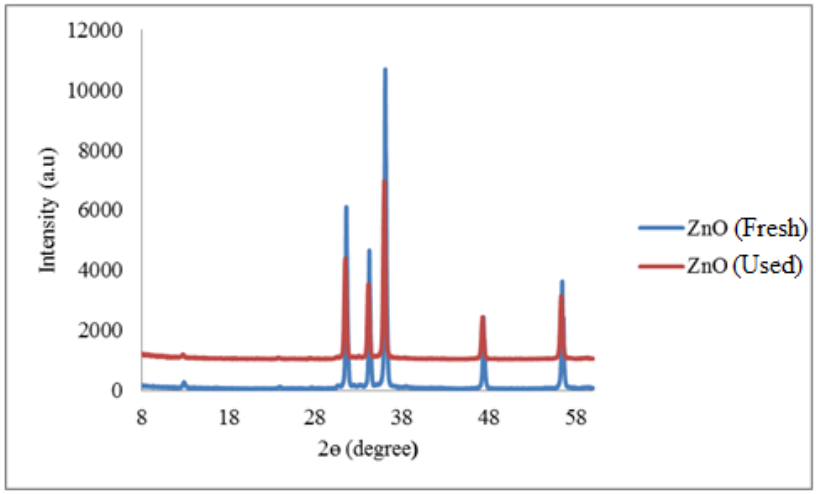

Fig. 3.40: XRD of fresh and used ZnO catalyst

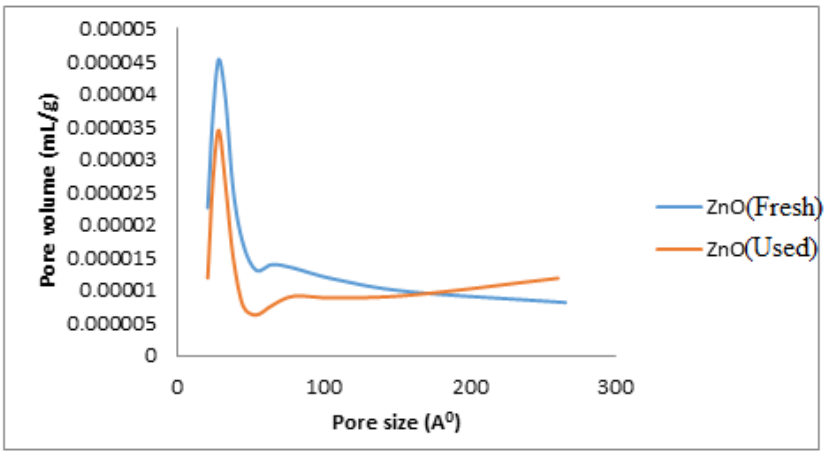

Fig. 3.41: Comparison of pore volume vs pore size for fresh and used ZnO catalyst

Table 3.12: Comparison of BET surface area, pore volume and pore size of fresh and used ZnO catalyst

Sample	BET Surface area (m^2/g)	Pore volume (cm^3/g)	Pore size (A^0)
Fresh ZnO	3.9745	0.012018	125.5911
Used ZnO	3.9769	0.016929	172.7230

3.4 General mechanism

The basic mechanism of semiconductor photocatalysis involves absorption of light by the catalyst and creation of electron-hole pair as the first step (reaction 98).

$$ZnO + h\nu \rightarrow ZnO\ (h^{+}_{vb}) + ZnO\ (e^{-}_{cb}) \qquad (98)$$

The electron is promoted from the valence band of the semiconductor to its conduction band, creating hole (+ ve charge) in the valence band. Both the electron and hole must be consumed so that the material can act as a catalyst. It is generally believed that both the electrons and holes can find low energy trap sites on a sub-picosecond time scale in the semiconductor [157]. They either recombine and dissipate the input energy as heat or react with electron acceptors and electron donors which are adsorbed on the semiconductor surface and/or trapped within the surrounding electrical double layer of the charged particles and produce strong oxidizing hydroxyl radicals [158].

The formation of hydroxyl radicals during solar irradiation of the aqueous suspension of ZnO is tested by the photoluminescence (PL) technique using terephthalic acid (TPA) as the probe molecule [159]. The hydroxyl radicals formed insitu in the system reacts with TPA and form 2-hydroxyl terephthalic acid (HTPA). The fluorescence intensity of HTPA formed is proportional to the formation of $^{\bullet}OH$ radicals in the system. The PL spectrum of the product HTPA is recorded in the range of 400-450 nm after every 5 min of irradiation. The excitation wavelength was 315 nm. The PL intensity at 425 nm corresponds to the concentration

of HTPA. Solar irradiation of the ZnO-TPA system shows gradual increase in the PL intensity at 425 nm with time of irradiation, as shown in figure 3.42 .This is attributed to the formation of HTPA and hence of $^{\bullet}OH$ as explained above. No PL was observed in the absence of either sunlight or ZnO thereby confirming the role of these two components on the formation of reactive $^{\bullet}OH$ radicals.

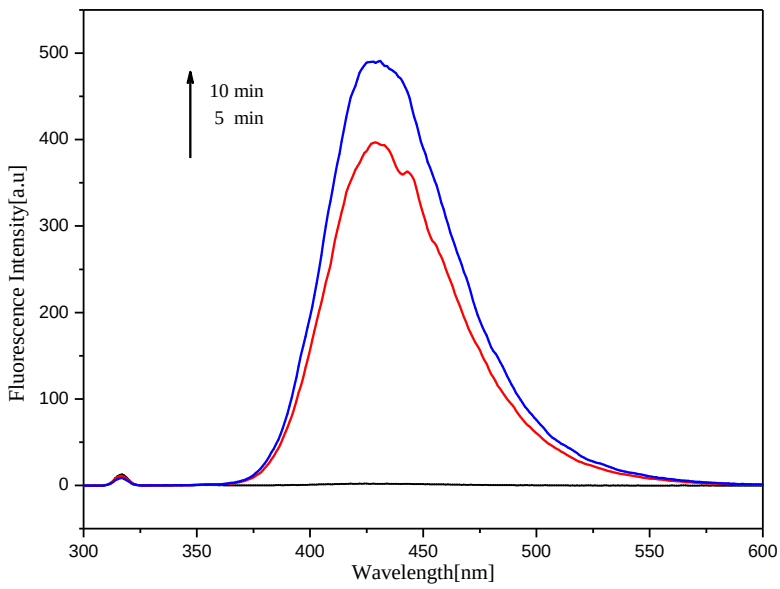

Fig. 3.42: PL spectral changes indicating the presence of $^{\bullet}OH$ radicals during ZnO photocatalysis

The •OH radicals formed as explained above can promote the oxidation of AMS as follows:

$$h^+ + e^- \rightarrow \text{Heat} \quad (99)$$

$$O_2 + e^- \rightarrow O_2^- \bullet \quad (100)$$

$$O_2^- \bullet + 2H^+ + e^- \rightarrow H_2O_2 \quad (101)$$

$$H^+ + O_2^- \bullet \rightarrow HO_2^{\bullet} \quad (102)$$

$h^{+}_{vb} + H_2O \rightarrow H^{+} + {}^{\bullet}OH$ (103)

AMS+ROS (H_2O_2, ${}^{\bullet}OH$, O_2^{-} ., $HO_2^{\bullet}$ etc.) →
Intermediate(s) →CO_2+H_2O+Salts (104)

The major intermediate is ACP in the current instance.

Various steps involved in the formation of more free radicals from H_2O_2 have been explained earlier (equations 67-73).

A simple schematic presentation of the general mechanism of formation of reactive free radicals, is given in figure 3.43 [160, 161].

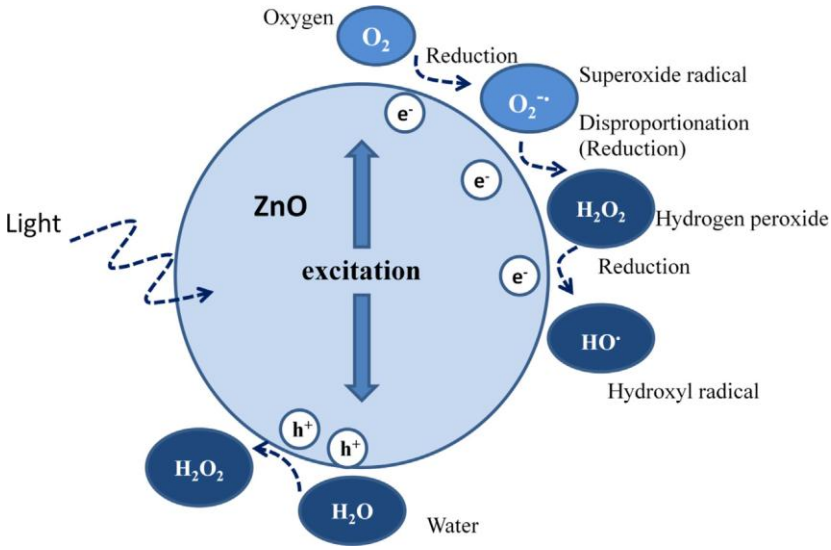

Fig. 3.43: Schematic presentation of the formation of reactive oxygen species (ROS) in ZnO photocatalysis

Possible steps involved in the photocatalytic degradation of AMS in presence of ZnO catalyst under sunlight irradiation may be shown as in figure 3.44.

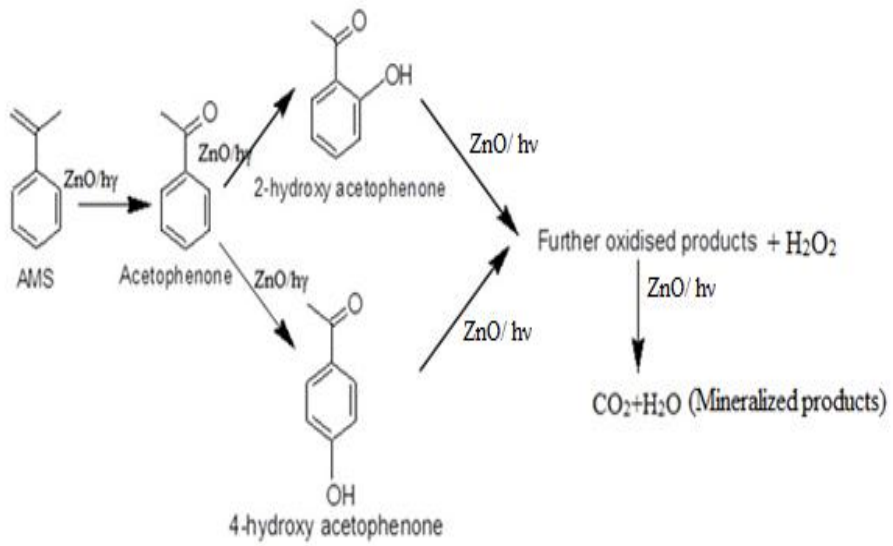

Fig. 3.44: Possible mechanism for the photocatalytic mineralization of AMS.

The H_2O_2 formed as above undergoes concurrent decomposition resulting in oscillation in its concentration. Relevant reaction steps are discussed and presented in reactions 60-73.

3.5 Conclusions

The photocatalytic degradation of trace amounts of α-methyl styrene (AMS) in water is investigated in the presence of ZnO as catalyst and sunlight as the energy source. The degradation proceeds efficiently and acetophenone (ACP) is identified as the major intermediate. Eventually, ACP also gets mineralized indicating the potential application of solar energy for the photocatalytic removal of toxic pollutants from water. H_2O_2 is concurrently formed in the process which enhances the degradation initially. The concentration of H_2O_2 does not increase beyond a critical limit which is explained based on the simultaneous and

competing formation and decomposition processes. AMS and ACP inhibit the degradation of one another. The degradation of AMS is slow in deaerated system, thereby confirming the role of O_2 in photo-catalytic processes. The reaction follows pseudo first order kinetics and parameters such as pH, substrate concentration and catalyst dosage play important role in determining the rate of degradation. The effect of various salts/anions and oxidants on the degradation of AMS is studied in detail. The anion may inhibit/enhance the degradation depending on the physico-chemical processes taking place on the surface and in the bulk as well as changes in the catalyst and substrate characteristics. Persulphate, iodate and H_2O_2 enhance the degradation individually, even though, their combination does not provide any additive effect. The catalyst can be recycled at least three times without loss in efficiency. Repeated washing with water followed by calcination at 250^0C can restore the catalytic activity fully. The study reiterates the possibility of using ZnO as a semiconductor oxide catalyst for the dual application of harvesting solar energy and the removal of hazardous pollutants from water.

.....ꕥ.....

Chapter 4

ZINC OXIDE MEDIATED SOLAR PHOTOCATALYTIC DEGRADATION OF ACETOPHENONE [ACP] IN WATER

Contents

4.1 Introduction

Acetophenone (ACP) is an intermediate in phenol manufacturing industry. Small amounts of ACP is present in the effluent water from such industries. It is also formed from the degradation of AMS, which is another major pollutant in the effluent water from phenol industry as explained in Chapter 3. Conventional secondary treatment techniques such as biological methods are found to be inadequate for the removal of the last traces of ACP from water. As photocatalysis was found to be an effective AOP for the removal of traces of many organic pollutants from water [36,37,102,104-106,162], including AMS as described in the previous chapter, the possibility of using the same for the removal of last traces of ACP in water is investigated using ZnO as the photocatalyst and sunlight as the energy source.

Not many studies are reported in literature on the degradation of ACP or its removal from water. Amereh et al. [163] investigated the photodegradation of a mixture of acetophenone and toluene in water in

presence of nano-TiO_2 powder supported on NaX zeolite. The study revealed that the TiO_2-zeolite composite shows better degradation efficiency compared to nano titanium oxide powder alone. Wen et al. [164] studied Pulsed Corona Discharge-Induced reactions of Acetophenone in water. The study shows that acetophenone degradation proceeds through the oxidative reaction pathway, in which molecular oxygen accelerates the degradation through photolysis and pyrolysis. Kohtani et al. [165] used coumarin dyes adsorbed on titanium dioxide (TiO_2, P25) for the hydrogenation of acetophenone using diisopropyl ethylamine (DIPEA) as the sacrificial reagent. The catalysts effectively hydrogenated acetophenone under visible light. The variation of Langmuir adsorption constant for the photodegradation of acetophenone over TiO_2 under different light intensities was studied by Xu et al. [125]. Their study reveals that the photo adsorption of ACP on TiO_2 is poor and depends on the light intensity. The photocatalytic activity of transition metal ion impregnated TiO_2 for the degradation of acetophenone and nitrobenzene in aqueous solution was investigated by Tayade et al. under UV irradiation [166]. However, no detailed studies on the photocatalytic degradation/mineralization of trace amounts of ACP in water seem to be reported so far. In this chapter, the photocatalytic mineralization of trace amounts of ACP in water using sunlight as the energy source and commercially available ZnO as catalyst is investigated in detail. The effect of various parameters such as catalyst dosage, initial concentration of ACP, pH, humic acid, externally added H_2O_2, electrolytes etc., on the rate of degradation is investigated in detail.

4.2 Experimental Details

4.2.1 Materials

ACP (98.0%) obtained from Merck, India Ltd was used as such without further purification. All other chemicals, including the catalyst ZnO are from the same source as described in Chapter 3. The materials were analyzed/characterized as explained therein.

4.2.2 Photocatalytic Experimental set up

The experimental set up and procedures used are the same as those described in Chapter 3.

4.2.3 Analytical Procedures

Perkin Elmer Auto System XL Gas Chromatograph (GC) is used for the analysis of ACP and intermediates during the degradation reaction using flame ionization detector and Elite 1301 column with hydrogen as the carrier gas. The calibration graph is obtained by multiple level calibration method. Different known concentrations of ACP solutions are prepared and each one of these solution is injected into the GC (1.0 µL). The procedure is repeated to get the average calibration value corresponding to the respective concentration to minimize the error. The instrument parameters are the same as those used for AMS analysis (section 3.2.2). The intermediates formed from ACP are also detected by GC. The calibration graph of ACP is shown in figure 4.1. During the reaction, samples from the reactor (2 mL) are taken at regular intervals, filtered and then injected (1 µL) into the GC. The peak area (response) corresponding to the remaining ACP is converted into concentration directly from the calibration curve.

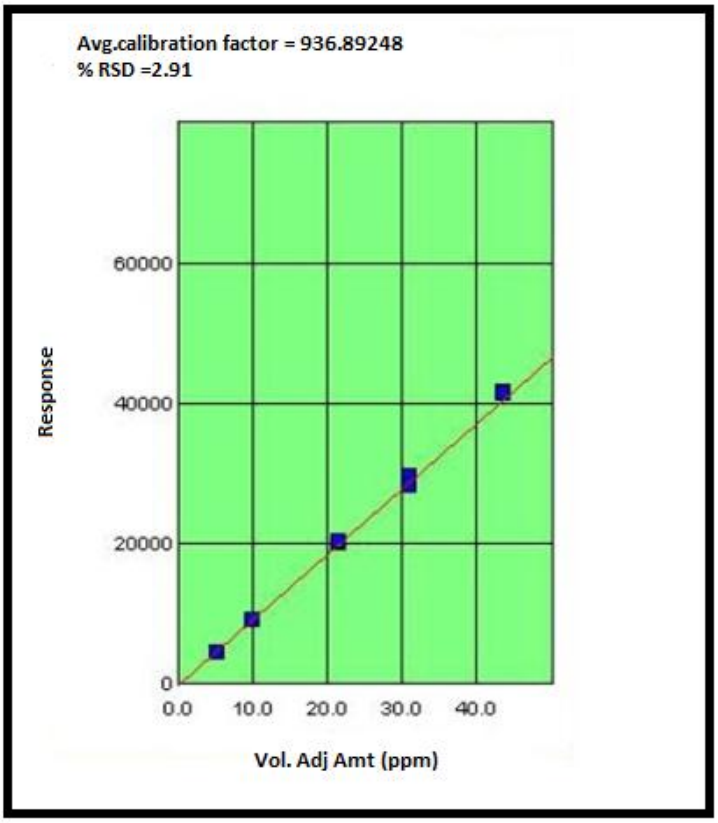

Fig. 4.1: Calibration graph for the Gas chromatographic analysis of Acetophenone.

4.3 Results and Discussion

Preliminary studies on the photocatalytic degradation of ACP (50 mg/L) were carried out in presence of sunlight, using ZnO (100 mg/L) as catalyst. The results are shown in figure 4.2.

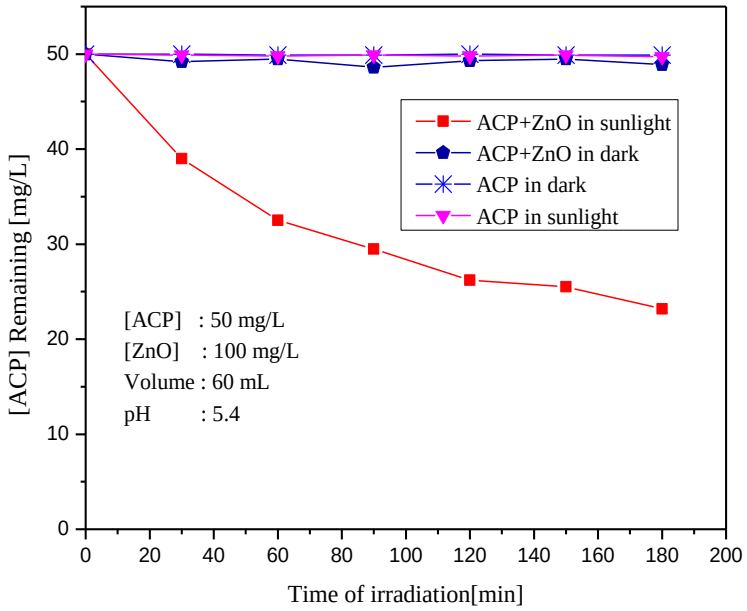

Fig. 4.2: Photocatalytic degradation of ACP on ZnO

More than 53% degradation was obtained after 3 hr of irradiation. No degradation was observed in the absence of either light or catalyst thereby confirming the role of both light and catalyst for the degradation. In order to verify whether the decrease in concentration is due to simple adsorption, the adsorption of ACP on ZnO under standard experimental conditions was investigated. The results are presented in table 4.1, which show that the adsorption of ACP over ZnO catalyst is negligible and is less than 4% even after 150 min. Hence the decrease in ACP concentration in presence of ZnO catalyst under sunlight irradiation is primarily due to its photodegradation/mineralization.

Table 4.1: Adsorption of ACP over ZnO at different time intervals
[ZnO]= 100 mg/L, Volume =60 mL

[ACP], mg/L	% Adsorption of ACP over ZnO catalyst after		
	30 min	90 min	150 min
5	4.0	4.0	4.0
10	2.0	3.0	4.0
20	2.0	3.0	2.5
30	1.7	2.0	3.3
40	2.8	2.0	3.0
50	1.6	2.8	1.0

Hydroxy acetophenone (HACP) is identified as the major reaction intermediate. A typical chromatogram showing ACP and the intermediate HACP is shown in figure 4.3.

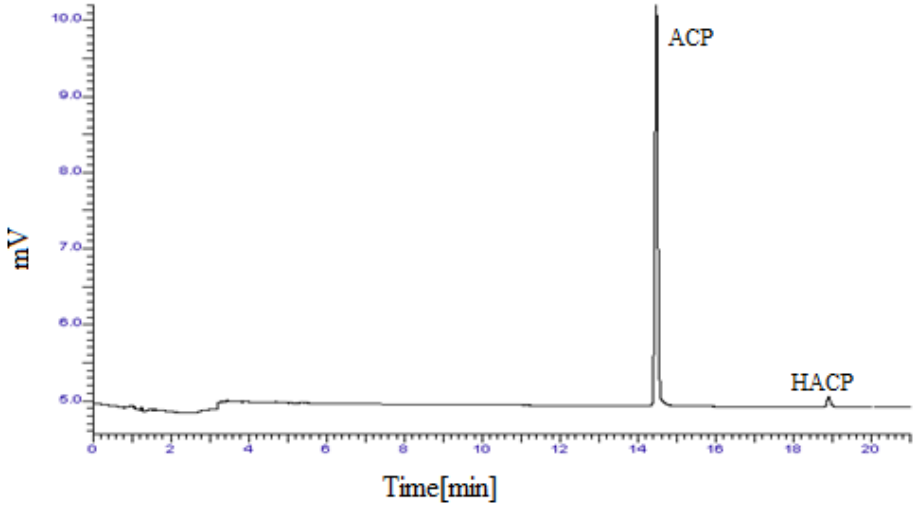

Fig. 4.3: Typical chromatogram showing ACP and HACP

The concentration of HACP was found to increase initially corresponding to decrease in ACP concentration. Eventually the decrease in ACP and increase in HACP level off (figure 4.4).

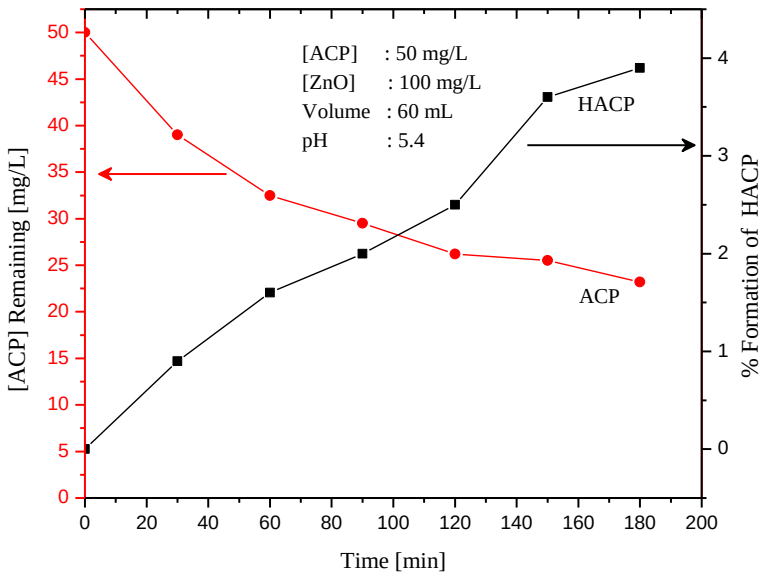

Fig. 4.4: Photocatalytic degradation of ACP and concurrent formation of HACP

The concentration of HACP in the system does not strictly correspond to the expected quantity from ACP degradation, indicating its degradation in parallel. From the chromatographic data it is seen that HACP formed insitu is decreasing with time upon continuous irradiation and eventually disappears (see figure 4.5). Small quantities of phenol is also detected as an intermediate by colorimetric method, which also get degraded on prolonged irradiation. This shows the potential of the photocatalytic process for the complete mineralization of the pollutant.

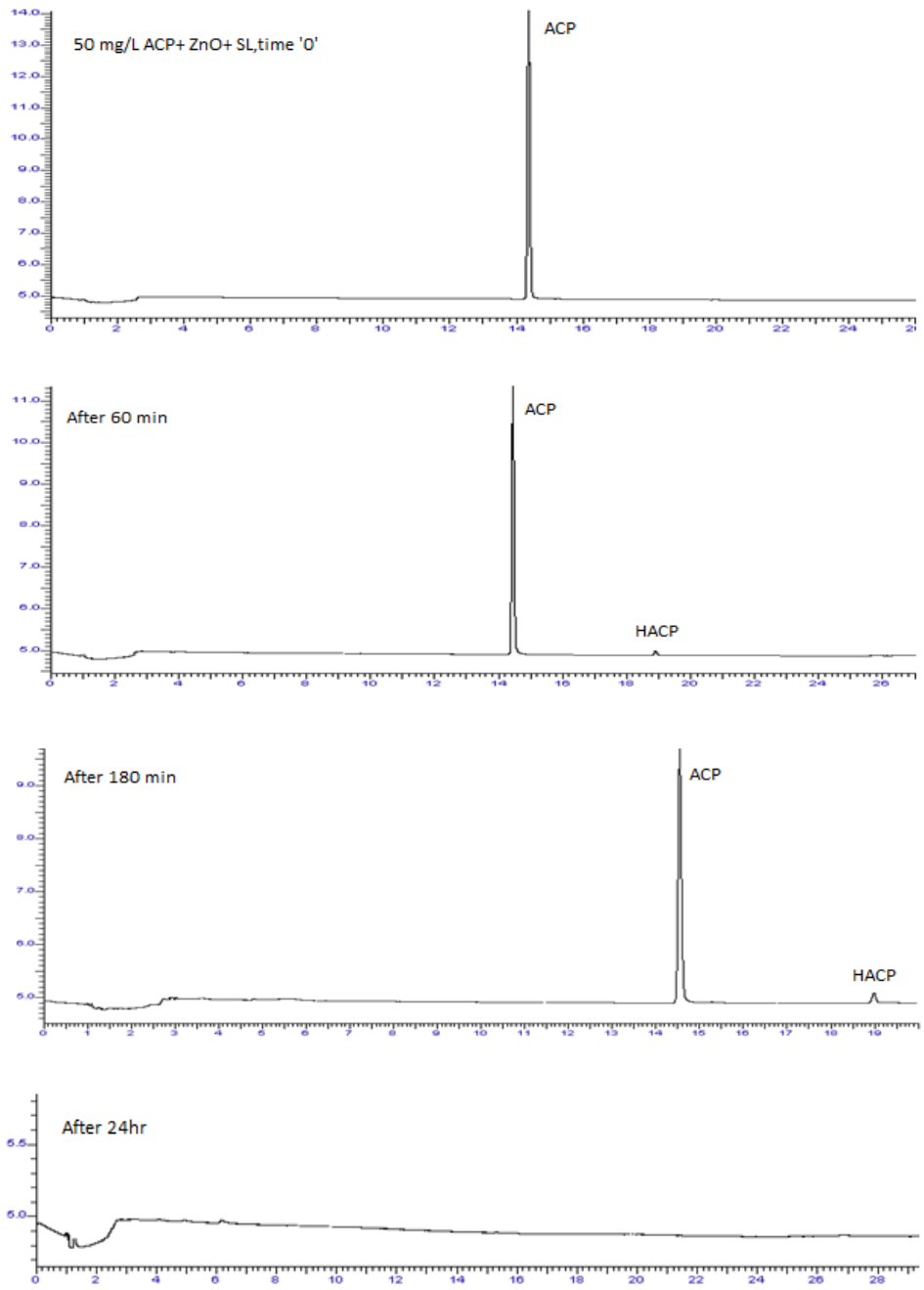

Fig. 4.5: Chromatogram showing the degradation of ACP

LC/MS analysis of the reaction products at the stage of 50% degradation (of ACP) showed the presence of more intermediates as listed in table 4.2.

Table 4.2: Intermediates formed during the solar photocatalytic degradation of ACP over ZnO

SL .No	Mass	Proposed structure
1	135	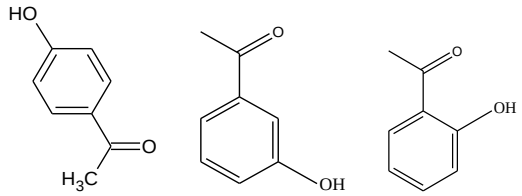
2	153	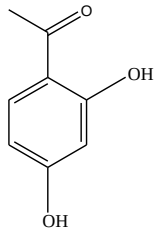
3	331	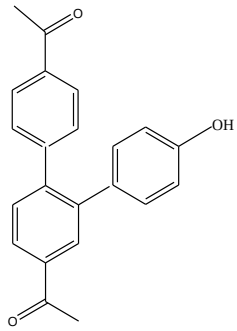

Generally it is known that the adsorption of the substrate on the catalyst surface is essential for the effective photocatalytic degradation though homogeneous reaction in the bulk phase also is reported to play a major role in many instances. The high degradation rate of ACP in spite

of its poor adsorption shows that the interactions with the reactive species and/or surface-generated reactive free radicals is mostly taking place in the bulk. This is in agreement with the observations of Turchi and Ollis [110] who demonstrated that though photocatalytic degradation depends on the adsorptive properties of the organic compounds on the surface, it is not an essential requirement for the reactions. The reactive $^{\bullet}OH$ radicals and other oxidizing species can diffuse into the bulk solution to interact with the organic pollutant. Since adsorption of the substrate is not a major factor, the decrease in rate of degradation with time is possibly due to decrease in the concentration of ACP and the competition between the reaction intermediates and ACP for the reactive free radicals. Other than HACP, only one minor (practically insignificant) intermediate is detected during the reaction which is identified as phenol. Eventually the intermediates also get degraded and mineralized as seen from their complete disappearance with time, as shown in figure 4.5.

4.3.1 Effect of catalyst dosage

The optimum catalyst loading for the effective photocatalytic degradation of ACP is investigated by varying the amount of ZnO in the range from 20 to 140 mg L^{-1} and keeping all other parameters constant. The results are plotted in figure 4.6.

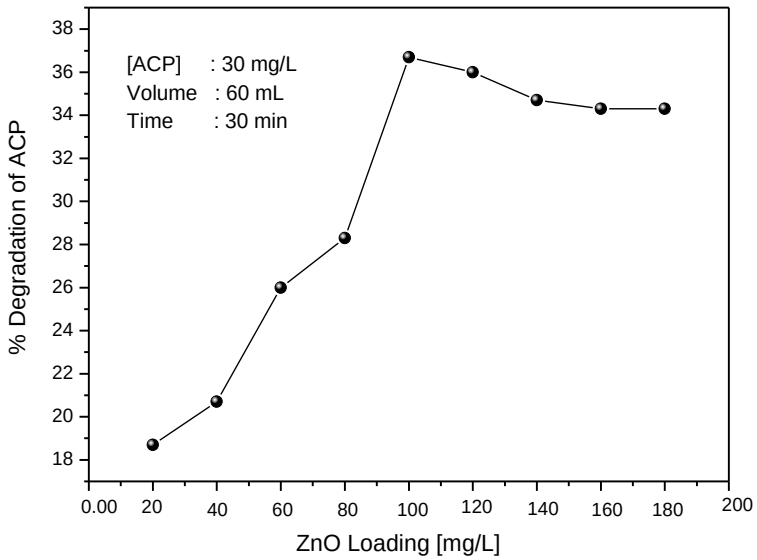

Fig. 4.6: Effect of catalyst dosage on the photocatalytic degradation of ACP under sunlight

The degradation of ACP increases with increase in catalyst loading upto 100 mg/L and stabilizes/decreases thereafter. The enhancement in the degradation rate with increase in catalyst loading is usually attributed to corresponding increase in the number of adsorption and interaction sites for the substrate and/or intermediates and more absorption of light quanta. But in the case of ACP, the adsorption over ZnO is not significant. Hence the role of the catalyst is maximizing the light absorption and the resultant increase in the generation of hydroxyl and other reactive radicals in the system. These reactive species result in increased interaction with the pollutant/intermediates, which account for the increasing degradation rate. However, increase in catalyst loading beyond the optimum will result only in the scattering and reduced passage of light through the suspension medium, thereby stabilizing or even

decreasing the rate of degradation. At higher catalyst loading beyond the optimum, there is possibility of aggregation of catalyst particle which reduces the number of available active surface sites. Also at higher catalyst loading, part of the activated zinc oxide gets deactivated through collision with ground state catalyst as described in the case of AMS degradation (Chapter 3). The optimum ZnO loading of 100 mg/L is chosen for further studies.

4.3.2 Effect of initial concentration of ACP

The effect of initial concentration of ACP in water on its photocatalytic degradation under sunlight was studied in the concentration range of 5-60 mg/L. The results (figure 4.7) show that the percentage degradation of ACP decreases as the initial concentration of ACP increases.

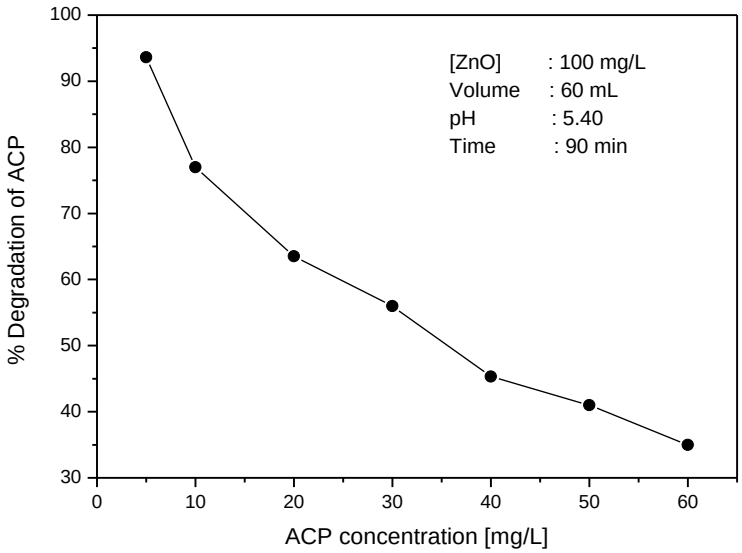

Fig. 4.7: Effect of concentration of ACP on its photocatalytic degradation

On the other hand, the rate of degradation increases steadily with increase in initial concentration of ACP and eventually stabilizes (figure 4.8). The graph also indicates that the rate follows variable kinetics at different ACP concentrations. The maximum kinetic rate of 2.4×10^{-1} mg/L/min was obtained at 50 mg/L of ACP concentration. This is followed by constant degradation rate at higher ACP concentration implying zero order kinetics.

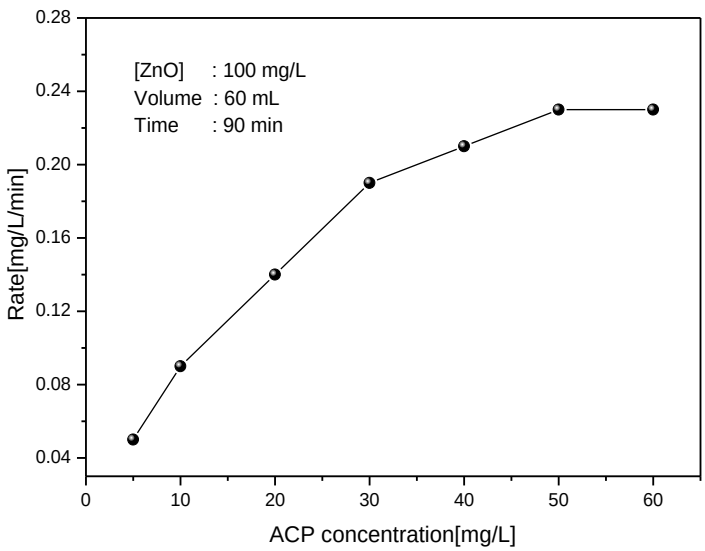

Fig. 4.8: Effect of concentration of ACP on its rate of degradation

The photocatalytic degradation of many pollutants is reported to follow pseudo first order kinetics [112-114]. The increase in the degradation rate with increase in concentration is normally explained based on the increase in adsorption of substrate on the catalyst surface. This will continue until the entire surface is fully covered and all the active sites are occupied. But in the present case this explanation is not applicable as the adsorption of ACP on ZnO is very small. But with

increase in ACP concentration, more substrate molecules will be available in the bulk as well as in the vicinity of the surface which can effectively interact with the surface generated reactive free radicals and ROS such as $^{\bullet}OH$ and H_2O_2. However, at higher concentrations beyond the optimum, at least a part of the incident light may be blocked and/or absorbed by ACP and the intermediates thereby reducing the photons available for effective catalyst activation. Moreover, major portion of the degradation reaction occurs in the region (reaction zone) close to the irradiated side, where the irradiation intensity is much greater than the other side. This retardation in the penetration of light, at longer distance from the light source, results in the decreased degradation [115-118]. With the increase in initial concentration of ACP, the requirement of catalyst surface needed for the generation of adequate concentration of reactive species in order to maintain corresponding degradation rate also increases. Since the intensity of illumination and catalyst concentration are kept constant, the relative number of ROS available for interacting with the ACP also decreases leading to stabilized/decreased rate of degradation. Once the concentration of the substrate is enough to interact with all the optimum available ROS and other reactive free radicals, any further increase cannot result in increased reaction. Hence the ACP removal becomes independent of its concentration. It is also possible that at higher substrate concentration, some of the reaction intermediates may get adsorbed onto the surface or remain in the bulk for relatively longer period and this will reduce the frequency of interaction between fresh ACP molecules and the ROS. Complete domination of the reaction system by the reactant/ intermediates can also result in suppression of the generation of surface

initiated reactive free radicals. At any point in time, there will be an optimum for the number of substrate molecules that can interact with the reactive free radicals generated by the surface. This optimum will depend on a number of parameters such as initial concentration of the substrate, intensity of illumination, wavelength of light, mass and type of photocatalyst, nature and concentration of the intermediates, type and geometry of photo reactor etc. Consequently, the measurements and calculations apply only to the specific reaction conditions and cannot be generalized.

The reciprocal plot of initial rate of degradation of ACP against its initial concentration yields a straight line graph (figure 4.9) indicating first order kinetics. This shows that the reaction follows Langmuir-Hinshelwood model modified to accommodate reactions occurring at solid-liquid interface [116,117].

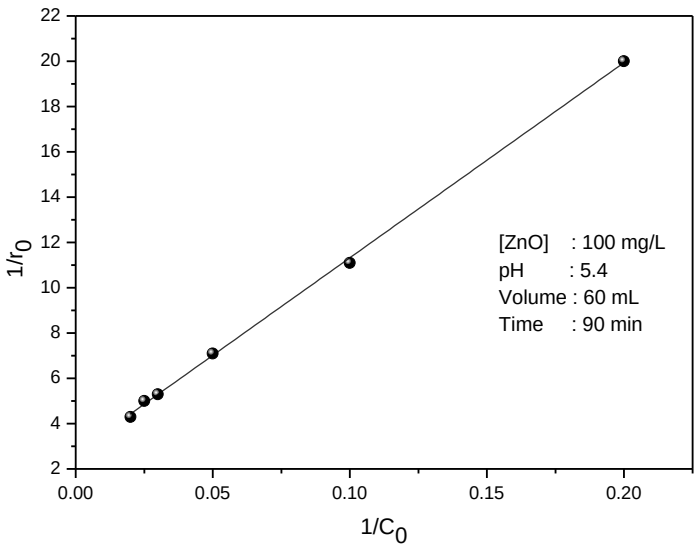

Fig. 4.9: Reciprocal plot of initial rate of ACP degradation versus its initial concentration.

The logarithmic plot of ln (C_0/C) vs time (t), where C_0 is the initial ACP concentration and C is the concentration remaining after time t (in the concentration range of 10-50 mg/L) gives straight lines (figure 4.10) that pass through the origin. This also reconfirms the pseudo first order kinetics.

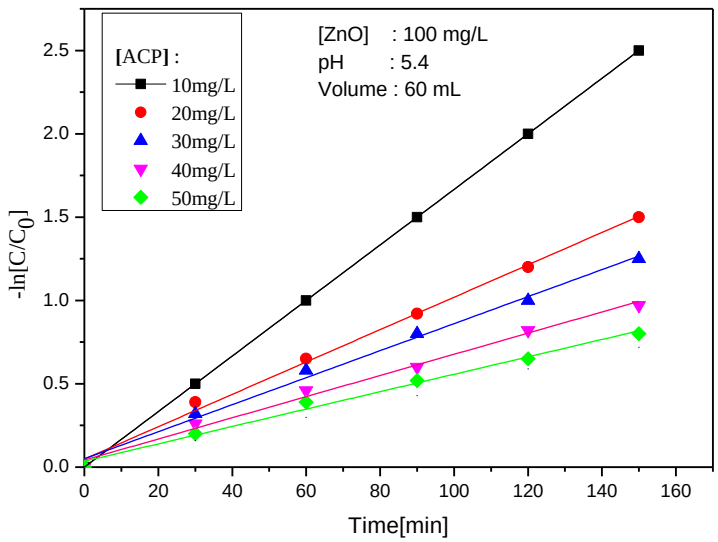

Fig. 4.10: Logarithmic plot for the degradation of ACP

The apparent rate constant k for each substrate concentration, represented by the slope of the curve is calculated and presented in table 4.3. It is observed that the rate constant decreases as the ACP concentration increases. This can be explained based on the reduction in the relative percentage fraction of the substrate which can effectively interact with the ROS. Details on this are discussed in Chapter 3, section 3.3.4.

Table 4.3: Pseudo first order rate constants for the photocatalytic degradation of ACP over ZnO.

Sl No	[ZnO], mg/L	[ACP], mg/L	k^r x 10^{-3} (min^{-1})
1	100	10	16.7
2	100	20	9.7
3	100	30	8.1
4	100	40	6.3
5	100	50	5.2

4.3.3 Effect of pH

The pH of the reaction medium can have significant effect on the aqueous phase photocatalytic process, as surface characteristics of the catalyst as well as the chemical nature of the substrate and species derived from them change with the pH. The point of zero charge (PZC) of ZnO is ~ 9.3. At pH values < 9.3, the catalyst's surface is positively charged and at pH values > 9.3 it is negatively charged. Depending on the ionic form of the organic compound, i.e., anionic, neutral or cationic, electrostatic attraction or repulsion takes place and the photodegradation rate can be enhanced or inhibited. The effect of pH on the photocatalytic degradation of ACP is investigated by varying the pH of the medium from 2 to 12 keeping other parameters constant. The results are presented in figure 4.11. It was found that pH has only moderate effect on the degradation of ACP in the range of 4 to 11, with marginal increase in the alkaline range. This is expected since the adsorption of ACP on the ZnO is very low and hence the pH which affects primarily the surface chemistry of the catalyst cannot influence any surface initiated process involving the substrate. The

very low degradation at pH=2 may be due to the corrosion of ZnO at lower pH and consequent decrease in the availability of active surface sites. Poulios et al. [123] also reported similar observations.

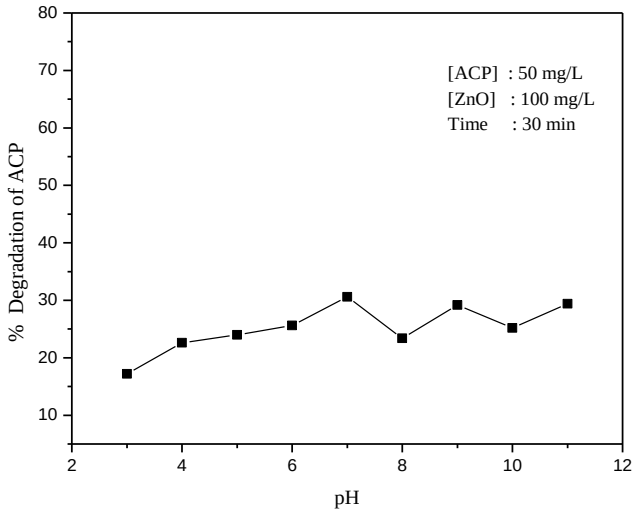

Fig. 4.11: Effect of pH on the photocatalytic degradation of ACP

The influence of pH on the photocatalytic activity of ZnO is often inconsistent and hence cannot be generalized. A complex interplay of many factors, i.e., chemistry of the surface, extent and mode of adsorption (of ACP, HACP and/or other minor unidentified intermediates in this case), concentration of reactive free radicals such as $^{\bullet}OH$ etc., determines the pH effect in many cases. Since the adsorption of the substrate is poor in the present case, the pH effect is mostly confined to the surface-initiated generation of reactive $^{\bullet}OH$ radicals and other ROS. Since the photocatalytic generation of reactive species is facilitated by both electrons and holes, the net effect at any particular pH may be more or less the same. This may be the reason for the absence of any significant

pH effect. Moderate enhancement in the alkaline pH, as explained in earlier chapter may be due to the increase in the availability of OH^- ions and consequently the reactive $^{\bullet}OH$ radicals.

4.3.3.1 Effect of pH on the adsorption of ACP over ZnO

The adsorption of ACP over ZnO is found to be negligible (table 4.1) under standard pH conditions, (pH ≈ 5.4). The effect of pH on the adsorption of ACP over ZnO catalyst in the pH range 3-12 also is investigated. The results show that pH has no significant effect on the adsorption of ACP on ZnO (table 4.4). Slightly higher decrease in the concentration of ACP in the supernatant at extreme alkaline pH (11-12) need not be due to surface adsorption only but also due to the change in the surface chemistry of ZnO and consequent likely interaction with the ACP. In any case, the increase is negligible and it may be concluded that pH has no effect on the adsorption of ACP on ZnO.

Table 4.4: Effect of pH on the adsorption of ACP over ZnO
[ACP]=50 mg/L, [ZnO] =100 mg/L, Volume =60 mL, Time=3 hr

pH	% Adsorption
At normal solution pH[5.40]	2.2
3	2.0
4	2.2
5	2.0
6	2.4
7	2.4
8	2.3
9	2.4
10	2.6
11	2.8
12	3.0

4.3.3.2 Corrosion of ZnO under solar photocatalysis at different pH

The corrosion study of ZnO catalyst in presence of ACP both in dark and under sunlight irradiation at two different exposure times (1and 4 hr) is investigated in detail by weight-loss method as described in section 3.3.6 of Chapter 3. The results presented in figure 4.12 clearly show that except under extreme acidic and alkaline pH, corrosion is not significant especially at the pH at which the ACP degradation is carried out (pH~ 5.4). Details are as discussed in section 3.3.6 of Chapter 3.

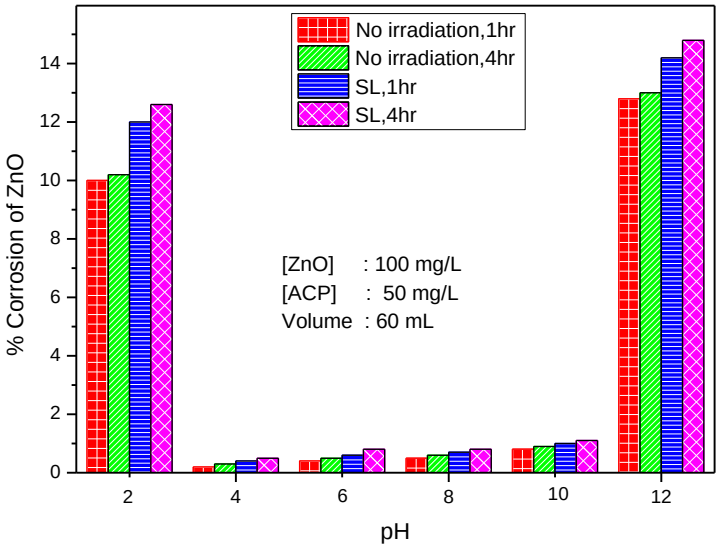

Fig. 4.12: Corrosion of ZnO at different pH in the presence and absence of solar irradiation

4.3.4 Formation and fate of the H_2O_2 formed during the ACP degradation

H_2O_2 is detected as a co-product as well as intermediate in the photocatalytic degradation of many organic compounds [37, 102, 103, 111,114,119]. However, its concentration does not increase in proportion

to the degradation of the pollutant and gets stabilized or decreases even before the pollutant degradation is complete. This has been explained as due to the oscillation in the concentration of H_2O_2 caused by its simultaneous formation and decomposition [113, 126]. The concentration of H_2O_2 formed during the photocatalytic degradation of ACP was determined by iodometric method. The concentration increases initially, decreases later and increases again (oscillation) as shown in figure 4.13. Depending on the domination of the formation or decomposition process, the net concentration of H_2O_2 at any point of time varies and this results in periodic crests and troughs in the concentration curve. Various steps leading to the concurrent formation and decomposition of H_2O_2 are discussed in detail in Chapter 3 (section 3.3.8).

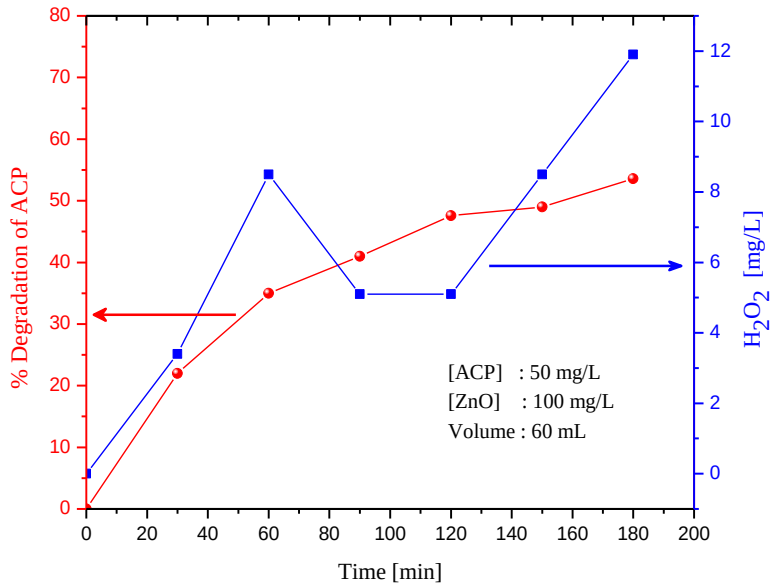

Fig. 4.13: Net concentration of H_2O_2 in the reaction system during the photocatalytic degradation of ACP on ZnO.

4.3.5 Effect of added H_2O_2

H_2O_2 is formed insitu in photocatalytic system as explained in previous section. H_2O_2 is also an effective oxidant which enhances the photocatalytic degradation of many pollutants by providing additional reactive $^{\bullet}OH$ radicals. Thus the degradation of ACP also is likely to be influenced by the H_2O_2 formed insitu. In this context, the effect of externally added H_2O_2 on the degradation of ACP at different concentrations is investigated. The results are shown in figure 4.14. H_2O_2 enhances the degradation of ACP moderately at all concentrations. However, the extent of enhancement stabilizes at higher concentration (>10 mg/L) of H_2O_2, especially in the early stages of reaction. However, at lower concentrations (<10 mg/L) of H_2O_2, initially there is enhancement followed by 'no effect' later on. This is consistent with the 'concentration-dependent effect' of H_2O_2 on the photocatalytic degradation of organics in water.

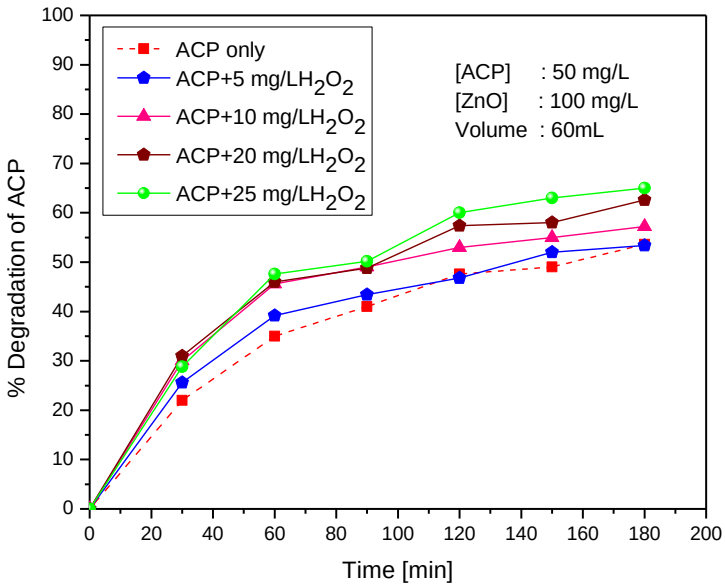

Fig. 4.14: Effect of added H_2O_2 on the photocatalytic degradation of ACP

This inconsistency in H_2O_2 effect, especially at later stage of reaction may be explained based on the dual role of H_2O_2 as a promoter as well as inhibitor in photocatalytic reactions [28,117]. The oscillation in the concentration of insitu formed H_2O_2 resulting from its concurrent formation and decomposition also may contribute to the inconsistency. As a result, the net concentration of H_2O_2 in the system is unpredictable at any time interval during the irradiation. The oscillation in the concentration of H_2O_2 and its dual role as a promotor or inhibitor are concentration-dependent while the concentration itself is dependent on the competing reactions taking place in the system [113]. The concentration of reactants, reaction conditions and the nature of interactions are important factors in this respect.

The enhancement of the degradation of organic pollutants (ACP here) by H_2O_2 is explained based on its role as an electron acceptor and consequent inhibition of the recombination of photogenerated electrons and holes. H_2O_2 can also produce reactive $^{\bullet}OH$ radicals as follows:

$$H_2O_2 + h\nu \rightarrow 2^{\bullet}OH \quad (105)$$

$$H_2O_2 + O_2^{-\bullet} \rightarrow {}^{\bullet}OH + OH^- + O_2 \quad (106)$$

$$H_2O_2 + e^- \rightarrow {}^{\bullet}OH + OH^- \quad (107)$$

These $^{\bullet}OH$ radicals can enhance the degradation of the pollutant. However, at higher concentrations of H_2O_2, either formed insitu or by external addition or both, it acts more as a scavenger of $^{\bullet}OH$ as well as holes as follows:

$$H_2O_2 + e^- \rightarrow {}^{\bullet}OH + OH^- \quad (108)$$

$$2OH^- + h^+ \rightarrow {}^{\bullet}OH + OH^- \quad (109)$$

$$H_2O_2 + 2\,h^+_{vb} \rightarrow O_2 + 2H^+ \quad (110)$$

$$H_2O_2 + {}^{\bullet}OH\,/h^+ \rightarrow HO_2\bullet + H_2O/H^+ \quad (111)$$

Thus H_2O_2 becomes a major competitor to the substrate for the ROS on the surface of the catalyst (or in the neighborhood) as well as in the solution bulk, resulting in its self-decomposition. Earlier studies have shown that the adsorption of H_2O_2 on ZnO is negligible and hence most of it will be in solution [127]. This also contributes to its competition with the substrate in the bulk. Hence the enhancing effect of added H_2O_2 is less prominent at higher concentration.

4.3.6 Effect of Humic acid

Humic substances which are naturally present in water are reported to enhance or inhibit the photocatalytic degradation of many water pollutants depending on the characteristic of the substrate, catalyst as well as the reaction conditions [28,140]. The effect of humic acid (HA) on the photocatalytic degradation of ACP using ZnO as catalyst under solar irradiation was investigated at different concentrations of the former and the results are plotted in figure 4.15. HA inhibits the degradation of ACP at all concentrations, and the extent of inhibition is dependent on the concentration of HA, the higher the concentration, greater the inhibition.

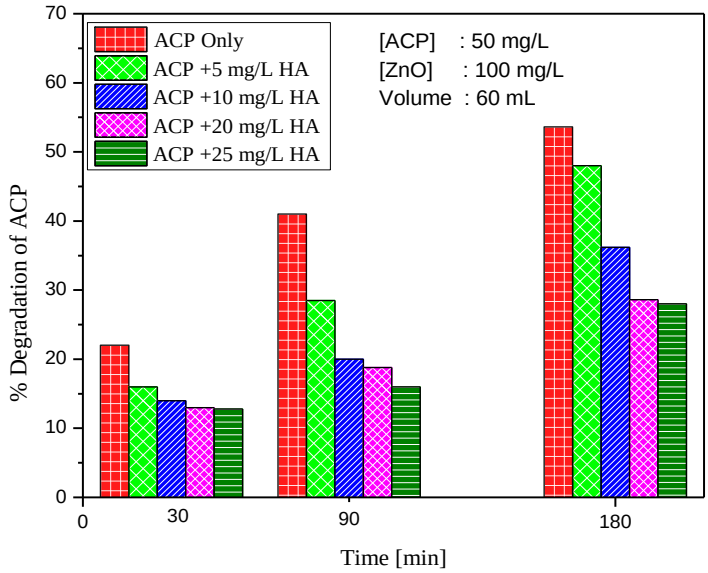

Fig. 4.15: Effect of Humic acid on the photocatalytic degradation of ACP

Natural organic matter such as HA present in water may absorb light, which in turn reduces the quantum of light available for the activation of the catalyst. This can inhibit the photocatalytic degradation. The formation of hydroxyl radical and the reactive H_2O_2 requires adequate light energy and hence any decrease in the quantum of energy received by the surface/system will adversely affect the degradation. HA can also act as an effective free radical scavenger which can consume ROS such as $^{\bullet}OH/HO_2^{\bullet}/O_2^{-\bullet}$. as shown in equations 112 and 113 [28,140]:

$$HA + h\nu \rightarrow HA^* \quad (112)$$

$$^{\bullet}OH,\ HO_2.\ O_2^{-\bullet}.\ \text{etc.} + HA^* \rightarrow \text{Intermediates} \rightarrow \text{Oxidized products} \quad (113)$$

The excited HA will decompose/get oxidized eventually. The results show that even low concentration of HA, which is comparable to that present in natural water in local streams and ponds, can inhibit the degradation of ACP.

4.3.7 Role of oxygen

It is established that in photocatalytic degradation reactions of organic pollutants, the reactive oxygen species generated during the irradiation of semiconductor oxide-aqueous suspensions play an important role. Both dissolved and adsorbed O_2 scavenge the electrons generated by the photo activation of the semiconductor oxide catalyst forming superoxide radical anion and other reactive species. Thus the recombination of photogenerated electrons and holes is inhibited. Hence both will be available for the formation of reactive free radicals. The role of dissolved O_2 and superoxide ion in TiO_2 photocatalysis was quantitatively demonstrated by Hirakawa et al. [142]. The role of dissolved O_2 on the ZnO mediated photocatalytic degradation of ACP was verified by deoxygenating the system with N_2 and carrying out the experiments under otherwise identical conditions. Subsequently, the suspensions were oxygenated by bubbling O_2 for 5 min. and the photocatalytic degradation is evaluated again. The results are shown in figure 4.16.

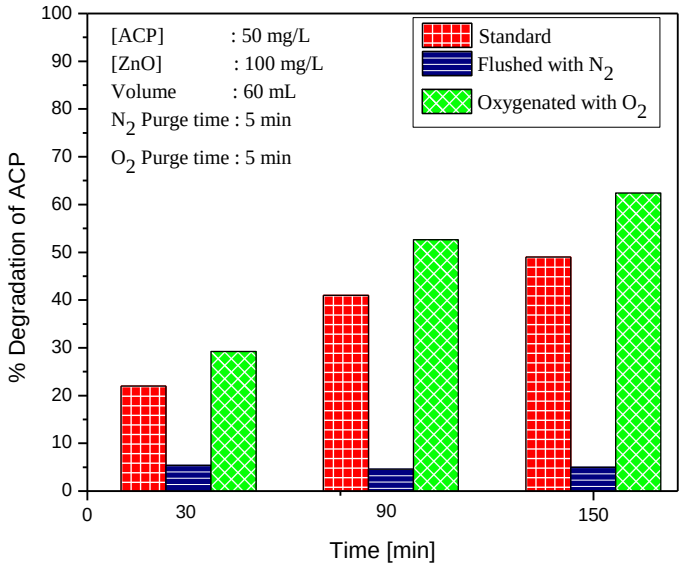

Fig. 4.16: Effect of O_2 on the photocatalytic degradation of ACP

The photocatalytic degradation of ACP is almost fully inhibited in the absence of O_2 at all time intervals. However, on oxygenating the suspension, the percentage degradation of ACP is significantly more. The slight degradation observed in the deaerated system may be due to the adsorbed and dissolved O_2, which cannot be fully removed by deaeration. In this case, the available O_2 is fully consumed in the first 30 min itself. That is the reason why the degradation is not proceeding further thereafter. The study conclusively establishes the role of O_2 in the photocatalytic degradation of organic pollutants.

4.3.8 Effect of salts/anions

The dissolved and suspended solids present in natural water may affect the efficiency of the photocatalytic degradation process. Even though the suspended solids can be removed by physical methods such as

filtration, decantation, sedimentation etc., the dissolved salts cannot be removed that easily. Hence any viable technology for the mineralization of organic pollutants in water must take the effect of these salts on the efficiency of the process also into consideration. Various inorganic ionic species present in the system can compete with the substrate as well as the intermediates for the active surface sites on the catalyst. They can also interact with the ROS and deactivate them. Other possible effects include; reducing the quantum of solar radiation reaching the catalyst surface, formation of unwanted byproducts etc. These processes can invariably affect the photocatalytic degradation and mineralization efficiency [123,125,157,167]. The effect of the salts/anions may be further complicated by factors such as pH, nature of catalyst, substrate, concentration of the species etc. In this context, the effect of some of the commonly encountered salts in municipal and industrial wastewater on the efficiency of ACP degradation is examined. The anions tested are fluoride (F^-), chloride (Cl^-), bromide (Br^-), iodide (I^-), sulphate (SO_4^{2-}), nitrate (NO_3^-), phosphate (PO_4^{3-}), acetate (CH_3COO^-), oxalate ($C_2O_4^{2-}$), carbonate (CO_3^{2-}) and bicarbonate (HCO_3^-). The investigation was carried out with different concentrations of these anions and at different reaction time intervals.

In the early reaction time of 30 min and at lower anion concentration (5 mg/L), all halide ions except bromide (which is an enhancer) mildly inhibit the degradation. PO_4^{3-} strongly inhibits the degradation while CO_3^{2-} and HCO_3^- inhibit the degradation slightly. SO_4^{2-} and $C_2O_4^{2-}$ enhance the degradation moderately such that $SO_4^{2-} > C_2O_4^{2-}$ (figure 4.17). However, NO_3^- and CH_3COO^- have no effect. The effect by various ions

under the above conditions (30 min, 5 mg/L) may be summarized as follows:

Inhibition: $PO_4^{3-} > HCO_3^- \approx I^- \approx CO_3^{2-} > F^- \approx Cl^-$

No effect: NO_3^-, CH_3COO^-

Enhancement: $SO_4^{2-} > Br^- > C_2O_4^{2-}$

Similarly the effect at higher reaction time of 120 min may be summarized as:

Inhibition: $PO_4^{3-} > I^- > HCO_3^- > C_2O_4^{2-} > Cl^- > CO_3^{2-}$

No effect: F^-, NO_3^-, CH_3COO^-

Enhancement: $Br^- > SO_4^{2-}$

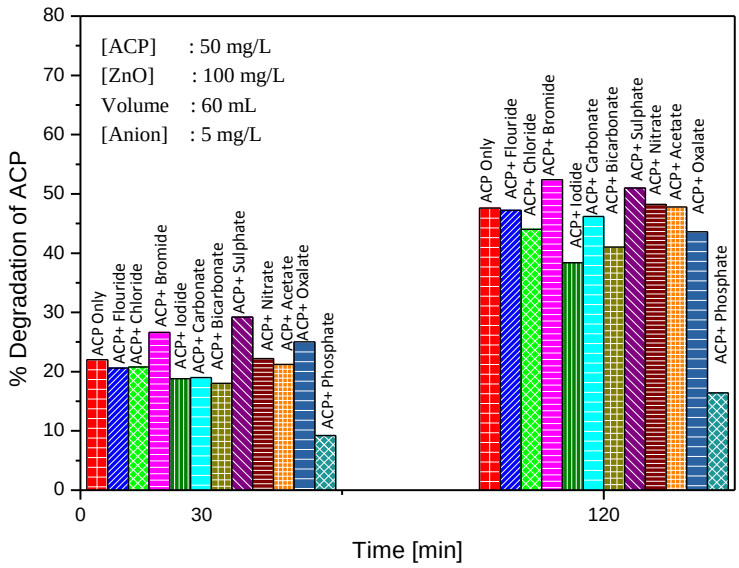

Fig. 4.17: Effect of anions on the degradation of ACP after different reaction times

The effect of anions at higher concentrations (20 mg/L) on the degradation of ACP at 30 min of reaction is given in figure 4.18.

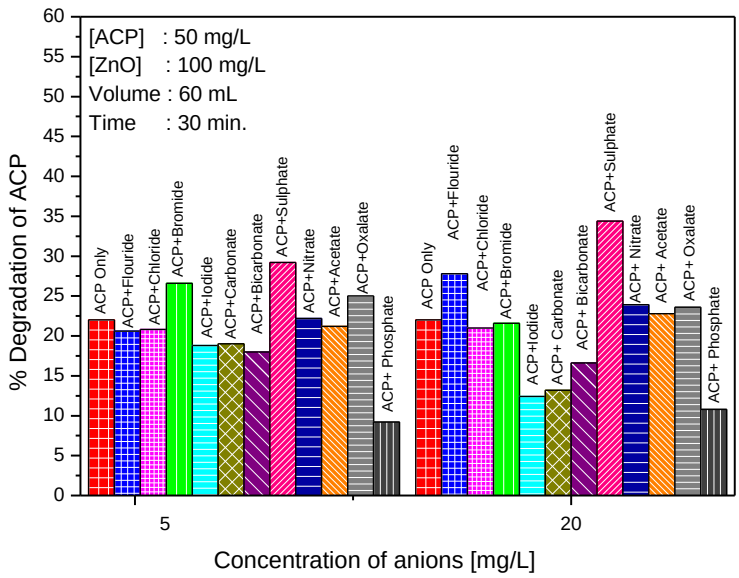

Fig. 4.18: Effect of various anions at different concentrations on the degradation of ACP

SO_4^{2-} and F^- function as enhancers at higher concentration.

PO_4^{3-}, HCO_3^-, CO_3^{2-} and I^- function as inhibitors. The effect after 30 min may be summarized as:

Inhibition: $PO_4^{3-} > I^- \geq CO_3^{2-} > HCO_3^-$

No effect: Cl^-, Br^-, CH_3COO^-, $C_2O_4^{2-}$, NO_3^-

Enhancement: $SO_4^{2-} > F^-$

The results clearly show that both concentration of the anions and the reaction time influence the anion effect on the degradation. Hence a detailed study of these two parameters with respect to each anion on the photocatalytic degradation of ACP is undertaken. The results are as follows:

a) Effect of F^-

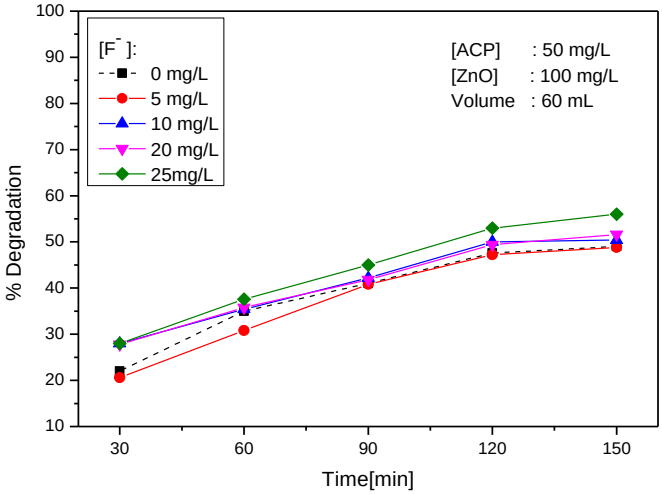

Fig. 4.19: Effect of concentration of F^- and reaction time on the photocatalytic degradation of ACP

Except at very low concentration of 5 mg/L, F^- has either 'no effect' or is a mild enhancer of the photocatalytic degradation of ACP.

b) Effect of Cl^-

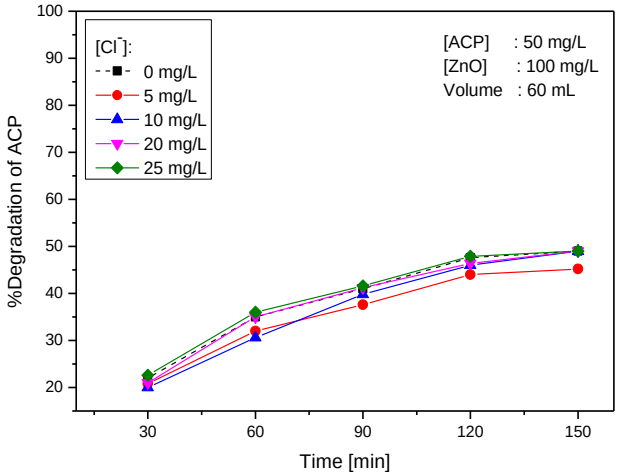

Fig. 4.20: Effect of concentration of Cl^- and reaction time on the photocatalytic degradation of ACP

Practically no effect or mild inhibition at all concentrations of Cl^-

c) Effect of Br^-

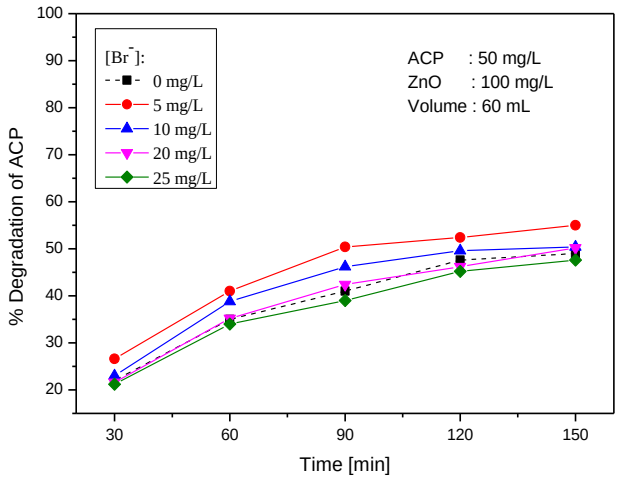

Fig. 4.21: Effect of concentration of Br^- and reaction time on the photocatalytic degradation of ACP

At lower concentration (5-15 mg/L), Br^- is an enhancer. At higher concentrations (>20mg/L) it has 'no effect'.

d) Effect of I^-

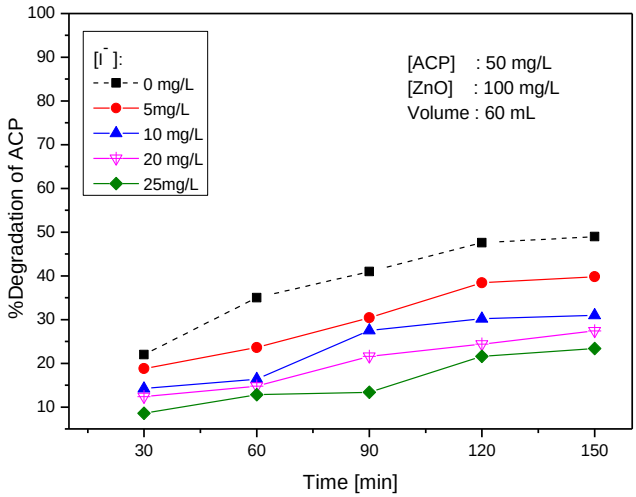

Fig. 4.22: Effect of concentration of I^- and reaction time on the photocatalytic degradation of ACP

I^- is a strong inhibitor at all concentrations and all reaction times.

e) Effect of CO_3^{2-}

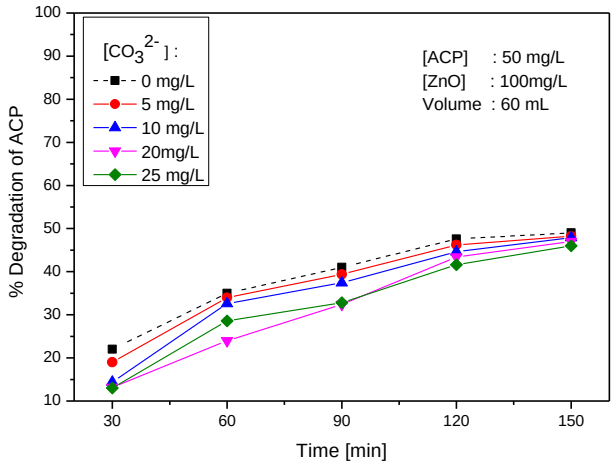

Fig. 4. 23: Effect of concentration of CO_3^{2-} and reaction time on the photocatalytic degradation of ACP

CO_3^{2-} is a mild inhibitor at all concentrations and all reaction times.

f) Effect of HCO_3^-

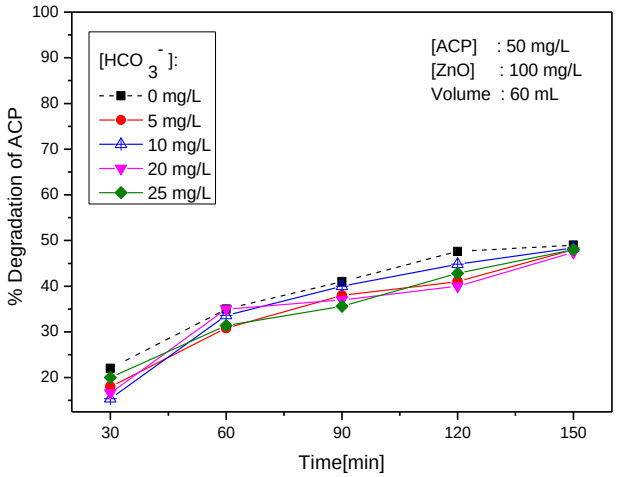

Fig. 4. 24: Effect of concentration of HCO_3^- and reaction time on the photocatalytic degradation of ACP

HCO_3^- is a mild inhibitor at all concentrations and reaction times.

g) Effect of SO_4^{2-}

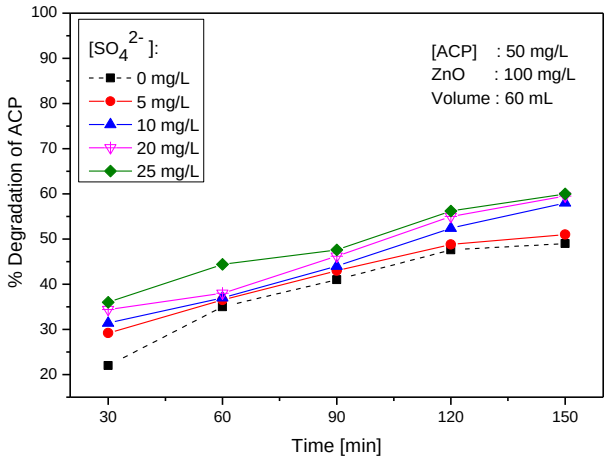

Fig. 4. 25: Effect of concentration of SO_4^{2-} and reaction time on the photocatalytic degradation of ACP

SO_4^{2-} is an enhancer at all concentrations and all reaction times.

h) Effect of NO_3^-

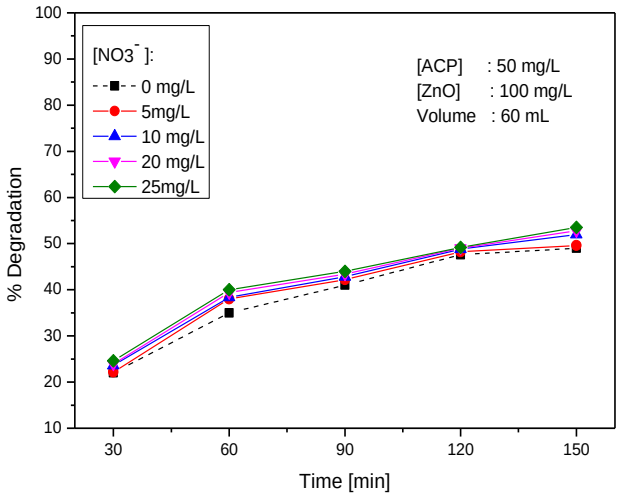

Fig. 4.26: Effect of concentration of NO_3^- and reaction time on the photocatalytic degradation of ACP

NO_3^- has practically no effect on the degradation of ACP.

i) Effect of PO_4^{3-}

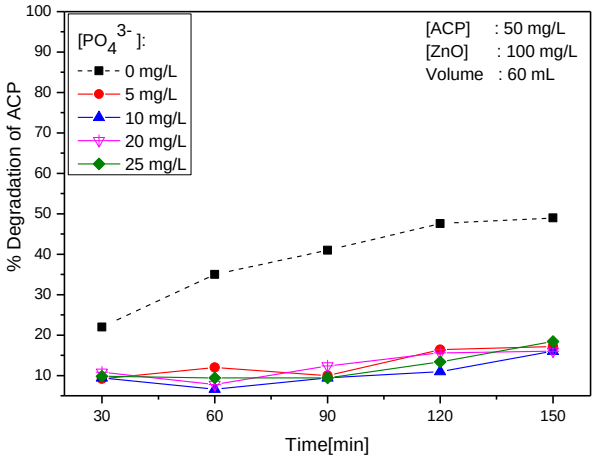

Fig.4.27: Effect of concentration of PO_4^{3-} and reaction time on the photocatalytic degradation of ACP

PO_4^{3-} is a strong inhibitor at all concentrations and all reaction times. However, the degree of inhibition is not much influenced by the concentration of the anion.

j) Effect of CH_3COO^-

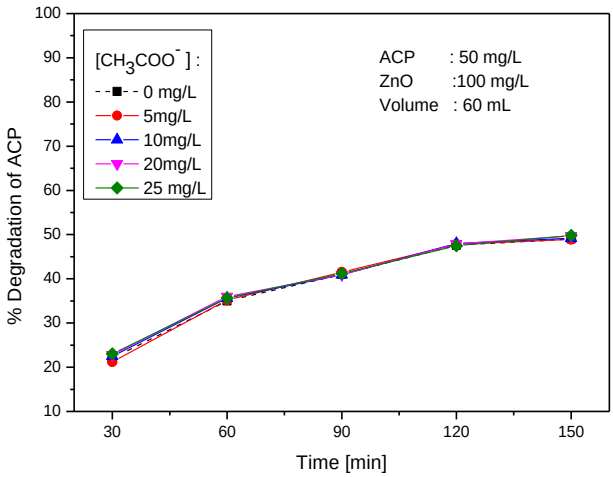

Fig. 4.28: Effect of concentration of CH_3COO^- and reaction time on the photocatalytic degradation of ACP

Acetate ion shows practically no effect on the degradation at all concentrations and reaction times.

k) Effect of $C_2O_4^{2-}$

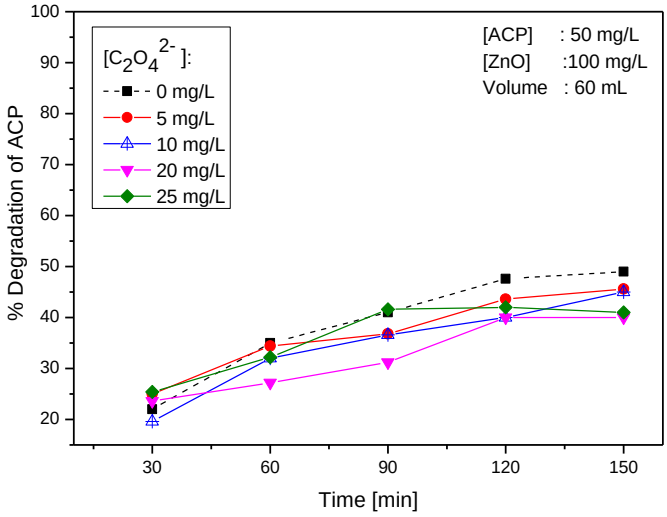

Fig. 4. 29: Effect of concentration of $C_2O_4^{2-}$ and reaction time on the photocatalytic degradation of ACP

$C_2O_4^{2-}$ has no effect in the early stages of reaction. Later on, the effect becomes inhibition, the degree of inhibition increasing moderately with increase in concentration.

The results confirm the earlier findings from this laboratory [127] that the effect of salts/anions on the photocatalytic degradation of water pollutants is dependent on their relative concentration and the relative abundance with respect to the substrate, reaction conditions, catalyst etc. SO_4^{2-} clearly enhances the degradation while I^-, PO_4^{3-}, CO_3^{2-}, HCO_3^- and $C_2O_4^{2-}$ are clear inhibitors. The relative efficiency of various anions on the photocatalytic degradation of ACP at different concentrations and reaction times are tabulated in table 4.5.

Table 4.5: Comparative effect of anions at various concentrations and reaction time on the photocatalytic degradation of ACP.
[ACP]=50 mg/L, [ZnO] = 100 mg/L, Volume =60mL

Time [min]	[Anion], mg/L	Comparative effect
30	5	Enhancement: $SO_4^{2-} > Br^- > C_2O_4^{2-}$ No effect: NO_3^-, CH_3COO^- Inhibition: $PO_4^{3-} > HCO_3^- \approx I^- \approx CO_3^{2-} > F^- \approx Cl^-$
	10	Enhancement: $SO_4^{2-} > F^-$ No effect: Br^-, NO_3^-, CH_3COO^- Inhibition: $PO_4^{3-} > I^- \approx CO_3^{2-} > HCO_3^- > C_2O_4^{2-} > Cl^-$
	20	Enhancement: $SO_4^{2-} > F^-$ No effect: Br^-, Cl^-, NO_3^-, CH_3COO^-, $C_2O_4^{2-}$ Inhibition: $PO_4^{3-} > I^- \geq CO_3^{2-} > HCO_3^-$
	25	Enhancement: $SO_4^{2-} > F^-$ No effect: Cl^-, Br^-, CH_3COO^-, NO_3^-, $C_2O_4^{2-}$ Inhibition: $I^- > PO_4^{3-} > CO_3^{2-} > HCO_3^-$
60	5	Enhancement: $Br^- > SO_4^{2-}$ No effect: CO_3^{2-}, $C_2O_4^{2-}$, NO_3^-, CH_3COO^- Inhibition: $PO_4^{3-} > I^- > HCO_3^- > F^- > Cl^-$
	10	Enhancement: $Br^- > SO_4^{2-}$ No effect: F^-, NO_3^-, HCO_3^-, CH_3COO^- Inhibition: $PO_4^{3-} > I^- > Cl^- > C_2O_4^{2-} > CO_3^{2-}$
	20	Enhancement: SO_4^{2-} No effect: F^-, Cl^-, Br^-, HCO_3^-, NO_3^-, CH_3COO^- Inhibition: $PO_4^{3-} > I^- > CO_3^{2-} > C_2O_4^{2-}$
	25	Enhancement: $SO_4^{2-} > F^-$ No effect: Cl^-, Br^-, NO_3^-, CH_3COO^- Inhibition: $PO_4^{3-} > I^- > CO_3^{2-} > HCO_3^- > C_2O_4^{2-}$
90	5	Enhancement: $Br^- > SO_4^{2-}$ No effect: F^-, CO_3^{2-}, NO_3^- Inhibition: $PO_4^{3-} > I^- > C_2O_4^{2-} > Cl^- \approx CH_3COO^- \approx HCO_3^-$
	10	Enhancement: $Br^- > SO_4^{2-}$ No effect: F^-, Cl^-, HCO_3^-, NO_3^- Inhibition: $PO_4^{3-} > I^- > CH_3COO^- > C_2O_4^{2-} > CO_3^{2-}$

	20	Enhancement: SO_4^{2-} No effect : F^-, Br^-, Cl^- , NO_3^-, CH_3COO^- Inhibition: PO_4^{3-} > I^- > $C_2O_4^{2-}$ > CO_3^{2-} > HCO_3^-
	25	Enhancement: SO_4^{2-} > F^- No effect : Cl^-, Br^-, NO_3^-, CH_3COO^-, $C_2O_4^{2-}$ Inhibition: PO_4^{3-} > I^- > CO_3^{2-} > HCO_3^-
120	5	Enhancement: Br^- > SO_4^{2-} No effect : F^-, NO_3^-, CH_3COO^- Inhibition: PO_4^{3-} > I^- > HCO_3^- > $C_2O_4^{2-}$ > Cl^-> CO_3^{2-}
	10	Enhancement: SO_4^{2-} No effect : F^-, Cl^-, Br^-, NO_3^-, CH_3COO^- Inhibition: PO_4^{3-} > I^- > $C_2O_4^{2-}$ > HCO_3^- > CO_3^{2-}
	20	Enhancement: SO_4^{2-} No effect : Cl^-, Br^-, SO_4^{2-} , NO_3^-, CH_3COO^- Inhibition: PO_4^{3-} > I^- > $C_2O_4^{2-}$ ≈ HCO_3^- > CO_3^{2-}
	25	Enhancement: SO_4^{2-} > F^- No effect : Cl^-, Br^-, NO_3^-, CH_3COO^- Inhibition: PO_4^{3-} > I^- > $C_2O_4^{2-}$ ≈ HCO_3^- > CO_3^{2-}
150	5	Enhancement: SO_4^{2-} >Br^- No effect : F^-, CO_3^{2-}, HCO_3^-, NO_3^-, CH_3COO^- Inhibition: PO_4^{3-} > I^- > Cl^- > $C_2O_4^{2-}$
	10	Enhancement: SO_4^{2-} No effect : F^-, Cl^-, Br^-, CO_3^{2-}, HCO_3^-, NO_3^-, CH_3COO^- Inhibition: PO_4^{3-} > I^- > $C_2O_4^{2-}$
	20	Enhancement: SO_4^{2-} No effect : F^-, Cl^-, Br^-, NO_3^-, CO_3^{2-}, HCO_3^-, CH_3COO^- Inhibition: PO_4^{3-} > I^- > $C_2O_4^{2-}$
	25	Enhancement: SO_4^{2-} > F^- No effect : Cl^-, Br^-, HCO_3^-, NO_3^-, CH_3COO^- Inhibition: PO_4^{3-} > I^- > $C_2O_4^{2-}$ > CO_3^{2-}

Thus it is seen that the effect depends on both the concentration of the anions and the reaction time in most cases. As explained in Chapter 3, the anions are known to interact with the reactive $^{\bullet}OH$ radicals and deactivate them. In this process they form the respective radical anions which are also good oxidants. Hence the inhibition caused by the quenching of $^{\bullet}OH$ radical is not significant in many cases. The anions also get adsorbed on the catalyst surface, thus blocking the surface sites from adsorption of the substrates and also inhibiting the formation of reactive species [168]. In the present case, the adsorption of ACP on the catalyst surface was found to be negligible. Hence the role of anions which get preferentially adsorbed on the surface may be mainly in inhibiting the formation of reactive species. The adsorption of anions on the catalyst surface also influences the adsorption of the intermediates formed from the ACP degradation, which will also result in a slowdown of the degradation and mineralization.

In the case of halides, the ions X^- can function as $^{\bullet}OH$ radical scavenger and form less active $X_2^{\cdot -}$ or $\bullet XOH^-$ radicals which can inhibit the degradation of the substrate, in this case ACP.

Halide ion can be thermodynamically oxidized by valence band holes. Thus the holes are scavenged. At the normal pH~ 6 of the reaction system, the halide ion can be oxidized to halogen radical as

$$X^- + h^+_{VB} \rightarrow {}^{\bullet}X \qquad (114)$$

It is also possible that $^{\bullet}X$ can meet with conduction band electron to form X^- back again as,

$$^{\bullet}X + e^- \rightarrow X^- \qquad (115)$$

Thus the effect is practically 'nil'. Effectively both holes and electrons are scavenged by the halides, thereby inhibiting the formation of reactive oxygen species and subsequently, the degradation of the organic pollutant. $^{\bullet}X$ can also attack organic pollutants through addition/ elimination reaction at a rate lower than that of the reactive free radicals.

Among halide ions, iodide ion exhibits greater inhibition towards ACP degradation probably due to its relatively bigger size. Hence I^- occupies the surface more effectively and the degradation intermediates are prevented from getting access to the catalyst surface. This results in reduction in the generation of reactive species as described in Chapter 3. However, the effect may be different in the case of different catalysts, substrates and reaction conditions as explained earlier.

In the case of F^-, the inconsistency reported in many earlier studies is observed here also. This may be explained as follows: F^- ions are known to enhance the scavenging of photogenerated electron by O_2 or superoxide formation thereby making the holes freely available for oxidation. This could have resulted in enhancement of the degradation, which is not observed here consistently. The interaction between the photo activated semiconductor oxide surface and the F^- ion may be more complicated depending on the nature of the surface as well as the substrate. Presence of multiple interactions on the surface and in the bulk may complicate the mechanism further. In the case of TiO_2, the inconsistent effect of F^- in photocatalysis is also explained based on the blocking of the active surface sites by the halide and consequent reactions. In such cases, the degradation of the organics proceeds mostly

through homogeneous $^{\bullet}OH$ radical reaction in the bulk. Depending on which of the multiple processes dominate at any point of time, at various concentration of the halides, the effect may vary from enhancement to 'no effect' or inhibition.

The enhancement by SO_4^{2-} can be attributed to the formation of $SO_4^{-\bullet}$ radical by interaction of the anion with the photo-generated holes:

$$SO_4^{2-} + h^+ \rightarrow SO_4^{-\bullet} \quad (116)$$

The $SO_4^{-\bullet}$ radical can also generate reactive $^{\bullet}OH$ radicals and accelerate the degradation process as follows:

$$SO_4^{-\bullet} + H_2O \rightarrow SO_4^{2-} + {}^{\bullet}OH + H^+ \quad (117)$$

$$SO_4^{-\bullet} + {}^{\bullet}OH + ACP \rightarrow \text{Intermediate 1} \rightarrow \text{Intermediate 2} \ldots\ldots \rightarrow CO_2 + H_2O + SO_4^{2-} \quad (118)$$

The presence of SO_4^{2-} can generate extra $^{\bullet}OH$ radicals in the system, which can enhance the degradation. The presence of two highly reactive free radical species ($^{\bullet}OH$ and $SO_4^{-\bullet}$) together can compensate for any inhibition caused by the depletion of surface sites taken up by sulphate ions.

Two strongly inhibiting anions in this case are PO_4^{3-} and I^-. The inhibition by I^- is explained earlier. Phosphate ion strongly inhibits the ACP degradation at all concentrations and reaction times. This has been explained on the basis of the preferential adsorption of PO_4^{3-} over the catalyst surface. Phosphate ion can block more active sites on the catalyst surface which reduces the amount of active species formed by the

interaction of the catalyst with photon. The preferential adsorption of PO_4^{3-} over ZnO has been proved by the FTIR spectra (Section 3.3.14).

The inhibition of the photocatalytic degradation by various anions can also be explained based on their ability to scavenge the reactive $^{\bullet}OH$ radicals. The scavenging rate constant of $^{\bullet}OH$ by various anions are discussed in Chapter 3. The scavenging of $^{\bullet}OH$ by the anion can generate corresponding radical anions. Even though these radical anions are less reactive compared to $^{\bullet}OH$ radical they are available in the system for longer period and can interact more frequently with the pollutant /intermediates as discussed in detail in Chapter.3. Hence the inhibition cannot be sustained consistently.

The general mechanism of inhibition by HCO_3^- and CO_3^{2-} can be explained as follows:

In the case of HCO_3^-, the anion reacts with $^{\bullet}OH$ radicals producing less reactive $CO_3^-\bullet$ anion radicals.

$$^{\bullet}OH + HCO_3^- \rightarrow CO_3^-\bullet + H_2O \quad (119)$$

HCO_3^- can also act as scavenger of h^+ on the catalyst surface.

$$HCO_3^- + h^+ \rightarrow HCO_3\bullet \quad (120)$$

$$HCO_3\bullet \rightarrow CO_3^-\bullet + H^+ \quad (121)$$

$CO_3^-\bullet$ is less reactive than $^{\bullet}OH$

HCO_3^- also forms negatively charged layer on the catalyst surface. Consequently, the surface will be interacting less with the substrate anion or the intermediates.

In the case of CO_3^{2-}, the deactivation of $^{\bullet}OH$ takes place as follows:

$$^{\bullet}OH + CO_3^{2-} \rightarrow CO_3^{-}\bullet + OH^{-} \quad (122)$$

The effect of every anion has to be individually evaluated in view of the complexity of interactions involving many ions and free radicals on the surface as well as in the bulk. In the case of ions with 'no effect', the 'inhibiting' and 'enhancing' factors may be compensating. However, this also depends on the relative concentration of the anion and the substrate.

The inhibitory pattern at various concentrations and reaction times cannot be explained based on the trapping of $^{\bullet}OH$ radical alone or the adsorption of anions on the surface of the catalyst. For example, the scavenging rate constant of $^{\bullet}OH$ by HCO_3^- or PO_4^{3-} is about 100 times smaller than Cl^- or SO_4^{2-} [146]. The reaction rate of $^{\bullet}OH$ with HCO_3^- is much lower than the reaction rate with many organic compounds (refer table 3.7 in Chapter 3). If the inhibition is due to the scavenging of $^{\bullet}OH$ by the anion, the inhibition by selected anions should have been in the order

$$SO_4^{2-} > Cl^- > HCO_3^- > CO_3^{2-} > PO_4^{3-}$$

But this is not the case as seen from the experiments. Hence other mechanisms as discussed in Chapter 3 also need to be considered.

In this context, the formation of an inorganic anion layer on the surface of the catalyst is important. As explained in Chapter 3, the efficiency of layer formation is related to the solubility of the salts. The

salts with higher solubility shows lower adsorption and layer formation. The solubility of various salts at 20^0C, their layer formation tendency and effect on pollutant degradation was discussed in detail in Chapter 3. Based on this criteria the order of inhibition by various interacting anions must be in the order:

$$F^- > HCO_3^- > PO_4^{3-} > Cl^- > CO_3^{2-} > SO_4^{2-} > CH_3COO^- > NO_3^-$$

No such correlation is seen here. However, it may be stated in general, based on the inhibition by anions such as CO_3^{2-}, HCO_3^-, I^-, PO_4^{3-} etc. that layer formation is a possible cause for the inhibition of photo catalytic degradation.

Thus scavenging of the $^{\bullet}OH$ radicals, formation of reactive radical anions, blocking of the active surface sites by adsorption and layer formation can generally explain the effect of various anions towards the photocatalytic degradation of ACP, with certain exceptions. Different factors are responsible to different degrees for the effect of different anions. The individual contribution by various factors can be assessed only by in-depth study of the 'anion effect' in photocatalysis.

The adsorption of ACP over ZnO is negligible under standard reaction conditions. Hence the presence of anions is not expected to make any major change in the adsorption characteristics. In any case, this is verified by measuring the adsorption of ACP in presence of various anions (table.4.6).

Table 4.6: Adsorption of ACP over ZnO in presence of various anions
[ACP]=50 mg/L, [ZnO] =100 mg/L, Volume = 60 mL, [Anion] =5 mg/L, Time = 2hr

Anion	% Adsorption of ACP
No anion	1.6
F^-	1.4
Cl^-	1.2
Br^-	1.2
I^-	1.4
CO_3^{2-}	1.2
HCO_3^-	1.6
SO_4^{2-}	1.8
NO_3^-	1.2
CH_3COO^-	1.2
$C_2O_4^{2-}$	1.2
PO_4^{3-}	1.8

Thus it is seen that the anions do not influence the adsorption of ACP over ZnO. The anion effect is not due to any major change in the pH of the medium. This is confirmed by measuring the pH of the medium in presence of the anions under the same conditions used for evaluating the anion effect. The results are presented in table 4.7.

Table 4 7: pH of ACP solution with ZnO in presence of various anions
[ACP] = 50 mg/L, [ZnO] =100 mg/L, [Anion] =5 mg/L, Time= 2 hr

Anion	pH
No anion	5.4
F^-	7.32
Cl^-	7.33
Br^-	7.33
I^-	7.35
CO_3^{2-}	9.4
HCO_3^-	7.52
SO_4^{2-}	7.32
NO_3^-	7.30
CH_3COO^-	7.75
$C_2O_4^{2-}$	7.20
PO_4^{3-}	7.80

The pH increases moderately in presence of the anions. However, as seen in the study of pH effect, the degradation is affected only moderately by the change in pH in the range of 5-9. In the case of CO_3^{2-}, the pH increases significantly. However, the degradation is unaffected even at this pH. Hence variation in pH caused by the anion is not a major factor that determines the anion effect at least in the range studied here.

The factors discussed here together with those explained in section 3.3.14 to 3.3.18 of Chapter 3 clearly illustrate that the effect of anions on the photocatalytic degradation of organic pollutants in water is inconsistent and unpredictable and it depends on the net effect of the interplay of a number of complimentary and opposing factors.

4.3.9 Effect of oxidants

Oxidizing agents such as persulphate and H_2O_2 are known to enhance the degradation of organic pollutants in water as demonstrated in Chapter 3. The effect of these oxidizing agents, i.e., KIO_3, $K_2S_2O_8$, and H_2O_2 on the degradation of ACP was investigated in detail. The results presented in figure 4.30 show that at the lower oxidant concentration of 5 mg/L, all the oxidants have only negligible effect on the degradation of ACP even though H_2O_2 enhances the degradation mildly. However, after longer time of reaction (120 min), KIO_3 shows 'no effect' while $K_2S_2O_8$ and H_2O_2 slightly enhance the degradation. It may be inferred that, practically these oxidants at 5 mg/L concentration have no significant effect on the degradation of ACP.

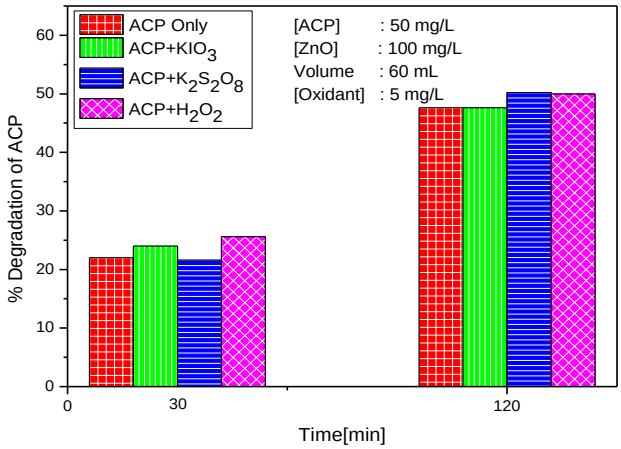

Fig. 4.30: Effect of oxidants on the degradation of ACP after different reaction times

The effect of higher concentration of the oxidants is investigated at 20 mg/L after a shorter time (30 min) of irradiation. The results are plotted in figure 4.31. All oxidants are observed to enhance the degradation at the higher concentration.

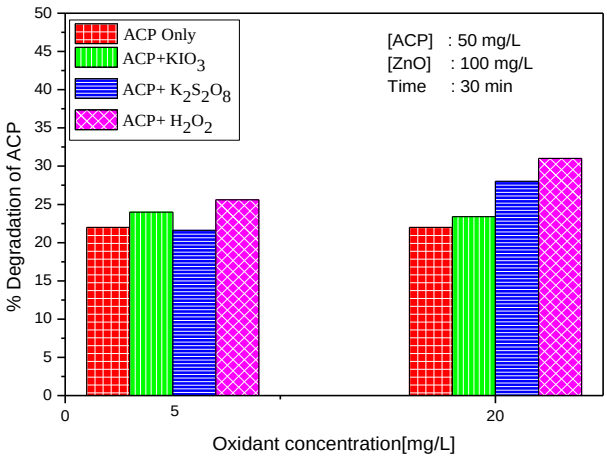

Fig. 4.31: Effect of oxidants at different concentrations on the degradation of ACP

The order of enhancement at the higher oxidant concentration (20 mg/L) is $H_2O_2 > K_2S_2O_8 > KIO_3$

The degree of enhancement by oxidants vary with time of reaction as well as concentration of the oxidant as seen in Table.4.8.

Table 4.8: Degree of Enhancement in ACP degradation in presence of oxidants.

Oxidant	% Enhancement with 5 mg/L oxidant		% Enhancement with 20 mg/L oxidant
	30 min	120 min	30 min
H_2O_2	+7.2	+4.8	+18.0
$K_2S_2O_8$	- 0.8	+5.2	+12.0
KIO_3	+ 4.0	0	+2.8

The effect of reaction time and concentration of the oxidant is investigated in detail and the results are presented in figures 4.30-4.33.

4.3.9.1 Effect of concentration of oxidants and reaction time on degradation of ACP

Result of the detailed investigation of the effect oxidants on the photocatalytic degradation of ACP at different concentration of oxidants and reaction time are plotted in the figures 4.32-4.34

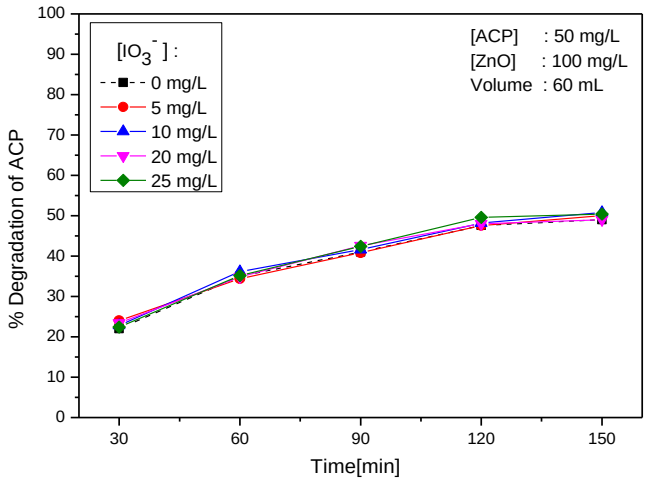

Fig. 4.32: Effect of concentration of the oxidant KIO_3 and reaction time on the photocatalytic degradation of ACP

Effect of KIO_3 on the degradation is negligible at least in the concentration range 0-25 mg/L, upto a reaction time of 150 min. Hence IO_3^- may not be of much use to enhance the photocatalytic degradation of ACP.

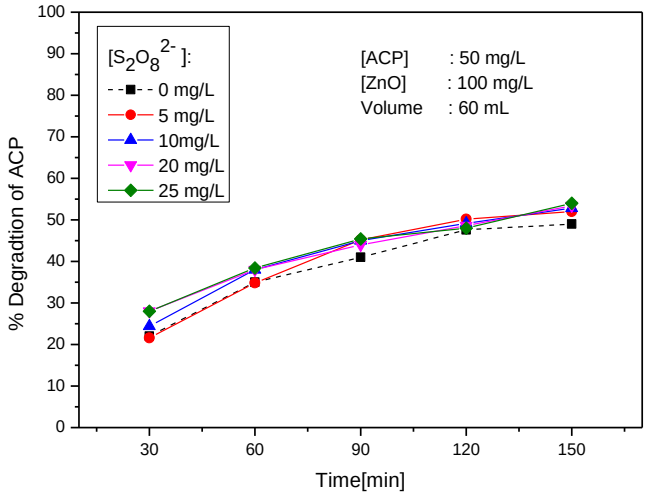

Fig. 4.33: Effect of concentration of the oxidant $K_2S_2O_8$ and reaction time on the photocatalytic degradation of ACP

The study shows that the use of $K_2S_2O_8$, which is a powerful oxidant under UV induced photocatalysis offers no significant enhancement in the solar photocatalytic degradation of ACP. The enhancement by $S_2O_8^{2-}$ is attributed to the concurrent generation of reactive $SO_4^{-\bullet}$ radical anion and $^{\bullet}OH$ radicals during the photocatalytic process. The absence of such enhancement in the current instance may be due to the fact that sunlight as such is not powerful enough (as UV source) to generate adequate concentration of ROS for facilitating the degradation of a highly recalcitrant molecule such as ACP.

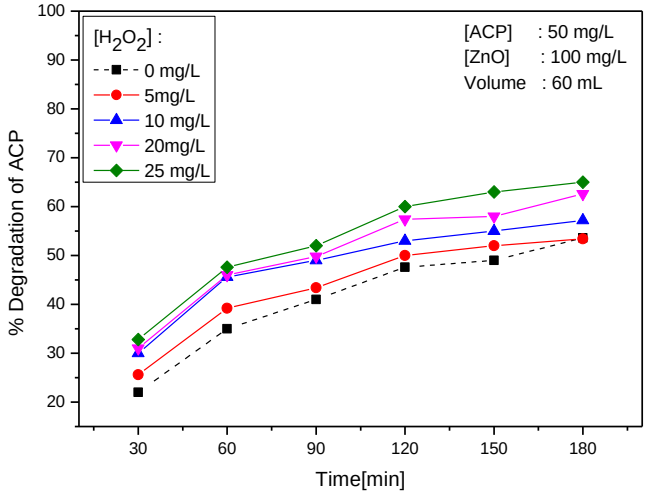

Fig. 4.34: Effect of concentration of the oxidant H_2O_2 and reaction time on the photocatalytic degradation of ACP

H_2O_2 remains as a moderately powerful oxidant at all concentrations. The enhancement increases with increase in concentration. The role of H_2O_2 as an electron acceptor and consequent inhibition of the recombination of electrons and holes can very well explain the enhancement in the photocatalytic degradation of ACP (by H_2O_2). Moreover, H_2O_2 can also produce more reactive $^{\bullet}OH$ radicals, which is also responsible for the enhancement as already discussed in Chapter 3 (section 3.3.10).

The two relatively powerful oxidants, i.e. $K_2S_2O_8$ and H_2O_2 are combined and the effect of the combination on the degradation of ACP is investigated. Results are plotted in figure 4.35.

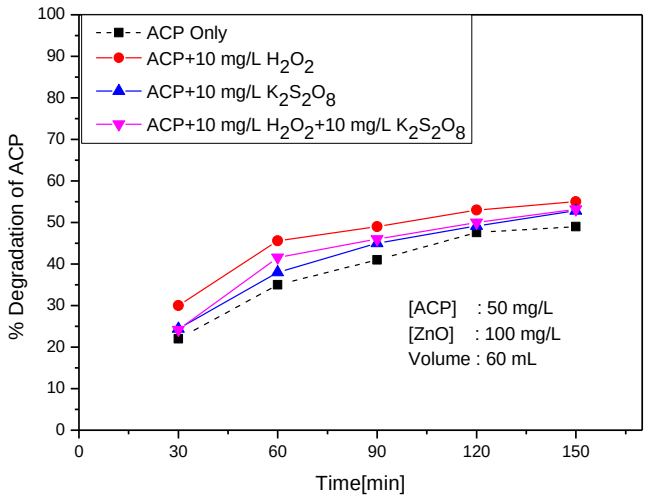

Fig. 4.35: Comparison of the effect of H_2O_2, $K_2S_2O_8$ and their combination on ACP degradation

The effect of the combination is more or less the same as that of H_2O_2 only. Actually $S_2O_8^{2-}$ mildly slows down the enhancing effect by H_2O_2. This may be due to the consumption of reactive $^{\bullet}OH$ radicals by $S_2O_8^{2-}$ as explained earlier. Corresponding generation of reactive $SO_4^{-\bullet}$ radical anion may not be efficient enough to compensate for the loss of $^{\bullet}OH$.

4.3.10 Recycling of the catalyst

The recycling efficiency of ZnO as a photocatalyst for the degradation of ACP is verified experimentally. The ZnO catalyst used for the degradation of ACP is separated from the reaction system by simple centrifugation, air dried at room temperature (~30^0C) and reused to evaluate the possibility of recycling. The photocatalytic activity is retained for multiple runs as shown in figure 4.36.

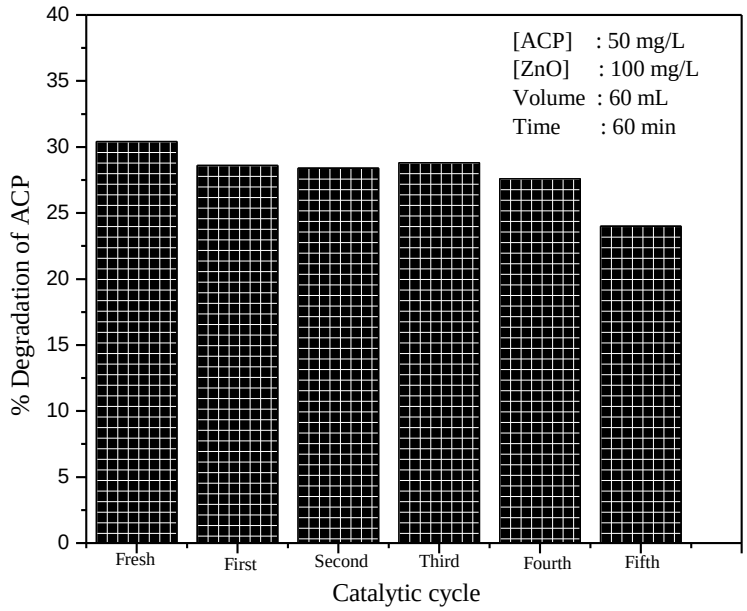

Fig. 4.36: Recycling of ZnO for the photocatalytic degradation of ACP

The catalyst remains active at least for 4 recycles before the activity decreases. This is an important factor for scaling up the process and eventual commercialization. Similar observations are made on the photocatalytic degradation of Alpha-methyl styrene on recycled ZnO as discussed in Chapter 3. Since the adsorption of ACP on ZnO is weak, decrease in the adsorption efficiency of ZnO cannot be a possible reason for the inhibition after 4th recycle. Formation of surface hydroxides may be another major factor leading to decreased activity of continuously recycled ZnO. Factors such as change in morphology of the catalyst and other physical characteristics can cause decrease in activity as discussed in Chapter 3. SEM image of the fresh and used ZnO (after 5th recycling) is shown in figure 4.37 (a) and (b) respectively.

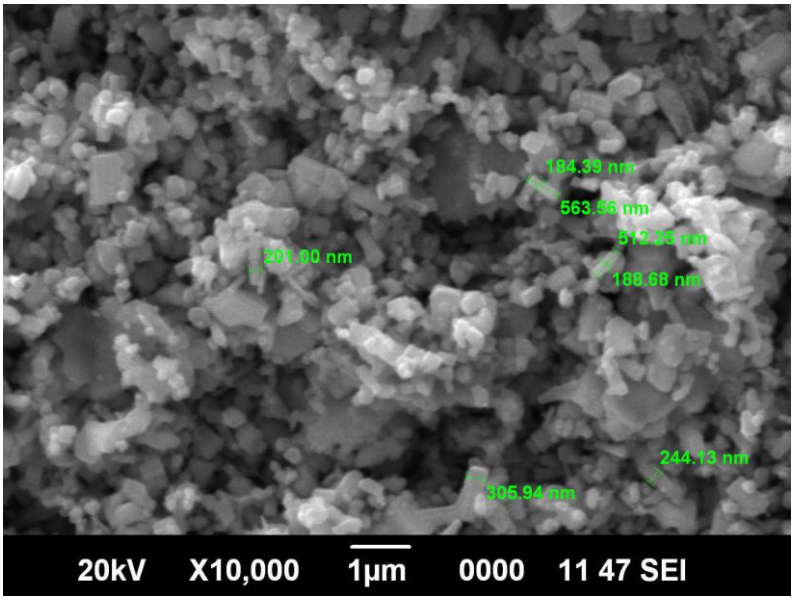

Fig. 4.37 (a): SEM of fresh ZnO

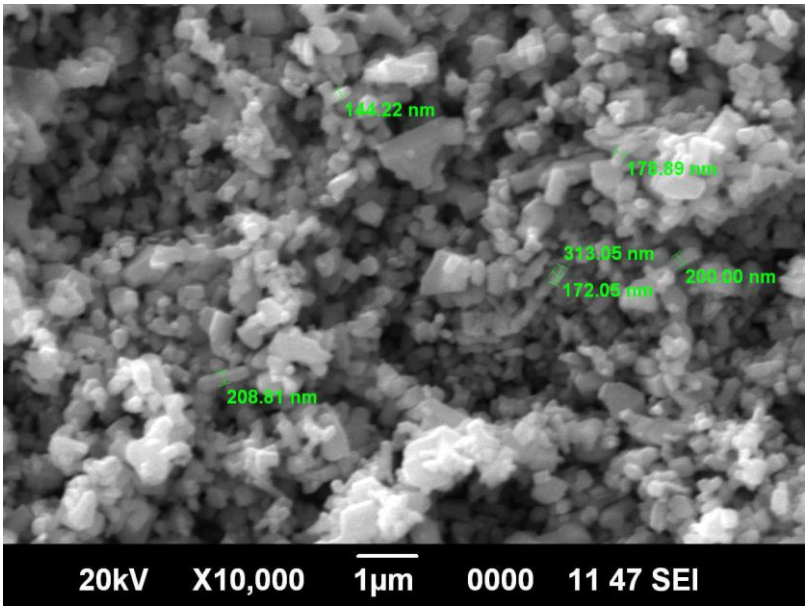

Fig. 4.37 (b): SEM of ZnO after 5th recycling

The images show that the particle size and shape have undergone changes after recycling. Even though ACP does not get adsorbed on the surface of ZnO, some of the intermediates which may be getting mineralized only slowly may be gradually accumulating on the surface with every recycling. The number of possible recyclings before the decline in activity may vary depending on the reaction conditions, chemistry of the substrate and its intermediates, reactor size and geometry.

A comparison of the XRD, BET surface area, pore size and pore volume of the used catalyst (after 5th recycle) with that of fresh ZnO is presented in figure 4.38-4.39 and table 4.9

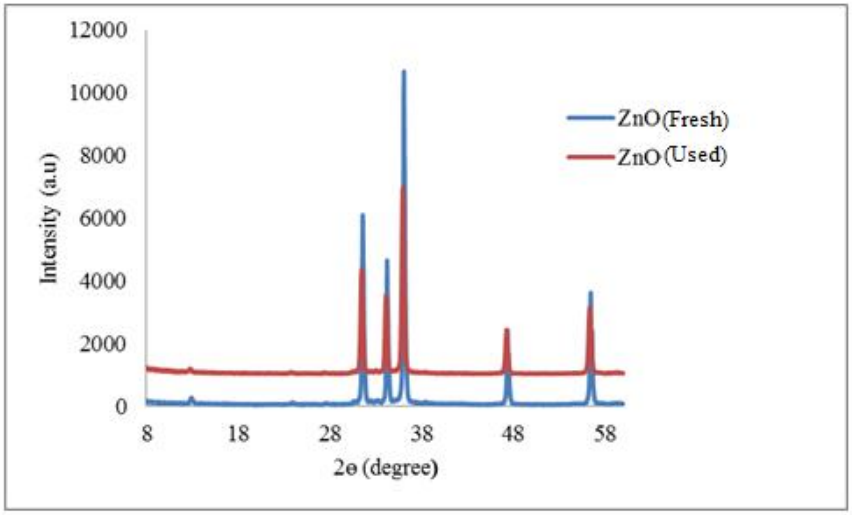

Fig. 4.38: Comparison of XRD of pure and used ZnO

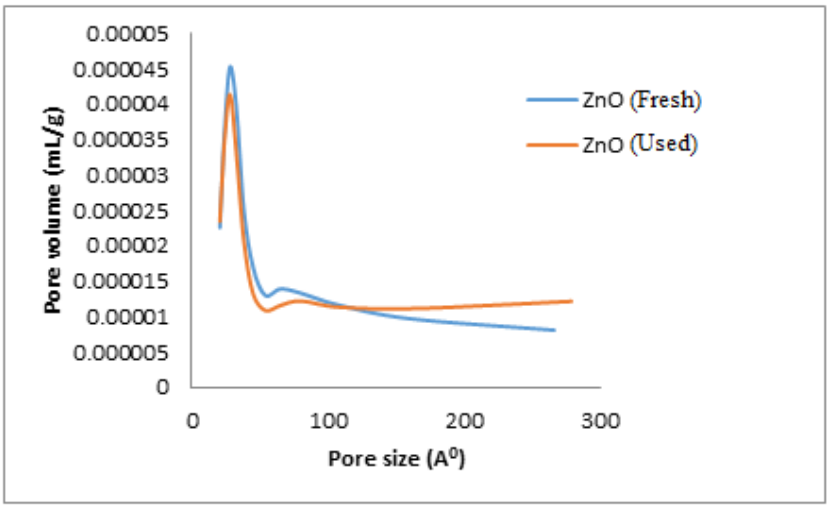

Fig. 4.39: Pore volume vs pore size for fresh and used ZnO catalyst**.**

Table 4.9: Comparison of BET surface area, pore volume and pore size for fresh and used ZnO catalyst

Sample	BET Surface area (m^2/g)	Pore volume (cm^3/g)	Pore size (A^0)
Fresh ZnO	3.9745	0.012018	125.5911
Used ZnO	4.1017	0.015171	151.4220

The parameters undergo only moderate changes with repeated use. Hence the catalyst remain active even after many recycles.

4.3.11 Regeneration of the catalyst

The adsorption/degradation efficiency of the ZnO catalyst after each recycle is presented in table 4.10. After 5th recycle the catalyst is washed with distilled water and calcined at 250^0C for 2 hr and its efficiency for ACP degradation is tested under identical conditions.

Table 4.10: Comparative adsorption and degradation of ACP over fresh and recycled ZnO
[ACP] =50 mg/L, [ZnO] = 100 mg/L

Catalyst cycle	% Adsorption after 60 min	% Degradation after 60 min
Fresh	2.3	35.0
First recycling	2.3	33.2
Second recycling	2.2	33.0
Third recycling	2.2	32.4
Fourth recycling	2.2	32.2
Fifth recycling	2.1	28.6
Sixth recycling(after washing and calcining at 250°C for 2hr)	2.3	36.8
Seventh recycling	2.3	36.2
Eighth recycling	2.2	35.5

After reactivation of the catalyst its activity is regained but the adsorption remains unaffected. This is expected as the adsorption of ACP over ZnO is negligible. The slight enhancement in degradation after activation may be due to desorption of some substrate/intermediates from the used catalyst thereby providing new sites for the adsorption of substrate/intermediate. Moreover, when more surface sites are available for activation, they can absorb more photons, which inturn may lead to the generation more ROS and consequent increase in degradation of ACP.

4.3.12 Mineralization of ACP in presence of ZnO/sunlight

The potential of a photocatalytic method for the removal of recalcitrant organic pollutants from water depends on its efficiency for complete mineralization of the pollutant. This is because in some cases even though the parent compound is degraded, the resultant intermediates formed from it may be more toxic than the original pollutant molecule. Hence it is important to ensure the complete degradation of both parent as

well as intermediates during the photocatalytic degradation. In the case of ACP, HACP is identified as the major reaction intermediate during its photodegradation. Small amount of phenol is also detected in the reaction system by colorimetric method. Upon continuous irradiation, both ACP and HACP disappear from the system as evident from the chromatographic analysis shown in the figure 4.5. The intermediate phenol is also completely removed from the system on prolonged irradiation. This is further confirmed by the progressive decrease in COD values which ultimately becomes zero after 26 hr of irradiation as shown in figure 4.40. The initial decrease in COD is very small compared to the degradation of ACP (the degradation is 75% while the COD decrease is only 25% in 5 hr). This shows that the intermediates are more stable and get mineralized only slowly. Eventual COD value of 'nil' confirms the potential of solar photocatalysis in presence of ZnO as an efficient technique for the removal of last traces of ACP pollutant from industrial effluents.

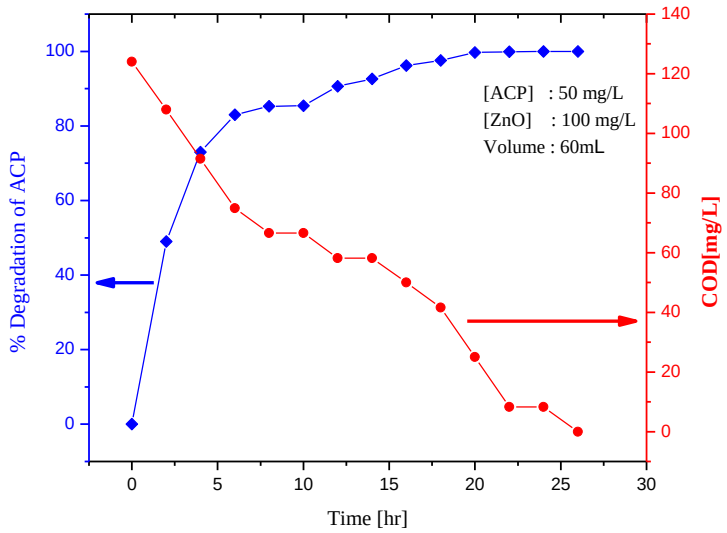

Fig. 4.40: Photocatalytic degradation of ACP and concurrent variation in COD

4.3.13 General mechanism

The general mechanism of photocatalysis is discussed in detail in Chapter 3. The first step in semiconductor photocatalysis is the absorption of light by the catalyst and creation of electron-hole pair:

$$ZnO + h\nu \rightarrow ZnO\ (h^{+}_{vb}) + ZnO\ (e^{-}_{cb}) \qquad (123)$$

Consequently, the electron is promoted from the valence band of the semiconductor to its conduction band creating corresponding hole (+ve charge) in the valence band. The semiconductor can function as an effective photocatalyst when both the electron and hole are consumed. It is generally accepted that both the electrons and holes can find low energy trap sites on a sub-picosecond time scale in the semiconductor [157]. The electrons and holes can recombine and dissipate the input energy as heat and in such case photocatalysis cannot take place. Alternatively, they can react with electron donors and electron acceptors which are adsorbed on the semiconductor surface and/or trapped within the surrounding electrical double layer of the charged particles to produce strong oxidizing $^{\bullet}OH$ radicals [128]. The formation of hydroxyl radicals during solar irradiation of the ACP solution in presence of ZnO is tested by the photoluminescence (PL) technique and is shown in figure 4.41, by similar procedure as described in Chapter 3 (section 3.4).

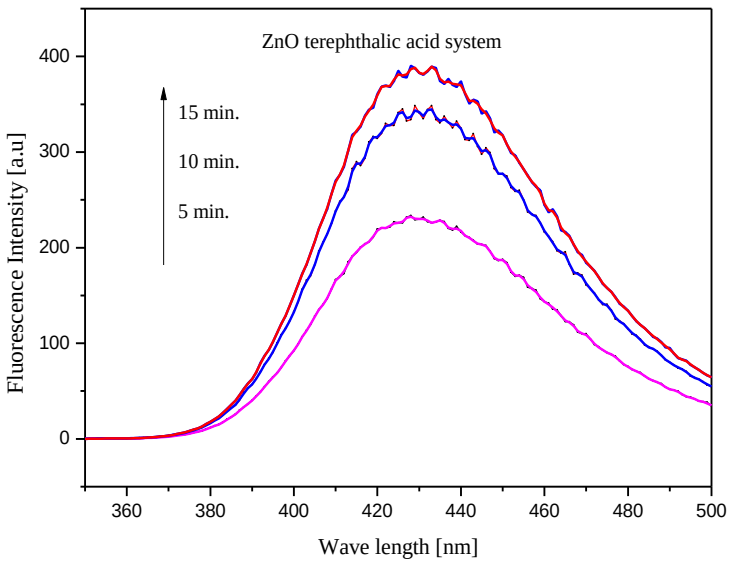

Fig. 4.41: PL spectra showing the presence of $^{\bullet}OH$ radicals during ZnO photocatalysis

These reactive free radicals can promote the oxidation of organic compounds as follows:

$$O_2 + e^- \rightarrow O_2^{-}\bullet \quad (124)$$

$$h^+ + H_2O \rightarrow H^+ + {}^{\bullet}OH \quad (125)$$

$${}^{\bullet}OH + RH \rightarrow H_2O + R^{\bullet} \quad (126)$$

$$R^{\bullet} + O_2 \rightarrow ROO^{\bullet} \rightarrow \text{Intermediate(s)} \rightarrow \rightarrow CO_2 + H_2O \quad (127)$$

RH is ACP and the major intermediate is HACP in the current instance.

Possible steps involved in the solar photocatalytic degradation of ACP in presence of ZnO catalyst leading to its mineralization [169] can be schematically presented as in figure 4. 42.

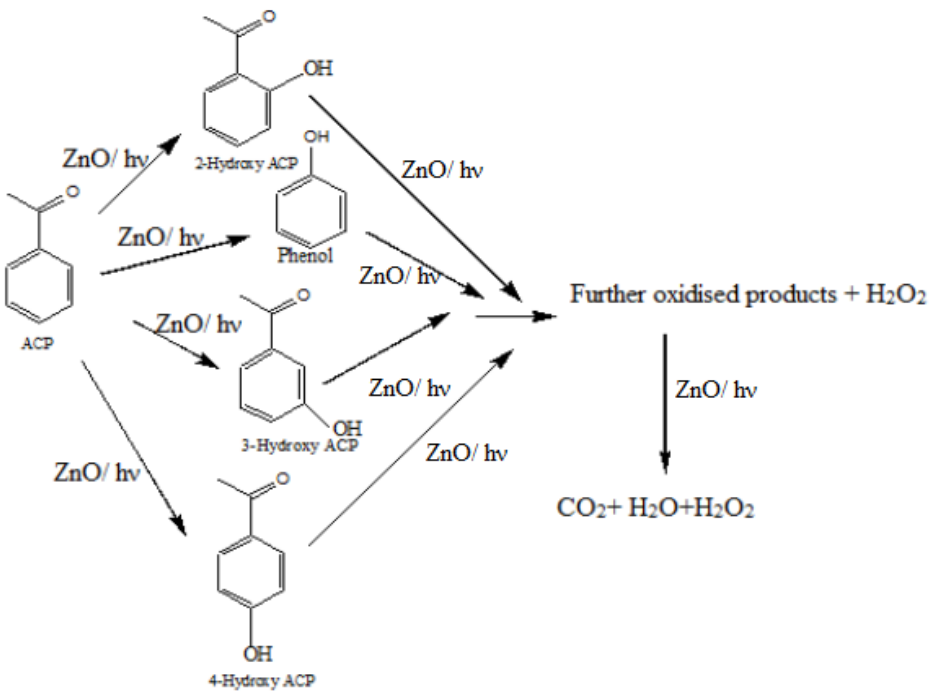

Fig. 4.42: Possible steps involved in the photocatalytic mineralization of ACP

The concurrent formation and decomposition of H_2O_2 and the oscillation phenomena that follows are already discussed earlier (Chapter 3, section 3.3.8)

4.4 Conclusions

The solar photocatalytic degradation of trace amounts of acetophenone in water is investigated using ZnO as the catalyst. The effect of various reaction parameters such as pH, concentration of pollutant, catalyst loading, presence of anions, oxidants etc., on the rate of photocatalytic degradation of ACP is investigated in detail. HACP is identified as the major reaction intermediate. Phenol is another intermediate

formed in traces. These intermediates also get mineralized on prolonged exposure to sunlight thereby showing the potential of this method for the safe removal of trace amounts of ACP from water. The concentration of concurrently formed H_2O_2 does not increase corresponding to the degradation of ACP and is oscillating with periodic crests and troughs. This phenomenon is attributed to the simultaneous and competing formation and decomposition processes. The inhibition of the degradation of ACP in deaerated system confirms the role of O_2 in the process. The role of various salts and common oxidants on the solar photocatalytic degradation of ACP is thoroughly investigated. The reusability study of the catalyst shows that it can be recycled at least four times with comparable efficiency. The formation of hydroxyl radical in the system is confirmed experimentally by photoluminescence technique. The study reiterates the possibility of using ZnO mediated photocatalysis as an efficient technique for the dual application of harvesting solar energy and the removal of hazardous pollutants such as ACP from water.

.....ꕥ.....

Chapter 5

ZINC OXIDE MEDIATED SOLAR PHOTOCATALYTIC DEGRADATION OF DIMETHYL PHENYLCARBENOL [DMPC] IN WATER

Contents

5.1 Introduction

Dimethyl phenyl carbenol (DMPC) or 2-Phenyl 2-propanol is obtained as a byproduct from many petrochemical industries especially from the production of phenol and acetone by the cumene oxidation process. It is a fragrance ingredient used in many products. It is used in decorative cosmetics, fine fragrances, shampoos, toilet soaps and other toiletries as well as in non-cosmetic products such as household cleaners and detergents. The effluent water from such industries invariably contains trace amounts of DMPC. Conventional methods such as biological methods are ineffective for removing the last traces of this pollutant from the waste water. Since photocatalysis is found to be an effective AOP for the removal of many toxic pollutants from water [19, 34, 36, 37, 105, 106, 170, 171], the same is investigated for the removal of trace amounts of DMPC from water.

Liu et al. [172] studied the transfer hydrogenolysis of DMPC to isopropylene using formic acid as the hydrogen donor over supported

palladium, platinum and ruthenium catalysts. They found that Pd/C (Pd supported on activated carbon) is an effective catalyst and formic acid is much better than formate salts or other hydrogen donating agents for the catalytic transfer hydrogenolysis of DMPC. A comprehensive review on the use of DMPC as a fragrance ingredient is made by Scognamiglio et al. [98]. To the best of our knowledge, no systematic investigation is reported so far on the removal of traces of DMPC from water, even though its presence in moderate concentration can be toxic [LD_{50}: 1400 mg/kg-oral (mouse)] as previously discussed in Chapter 2.

In this chapter, the results on the investigation of the photocatalytic degradation of DMPC in presence of commercial ZnO as the catalyst and solar energy as the source of activation are reported and discussed.

5.2 Experimental Details

5.2.1 Materials

DMPC (99.7%) was obtained from Aldrich (India) and used as such without further purification. Zinc oxide was obtained from Merck Chemical Company (India). LR grade H_2O_2 and HCl were from Nice chemicals (India). Milli-pore water was used for the preparation of standard solutions. All other chemicals used are of reagent grade or equivalent and are used as such without further purification.

5.2.2 Analytical Procedures

Perkin Elmer Auto System XL Gas Chromatograph described earlier is used for the analysis of DMPC and the intermediates formed during the degradation reaction using flame ionization detector and Elite 1301 column with hydrogen as the carrier gas. The calibration graph is prepared by

multiple level calibration method, where different known concentrations of DMPC are prepared and each of these solutions is injected into the GC [1.0 µL). The procedure is repeated to get the average calibration value corresponding to the respective concentration in order to minimize the error. The instrument parameters are the same as those used for AMS analysis as described in section 3.2.2. The calibration graph for DMPC is shown in figure 5.1.

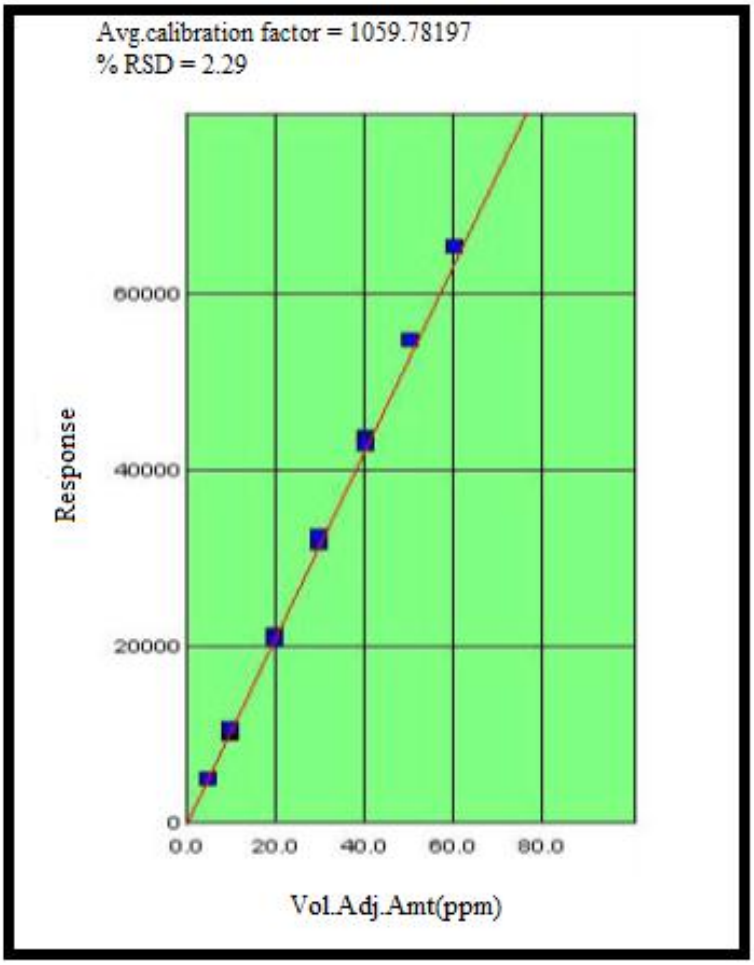

Fig. 5.1: Calibration graph for DMPC analysis

The ZnO catalyst used in this study is the same as that used for the investigations on AMS and ACP degradation. The analysis of H_2O_2 and COD determination were done in the same way as described in Chapter 3.

5.2.3 Adsorption study

Adsorption of DMPC over ZnO catalyst was measured using the standard procedure as described in Chapter 3, replacing AMS by DMPC.

5.2.4 Photocatalytic Experimental set up

The photocatalytic degradation of DMPC was investigated by the same procedure using the same jacketed Pyrex reactor as described in the case of AMS and ACP. Sampling and analytical procedures were also the same as described.

5.3 Results and Discussion

5.3.1 Catalyst characterization

The catalyst ZnO is characterized as described in earlier chapters.

5.3.2 Preliminary experiments

Preliminary study of the solar photocatalytic degradation of DMPC (30 mg/L) was carried out using commercial ZnO (100 mg/L) and the results are shown in figure 5.2.

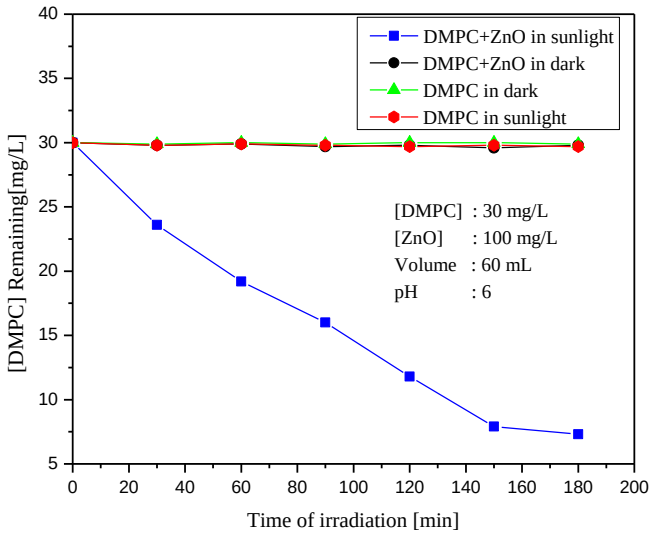

Fig. 5.2: Photocatalytic degradation of DMPC over ZnO in sunlight

More than 75% degradation was observed within 3 hr (180 min) of irradiation. No degradation was noticed in the absence of either light or catalyst, confirming the role of both factors in the degradation process. In the absence of irradiation, there is practically no change in the concentration of DMPC even in presence of ZnO, indicating that the adsorption also is negligible. This is reconfirmed by conducting the adsorption experiments at different concentrations of DMPC by the standard method explained earlier. The results tabulated in table 5.1 show that the adsorption of DMPC over ZnO catalyst is negligible and is not more than 2% even after 6hr.

Table 5.1: Adsorption of DMPC over ZnO
[ZnO]=140 mg/L, Time=6 hr

Initial [DMPC], mg/L]	[DMPC] after 6 hr, mg/L	% Adsorption
10	9.90	1.0
20	19.8	1.0
30	29.6	1.3
40	39.6	1.0
50	49.4	1.2

Since the adsorption of DMPC on ZnO surface was found to be negligible, the reduction in DMPC concentration in presence of ZnO under solar irradiation is entirely due to its photocatalytic degradation. As described in Chapters 3 and 4, even though adsorption of the substrate on the surface of the catalyst is assumed to be a prerequisite for effective photocatalytic degradation process, the high rate of DMPC degradation despite its poor adsorption suggests that the interaction between the surface generated reactive free radicals and the substrate can take place in the bulk as well. This is in agreement with the observation of Turchi and Ollis [110] that the reactive $^{\bullet}OH$ radicals and other oxidizing species can diffuse into the bulk solution and interact with the organic pollutant. The decrease in the rate of DMPC degradation with time may be attributed to decrease in its concentration as well as due to the competition between the various intermediates formed and the DMPC molecules for the reactive free radicals in the system. Acetophenone, AMS, and another unidentified compound are detected as the intermediates using gas chromatography. Phenol in traces is also detected by colorimetric method as described in Chapter 4. All these intermediates have only short lifetime and disappear on continuous irradiation thereby showing that they also get degraded faster. Consequently, their concentration in the reaction system does not increase much with time of irradiation. The gradual disappearance of DMPC as well as the formation and degradation of the reaction intermediates with time of irradiation is shown in figure 5.3.

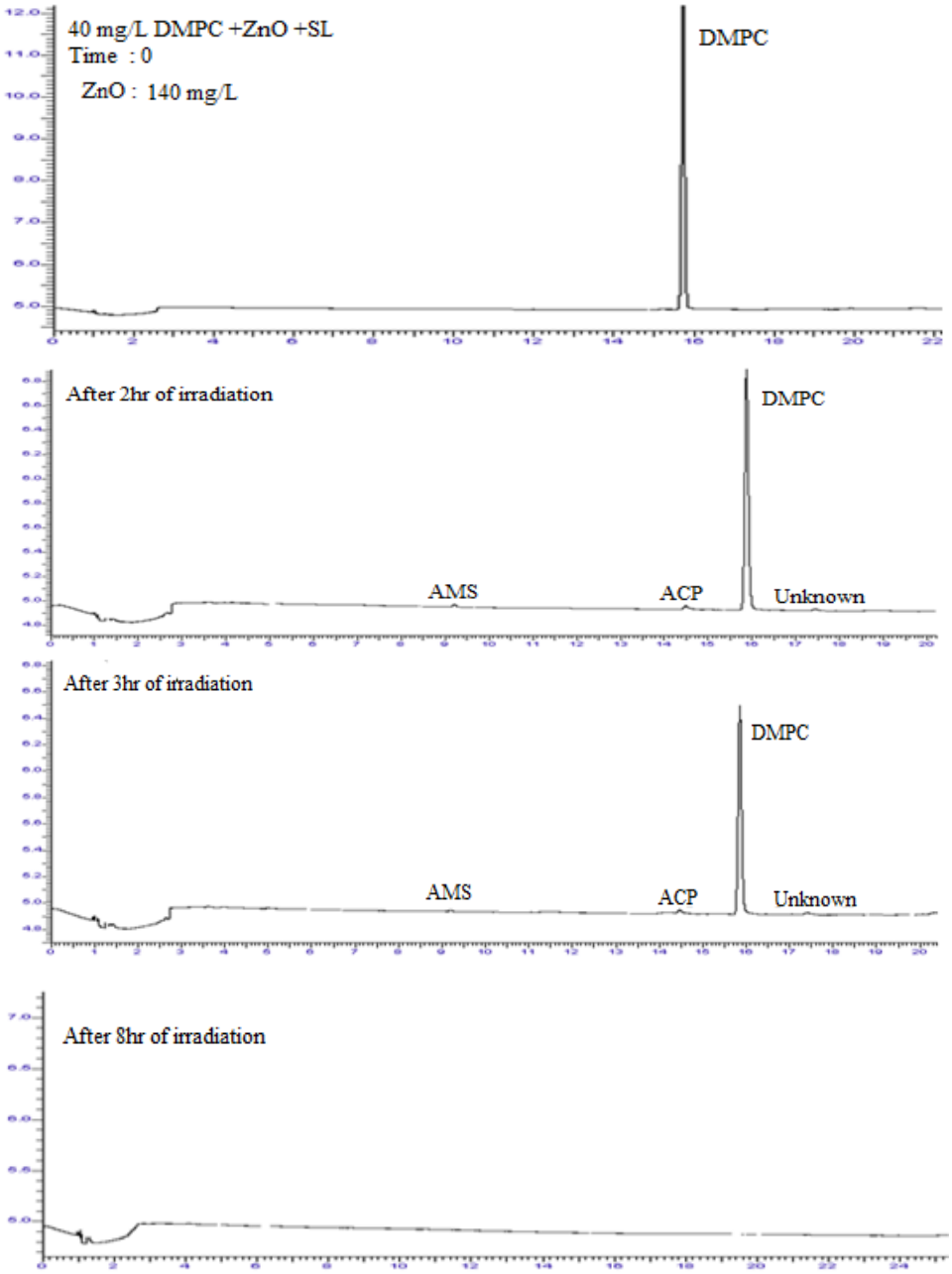

Fig. 5.3: Gas chromatogram showing the degradation of DMPC and formation/ degradation of intermediates

LC/MS analysis of the reaction system at the stage of 50% degradation (of DMPC) showed the presence of more intermediates as in table 5.2

Table 5.2: Intermediates formed during the solar photocatalytic degradation of DMPC over ZnO

SL No	Mass	Proposed structure
1	135	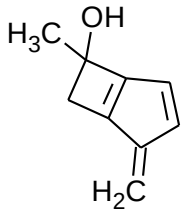
2	151	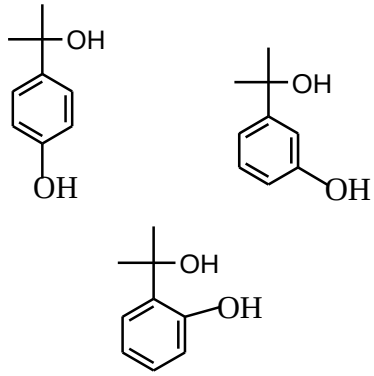

5.3.3 Effect of catalyst dosage

The economic and effective catalyst loading for DMPC (30 mg/L) degradation in sunlight was identified by carrying out the degradation study at different ZnO loading ranging from 20 to 160 mg/L, keeping all other parameters constant. The result is shown in figure 5.4.

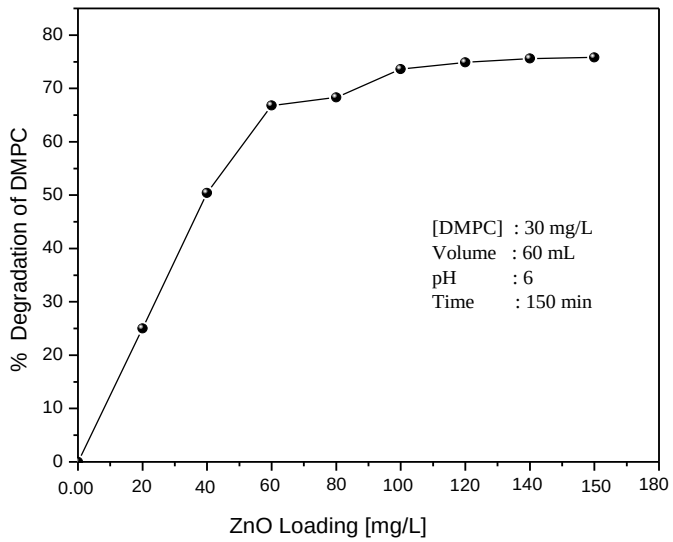

Fig. 5.4: Effect of catalyst loading on the photocatalytic degradation of DMPC

The degradation of DMPC increases with increase in ZnO loading steeply upto 60 mg/L, slowly thereafter upto 100 mg/L and then stabilizes. As the adsorption of DMPC on the ZnO surface is negligible, the increase in degradation with increase in ZnO loading cannot be attributed to the increase in the number of adsorption/ interaction sites for the substrate. Hence the role of catalyst is only maximizing the light absorption and consequent increase in the generation of hydroxyl and other reactive radicals in the system. These radicals will interact with the substrate/intermediate leading to the enhanced degradation of the pollutant. When the catalyst loading is increased beyond the optimum, it results in scattering and reduced passage of light through the suspension. At higher loading, there is also the possibility of aggregation of catalyst particles, which in turn results in decrease in the number of available active surface sites and stabilization/decrease in the rate of $^{\bullet}OH$ radical

generation. At higher ZnO loading, part of the initially activated ZnO gets deactivated by collision with catalyst in the ground state as described in Chapters 3 and 4. Since the optimum ZnO loading for DMPC degradation is in the range 100 to 160 mg/L, any dosage in this range should have been chosen as the optimum. Since there is no negative effect at higher loading, 140 mg/L is chosen as the optimum to take advantage of higher dosage, if any, while optimizing other parameters.

5.3.4 Effect of initial concentration of DMPC

The effect of initial concentration of DMPC in water on its photocatalytic degradation under sunlight was investigated using ZnO as catalyst. The concentration of DMPC is kept in the range 10 to 50 mg/L. The results are plotted in figure 5.5.

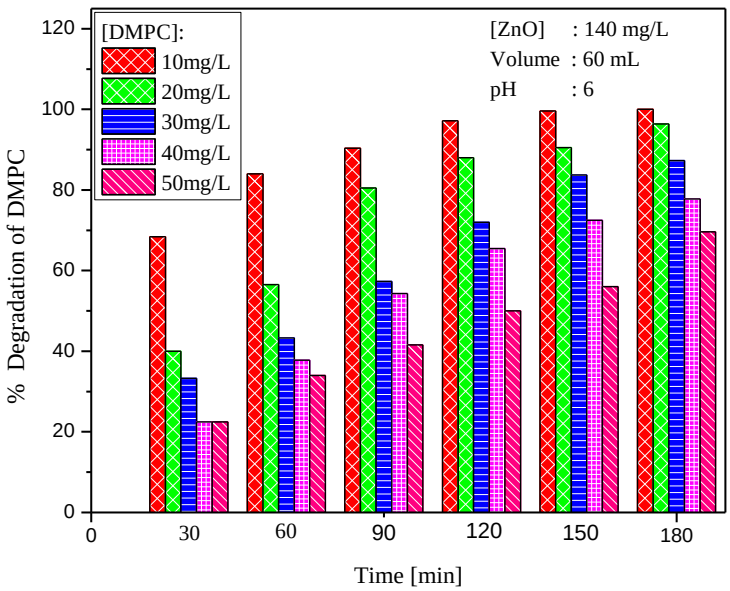

Fig. 5.5: Effect of concentration of DMPC on its percentage photocatalytic degradation

The results show that the percentage degradation of DMPC decreases as its initial concentration increases at all time intervals. However, rate of DMPC degradation was found to increase with increase in initial concentration and stabilizes eventually (figure 5.6.).

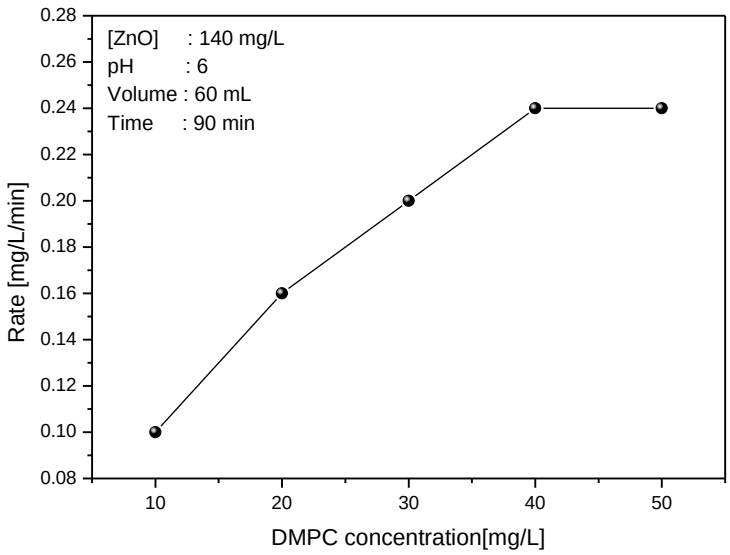

Fig. 5.6: Effect of initial concentration of DMPC on its photocatalytic degradation rate

The rate indicates variable kinetics at different concentrations of DMPC. The maximum rate of 2.4 x10^{-1} mg/L/min was obtained with initial DMPC concentration of 40 mg/L. Since the adsorption of DMPC on the ZnO catalyst is very small, the increase in the rate of the reaction with increase in substrate concentration is not due to the increase in the adsorption of DMPC molecules on the ZnO surface. At higher DMPC concentration, more molecules will be available in the bulk of the solution as well as in the neighborhood of the surface which can effectively

interact with the surface generated free radicals and other ROS. This is similar to the case of ACP degradation as discussed in Chapter 4. But at concentrations higher than the optimum value, at least a part of the incident light may be absorbed/blocked by DMPC and the intermediates formed from it. Hence the photons available for the activation of the catalyst is reduced. This leads to decrease in the reaction rate. When the initial concentration of DMPC increases, the requirement for the catalytic surface which is necessary for maintaining the degradation rate also increases. But as the intensity of illumination and catalyst amount are kept constant, the relative amount of ROS which are generated and available for interacting with DMPC decreases. This accounts for the decreased degradation rate. At high substrate concentration, some of the abundantly available reaction intermediates may get adsorbed onto the surface or remain in the bulk for a relatively longer period, which results in less frequent interaction between fresh DMPC molecules and reactive oxygen species. The mechanism is similar to that described in the case of ACP degradation in Chapter 4.

The reciprocal plot of initial rate of degradation of DMPC ($1/r_0$) against its initial concentration ($1/C_0$) yields a straight line graph (figure 5.7), indicating that the degradation follows pseudo first order kinetics and Langmuir-Hinshelwood model, modified to accommodate the reactions occurring at solid-liquid interface.

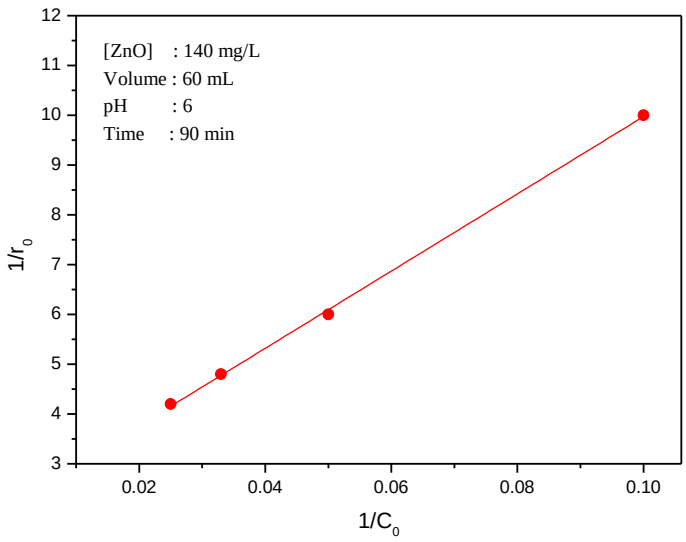

Fig. 5.7: Reciprocal plot of initial degradation rate of DMPC versus its initial concentration

The plot of $-\ln(C/C_0)$ against irradiation time (t) in the concentration range 10-40 mg/L of DMPC gives straight lines (figure 5.8), which also reconfirms the pseudo first order kinetics.

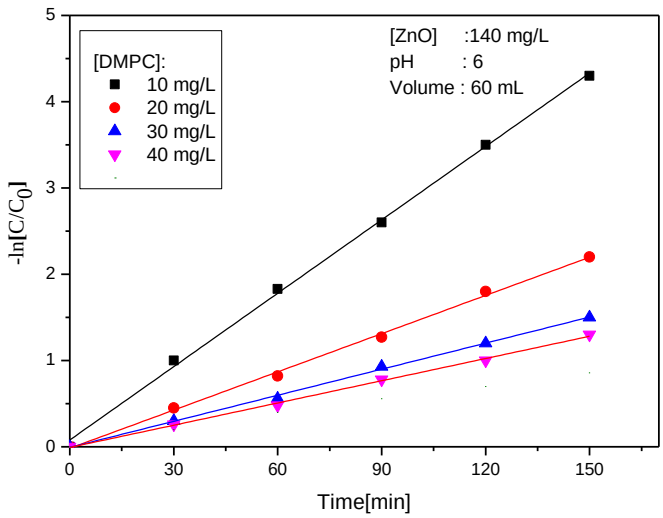

Fig. 5.8: Logarithmic plot of pseudo first order kinetics for the degradation of DMPC

The apparent rate constant k for the degradation of DMPC at different concentrations as obtained from the slopes of corresponding lines is tabulated in table 5.3.

Table 5.3: Pseudo first order rate constants for the photocatalytic degradation over ZnO.

Sl No	[ZnO], mg/L	[DMPC], mg/L	k^r x 10^{-3} (min^{-1})
1	140	10	28.3
2	140	20	14.7
3	140	30	10
4	140	40	8.5

The rate constant decreases with increase in DMPC concentration. For a fixed catalyst loading, there is finite number of reactive species which are available for interaction with the substrate. At higher concentration, the number of substrate molecule is excessive. Hence the fraction of substrate molecules which can interact effectively with the reactive species is reduced. This explains the decrease in the apparent rate constant. This is similar to the decrease in rate constant observed with AMS degradation as discussed in section 3.3.4. Similar case of decrease in the rate constant and the order of the reaction at higher substrate concentration was reported by others also [114,116,118].

5.3.5 Effect of pH

As explained in the case of AMS and ACP degradation in Chapters 3 and 4 respectively, pH of the reaction medium has a significant role in many aqueous phase photocatalytic processes. The effect of pH on the photocatalytic degradation of DMPC was investigated in detail by varying

the pH of the reaction medium from 2 to 12 and keeping all other parameters constant. The results are shown in figure 5.9.

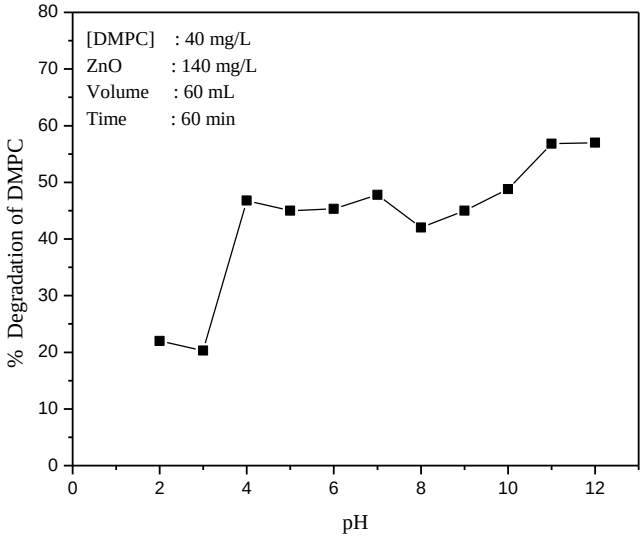

Fig. 5.9: Effect of pH on the photocatalytic degradation of DMPC

The comparatively very small degradation rate observed in the range of pH=2-3 may be due to the corrosion of the ZnO catalyst at lower pH, which in turn reduces the availability of active surface sites for adsorption of the intermediate and the generation of reactive species. It is seen that pH has no significant effect on the degradation of DMPC in the pH range 4 to 10 even though a slight decrease in degradation was observed at pH=8, which may be treated as within the limits of experimental error. Enhancement in the degradation rate is observed at the higher pH of >11.

The effect of pH on the adsorption of DMPC on ZnO is experimentally verified and the results are given in table.5.4.

Table 5.4: Effect of pH on the adsorption of DMPC over ZnO
[DMPC]=40 mg/L, [ZnO] =140 mg/L, Volume =60 mL, Time=3 hr

pH	% Adsorption
At normal solution pH[6]	1.5
3	2.5
4	1.3
5	2.5
6	2.0
7	2.0
8	1.8
9	1.0
10	1.5
11	3.0
12	2.8

The adsorption is very small at all pH ranges as is evident from the table 5.4. Hence there is no direct correlation between the degradation and the adsorption. The slight enhancement in the degradation at alkaline pH range may be attributed to the generation of more hydroxyl radicals. The effect of pH on the degradation of DMPC was found to be fairly constant both above and below the Point of Zero charge (PZC) of ZnO (9.3). Hence correlation of pH effect with the PZC is not applicable in this case.

The absence of any significant pH effect on the degradation except under extreme acidic and alkaline conditions also confirms that the role of surface characteristics of ZnO which depend on pH, is not significant in the case of degradation of DMPC.

5.3.5.1 Corrosion of ZnO under solar photocatalysis at different pH

The corrosion of ZnO catalyst at different pH under photocatalytic condition was investigated as explained in previous chapters using 60 mL

of DMPC solution(40 mg/L) and 140 mg/L of ZnO. The results presented in figure 5.10 clearly show that there is no significant corrosion of ZnO at the pH at which solar photocatalytic degradation of DMPC was carried out (pH ~ 6). The results also show that solar irradiation does not change the pattern of corrosion at all pH.

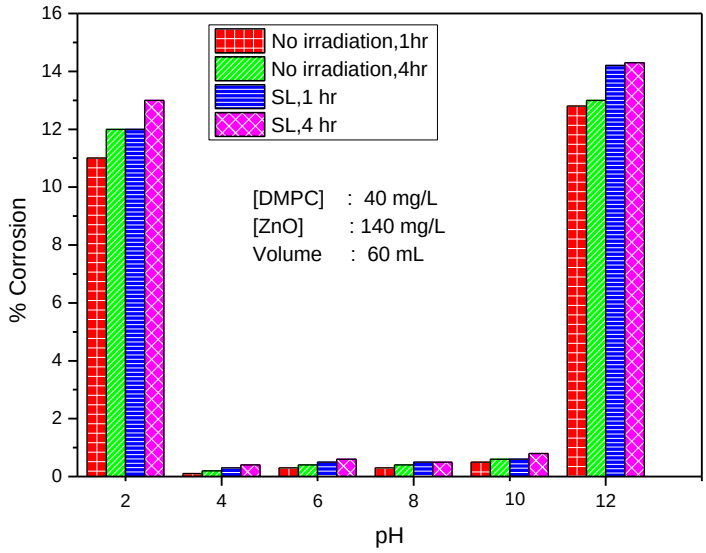

Fig. 5.10: Corrosion of ZnO at different pH in the presence and absence of solar irradiation

5.3.6 Role and fate of H_2O_2 formed during DMPC degradation

As described in Chapters 3 and 4, H_2O_2 was detected as a co-product/intermediate during the photocatalytic degradation of many organic compounds [33, 36, 37, 102, 116, 119]. The presence of H_2O_2 was detected during the photocatalytic degradation study of DMPC also. The concentration of H_2O_2 was determined quantitatively at different time intervals and the results are plotted in figure 5.11.

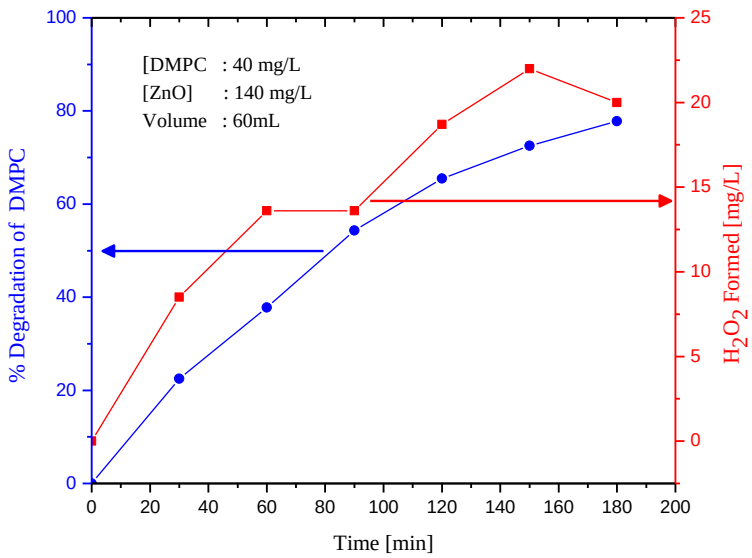

Fig. 5.11: Formation of H_2O_2 during the photocatalytic degradation of DMPC in presence of ZnO

It was observed that the concentration of H_2O_2 increases initially, reaches a steady state, increases again and then starts decreasing. At the same time, the degradation of DMPC continues to increase. The periodic increase and decrease in the concentration of H_2O_2 during the photocatalytic degradation of organic pollutants in water has been reported earlier as well as in Chapters 3 and 4 of this thesis. The phenomenon is due to the simultaneous formation and decomposition of H_2O_2, which results in oscillation in the concentration [113,126]. Details are discussed in previous chapters.

5.3.7 Effect of added H_2O_2

H_2O_2 is an oxidizing agent and is reported to enhance the photodegradation of many organic pollutants by providing additional reactive $^{\bullet}OH$ radicals. In the current instance, H_2O_2 is formed insitu and

this may be influencing the rate of degradation by generating and consuming the $^{\bullet}OH$ radicals. The effect of adding H_2O_2 on the photocatalytic degradation of DMPC at different concentrations was investigated and the results are shown in figure 5.12.

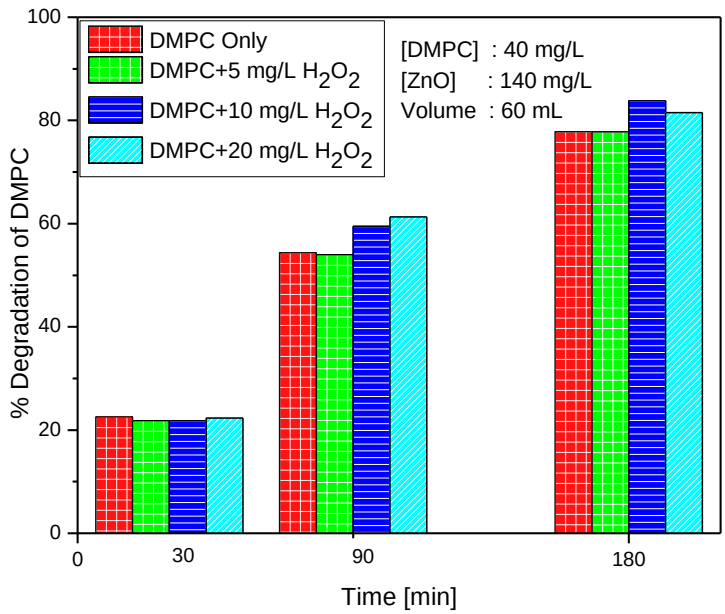

Fig. 5.12: Effect of H_2O_2 on the photocatalytic degradation of DMPC

It was observed that externally added H_2O_2 has no significant effect on the DMPC degradation at the beginning of the reaction at least in the range 5-20 mg/L. A slight enhancement in the degradation was observed at later stages for higher H_2O_2 concentrations of 10 and 20 mg/L.

H_2O_2 itself is a good oxidant. Under photocatalytic conditions, H_2O_2 can give rise to reactive $^{\bullet}OH$ and other free radicals as follows:

$$H_2O_2 + h\nu \rightarrow 2^{\bullet}OH \qquad (128)$$

$$H_2O_2 + O_2^{-\bullet} \rightarrow {}^{\bullet}OH + OH^- + O_2 \quad (129)$$

$$H_2O_2 + e^- \rightarrow {}^{\bullet}OH + OH^- \quad (130)$$

$$2OH^- + h^+ \rightarrow {}^{\bullet}OH + OH^- \quad (131)$$

$$H_2O_2 + 2\,h_{vb+} \rightarrow O_2 + 2H^+ \quad (132)$$

Concurrently, the H_2O_2 may be interacting with at least some of the reactive ${}^{\bullet}OH$ radicals forming less reactive $HO_2\bullet$ radicals as follows:

$$H_2O_2 + {}^{\bullet}OH \rightarrow HO_2^{\bullet} + H_2O \quad (133)$$

Thus some of the H_2O_2 molecules are decomposing and at least some of the insitu formed ${}^{\bullet}OH$ radicals are consumed. At the same time, the formation of H_2O_2 by interaction between the free radicals also takes place. Thus simultaneous formation and consumption of ${}^{\bullet}OH$ may balance each other at some stage, especially at lower H_2O_2 concentration. Hence 'no effect' at lower concentration of H_2O_2. However, at higher concentration of H_2O_2 at least some of the ${}^{\bullet}OH$ radicals may not be getting deactivated by coupling and instead will interact with the more readily available H_2O_2 to form $HO_2\bullet$ which is also reasonably active ROS. At higher substrate concentration, its interaction with the ROS also will be more frequent resulting in enhanced degradation of DMPC. However, because of the multiple interactions involving too many ROS, the net effect may be practically inconsistent and may even eventually lead to inhibition. The dual role played by H_2O_2 as an enhancer as well as inhibitor is reported earlier by other workers also [117, 126] as explained in detail in Chapter 3.

5.3.8 Effect of humic acid

The presence of humic substances in water can influence the photocatalytic degradation of organic pollutants positively or negatively as discussed in Chapters 3 and 4 in detail. The effect depends on the characteristics of the substrate, catalyst as well as the reaction conditions [27, 139]. The influence of humic acid (HA) on the photocatalytic degradation of DMPC was investigated by adding different concentrations of HA and following the degradation of DMPC at regular time intervals. The results are plotted in figure 5.13. It was found that the presence of humic acid inhibit the degradation of DMPC at all time intervals. The extent of inhibition depends on the concentration of HA in the system as in the case of both AMS and ACP degradation described in Chapters 3 and 4 respectively.

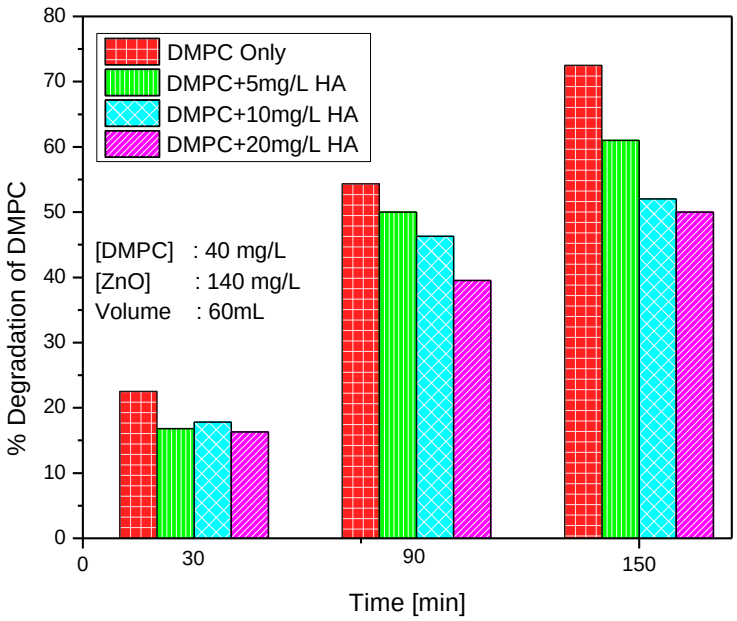

Fig. 5.13: Effect of Humic acid [HA] on the photocatalytic degradation of DMPC

Humic acid can absorb light which reduces the light quanta available for catalyst activation which in turn affects the generation of hydroxyl radicals and other reactive species. This results in inhibition of the degradation reaction. Moreover, HA can also act as a free radical scavenger which can consume ROS as described in Chapters 3 and 4. The net effect is the inhibition in the degradation of DMPC.

5.3.9 Role of Dissolved Oxygen

Dissolved oxygen has an important role in aqueous phase photocatalytic degradation reactions. The O_2 molecules act as scavengers for the photogenerated electrons thereby preventing the possible electron-hole recombination reactions as discussed in Chapter 3. Presence of oxygen is also important for the oxidation of pollutant as well as the intermediates formed from it, eventually leading to their complete mineralization. To establish the role of dissolved oxygen in the photocatalytic degradation of DMPC, three parallel experiments were conducted under identical conditions. In the first experiment, the degradation was carried out under normal reaction conditions with natural dissolved oxygen present in the system. In the second experiment, the dissolved oxygen present in the system is removed by bubbling N_2 gas through the solution and in the third, more oxygen is supplied to the system by passing O_2 through the solution. The results are shown in figure 5.14.

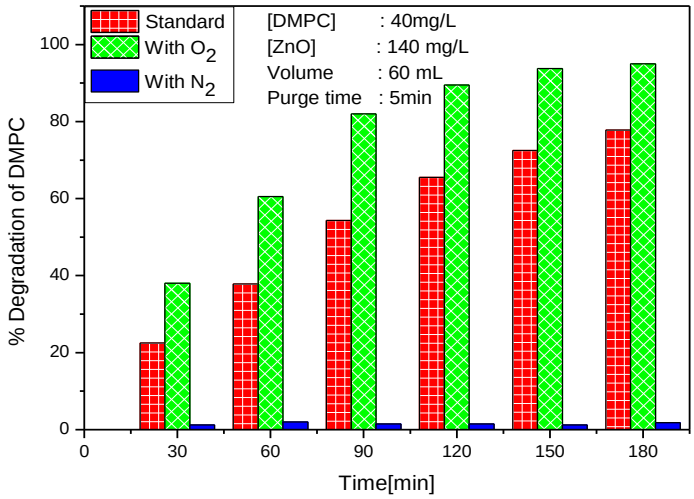

Fig. 5.14: Effect of O_2 on the photocatalytic degradation of DMPC on ZnO

It was clear that in the deaerated system the degradation of DMPC was inhibited and the degradation was less than 2% at all time intervals. The slight degradation observed in the deaerated system may be due to the residual adsorbed/dissolved oxygen present in the system, which is not removed completely by N_2. But this available dissolved oxygen was completely consumed within 30 min of irradiation as indicated by the constant degradation of DMPC at all time intervals. This is similar to the observation in the case of ACP as described in Chapter 4. When the system is enriched with extra O_2, the percentage degradation of DMPC increases at all time intervals compared to the normal system. However, after 150 min, the percentage degradation of DMPC stabilizes in the oxygen enriched system. The decrease in degradation of DMPC in the deaerated system can be explained based on the reduction in the amount of reactive oxygen species generated by the photo activation of ZnO catalyst. In the absence of O_2, which traps the photogenerated electron,

the holes and electrons will recombine and get deactivated. The higher rate of DMPC degradation both in natural and O_2 enriched system is due to the prevention of electron-hole recombination and consequent generation of more ROS which can interact with the pollutant /reaction intermediates as already explained in Chapters 3 and 4.

5.3.10 Detection and identification of reaction intermediates

During the photocatalytic degradation of DMPC three reaction intermediates i.e., AMS, ACP and an unidentified intermediate were detected by gas chromatography. Phenol is formed as a minor intermediate and its concentration at different time intervals was determined quantitatively by colorimetric analysis by measuring the absorbance of the coloured complex formed by phenol with 4-aminoantipyrene at 500 nm. The chromatogram showing the peaks of AMS, ACP and unknown intermediate during the DMPC degradation is shown in figure 5.15.

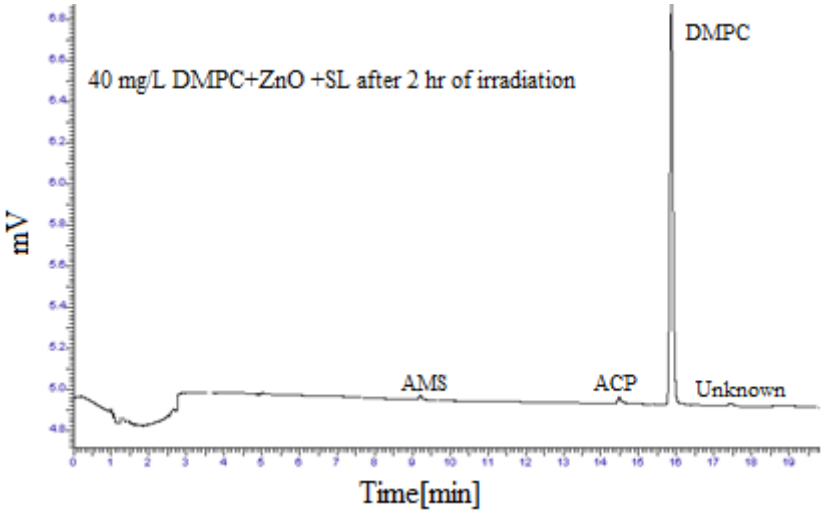

Fig. 5.15: Gas chromatogram showing DMPC, AMS, ACP and unknown intermediate.

As the degradation of DMPC is in progress, the concentration of these intermediates gradually increases and reaches a maximum level, then decreases as the irradiation continues. The concentrations of the intermediates after different periods of irradiation is shown in table.5.5.

Table 5.5: Formation of intermediates during the photocatalytic degradation of DMPC

[DMPC]=40 mg/L, [ZnO] =140 mg/L, Volume=60 mL

Time of irradiation[min]	% Degradation of DMPC	[AMS] [mg/L]	[Phenol] formed [mg/L]	[ACP] formed [mg/L]	Unidentified Intermediates formed [%]
0	0	0	0	00	0
30	22.5	0.18	0.21	0.12	0.16
60	37.8	0.12	1.9	0.16	0.24
90	54.3	0.08	2.1	0.25	0.45
120	65.5	0.06	2.3	0.27	0.71
150	72.5	0.06	2.3	0.22	0.74
180	77.8	0.02	2.2	0.19	0.62

The stabilization of the concentration of intermediates shows that the rates of their formation and degradation are approximately same. Later, as the concentration of DMPC has decreased, the degradation rate of the intermediates is accelerated. Hence the concentration of the intermediates begins to decrease and eventually becomes 'nil', indicating complete mineralization, as seen from the COD measurements (see section 5.3.14).

5.3.11 Effect of reaction intermediates on the degradation of DMPC

5.3.11.1 Effect of phenol

The effect of the reaction intermediate phenol on the photocatalytic degradation of DMPC is investigated in detail by adding varying amounts

of phenol to the reaction system at different time intervals. The results are shown in the figure 5.16. The percentage degradation of DMPC decreases in presence of externally added phenol at all time intervals and the extent of inhibition increases with increase in phenol concentration. The decrease in the degradation can be attributed to the competition between the DMPC and phenol as well as other intermediates for various ROS.

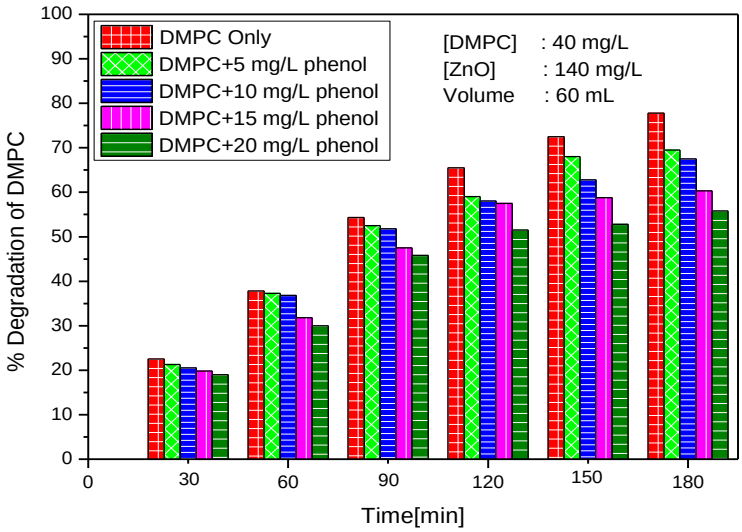

Fig. 5.16: Effect of phenol on the photocatalytic degradation of DMPC

Since there is competition between DMPC and phenol for the ROS, corresponding decrease is expected in the degradation of phenol in presence of DMPC also. The effect of DMPC on the degradation of phenol was also investigated at different DMPC concentrations. The results shown in figure 5.17 indicate that the addition of DMPC has very little influence on the degradation of phenol. The slight inconsistency in the concentration of phenol at various concentrations of DMPC can be

due to the insitu formation of phenol and its concurrent decomposition. In general, it may be concluded that the effect of DMPC on the degradation of phenol is negligible. This further indicates that the phenol which is generated insitu during the degradation of DMPC, is getting degraded and mineralized efficiently. Hence the concentration of phenol in the system is always quite low and even undetectable at times.

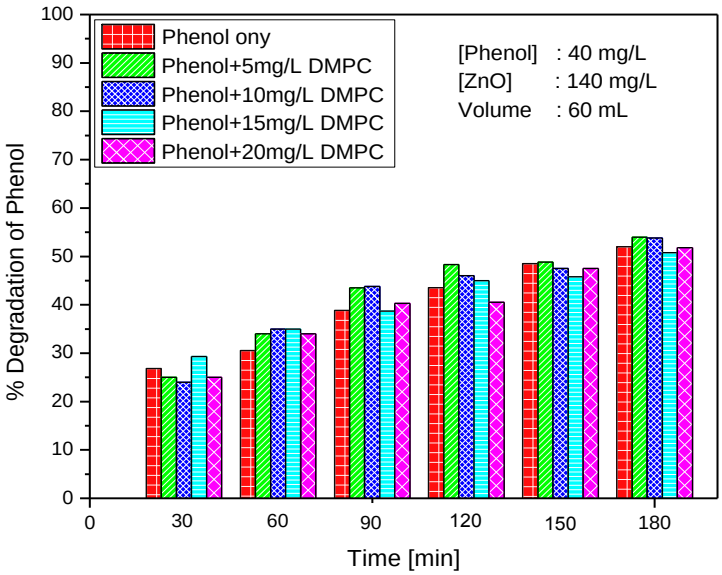

Fig. 5.17: Effect of DMPC on the photocatalytic degradation of Phenol

5.3.11.2 Effect of ACP

ACP was identified as another intermediate formed during the photocatalytic degradation of DMPC. The effect of the externally added ACP on the DMPC degradation is tested and the results are presented in figure 5.18. In the initial stage of the reaction, ACP inhibits the DMPC degradation at all concentrations. But the inhibition becomes weaker with time.

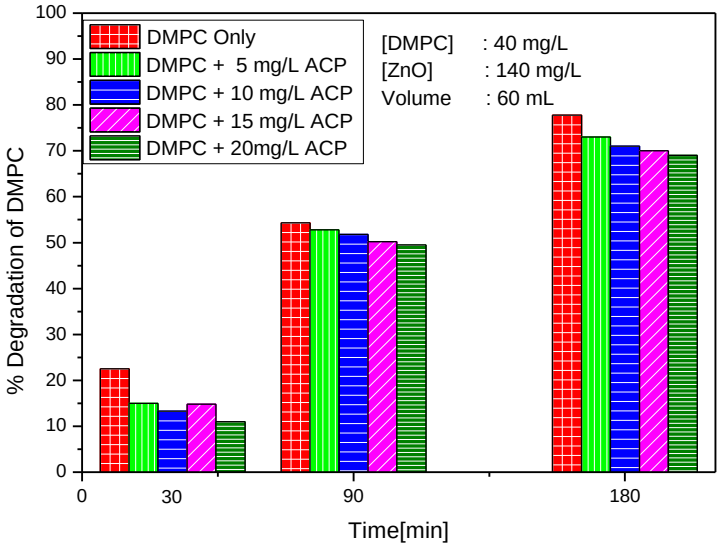

Fig. 5.18: Effect of Acetophenone (ACP) on the photocatalytic degradation of DMPC

The effect of DMPC on the degradation of ACP is negligible. Similarly the effect of AMS on the degradation of DMPC and vice versa is not much significant. Consequently, the degradation of insitu formed AMS and ACP also will proceed smoothly. Hence the net concentration of these two compounds in the system at any point of time during the photocatalytic process will be very small. More details on these studies are given in Chapter 7 (section 7.3.1).

5.3.12 Effect of salts/anions

As explained in Chapters 3 and 4, industrial effluent water often contains a variety of salts/anions, which can influence the photocatalytic degradation of pollutants present in the system. Hence it is important to study the effect of various salts or anions on the rate of degradation of the pollutants in order to develop an effective photocatalytic method for their

removal. The effects of various anions on the photocatalytic degradation of AMS and ACP are discussed in detail in previous chapters. In this chapter, the study is extended to the photocatalytic degradation of DMPC. The anions tested are the halides, sulphate, nitrate, carbonate, bicarbonate, oxalate, acetate and phosphate. The results are plotted in figures 5.19 and 5.20.

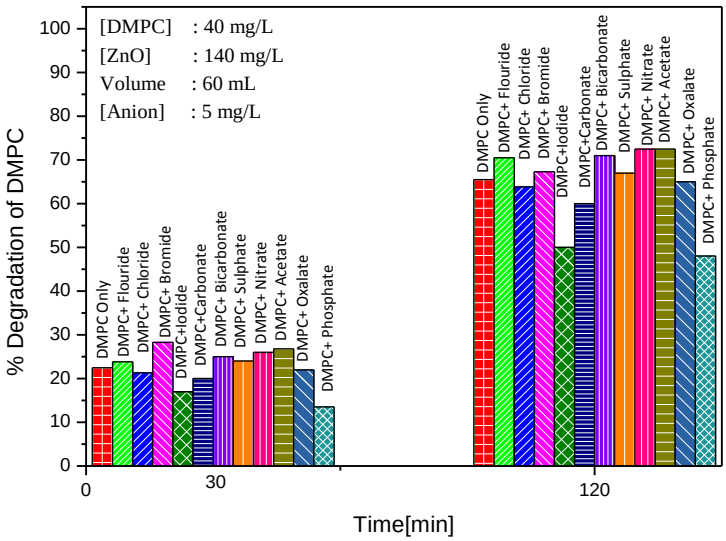

Fig. 5.19: Effect of different anions on the degradation of DMPC at different reaction times

As in the case of the degradation of AMS and ACP, in the case of DMPC also, the effect of various anions on its photocatalytic degradation was found to depend on the concentration of the anions and the time of irradiation. At low anion concentration of 5 mg/L, bromide, nitrate and acetate ion enhance the degradation of DMPC moderately at the initial time of reaction (30 min). PO_4^{3-}, I^- and CO_3^{2-} inhibit the degradation. Other ions have practically no effect. At the same concentration of anion after 120 min, PO_4^{3-}, I^- and CO_3^{2-} continue to be good inhibitors, while CH_3COO^-, NO_3^-, HCO_3^- and F^- may be considered as mild enhancers.

Other anions (Br^-, Cl^-, SO_4^{2-} and $C_2O_4^{2-}$) can be considered as having practically no effect, after this time period (120 min).

The effect of various anions may be summarized as follows:

<u>After 30 min of irradiation</u>

Inhibition: $PO_4^{3-} > I^- > CO_3^{2-}$

No effect: $F^- \approx Cl^- \approx HCO_3^- \approx SO_4^{2-} \approx C_2O_4^{2-}$

Enhancement: $Br^- > CH_3COO^- \geq NO_3^-$

<u>After 120 min of irradiation</u>

Inhibition: $PO_4^{3-} > I^- > CO_3^{2-}$

No effect: $Cl^- \approx Br^- \approx SO_4^{2-} \approx C_2O_4^{2-}$

Enhancement: $F^- \approx NO_3^- \approx HCO_3^- \approx CH_3COO^-$

At higher concentration of the anion (20 mg/L), the effect at 30 min (figure 5.20) is as follows:

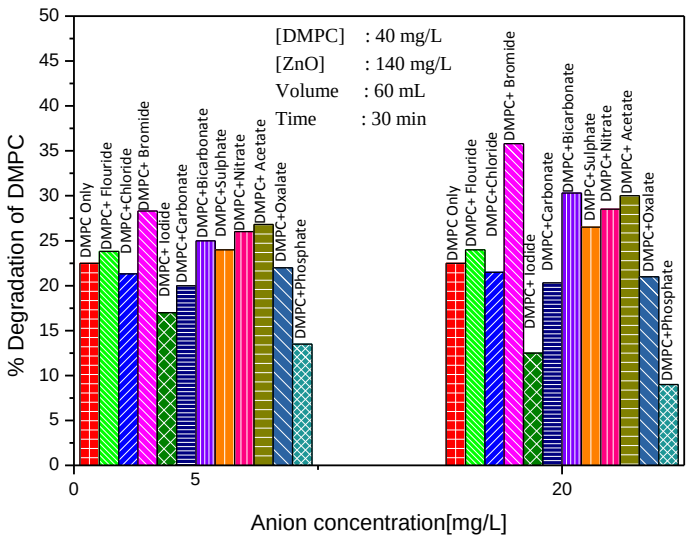

Fig. 5.20: Effect of concentration of anions on the degradation of DMPC

Inhibition: $PO_4^{3-} > I^- > CO_3^{2-} \approx C_2O_4^{2-}$

No effect: F^-, Cl^-

Enhancement: $Br^- > HCO_3^- \approx CH_3COO^- > NO_3^- > SO_4^{2-}$

The trend in the effect of the anions remain fairly the same at the two concentrations (5 and 20 mg/L) and two reaction periods (30 min and 120 min) studied here with only minor variations. In any case, detailed investigations of the effect of all these anions at different concentrations and reaction times was carried out as done in the case of AMS and ACP and the results are plotted in figures 5.21-5.31.

a) Effect of F^- :

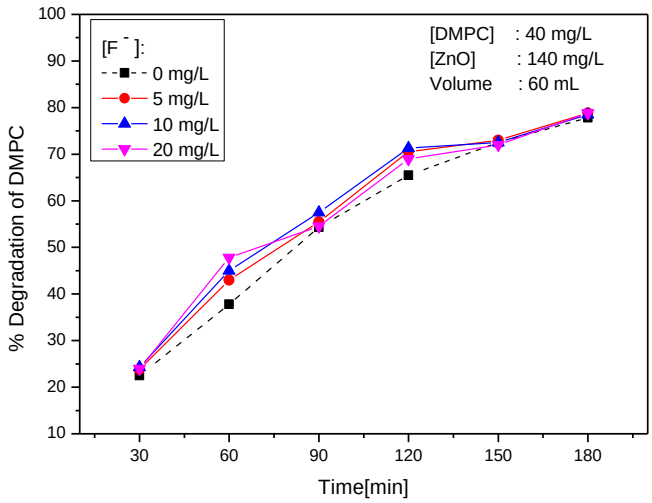

Fig. 5.21: Effect of concentration of fluoride ion (F^-) and reaction time on the photocatalytic degradation of DMPC.

Initially F^- has no effect on the degradation. However with time, it becomes a mild enhancer at all concentrations and eventually the effect is again 'nil', when most of the DMPC has already degraded.

b) Effect of Cl^- :

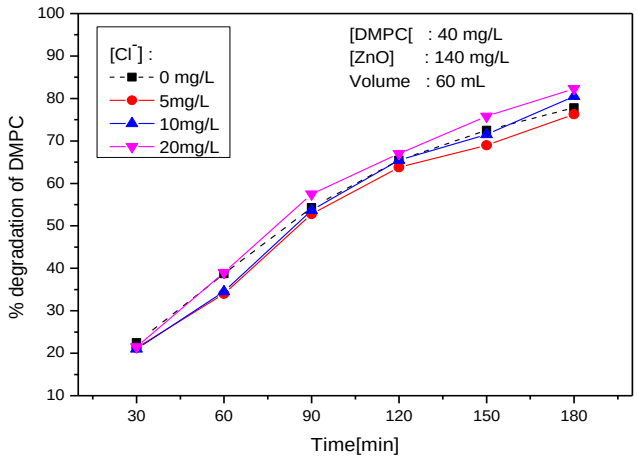

Fig. 5.22: Effect of concentration of chloride ion (Cl^-) and reaction time on the photocatalytic degradation of DMPC

Cl^- is found to have practically no effect (or mild enhancement) on the degradation. For all practical purposes, the effect can be treated as 'nil'.

c) Effect of Br^-

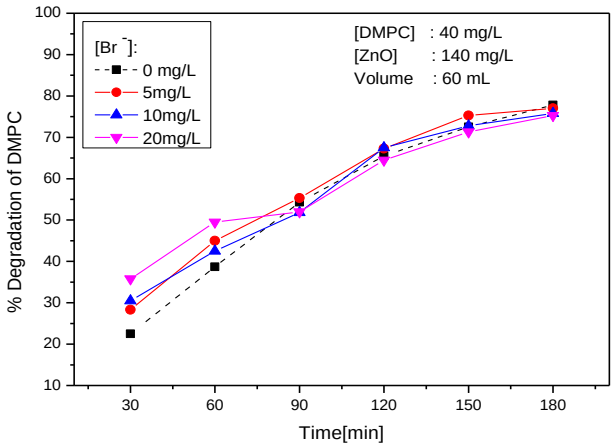

Fig. 5.23: Effect of concentration of bromide ion (Br^-) and reaction time on the photocatalytic degradation of DMPC'

Br^- is found to be a moderate enhancer in the early stages of the reaction. With time, the degree of enhancement decreases and eventually it becomes insignificant.

d) Effect of I^-

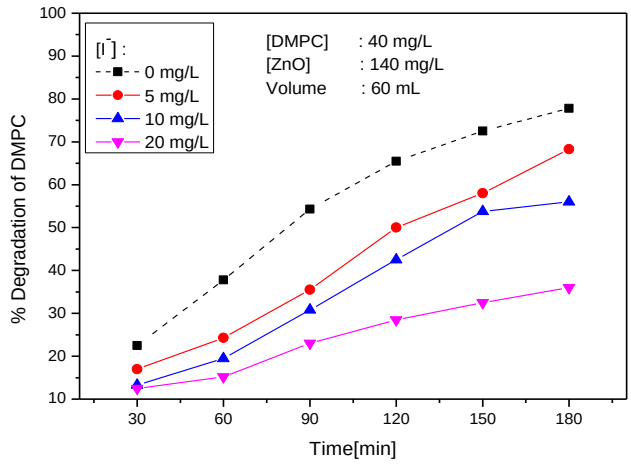

Fig. 5.24: Effect of concentration of iodide ion (I^-) and reaction time on the photocatalytic degradation of DMPC

I^- is observed to be a strong inhibitor, with the inhibition increasing with increase in its concentration.

e) Effect of CO_3^{2-}

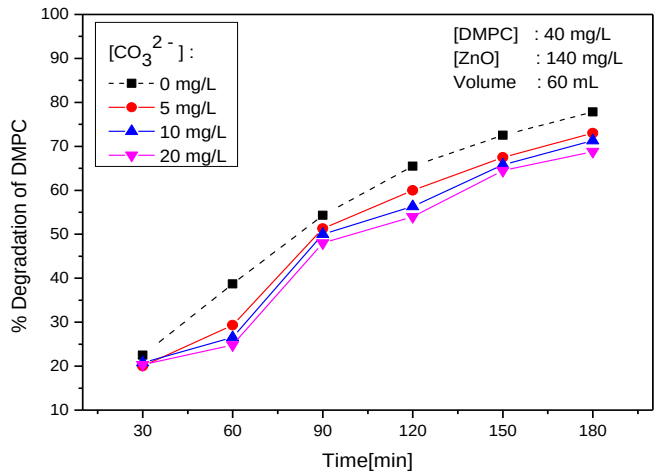

Fig. 5.25: Effect of concentration of carbonate ion (CO_3^{2-}) and reaction time on the photocatalytic degradation of DMPC.

CO_3^{2-} is a moderate inhibitor at all concentrations and all reaction times.

f) Effect of HCO_3^-

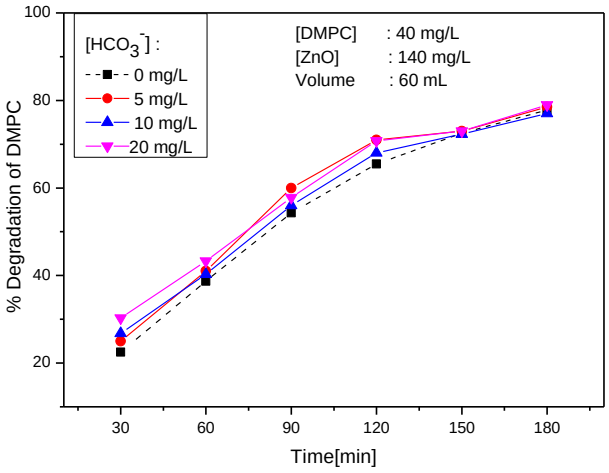

Fig. 5.26: Effect of concentration of bicarbonate anion (HCO_3^-) and reaction time on the photocatalytic degradation of DMPC.

The effect of HCO_3^- can be considered as 'mild enhancement' at lower reaction times, the effect increasing with increase in concentration. At later stages of the reaction, the effect is negligible.

g) Effect of NO_3^-

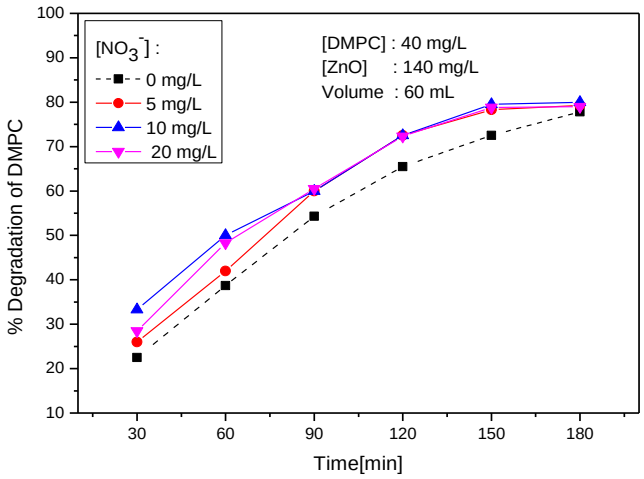

Fig. 5.27: Effect of concentration of nitrate ion (NO_3^-) and reaction time on the photocatalytic degradation of DMPC

NO_3^- is an enhancer at all concentrations and all reaction times.

h) Effect of PO_4^{3-}

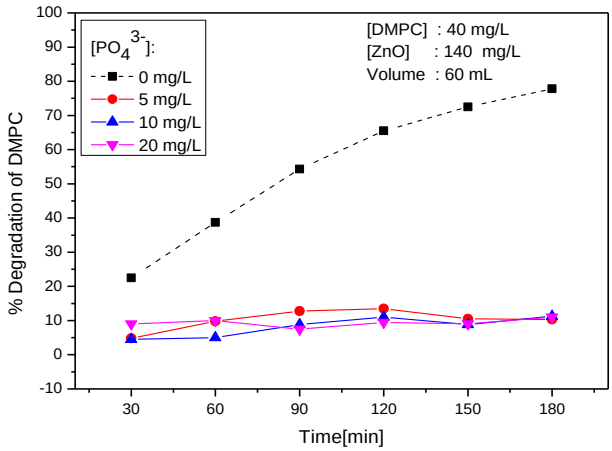

Fig. 5.28: Effect of concentration of phosphate ion (PO_4^{3-}) and reaction time on the photocatalytic degradation of DMPC.

PO_4^{3-} is a strong inhibitor of the degradation of DMPC at all concentrations and reaction times.

i) Effect of CH_3COO^-

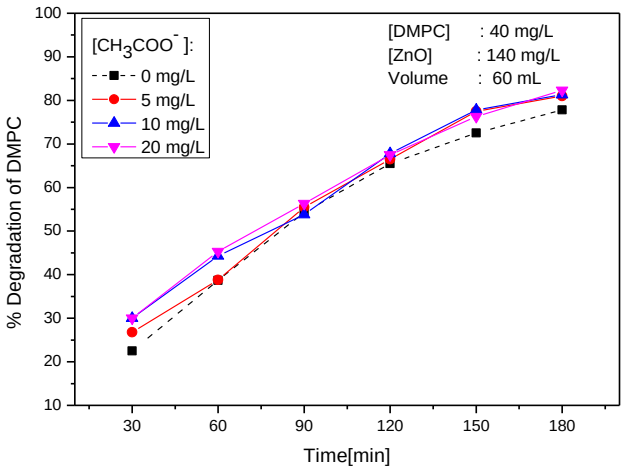

Fig. 5.29: Effect of concentration of acetate ion (CH_3COO^-) and reaction time on the photocatalytic degradation of DMPC.

CH_3COO^- can be considered as a 'mild enhancer' at all concentrations and reaction times

j) Effect of $C_2O_4^{2-}$

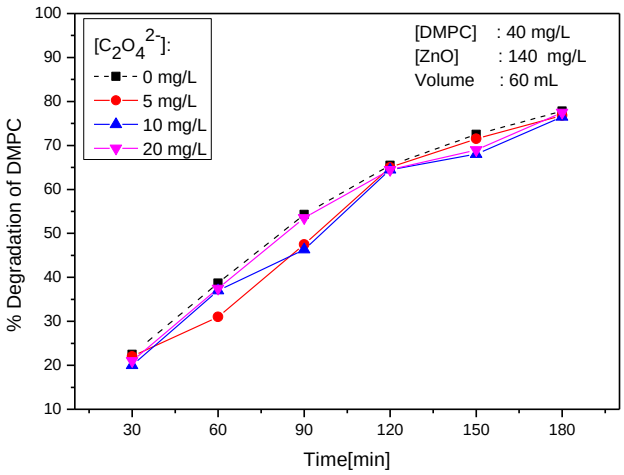

Fig. 5.30: Effect of concentration of oxalate ion ($C_2O_4^{2-}$) and reaction time on the photocatalytic degradation of DMPC.

$C_2O_4^{2-}$ can be treated as a 'mild inhibitor' or having 'no effect', depending on the concentration and reaction time

k) Effect of SO_4^{2-}

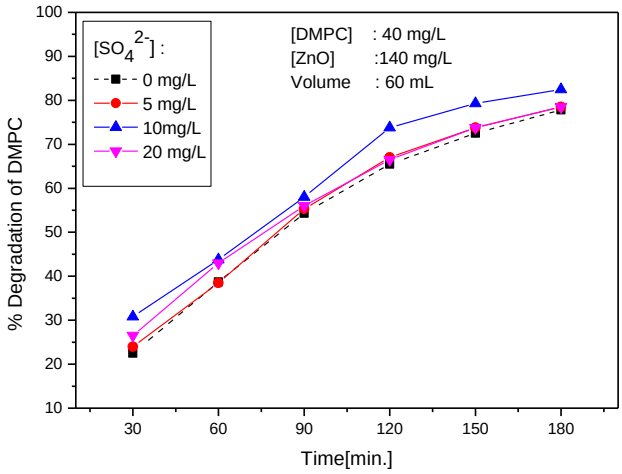

Fig. 5.31: Effect of concentration of sulphate ion (SO_4^{2-}) and reaction time on the photocatalytic degradation of DMPC.

At lower concentration, SO_4^{2-} has no effect on the degradation of DMPC. At higher concentration, it is a mild enhancer at all reaction times.

The study shows that the effect of anions on the photocatalytic degradation of DMPC follows more or less consistent trend with respect to the concentration of the ions as well as the reaction time. This is contrary to the effect of anions on the photocatalytic degradation of many other pollutants, where the concentration of the ions and reaction times alter the nature of the influence significantly. Phosphate and iodide ions act as strong inhibitors at all concentrations and at all irradiation times. CO_3^{2-} also functions as a mild inhibitor. Chloride and oxalate ions have practically little effect in many instances. Fluoride, bromide, bicarbonate, nitrate, sulphate and acetate ions act as enhancers at different concentrations and reaction times, though at varying degrees.

The inhibitory effect of halide ions such as iodide and chloride can be due to the fact that the halide ion, X^- acts as a radical scavenger and forms less active $X_2\bullet^-$ or XOH^-, which in turn can inhibit the degradation of the pollutant as explained earlier in Chapter 4. The size of the halide ion may also have effect on its ability to enhance/inhibit the degradation (see table 3.9). Iodide ion is having a bigger size followed by bromide, chloride and fluoride ions. As the size of the halide ion increases, it covers a greater surface area of the catalyst which results in decrease in the area available for the adsorption of pollutant/intermediates on the catalyst surface which results in decrease in the degradation rate. Moreover, the adsorbed halide ion prevents the catalyst activation by

preventing the sunlight from reaching the catalyst surface. However, in spite of its bigger size compared to chloride ion, bromide ion is a strong enhancer compared to the former. The effect of F^- also does not fit into this concept. Hence it may be inferred that, just as in the case of many other photocatalytic processes, the effect of halide ions does not follow a predictable or consistent pattern.

The greater inhibition shown by the phosphate ion can be explained as due to the preferential adsorption of the trivalent phosphate ion on the catalyst surface and the consequent reduction in the available active sites for the adsorption of pollutant/intermediates. This preferential adsorption also leads to the poor activation of the catalyst and hence the generation of ROS also is inhibited. This results in decreased degradation rate as already explained in Chapter 3. The enhancement by various anions may be due to the formation of reactive radical anions, which are formed by the interaction of the anions with the photogenerated holes as well as with $^{\bullet}OH$ radicals. The relative oxidation potential of the radical anions, reactivity of the substrate, nature of intermediates, adsorption of various components on the catalyst surface etc. determine the efficiency of respective radical anion species as enhancers, as already discussed in Chapter 4.

Comparative effect of the anions at various concentrations and reaction times on the degradation of DMPC is summarized qualitatively in table 5.6.

Table 5.6: Qualitative comparison of effect of anions at various concentrations and reaction times on the photocatalytic degradation of DMPC

Time of reaction, min	[Anion], mg/L	Comparative effect
30	5	Enhancement: $Br^- > CH_3COO^- \geq NO_3^-$ No effect: F^-, Cl^-, HCO_3^-, SO_4^{2-}, $C_2O_4^{2-}$ Inhibition: $PO_4^{3-} > I^- > CO_3^{2-}$
	10	Enhancement: $Br^- > NO_3^- > SO_4^{2-} > CH_3COO^-$ No effect: F^-, Cl^-, CO_3^{2-}, HCO_3^-, $C_2O_4^{2-}$ Inhibition: $PO_4^{3-} > I^-$
	20	Enhancement: $Br^- > HCO_3^- \geq CH_3COO^- > NO_3^- > SO_4^{2-}$ No effect: F^-, Cl^- Inhibition: $PO_4^{3-} > I^- > CO_3^{2-} \approx C_2O_4^{2-}$
60	5	Enhancement: $Br^- > F^- > NO_3^-$ No effect: Cl^-, HCO_3^-, CH_3COO^-, SO_4^{2-} Inhibition: $PO_4^{3-} > I^- > CO_3^{2-} > C_2O_4^{2-}$
	10	Enhancement: $NO_3^- > F^- > CH_3COO^- > SO_4^{2-} > Br^-$ No effect: Cl^-, HCO_3^-, $C_2O_4^{2-}$ Inhibition: $PO_4^{3-} > I^- > CO_3^{2-}$
	20	Enhancement: $Br^- > NO_3^- > F^- > CH_3COO^- > HCO_3^- > SO_4^{2-}$ No effect: Cl^-, $C_2O_4^{2-}$ Inhibition: $PO_4^{3-} > I^- > CO_3^{2-}$
90	5	Enhancement: $NO_3^- = HCO_3^-$ No effect: F^-, Cl^-, Br^-, CH_3COO^-, SO_4^{2-} Inhibition: $PO_4^{3-} > I^- > C_2O_4^{2-} > CO_3^{2-}$
	10	Enhancement: $NO_3^- > SO_4^{2-}$ No effect: F^-, Cl^-, Br^-, HCO_3^-, CH_3COO^- Inhibition: $PO_4^{3-} > I^- > C_2O_4^{2-} > CO_3^{2-}$

	20	Enhancement: NO_3^- No effect: F^-, Cl^-, Br^-, HCO_3^-, SO_4^{2-}, CH_3COO^-, $C_2O_4^{2-}$ Inhibition: $PO_4^{3-} > I^- > CO_3^{2-}$
120	5	Enhancement: $NO_3^- > F^- \approx HCO_3^- \approx CH_3COO^-$ No effect: Cl^-, Br^-, SO_4^{2-}, $C_2O_4^{2-}$ Inhibition: $PO_4^{3-} > I^- > CO_3^{2-}$
	10	Enhancement: $SO_4^{2-} > NO_3^- > F^-$ No effect: Cl^-, Br^-, HCO_3^-, CH_3COO^-, $C_2O_4^{2-}$ Inhibition: $PO_4^{3-} > I^- > CO_3^{2-}$
	20	Enhancement: $NO_3^- > HCO_3^- > F^-$ No effect: Cl^-, Br^-, SO_4^{2-}, CH_3COO^-, $C_2O_4^{2-}$ Inhibition: $PO_4^{3-} > I^- > CO_3^{2-}$
150	5	Enhancement: $NO_3^- > CH_3COO^-$ No effect: F^-, Cl^-, Br^-, HCO_3^-, SO_4^{2-}, $C_2O_4^{2-}$ Inhibition: $PO_4^{3-} > I^- > CO_3^{2-}$
	10	Enhancement: $NO_3^- \approx SO_4^{2-} > CH_3COO^-$ No effect: F^-, Cl^-, Br^-, HCO_3^- Inhibition: $PO_4^{3-} > I^- > CO_3^{2-} > C_2O_4^{2-}$
	20	Enhancement : $NO_3^- > CH_3COO^-$ No effect: F^-, Cl^-, Br^-, HCO_3^-, SO_4^{2-}, $C_2O_4^{2-}$ Inhibition: $PO_4^{3-} > I^- > CO_3^{2-}$
180	5	Enhancement: CH_3COO^- No effect: F^-, Cl^-, Br^-, HCO_3^-, SO_4^{2-}, NO_3^-, $C_2O_4^{2-}$ Inhibition: $PO_4^{3-} > I^- > CO_3^{2-}$
	10	Enhancement: $SO_4^{2-} > CH_3COO^-$ No effect: F^-, Cl^-, Br^-, HCO_3^-, NO_3^-, $C_2O_4^{2-}$ Inhibition: $PO_4^{3-} > I^- > CO_3^{2-}$
	20	Enhancement: CH_3COO^- No effect: F^-, Cl^-, Br^-, HCO_3^-, NO_3^-, SO_4^{2-}, $C_2O_4^{2-}$ Inhibition: $PO_4^{3-} > I^- > CO_3^{2-}$

Except for the strong enhancement (NO_3^-, CH_3COO^-) and strong inhibition (PO_4^{3-}, I^-), the relative effect of the anions is mild and not strictly consistent. Further, the effect is subject to minor variations under respective reaction conditions.

The pH on the reaction system in presence of various anions is measured to study the effect of anions on the pH and the results are presented in table 5.7.

Table 5.7: pH of DPMC solution with ZnO in presence of various anions
[DMPC]= 40 mg/L, [ZnO] =140 mg/L, [Anion] =5 mg/L, Time= 2 hr

Anion	pH
No anion	6.0
F^-	7.40
Cl^-	7.40
Br^-	7.40
I^-	7.43
CO_3^{2-}	9.32
HCO_3^-	7.55
SO_4^{2-}	7.42
NO_3^-	7.46
CH_3COO^-	7.41
$C_2O_4^{2-}$	7.87
PO_4^{3-}	7.86

Except in the case of CO_3^{2-}, which increases the pH moderately, the effect is only a mild increase in all other cases. Hence, the varying effect of anions on the degradation of DMPC cannot be attributed to any change in pH. The slight increase in degradation observed at alkaline pH (figure 5.9) is not seen in presence of CO_3^{2-} in spite of the increase in pH in its presence. Hence the net effect of CO_3^{2-} may be treated as clear inhibition and not an indirect effect of pH.

The adsorption of DMPC on ZnO is already verified and found to be negligible. The adsorption remains unchanged in the presence of anions (table 5.8). Hence the preferential adsorption by anions also cannot be a general reason for the anion effect.

Table 5.8: Adsorption of DMPC over ZnO in presence of anions
[DMPC]=40 mg/L, [ZnO] =140 mg/L, Volume=60 mL,
[Anion] =5 mg/L, Time = 2 hr

Anion	% Adsorption of DMPC
No anion	0.5
F^-	1.7
Cl^-	0.5
Br^-	1.5
I^-	0.6
CO_3^{2-}	1.7
HCO_3^-	2.6
SO_4^{2-}	3.0
NO_3^-	2.7
CH_3COO^-	1.2
$C_2O_4^{2-}$	2.0
PO_4^{3-}	2.7

The effect of anions on the photocatalytic degradation of DMPC can also be explained as done in the case of AMS and ACP. In the case of DMPC, the preferential adsorption by anions do not affect the adsorption of the substrate which is only negligible even in the absence of anions. However, the efficiency of photo activation of the surface and consequent generation of ROS can be affected by the anions. The specific reason for enhancement/inhibition/no effect may be more or less the same as discussed in earlier chapters.

5.3.13 Effect of oxidants

The effect of the two commonly used oxidants i.e., $S_2O_8^{2-}$ and IO_3^- at different concentrations on the solar photocatalytic degradation of DMPC with ZnO catalyst was investigated in detail. Comparative effect of these oxidants at different reaction times and at different concentrations are presented in figures 5.32 and 5.33 respectively. The effect of oxidants was found to be dependent on both the concentration of the added oxidant and the time of irradiation. This is similar to the observation made in the case of AMS and ACP degradation reported in earlier chapters. The effect of another common oxidant H_2O_2 on the degradation of DMPC is reported earlier in this chapter itself. For comparative purpose, the data is incorporated in figures 5.32 and 5.33 also.

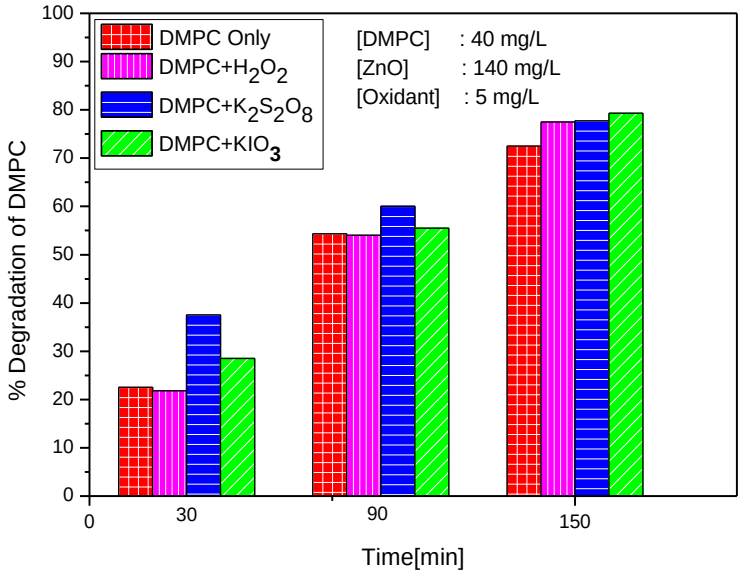

Fig. 5.32: Effect of oxidants on the photocatalytic degradation of DMPC after different reaction times.

At lower oxidant concentration (5 mg/L) and at the lower reaction time (30 min), H_2O_2 has little effect, while persulphate and iodate enhance the degradation. Persulphate is a better oxidant than iodate. However, the enhancement slows down with time and after ~150 min, the enhancing effect of all these oxidants is mild or even practically 'nil'. In the early stage of irradiation (30 min), both $S_2O_8^{2-}$ and IO_3^- enhance the degradation even at higher concentration (figure 5.33). However, the concentration effect is not much and $S_2O_8^{2-}$ remains a better enhancer than IO_3^- at all concentrations. Since the enhancing effect in the early stages is not seen at the later stages and the degradation becomes comparable with and without the oxidant, it is possible that some of the anions formed from the oxidants may be even functioning as inhibitors at later stages of the reaction. Eventually, the enhancing and inhibiting interactions balance thereby making the oxidant effect 'negligible'.

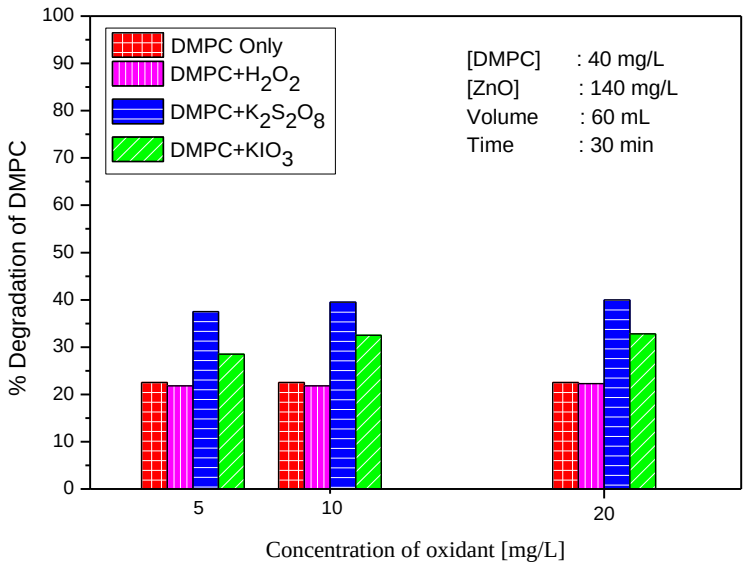

Fig. 5.33: Effect of oxidants at different concentrations on the photocatalytic degradation of DMPC

Detailed investigation of the effect of these oxidants at different concentrations and at different reaction times was carried out and the results are shown in figures 5.34-5.36.

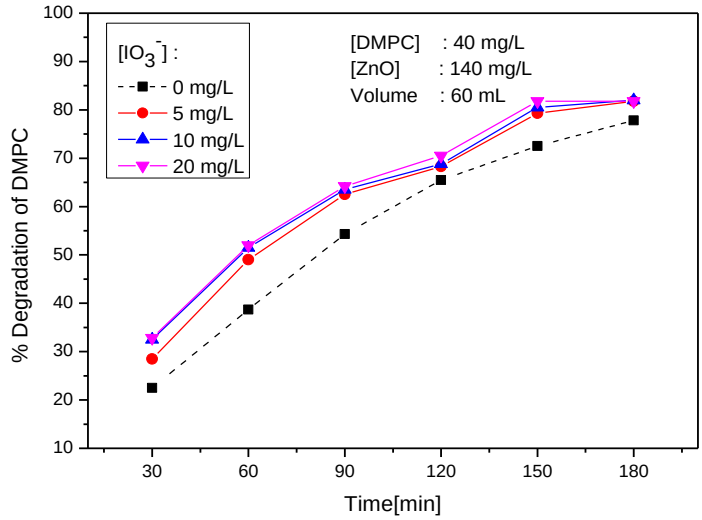

Fig. 5.34: Effect of concentration of potassium iodate and reaction time on the photocatalytic degradation of DMPC.

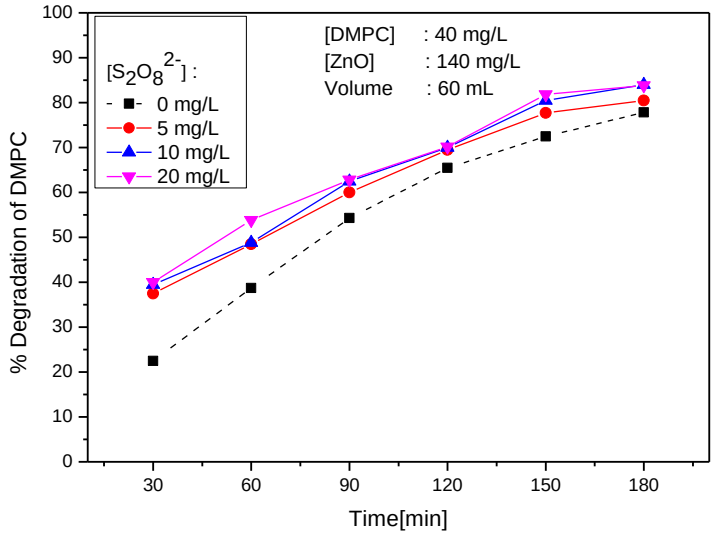

Fig. 5.35: Effect of concentration of persulphate and reaction time on the photocatalytic degradation of DMPC.

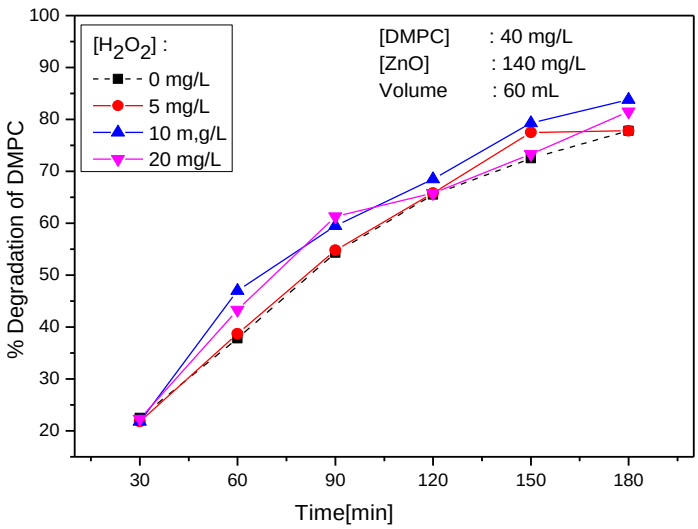

Fig. 5.36: Effect of concentration of H_2O_2 and reaction time on the photocatalytic degradation of DMPC.

The study indicates that these oxidizing agents enhance the photocatalytic degradation of DMPC in the early stages of the reaction in the order:

$$S_2O_8^{2-} > IO_3^- > H_2O_2$$

The enhancement by persulphate ion is attributed to the generation of highly reactive sulphate radical anion ($SO_4^{-\bullet}$) under UV irradiation both thermally and photochemically. These radical anions can react with H_2O to produce highly reactive $^{\bullet}OH$ radicals. Both $SO_4^{-\bullet}$ and $^{\bullet}OH$ are responsible for the enhancement as already discussed in Chapter 3. The enhancement by the persulphate ion slowly diminishes with time due to the accumulation SO_4^{2-} in the system, which acts as an inhibitor. The concentration as well as time-dependent role played by H_2O_2 as an enhancer/inhibitor is already discussed in Chapter 3. The enhancement by IO_3^- is also discussed in Chapter 3, section 3.3.19.

In the case of the pollutants AMS and ACP reported in previous chapters, combination of oxidants does not produce any additive effect. In any case, a typical combination of $S_2O_8^{2-}$ and H_2O_2 is tested in the case of DMPC also. Comparative effect of H_2O_2 and $K_2S_2O_8$ individually and their combination on the photocatalytic degradation of DMPC was conducted using 10 mg/L of the oxidants under identical conditions and the results are plotted in figure 5.37. The results show that except for H_2O_2 at the initial stage (30 min) of the reaction, the oxidants show slight enhancement towards DMPC degradation. However, the enhancement by the combination is always slightly less than that by the individual oxidants. This may be due to the complex interactions and resultant deactivation of at least some of the reactive free radicals.

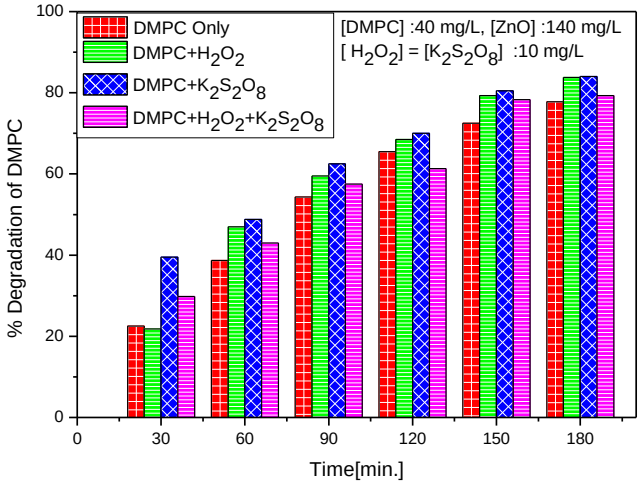

Fig. 5.37: Comparison of the effect of H_2O_2, $K_2S_2O_8$ and their combination on the photocatalytic degradation of DMPC

The study shows that the use of H_2O_2, $K_2S_2O_8$ or their combination has no significant advantage in the photocatalytic purification of water contaminated with DMPC in presence of ZnO under sunlight.

5.3.14 Mineralization of DMPC in presence of ZnO/sunlight

Complete mineralization of the pollutant and the intermediates formed from it is very important for the commercialization of the photocatalytic technology for pollution abatement. In some cases the intermediates formed from the pollutant may be more hazardous than the pollutant itself thereby requiring their complete removal from the system by way of mineralization. In the present case of DMPC degradation also, one of the intermediates detected was phenol, which is more toxic than DMPC [Mouse LD_{50} (oral) of DMPC=1400 mg/kg, Mouse LD_{50} (oral) of phenol=270 mg/kg]. Hence detailed investigation on the complete mineralization of DMPC during the photocatalytic degradation under sunlight with ZnO as catalyst was carried out. The results are shown in figure 5.38.

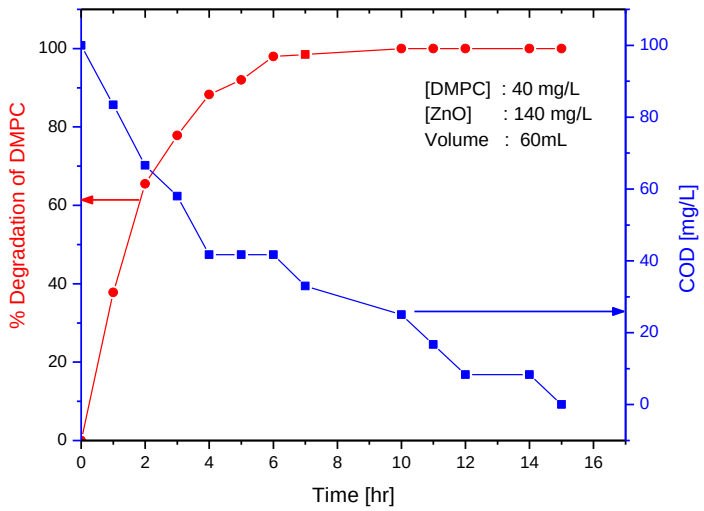

Fig. 5.38: Mineralization of DMPC under sunlight with ZnO catalyst

After 4 hr of irradiation, more than 88% DMPC degradation was achieved with decrease in the COD value from 100 mg/L to 41 mg/L.

After 6 hr even though DMPC degradation was complete, the COD value remains the same, which indicates that the intermediates are still present in the system without getting mineralized. On prolonged irradiation, the COD value gradually decreases and finally becomes zero after 15 hr of irradiation, indicating the complete mineralization of DMPC and the intermediates formed from it. Thus, the study clearly reveals that ZnO mediated sunlight induced photocatalysis can be effectively used as a powerful AOP for the complete removal of DMPC from water.

5.3.15 Reuse of ZnO catalyst

The possibility of reuse of the ZnO catalyst for DMPC degradation was investigated by separating the used ZnO from the system by filtration followed by air drying at room temperature (30°C). This catalyst was tested again to evaluate its reusability and the results are plotted in figure 5.39.

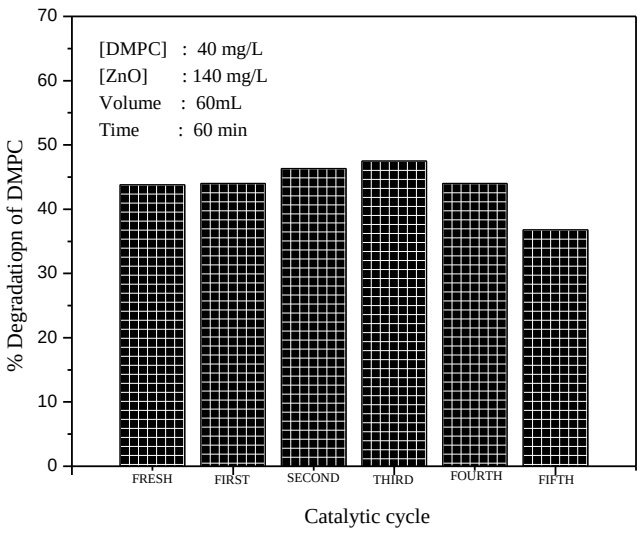

Fig. 5.39: Recycling of ZnO for the photocatalytic degradation of DMPC in SL

The study clearly shows that the catalyst remains active without any significant loss in its activity at least for 4 cycles. The decrease in the catalytic activity after fourth cycle may be due to the deactivation of some of the catalytic sites and consequent decrease in the adsorption of the intermediates (DMPC does not get adsorbed on ZnO), compared to that on the fresh catalyst. Formation of surface hydroxides along with other factors such as loss of catalyst during filtration, as described in detail in Chapters 3 and 4 can be another reason for the decrease in activity. As already discussed, the number of possible recycling depends upon many factors such as reaction conditions, chemistry of the substrate and the intermediates, reactor size and geometry etc. This study indicates that the ZnO catalyst can be economically reused for the photocatalytic degradation of DMPC in water.

A comparison of the used ZnO catalyst with fresh ZnO in terms of XRD, BET, pore size and pore volume is presented in figures 5.40-5.41 and table 5.9.

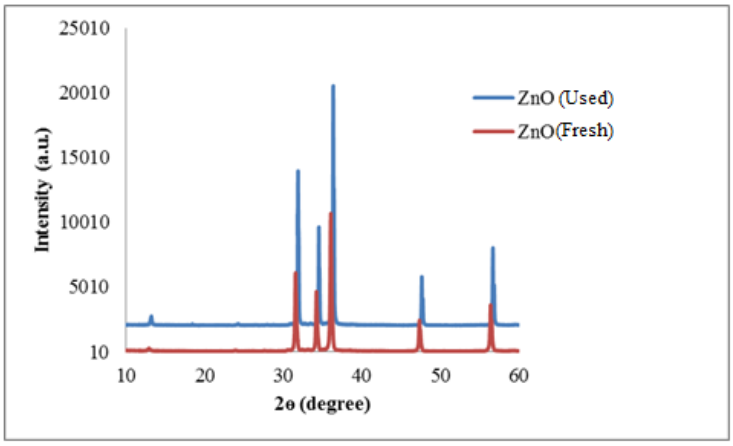

Fig. 5.40: XRD of fresh and used ZnO

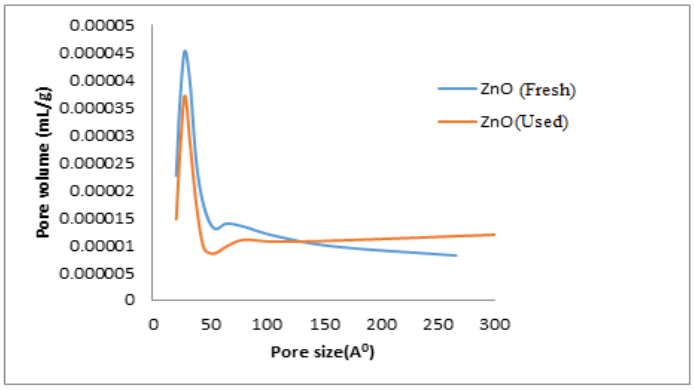

Fig. 5.41: Pore volume vs pore size for fresh and used ZnO catalyst

Table 5.9: Comparison of BET surface area, pore volume and pore size of fresh and used ZnO catalyst

Sample	BET Surface area (m^2/g)	Pore volume (cm^3/g)	Pore size (A^0)
Fresh ZnO	3.9745	0.012018	125.5911
Used ZnO	3.9481	0.016760	172.9292

The characteristics of fresh and used ZnO as above clearly show that the physicochemical parameters remain more or less unchanged with use. This may be the reason for sustaining the photocatalytic activity even after repeated use.

5.4 Mechanism

The basic mechanism of the solar photocatalytic mineralization of DMPC in water is similar to that discussed in Chapters 3 and 4, which may be summarized as follows:

$$ZnO + h\nu \rightarrow e_{cb}^- + h_{vb}^+ \quad (134)$$

$$O_2 + e_{cb}^- \rightarrow O_2^{-}\bullet \quad (135)$$

$$h_{vb}^+ + H_2O \rightarrow {}^{\bullet}OH + H \quad (136)$$

$$O_2^{-}\bullet + 2H^+ + e^- \rightarrow H_2O_2 \quad (137)$$

$$O_2^{-}\bullet + H^+ \rightarrow HO_2^{\bullet} \quad (138)$$

$$\text{DMPC} + \text{ROS } (H_2O_2,\ {}^{\bullet}OH,\ O_2^{-}\bullet,\ HO_2\bullet \text{etc}) \rightarrow \text{Intermediate(s)} \rightarrow CO_2 + H_2O + \text{Salts} \quad (139)$$

The formation of H_2O_2 and the complete mineralization (COD ≈ 0) leading to CO_2 and H_2O are confirmed from this study.

Considering the intermediates identified and the possible interaction between DMPC and the reactive $^{\bullet}OH$ radicals, the possible steps involved in the mineralization can be schematically represented as shown in figure 5.42. Some intermediates are not detected in GC analysis possibly because they are getting degraded faster than DMPC or phenol.

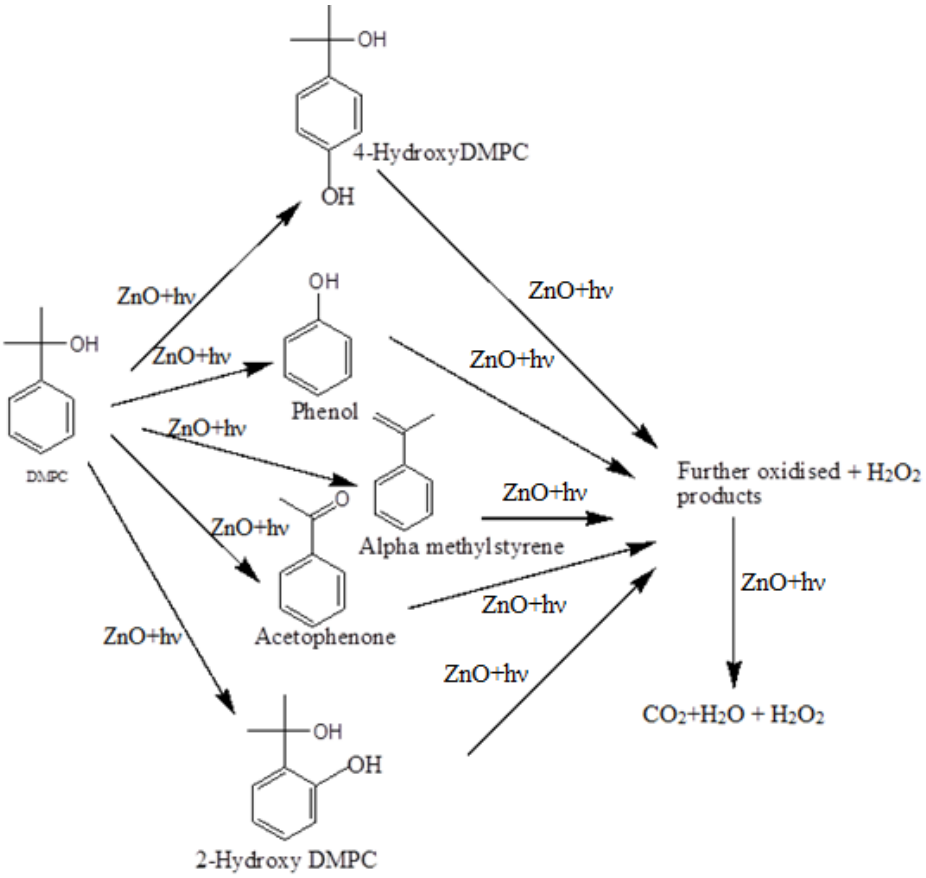

Fig. 5.42: Possible mechanism for the solar photocatalytic mineralization of DMPC in presence of ZnO

5.5 Conclusions

ZnO mediated photocatalytic degradation of small amount of DMPC in water was investigated in detail using sunlight as the energy source. The effect of various parameters such as catalyst dosage, pH, initial concentration of DMPC, externally added H_2O_2, humic acid, insitu formed intermediates etc., on the DMPC degradation was studied in detail. Acetophenone, AMS and phenol were identified as the major reaction intermediates along with one unidentified intermediate. The effect of various anions and oxidants likely to be present in water on the degradation of the pollutant was investigated. The effect varied from 'enhancement' to 'no effect' or 'inhibition' depending upon the reaction conditions and the chemistry of the reaction system. NO_3^- and CH_3COO^- were clear enhancers while PO_4^{3-} and I^- were strong inhibitors. The degradation was inhibited in deaerated system reconfirming the role of dissolved oxygen in the photocatalytic process. Complete mineralization of the pollutant was confirmed by the reduction in the COD value to zero after prolonged irradiation. The catalyst could be reused at least four times without any significant loss in its activity thereby demonstrating the potential of the method for commercial application by harvesting solar energy.

.....ꕥ.....

Chapter 6

ZINC OXIDE MEDIATED SOLAR PHOTOCATALYTIC DEGRADATION OF 2-METHYL BENZOFURAN [2-MBF] IN WATER

Contents

6.1 Introduction

2-Methyl benzofuran (2-MBF) is formed as a byproduct during the production of phenol by cumene oxidation process. Hence the industrial effluent water from phenol manufacturing processes may become contaminated with 2-MBF. Conventional secondary treatment methods are adequate for removing this pollutant from water to satisfy the statutory requirements. However, the accumulation of even traces of this contaminant in the environment may be harmful in the long run. In this context, the application of heterogeneous photo catalysis, which is emerging as a viable Advanced Oxidation Process for the total mineralization of most of organic pollutants [19,170,173-179] is investigated. ZnO is used as the catalyst and sunlight is used as the energy source. To the best of our knowledge, photocatalytic degradation of 2-MBF is not reported in the literature so far. The chemical structure of 2-MBF is presented in Chapter 2.

6.2 Experimental Details

6.2.1 Materials

2-MBF (97%) was obtained from Aldrich (India) and used as such without further purification. All other chemicals and the ZnO catalyst are from the same respective sources as described in Chapter 3. The characterization of the catalyst and the analysis of the materials were done as explained earlier.

6.2.2 Photocatalytic Experimental set up

The photocatalytic degradation study of 2-MBF was carried out in the same jacketed pyrex reactor as described in previous chapters.

6.2.3 Analytical Procedure

Perkin Elmer Auto System XL Gas Chromatograph was used for the analysis of 2-MBF in water using flame ionization detector and Elite 1301 column with hydrogen as the carrier gas. The calibration graph is obtained by multiple level calibration method similar to that explained in Chapter 3. The instrument parameters are the same as that for AMS analysis. The calibration graph of 2-MBF is shown in figure 6.1. The sampling and analysis are done in the same manner as explained in Chapter 3.

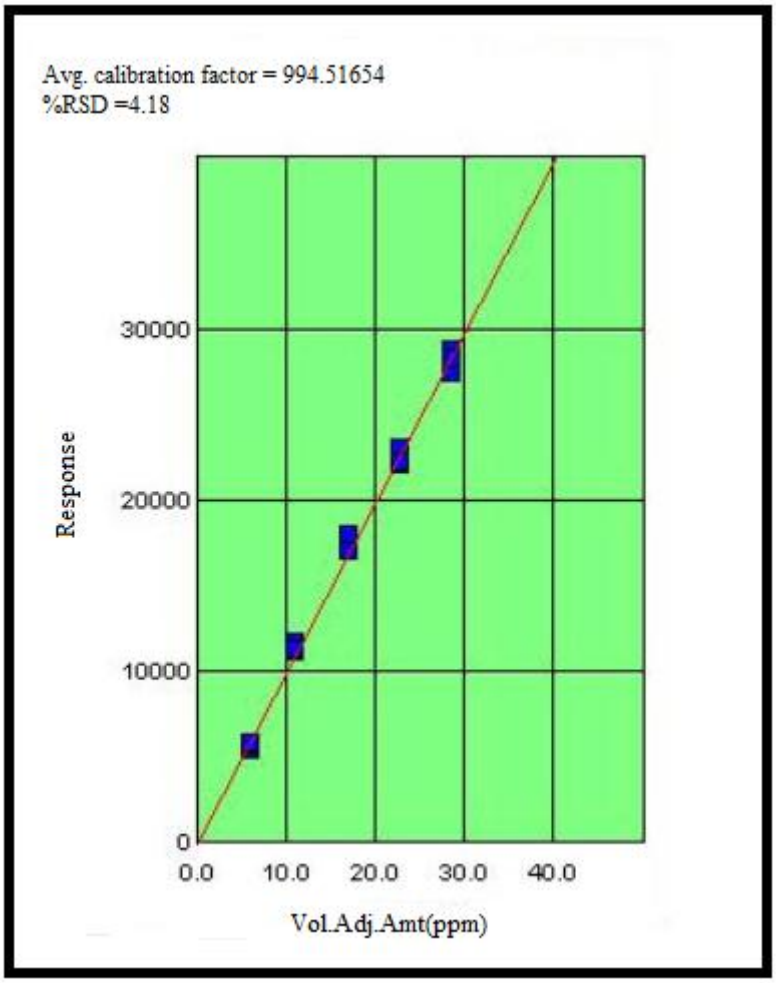

Fig. 6.1: Calibration graph for 2-MBF analysis by GC

6.2.4 Adsorption study

Adsorption study of 2-MBF over ZnO catalyst was done in the same manner as for AMS as described in Chapter 3.

6.3 Results and Discussion

6.3.1 Preliminary experiments

Preliminary investigation of the photocatalytic degradation of 2-MBF (25 mg/L) was carried out under sunlight irradiation using commercial ZnO (80 mg/L) as catalyst. The results are shown in figure 6.2.

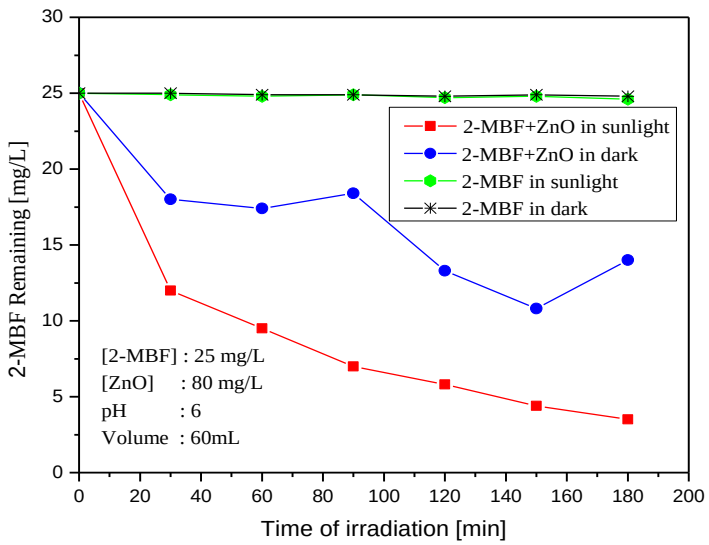

Fig. 6.2: Degradation of 2-MBF under different conditions

More than 87% degradation was obtained in 3 hr of irradiation in presence of ZnO. No degradation was observed when the experiment was carried out under identical conditions in the absence of either light or catalyst, thereby establishing the essential role of both light and catalyst. Adsorption measurements showed that the adsorption of 2-MBF on ZnO catalyst is very high. Hence significant reduction in 2-MBF concentration in the absence of light is due to adsorption on ZnO. The adsorption of 2-MBF at different concentrations over ZnO in the dark is measured and the results are shown in table 6.1.

Table 6.1: Adsorption of 2-MBF over ZnO
[2-MBF] =25 mg/L, [ZnO] = 80 mg/L

Initial [2-MBF], mg/L	[2-MBF] adsorbed after 3hr, mg/L	Adsorption of 2-MBF, mg/g of ZnO
10	6.5	81.2
15	11.2	140
20	10.7	133
25	11.0	137.5

The results show that the adsorption of 2-MBF on the ZnO surface increases with increase in concentration of the substrate and the optimum adsorption over ZnO is 11.2 mg over 0.08 g of ZnO (140 mg/g). This probably indicates that once the surface is fully covered, further adsorption does not takes place, thereby excluding the possibility of multilayer adsorption.

Chromatographic analysis of the photocatalytic reaction products at different intervals of irradiation shows the formation of ACP and three unidentified compounds (A, B and C) (figure 6.3). As explained in previous chapters, the photocatalytic degradation is primarily due to the interaction of the substrate molecule with the insitu formed reactive $^{\bullet}OH$ radical and other oxidizing species, both on the catalyst surface as well as in the bulk of the solution. The unidentified compounds are not observed consistently. Periodically they are detected and then they disappear. They may be the hydroxylated 2-MBFs formed as intermediates during the reaction. They are degrading very fast and are hence not detected often. On continuous irradiation, the pollutant as well as the intermediates disappear completely from the system, thereby establishing the potential of this method for the mineralization of 2-MBF in water matrix.

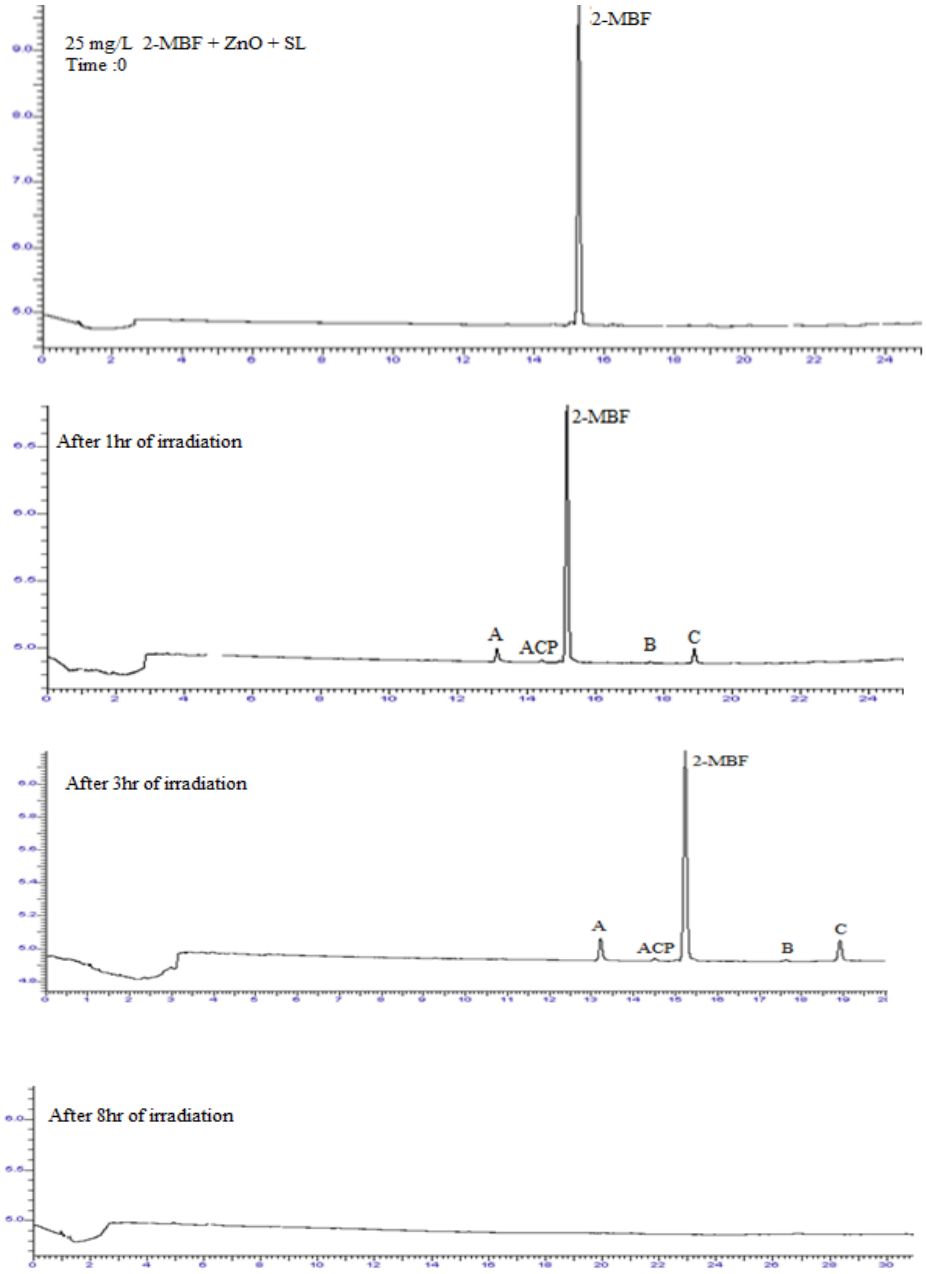

Fig. 6.3: Gas chromatogram showing the degradation of 2-MBF and formation of intermediates

The other intermediates identified using LC/MS are shown in table 6.2.

Table 6.2: Intermediates formed during the solar photocatalytic degradation of 2-MBF with ZnO

SL No	Mass	Structure
1	93	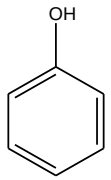
2	119	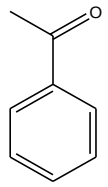
3	121	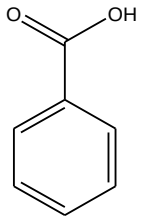
4	137	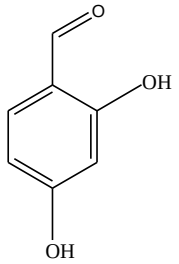
5	147	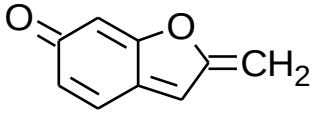

6	148	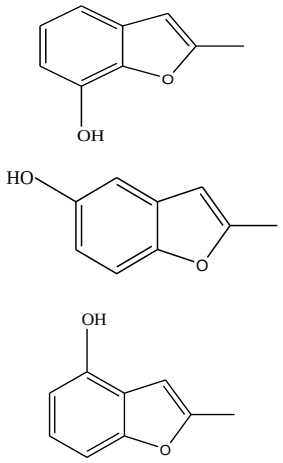
7	149	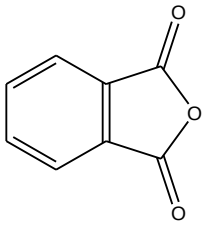
8	165	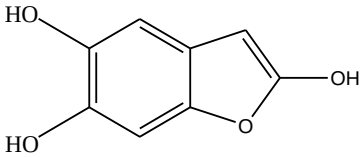

6.3.2 Effect of catalyst dosage

The optimum ZnO loading for the photocatalytic degradation of 2-MBF in water under sunlight is determined by carrying out the reactions using various catalyst dosage in the range 10 mg/L to 100 mg/L under otherwise identical conditions. The results are plotted in figure 6.4.

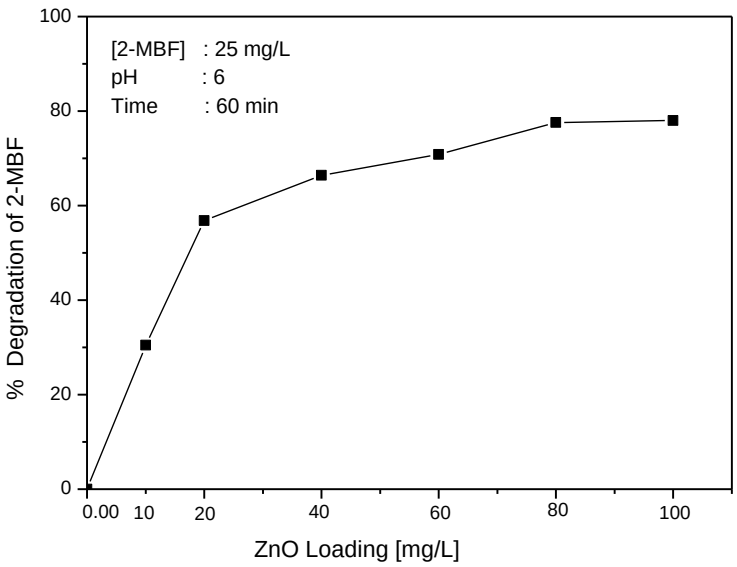

Fig. 6.4: Effect of catalyst loading on the photocatalytic degradation of 2-MBF

The degradation of 2-MBF increases steeply with increase in catalyst loading upto 20 mg/L and slowly thereafter. Eventually, the degradation stabilizes at 80 mg/L. The increase in degradation with increase in catalyst loading may be due to the increase in the number of adsorption sites available for the substrate as well as the generation of more reactive $^{\bullet}OH$ and other radicals in the system. Interaction of the substrate with the reactive free radicals is the primary step in photocatalytic processes. Hence enhancement of the formation of reactive species will result in enhancement in the degradation. Beyond the optimum dosage, further increase in catalyst loading results in the stabilization of the degradation. This may be due to the aggregation of the catalyst particles at higher concentration resulting in decrease

in the number of accessible active sites for the adsorption of substrate/intermediate. Other possible reasons, explained in previous chapters and applicable in this context can be summarized as follows: Higher catalyst loading results also in the scattering and reduced passage of light through the suspension. Hence availability of light energy for catalyst activation and subsequent generation of ROS also decreases. At higher ZnO loading, part of the initially activated ZnO gets deactivated by collision with catalyst in the ground state as described in the case of the degradation of both AMS and ACP in Chapters 3 and 4 respectively.

Since the optimum loading of ZnO for 2-MBF degradation was found to be 80 mg/L, all further studies were carried out using this dosage, unless indicated otherwise.

6.3.3 Effect of initial concentration of 2-MBF

The effect of initial concentration of 2-MBF on its photocatalytic degradation was investigated in the concentration range 5 to 30 mg/L. The study was limited in this range and higher concentration was not considered due to the poor solubility of 2-MBF in water above this range. The results are shown in figure 6.5. The rate of degradation increases with increase in concentration.

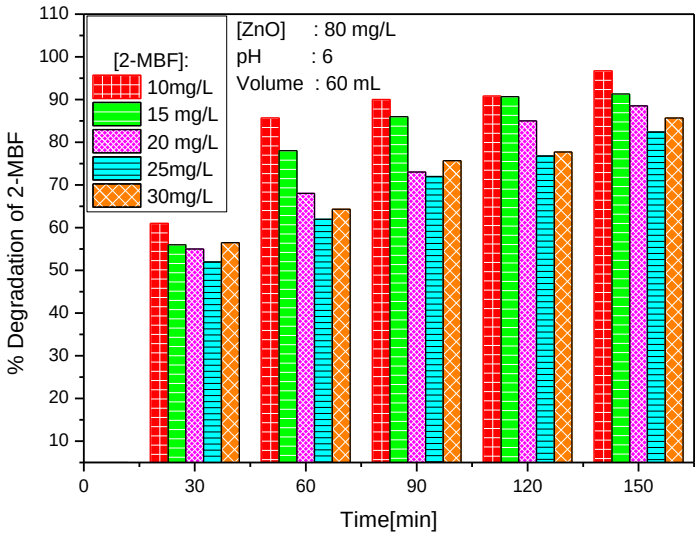

Fig. 6.5: Effect of concentration of 2-MBF on its photocatalytic degradation

As expected, rate of degradation steadily increases with increase in 2-MBF concentration as shown in figure 6.6.

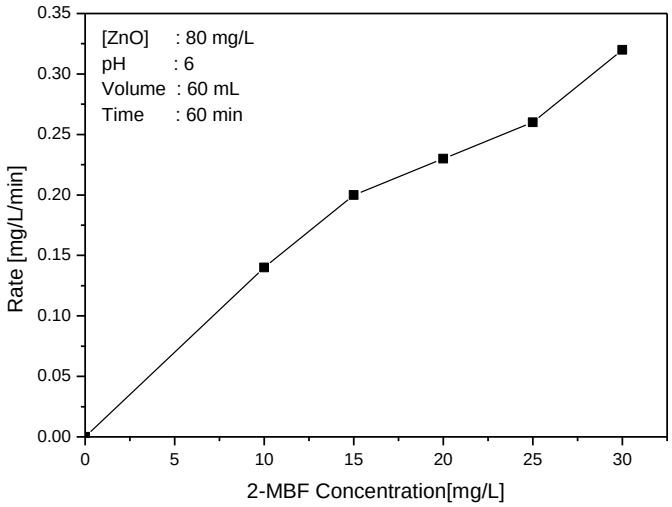

Fig. 6.6: Effect of initial concentration of 2-MBF on its photocatalytic degradation rate.

As the adsorption of 2-MBF over ZnO is high, the increase in the rate of degradation with increase in concentration may be at least partially due to increased adsorption of the substrate on the surface. With increasing concentration, the presence of substrate molecules will be more in the bulk of the solution as well. Consequently, there will be more frequent interaction with various ROS on the surface as well as in the bulk resulting in increased degradation. This is similar to the case of substrate concentration effect on the degradation of AMS as discussed in Chapter 3.

The reciprocal plot of initial rate of degradation of 2-MBF ($1/r_0$) against respective initial concentration ($1/C_0$) gives a straight line graph as shown in figure 6.7. This is a clear indication that the degradation is of first order kinetics. This is in accordance with the Langmuir-Hinshelwood model, modified to accommodate the reactions occurring at solid-liquid interface [116, 117]. Details of the kinetics are explained in previous chapters.

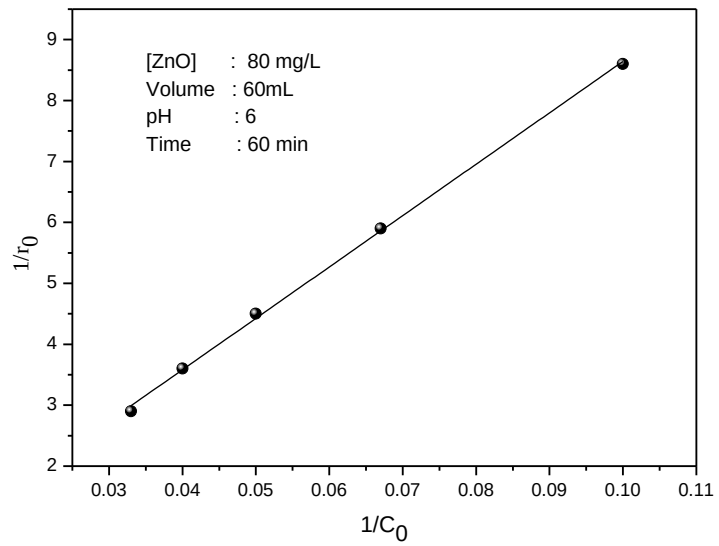

Fig. 6.7: Reciprocal plot of initial rate of degradation of 2-MBF versus its initial concentration

Similarly the logarithmic plot of -ln [C/C_0] versus the irradiation time (t) for the degradation yields straight lines passing through the origin as shown in the figure 6.8. This reconfirms pseudo first order kinetics, at least in the concentration range studied here.

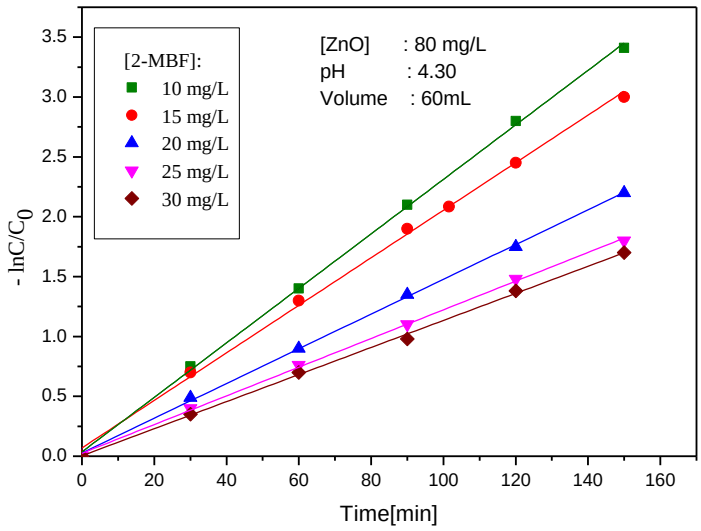

Fig. 6.8: Logarithmic plot of pseudo first order kinetics for the degradation of 2-MBF

The apparent rate constant, k for the degradation of 2-MBF at different concentrations [10 to 30 mg/L] is computed from the slopes of the corresponding lines in figure 6.8 and is tabulated in table 6.3.

Table 6.3: Pseudo first order rate constants for the photocatalytic degradation 2-MBF.

Sl No	[ZnO], mg/L	[2-MBF], mg/L	k x 10^{-3} (min^{-1})
1	80	10	22.7
2	80	15	19.9
3	80	20	14.5
4	80	25	11.9
5	80	30	11.3

The results show that as the concentration of 2-MBF increases, the rate constant decreases. For a given catalyst loading, the number of reactive species available for interaction with the substrate molecule is constant. However, at high concentration, the number of substrate molecules is excessive and hence the relative concentration of the substrate molecules, which can effectively interact with the reactive species is reduced. Hence the rate constant decreases. This observation is similar to the decrease in rate constant observed in the case of other substrates as described in previous chapters.

6.3.4 Effect of pH

As already discussed in Chapters 3, 4 and 5, the pH of the reaction medium plays an important role in many aqueous phase photocatalytic reactions because of the change in the surface characteristics of the catalyst as well as the chemical nature of the substrate and the intermediates formed from them. The Point of Zero Charge (PZC) of ZnO is ~ 9.3. At pH values < 9.3, the catalyst's surface is positively charged and at pH values > 9.3 it is negatively charged. Depending on the ionic form of the organic compound, i.e., anionic, neutral or cationic, electrostatic attraction or repulsion takes place and the photodegradation rate can be enhanced or inhibited. The results of the investigation of the effect of pH on the photocatalytic degradation of 2-MBF in the pH range 3 to 11 are presented in figure 6.9.

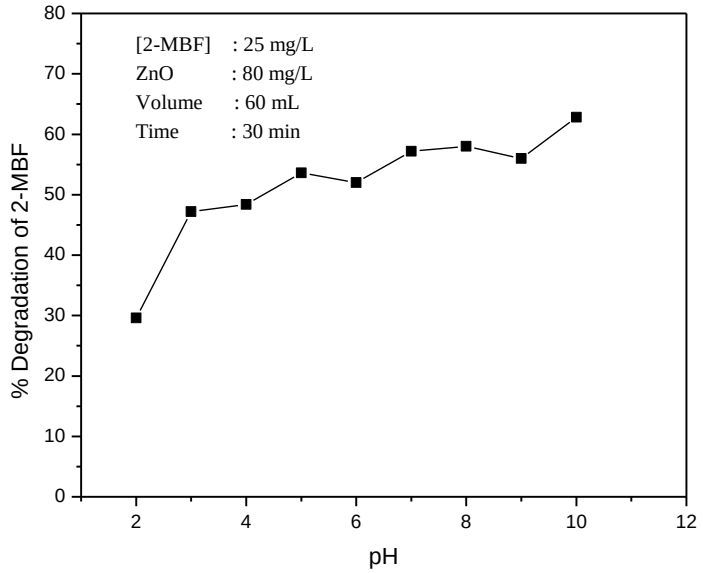

Fig. 6.9: Effect of pH on the photocatalytic degradation of 2-MBF

The results show that the degradation of 2-MBF increases steeply with increase in pH from 2 to 3. Thereafter the increase in degradation with pH is slower. Minor fluctuations in the range 5-7 may be treated as 'practically no change' within the limits of experimental error. The slow degradation observed at pH 2 may be due to the photocorrosion of the ZnO catalyst at lower pH which results in reduction in the number of active sites for the adsorption of substrate/intermediate [123]. This also reduces the formation of ROS which can interact with the pollutant/intermediates and slow down the resultant degradation. The high adsorption of 2-MBF and the reaction intermediates on the ZnO surface at extreme acidic pH also may lead to almost complete surface coverage, which makes the photo activation of ZnO surface less efficient. This results in decreased rate of formation of $^{\bullet}OH$ and other ROS, resulting in lower degradation of 2-MBF. The moderate increase in degradation

observed in the alkaline range may be due to the generation of more hydroxyl radicals from the available OH^- ions. The effect of pH on the rate of 2-MBF degradation is computed and the results are presented in table. 6.4.

Table 6.4: Effect of pH on the rate of 2-MBF degradation
[2-MBF]=25 mg/L, [ZnO] = 80 mg/L, Volume = 60 mL, Time =30 min

pH	Rate [mg/L/min]
3	0.25
4	0.39
5	0.40
6	0.45
7	0.43
8	0.48
9	0.48
10	0.47
11	0.52

The rate of the 2-MBF degradation increases initially with increase in pH. Thereafter, the rate is almost steady in the range of pH 6-10. The maximum degradation rate of 5.2×10^{-1} mg/L/min was observed at pH=11. Complex interplay of many factors, i.e. chemistry of the catalyst surface, substrate and the intermediates, extent and mode of adsorption of 2-MBF and intermediates, relative concentration of reactive free radicals such as $^{\bullet}OH$ etc., determines the pH effect in many cases as discussed in previous chapters.

The effect of pH on the adsorption of 2-MBF over ZnO is presented in table 6.5.

The percentage adsorption is low in the acidic pH probably due to the photocorrosion of the catalyst in this range as described earlier. The adsorption increases with increase in pH and remains fairly steady in the range 4-11. This is in agreement with the effect of pH on the degradation, thus confirming the relation between adsorption and degradation, at least in the case of highly adsorbing substrates.

Table 6.5: The effect of pH on the adsorption of 2-MBF over ZnO
[2-MBF] = 25 mg/L, [ZnO] =80 mg/L, Volume =60 mL, Time =3 hr

pH	% Adsorption
At normal solution pH[6.0]	44.6
2	27.2
3	38.4
4	43.6
5	44.8
6	45.0
7	45.6
8	45.6
9	45.8
10	46.0
11	46.2

6.3.5 Corrosion of ZnO under solar photocatalysis at different pH

The corrosion of ZnO catalyst at different pH under the experimental conditions was investigated by weight-loss method as explained in Chapter 3 using 60 ml 2-MBF solution (25 mg/L) and 80 mg/L ZnO. The results are presented in figure 6.10. The corrosion is fairly same as in the case of AMS, ACP and DMPC as explained in previous chapters. Since the investigation of the photocatalytic degradation of 2-MBF is carried out at pH ~ 6, corrosion can be considered as negligible under the conditions of the study.

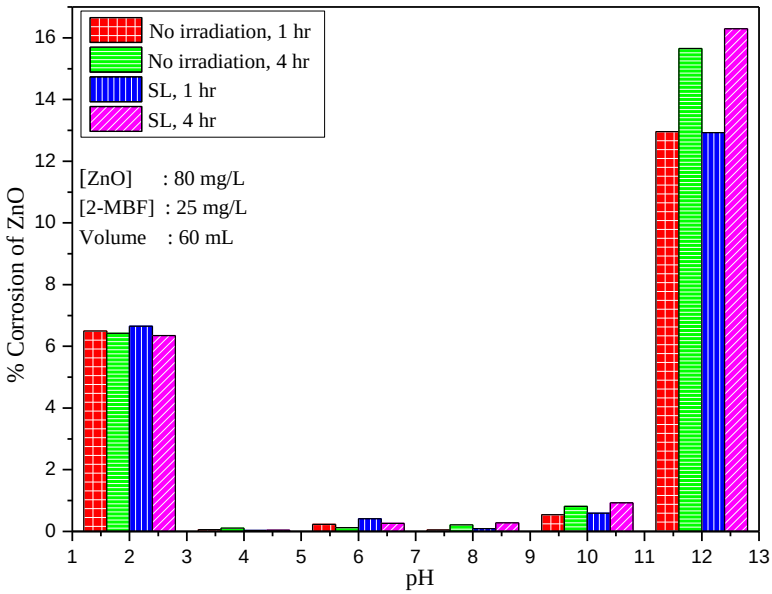

Fig. 6.10: Corrosion of ZnO at different pH in the presence and absence of solar irradiation.

6.3.6 Formation of intermediates during the photocatalytic degradation of 2-MBF

During the solar photocatalytic degradation of 2-MBF in presence of ZnO catalyst, four intermediates are detected by GC. One of them is identified as ACP and the other three are unidentified and are labelled as A, B, and C as shown in gas chromatogram in figure 6.11. (Also please see section 6.3.1). The unidentified intermediates may be hydroxylated 2-MBFs as mentioned earlier. However, they get degraded at the same rate as that of the parent compound 2-MBF, and hence do not increase with time and are not even detected in many instances. Other trace intermediates detected by LC/MS are listed in table 6.2.

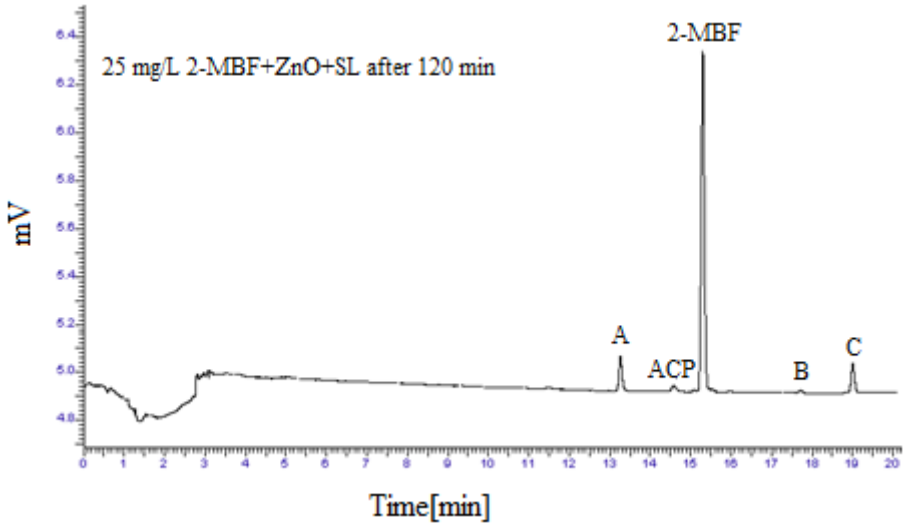

Fig. 6.11: Gas chromatogram showing intermediates

In addition to the intermediates detected as above, small quantities of phenol was also detected as an intermediate by colorimetric method, using the procedure described in Chapter 3. However, on continuous irradiation phenol disappears indicating that it is getting degraded faster.

The quantity of phenol in the system at different reaction intervals is estimated and the results are shown in figure 6.12. As the degradation of 2-MBF proceeds, the formation of phenol in the system gradually increases, reaches a maximum value and then decreases. Eventually, phenol also is completely degraded.

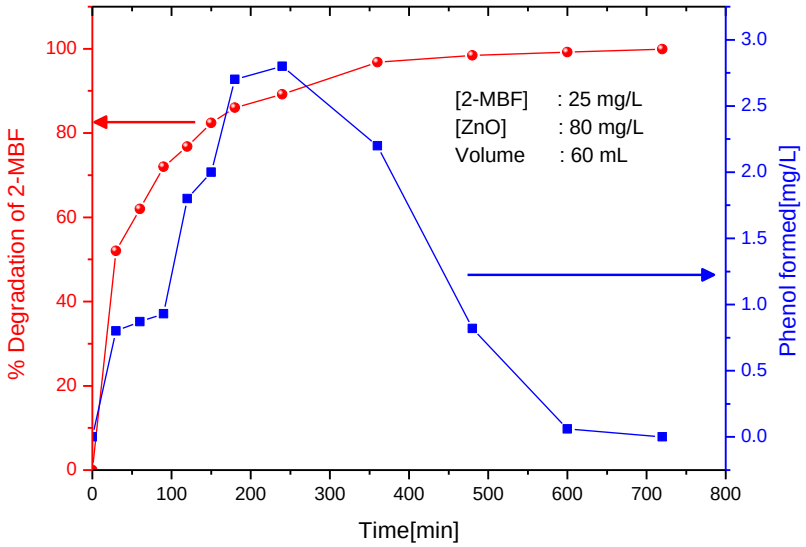

Fig. 6.12: Formation and degradation of phenol during the photocatalytic degradation of 2-MBF

6.3.7 Effect of externally added phenol on the degradation of 2-MBF

In order to verify whether the insitu formed phenol will interfere with the degradation of 2-MBF, the role of externally added phenol on the degradation of 2-MBF was investigated in detail. The results are presented in figure 6.13. It is seen that phenol inhibits the degradation of 2-MBF slightly. The extent of inhibition is not affected by the increase in concentration of added phenol or reaction time.

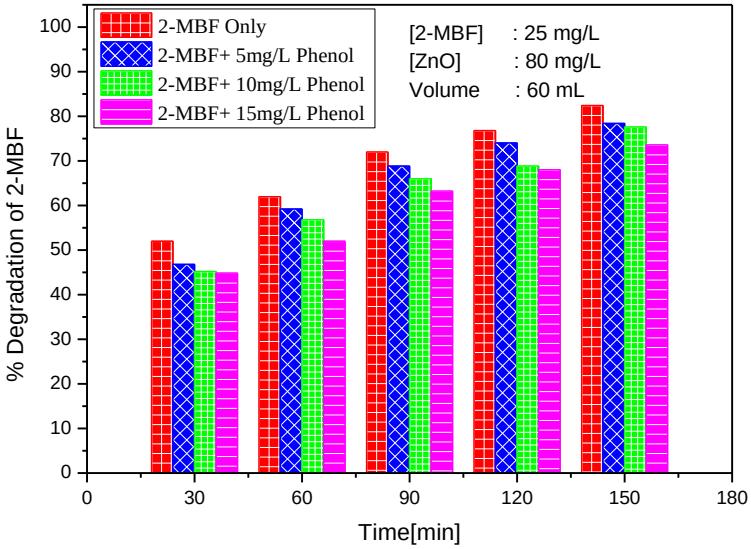

Fig. 6.13: Effect of phenol on the photocatalytic degradation of 2-MBF

6.3.8 Effect of 2-MBF on the phenol degradation

Since it is observed that phenol influences the degradation of 2-MBF, though slightly, it is relevant to see how 2-MBF will influence the photocatalytic degradation of phenol. In this context the effect of externally added 2-MBF on the degradation of phenol was studied at different concentrations of the former. The 2-MBF added inhibits the degradation of phenol moderately at all concentrations and at all time intervals as shown in figure 6.14.

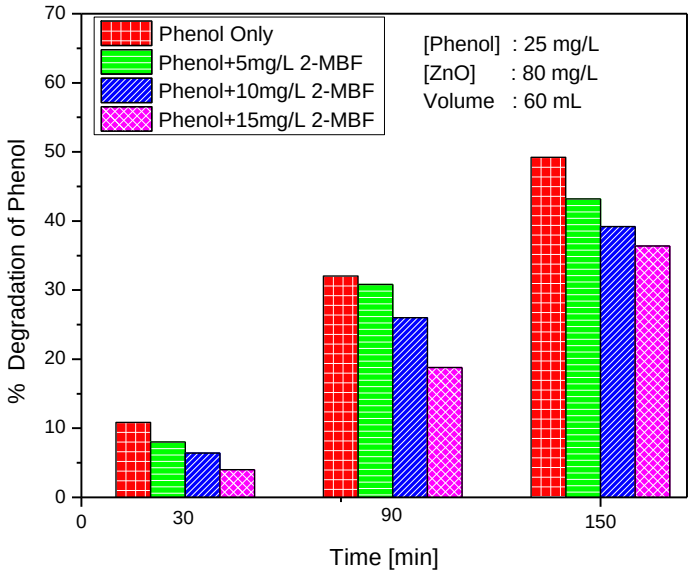

Fig. 6.14: Effect of 2-MBF on the photocatalytic degradation of phenol

The extent of inhibition is directly related to the concentration of added 2-MBF. This indicates that the insitu formed phenol will not be getting degraded easily in presence of 2-MBF. Hence the very low concentration of phenol in the reaction system implies its very low rate of formation. This may be the reason for its inconsistent and/or negligible presence during the degradation of 2-MBF at different times of irradiation. Hence phenol need not be considered as an intermediate of any consequence during the photocatalytic degradation of 2-MBF. The inhibition of the degradation of phenol by 2-MBF can be explained on the basis of the competition between the two as well as the intermediate formed from them for available active sites on the surface and also for the ROS. The relative adsorption of 2-MBF and phenol on ZnO from a combination of the two is experimentally tested and the results are shown in table 6.6.

Table 6.6: Adsorption of 2-MBF and Phenol over ZnO
[2-MBF] = 25 mg/L, [Phenol] = 25 mg/L, [ZnO] = 80 mg/L,

Time[min]	% Adsorption of 2-MBF	% Adsorption of Phenol
30	40.4	6.2
60	43.6	6.4
120	41.2	6.0
180	42.0	6.0

The table shows that the 2-MBF gets preferentially more adsorbed over ZnO which in turn results in the lower adsorption/degradation of phenol. Hence 2-MBF can inhibit the degradation of phenol more than the latter can inhibit the degradation of the former. In any case, since the formation of phenol itself is only in minor amounts, it may not be influencing the rate of degradation of 2-MBF much.

6.3.9 Formation of H_2O_2

H_2O_2 was detected as a byproduct during the photocatalytic degradation of many organic pollutants [36, 37, 102,113,118], as described in previous chapters. The concentration of H_2O_2 formed during the photocatalytic degradation of 2-MBF was quantitatively determined by iodometric method and the results are shown in figure 6.15. As in the case of AMS, ACP and DMPC degradation reactions, the concentration of H_2O_2 is inconsistent and non-reproducible at any time period of irradiation in this case also. As in earlier cases, the periodic increase and decrease in the concentration of H_2O_2 can be explained based on the oscillation in its concentration resulting from concurrent formation and decomposition. At the same time, the degradation of 2-MBF continues to

increase with time. Various possible steps leading to the formation and decomposition of H_2O_2 and the mechanism of oscillation were described in detail in Chapter 3.

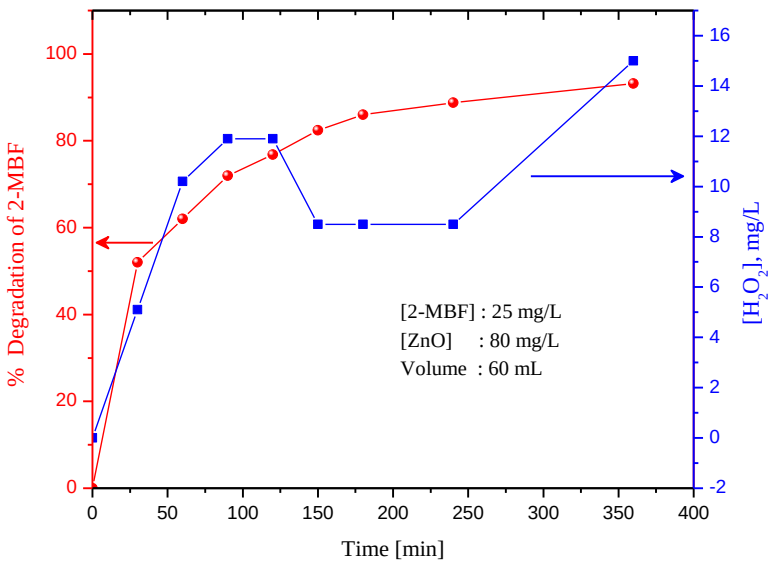

Fig. 6.15: Formation and fate of H_2O_2 during the photocatalytic degradation of 2-MBF on ZnO.

6.3.10 Effect of externally added H_2O_2 on the photocatalytic degradation of 2-MBF

The role of H_2O_2 as 'inhibitor', 'having no effect', or 'as an enhancer' of photocatalytic degradation of organic pollutants has been illustrated in many studies [180, 181] as well as in earlier chapters of this thesis. In this context, the effect of externally added H_2O_2 on the photocatalytic degradation of 2-MBF was investigated by adding varying amounts of H_2O_2 into the reaction system under identical conditions. The results of the investigation are plotted in figure 6.16.

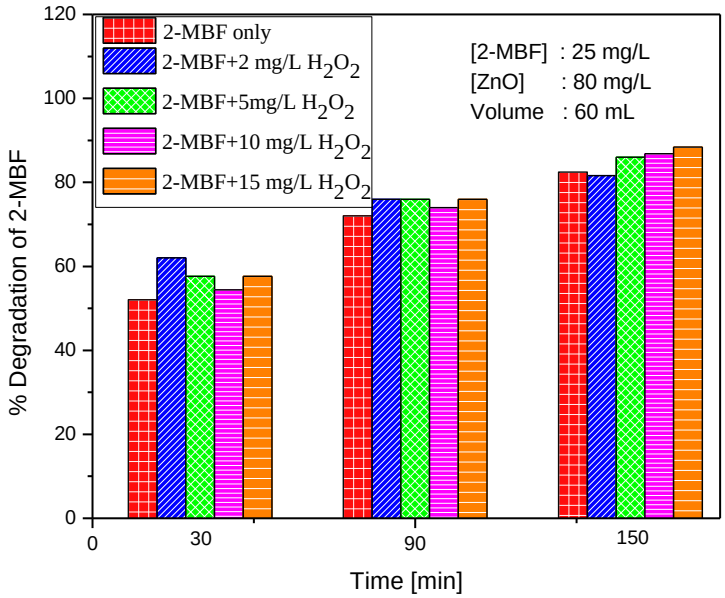

Fig. 6.16: Effect of added H_2O_2 on the photocatalytic degradation of 2-MBF

It is found that externally added H_2O_2 has either 'practically no effect' or 'slightly enhances' the degradation of 2-MBF at all concentrations and reaction times. The enhancement is relatively more pronounced at lower H_2O_2 concentration in the early stages of reaction (i.e., 30 min here). As demonstrated in earlier chapters, H_2O_2 acts as a promotor as well as an inhibitor depending upon its concentration and reaction conditions. In the initial stage of the reaction the concentration of in situ formed H_2O_2 is very small and hence the externally added H_2O_2 can enhance the degradation by providing additional hydroxyl radical in the system. But above a critical concentration, H_2O_2 can act as a scavenger of hydroxyl radical. This dual role of H_2O_2 as well as the competition between H_2O_2 and the substrate/intermediates for the active sites and various ROS leads only to a slight enhancement in the

degradation of 2-MBF or balances the simultaneous enhancement and inhibition. The mechanism by which H_2O_2 acts both as an enhancer as well as inhibitor of photocatalytic degradation of organics is demonstrated in section 4.3.5 in Chapter 4.

6.3.11 Effect of Humic acid [HA]

Humic substances which are naturally occurring biogenic heterogeneous organic substances can influence the photocatalytic degradation of organic pollutants in water [28,140] as discussed in Chapter 3. Their effect can be positive or negative depending on the nature of the pollutants. The effect of humic acid (HA) on the degradation of AMS, ACP and DMPC are discussed in previous chapters. The effect of HA on the solar photocatalytic degradation of 2-MBF was investigated with ZnO catalyst at different HA concentrations and the results are given in figure 6.17.

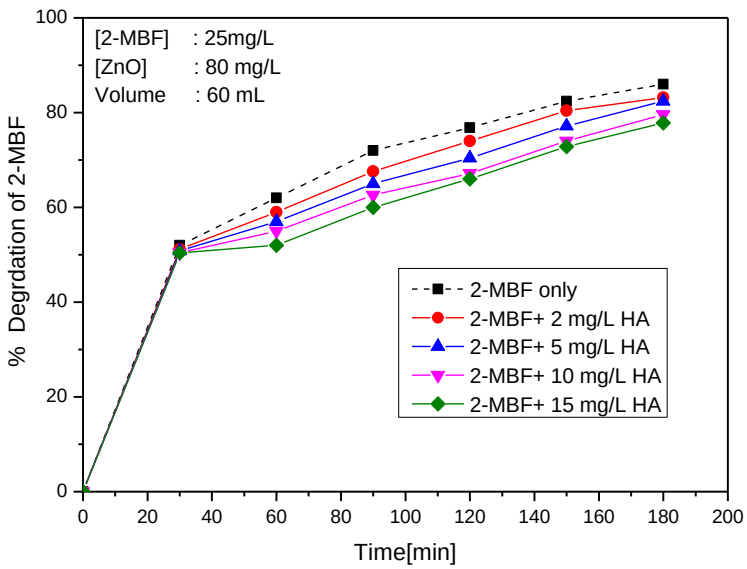

Fig. 6.17: Effect of Humic acid on the photocatalytic degradation of 2-MBF

The results reveal that at lower reaction time HA has no significant effect on the degradation of 2-MBF whereas moderate reduction in 2-MBF degradation was observed at later stages of the reaction. The extent of inhibition increases with increase in the HA concentration. HA is known to absorb a fraction of the sunlight which decreases the energy available for the activation of the ZnO catalyst. Hence the generation of hydroxyl radical and other reactive species, which are responsible for the degradation reaction will be less and this will inhibit the degradation of 2-MBF. Humic acid can also act as a free radical scavenger, which will consume the ROS [28, 140]. Both these factors contribute to inhibition of the degradation by HA as discussed in detail in Chapter 3, section 3.3.11.

6.3.12 Role of dissolved oxygen

Dissolved O_2 has a significant role in the aqueous phase photocatalytic degradation process as described in previous chapters. The dissolved O_2 acts as a scavenger for the photogenerated electrons and forms superoxide radical anions and other reactive species thereby preventing the electron-hole recombination. Thus both electrons and holes can participate in the degradation reaction. This role of dissolved O_2 in the photocatalytic degradation of 2-MBF was confirmed by carrying out the degradation in deaerated as well as O_2 enriched systems under identical conditions. The results are shown in figure 6.18.

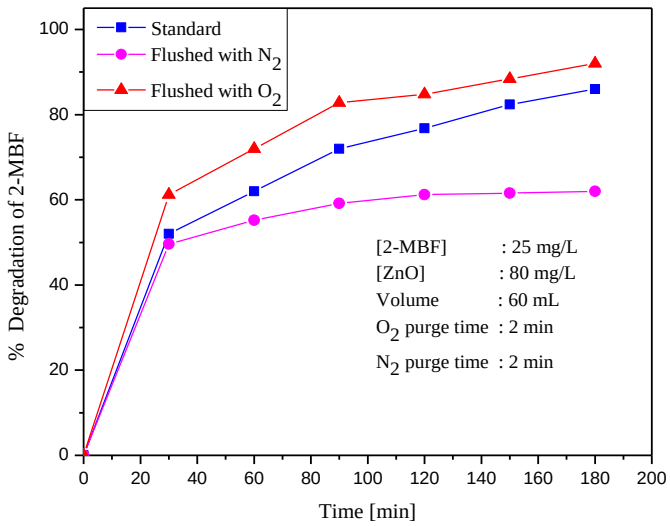

Fig. 6.18: Effect of O_2 on the photocatalytic degradation of 2-MBF

When the dissolved O_2 in the system is removed by bubbling N_2, the percentage degradation of 2-MBF decreased considerably. The extent of degradation in the deaerated system remains almost constant, after the initial degradation for the 3 hr irradiation time tested here. Moderate initial degradation even after the deaeration may be attributed to the small amount of oxygen still present in the system which cannot be removed by N_2 purging for short duration. When the system is enriched with O_2 by bubbling the gas through the solution, the percentage degradation of 2-MBF is increased. This also reconfirms the role of dissolved O_2 in the photocatalytic degradation of 2-MBF.

6.3.13 Effect of anions/salts

The presence of various anions/salts in industrial effluent water is known to affect the photocatalytic degradation. This is demonstrated in the case of the degradation of AMS, ACP and DMPC in previous

chapters. They can either compete with the substrate/intermediates for available active sites on the catalyst or deactivate the ROS by interacting with them. They can also lead to the formation of undesirable byproducts and can reduce the light quanta reaching the catalyst surface for effective catalyst activation as described in Chapter 4. As already discussed, the effect of anions/salts may be further complicated by factors such as pH, nature of the catalyst and the pollutant, concentration of the species etc. The effect of some of the anions such as fluoride (F^-), chloride (Cl^-), bromide (Br^-), iodide (I^-), sulphate (SO_4^{2-}), nitrate (NO_3^-), phosphate (PO_4^{3-}), acetate (CH_3COO^-), oxalate ($C_2O_4^{2-}$), carbonate (CO_3^{2-}) and bicarbonate (HCO_3^-) on the photocatalytic degradation of 2-MBF was investigated in detail using different concentrations of these ions at different irradiation times. The results are plotted in figures 6.19 and 6.20.

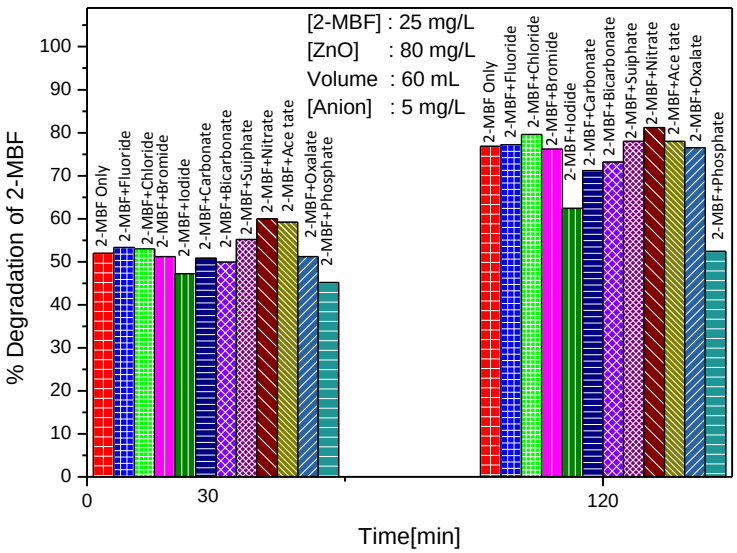

Fig. 6.19: Effect of anions on the photocatalytic degradation of 2-MBF at different reaction times

At low anion concentration (5 mg/L) and in the early stage of degradation i.e., initial reaction time of 30 min, I^- and PO_4^{3-} inhibit the degradation of 2-MBF in the order $PO4^{3-} > I^-$, while NO_3^-, CH_3COO^- and SO_4^{2-} (to a slight extent) enhance the degradation in the order $NO_3^- \approx CH_3COO^- > SO_4^{2-}$. F^-, Cl^-, Br^-, CO_3^{2-}, HCO_3^- and $C_2O_4^{2-}$ have no significant effect. At later stage of the reaction (120 min), the enhancement has become negligible. Only NO_3^- is a mild enhancer, while PO_4^{3-}, I^-, CO_3^{2-} and HCO_3^- inhibit the degradation. Other ions have practically no effect. The efficiency of anions at 30 and 120 min can be summarized as:

<u>After 30 min of irradiation</u>:

Enhancement: $NO_3^- \approx CH_3COO^- > SO_4^{2-}$
No effect: F^-, Cl^-, Br^-, CO_3^{2-}, $C_2O_4^{2-}$, HCO_3^-
Inhibition: $PO_4^{3-} > I^-$

<u>After 120 min of irradiation</u>:

Enhancement: NO_3^- is a mild enhancer. No significant enhancement by any other anions
No effect: NO_3^-, Cl^-, F^-, Br^-, SO_4^{2-}, $C_2O_4^{2-}$, CH_3COO^-
Inhibition: $PO_4^{3-} > I^- > HCO_3^- \approx CO_3^{2-}$

At higher anion concentration (15 mg/L) and at the initial stage of the reaction (30 min), almost similar trend is followed as shown in figure 6.20.

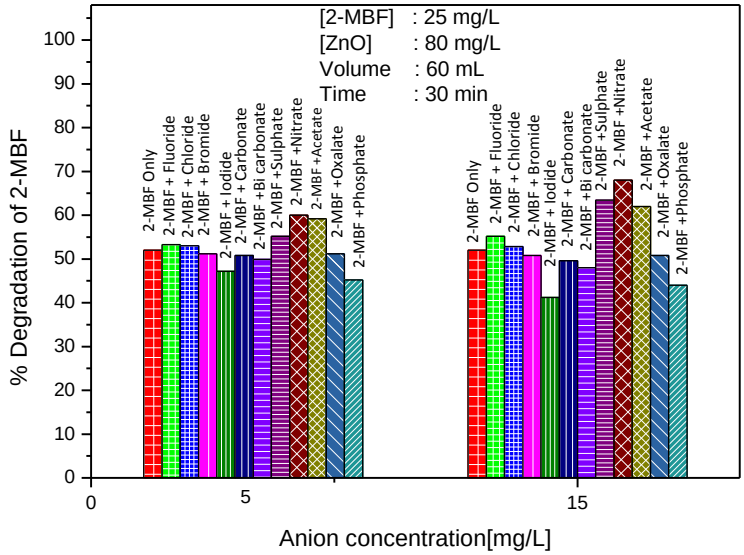

Fig. 6.20: Effect of various anions at different concentration on the degradation of 2-MBF

The effect is as follows:

Enhancement: $NO_3^- > SO_4^{2-} \approx CH3COO^-$

No effect: F^-, Cl^-, Br^-

Inhibition: $I^- \approx PO_4^{3-} > HCO_3^- \approx CO_3^{2-} \approx C_2O_4^{2-}$

Results of detailed investigation of the effect of various anions on the degradation of 2-MBF at different anion concentrations and reaction times are presented in figures 6.21-6.31.

a) Effect of F^-

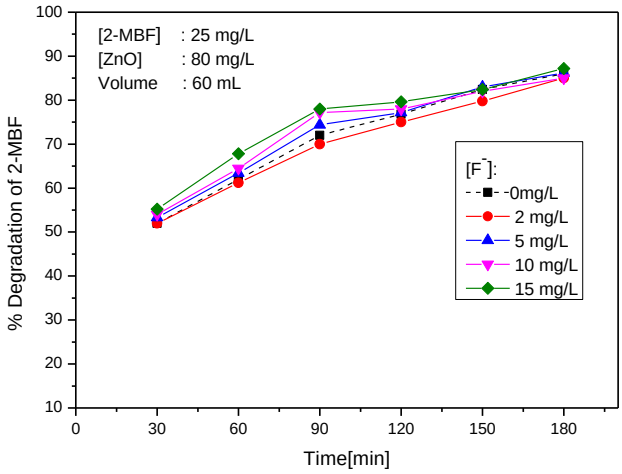

Fig. 6.21: Effect of concentration of F^- and reaction time on the photocatalytic degradation of 2-MBF.

The results show practically no effect or mild enhancement at all reaction times and concentrations. Eventually, even the 'mild enhancement' becomes 'no effect'.

b) Effect of Cl^-

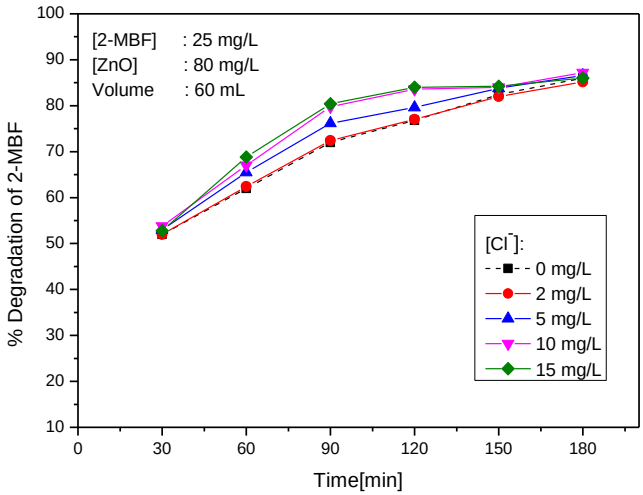

Fig. 6.22: Effect of concentration of Cl^- and reaction time on the photocatalytic degradation of 2-MBF.

The results are similar to those in the case of F^- and show 'no effect' in the early and later stages of the reaction. The mild enhancement in between may be due to the interaction of the anions with the multitude of ROS and the generation of radical anions as explained earlier. However, eventually the ROS also get deactivated by interactions among themselves and the effect becomes 'nil'.

c) Effect of Br^-

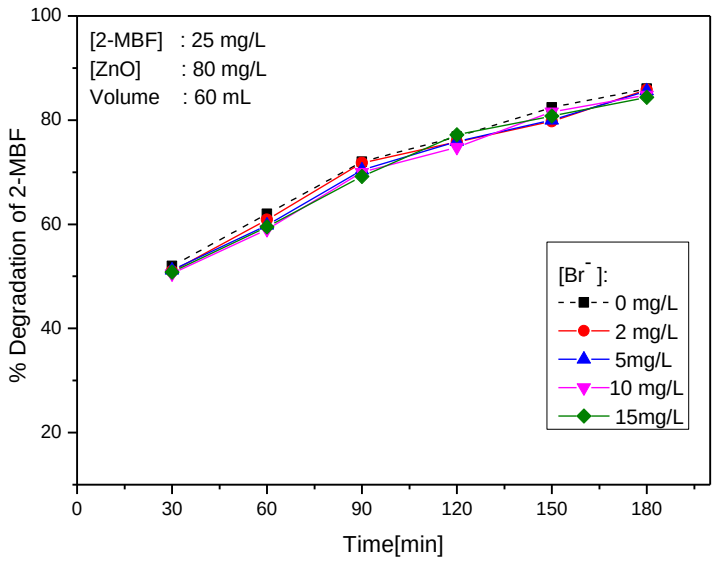

Fig. 6.23: Effect of concentration of Br^- and reaction time on the photocatalytic degradation of 2-MBF.

Br^- has practically 'no effect' at all concentrations and reaction times.

d) Effect of Γ

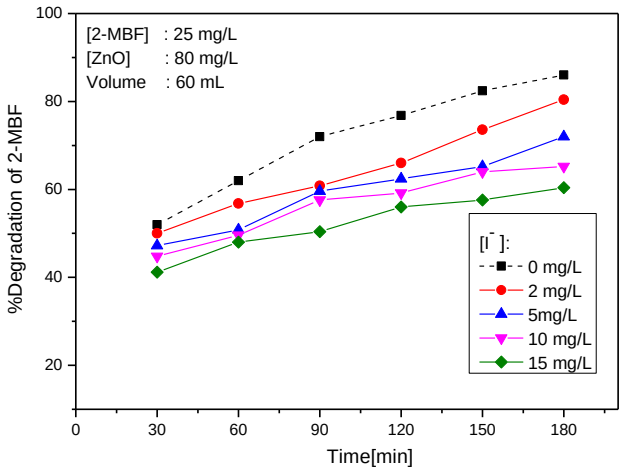

Fig. 6.24: Effect of concentration of I^- and reaction time on the photocatalytic degradation of 2-MBF.

I^- is a strong inhibitor at all concentrations and reaction times.

e) Effect of CO_3^{2-}

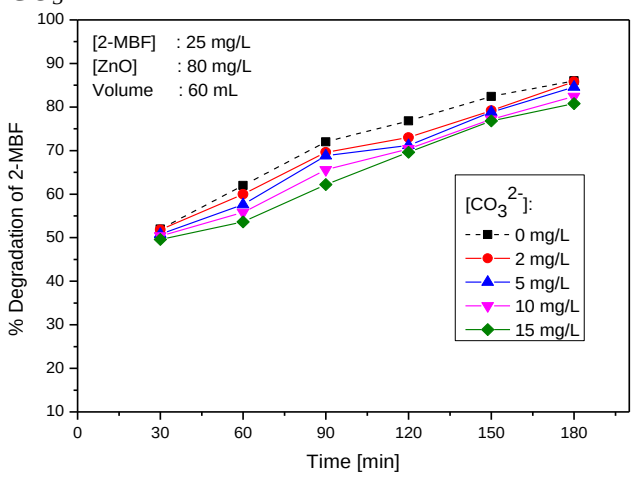

Fig. 6.25: Effect of concentration of CO_3^{2-} and reaction time on the photocatalytic degradation of 2-MBF.

CO_3^{2-} is a mild inhibitor at all concentrations and reaction times. At early stages of the reaction and at lower concentration, the effect may be treated as 'nil'.

f) Effect of HCO_3^-

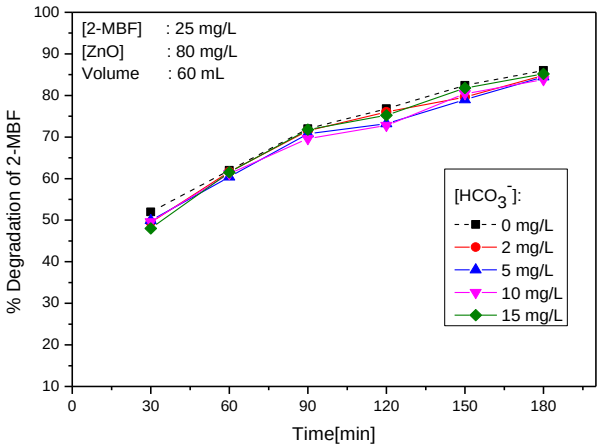

Fig. 6.26: Effect of concentration of HCO_3^- and reaction time on the photocatalytic degradation of 2-MBF.

The effect of bicarbonate ion can be considered as 'practically no effect' at all concentrations and all reaction times.

g) Effect of SO_4^{2-}

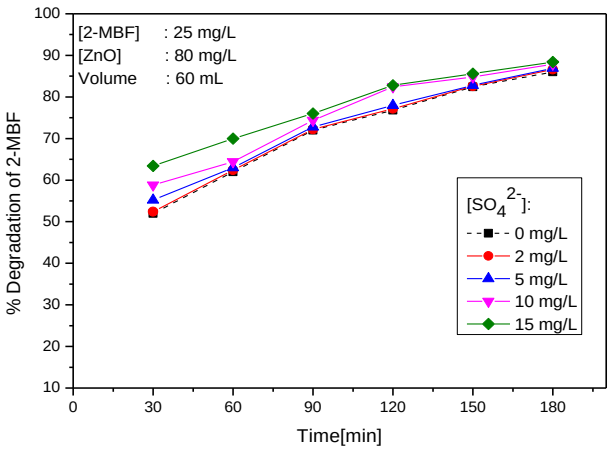

Fig. 6.27: Effect of concentration of SO_4^{2-} and reaction time on the photocatalytic degradation of 2-MBF.

SO_4^{2-} can be considered as a mild enhancer at all concentrations and reaction times.

h) Effect of NO_3^-

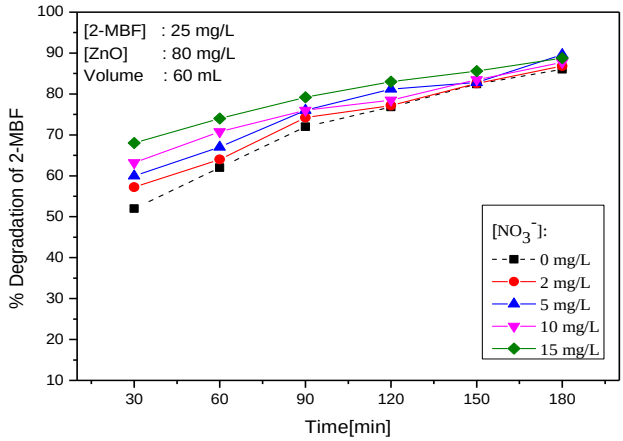

Fig. 6.28: Effect of concentration of NO_3^- and reaction time on the photocatalytic degradation of 2-MBF.

NO_3^- is a consistent enhancer of the degradation of 2-MBF. Towards the later stages of the reaction, as the concentration of 2-MBF is very small, the enhancement is not much pronounced.

i) Effect of PO_4^{3-}

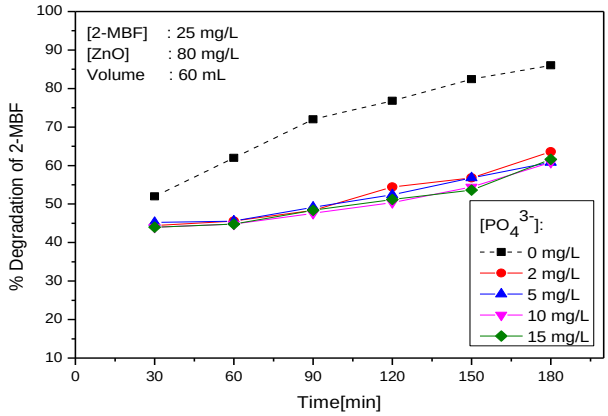

Fig. 6.29: Effect of concentration of PO_4^{3-} and reaction time on the photocatalytic degradation of 2-MBF.

As expected from the results of many previous studies, PO_4^{3-} is a strong inhibitor of the degradation of 2-MBF at all concentrations and all reaction times.

j) Effect of CH_3COO^-

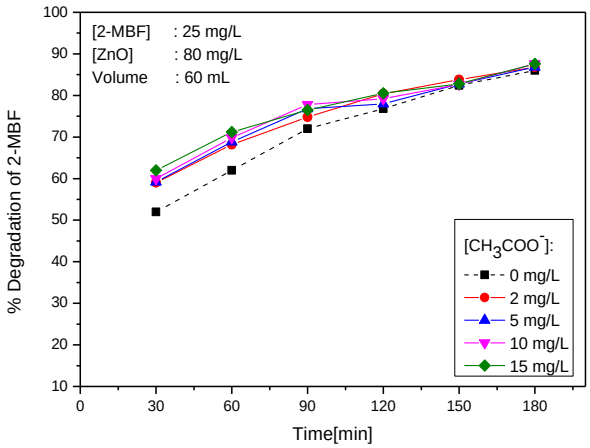

Fig. 6.30: Effect of concentration of CH_3COO^- and reaction time on the photocatalytic degradation of 2-MBF.

Acetate is a mild enhancer at all concentrations in the earlier stage of the reaction. Eventually, when the concentration of the pollutant becomes very small, the 'enhancement' becomes 'no effect'

k) Effect of $C_2O_4^{2-}$

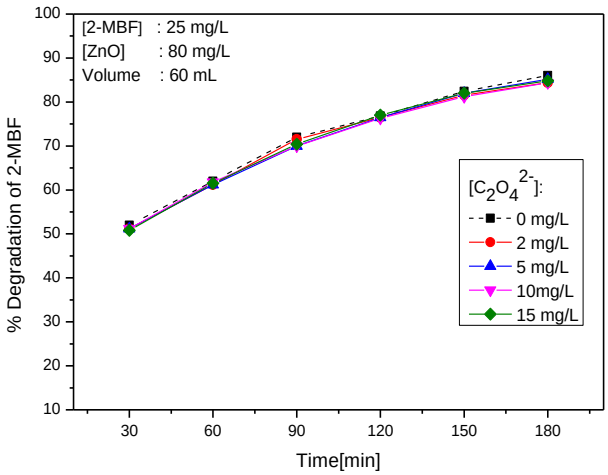

Fig. 6.31: Effect of concentration of $C_2O_4^{2-}$ and reaction time on the photocatalytic degradation of 2-MBF.

Oxalate has practically 'no effect' at all concentrations and reaction times.

The study clearly shows that the effect of various anions on the photocatalytic degradation of 2-MBF depends on the concentration of the anion as well as the reaction time. However, the effect is not as pronounced as in the case of other substrates discussed in earlier chapters. Only the inhibition by PO_4^{3-} and I^- remains consistent throughout. This indicates that in the case of strongly adsorbing pollutants, the effect of most of the anions is not that significant.

The relative efficiency of various anions on the photocatalytic degradation of 2-MBF at different concentrations and reaction times are computed and summarized in table 6.7.

Table 6.7: Comparative effect of anions at various concentrations and reaction times on the photocatalytic degradation of 2-MBF.
[2-MBF] = 25 mg/L, [ZnO] = 80 mg/L, Volume = 60 mL

Time, min.	[Anions], mg/L	Comparative effect
30	2	Enhancement: $CH_3COO^- \approx NO_3^-$ No effect: F^-, Cl^-, Br^-, CO_3^{2-}, SO_4^{2-}, $C_2O_4^{2-}$ Inhibition: $PO_4^{3-} > HCO_3^- > I^-$
	5	Enhancement: $NO_3^- \approx CH_3COO^- > SO_4^{2-}$ No effect: F^-, Cl^-, Br^-, CO_3^{2-}, HCO_3^-, $C_2O_4^{2-}$ Inhibition: $PO_4^{3-} > I^-$
	10	Enhancement: $NO_3^- > CH_3COO^- > SO_4^{2-}$ No effect: F^-, Cl^-, Br^-, CO_3^{2-}, HCO_3^-, $C_2O_4^{2-}$ Inhibition: $PO_4^{3-} > I^-$
	15	Enhancement: $NO_3^- > SO_4^{2-} \approx CH_3COO^-$ No effect: F^-, Cl^-, Br^- Inhibition: $I^- \approx PO_4^{3-} > HCO_3^- \approx CO_3^{2-} \approx C_2O_4^{2-}$
	2	Enhancement: $CH_3COO^- > NO_3^-$ No effect: F^-, Cl^-, Br^-, HCO_3^-, $SO_4^{2-} \approx C_2O_4^{2-}$ Inhibition: $PO_4^{3-} > I^- > CO_3^{2-}$

60	5	Enhancement: CH_3COO^- >NO_3^- > Cl^- No effect: F^-, Br^-, HCO_3^-, SO_4^{2-}, $C_2O_4^{2-}$ Inhibition: PO_4^{3-} > I^- = CO_3^{2-}
	10	Enhancement: NO_3^- > CH_3COO^- > Cl^- ≈ SO_4^{2-} No effect: F^-, Br^-, HCO_3^-, $C_2O_4^{2-}$ Inhibition: PO_4^{3-} > I^- > CO_3^{2-}
	15	Enhancement: NO_3^- > CH_3COO^- > SO_4^{2-} > Cl^- > F^- No effect: Br^-, HCO_3^-, $C_2O_4^{2-}$ Inhibition: PO_4^{3-} > I^- > CO_3^{2-}
90	2	Enhancement: CH_3COO^- > NO_3^- No effect: F^-, Cl^-, Br^-, HCO_3^-, SO_4^{2-}, $C_2O_4^{2-}$ Inhibition: : PO_4^{3-} > I^- > CO_3^{2-}
	5	Enhancement: CH_3COO^- >NO_3^- > Cl^- No effect: F^-, Br^-, HCO_3^-, SO_4^{2-}, $C_2O_4^{2-}$ Inhibition: PO_4^{3-} > I^- > CO_3^{2-}
	10	Enhancement: Cl^- > CH_3COO^- > F^-> NO_3^- > SO_4^{2-} No effect :Br^-, $C_2O_4^{2-}$, HCO_3^- Inhibition: PO_4^{3-} > I^- > CO_3^{2-}
	15	Enhancement: Cl^- > NO_3^- > F^- > CH_3COO^- > SO_4^{2-} No effect: Br^-, HCO_3^-, $C_2O_4^{2-}$ Inhibition: PO_4^{3-} > I^- > CO_3^{2-}
120	2	Enhancement: Nil No effect: F^-, Cl^-, Br^-, HCO_3^-, SO_4^{2-}, NO_3^-, CH_3COO^-, $C_2O_4^{2-}$ Inhibition: PO_4^{3-} > I^- > CO_3^{2-}
	5	Enhancement: Nil No effect: NO_3^-, Cl^-, F^-, Br^-, SO_4^{2-}, $C_2O_4^{2-}$, CH_3COO^- Inhibition: PO_4^{3-} > I^- > HCO_3^- ≈ CO_3^{2-}
	10	Enhancement: Cl^- > SO_4^{2-} No effect: F^-, Br^-, NO_3^-, CH_3COO^-, $C_2O_4^{2-}$, HCO_3^- Inhibition: PO_4^{3-} > I^- > CO_3^{2-}
	15	Enhancement: Cl^-> NO_3^- > SO_4^{2-} > CH_3COO^- No effect: F^-, Br^-, HCO_3^-, $C_2O_4^{2-}$ Inhibition: PO_4^{3-} > I^- > CO_3^{2-}

150	2	Enhancement: Nil No effect: F^-, Cl^-, NO_3^-, SO_4^{2-}, $C_2O_4^{2-}$, CH_3COO^-, HCO_3^-, Br^- Inhibition: $PO_4^{3-} > I^- > CO_3^{2-}$
	5	Enhancement: Nil No effect: F^-, Cl^-, HCO_3^-, SO_4^{2-}, NO_3^-, CH_3COO^-, $C_2O_4^{2-}$ Inhibition: $PO_4^{3-} > I^- > Br^- > CO_3^{2-}$
	10	Enhancement: Nil No effect: F^-, Cl^-, Br^-, HCO_3^-, NO_3^-, SO_4^{2-}, CH_3COO^-, $C_2O_4^{2-}$ Inhibition: $PO_4^{3-} > I^- > CO_3^{2-}$
	15	Enhancement: Nil No effect: F^-, Cl^-, Br^-, HCO_3^-, NO_3^-, SO_4^{2-}, CH_3COO^-, $C_2O_4^{2-}$ Inhibition: $PO_4^{3-} > I^- > CO_3^{2-}$
180	2	Enhancement: Nil No effect: F^-, Cl^-, Br^-, CO_3^{2-}, HCO_3^-, NO_3^-, SO_4^{2-}, $C_2O_4^{2-}$, CH_3COO^- Inhibition : $PO_4^{3-} > I^-$
	5	Enhancement: Nil No effect: F^-, Cl^-, Br^-, CO_3^{2-}, HCO_3^-, NO_3^-, SO_4^{2-}, CH_3COO^-, $C_2O_4^{2-}$ Inhibition : $PO_4^{3-} > I^-$
	10	Enhancement: Nil No effect: F^-, Cl^-, Br^-, HCO_3^-, NO_3^-, SO_4^{2-}, CH_3COO^-, $C_2O_4^{2-}$ Inhibition : $PO_4^{3-} > I^- > CO_3^{2-}$
	15	Enhancement: Nil No effect: F^-, Cl^-, Br^-, HCO_3^-, NO_3^-, SO_4^{2-}, CH_3COO^-, $C_2O_4^{2-}$ Inhibition: $I^- > PO_4^{3-} > CO_3^{2-}$

These results clearly confirm the findings of our earlier study of the effect of anions on the photocatalytic degradation of AMS, ACP and DMPC. The effect of anions depends on their concentration and the reaction time. Ions like nitrate and acetate act as enhancers while iodide and phosphate are

clear inhibitors consistently. In the case of many salts, at very low concentration (e.g. 2 mg/L), the effect may not be very distinct and hence the inconsistency. Similarly the results towards later stages of reaction, when most of the substrate has already degraded, have to be analyzed cautiously. However, a general trend is clearly visible in all these cases. Hence it may be concluded that the effect of anions on the rate of degradation of organic pollutants cannot be predicted precisely as it depends on the interplay of a number of parameters related to the reaction and reactants.

The possibility of the anions changing the pH of the reaction suspension and the consequent effect on the degradation of 2-MBF is checked by measuring the pH of the system in presence of respective anions (table 6.8). Except in the case of carbonate ions, the pH remains fairly the same at ~ 7.5. The pH effect in figure 6.9 shows that the degradation of 2-MBF does not change much in the range 5-10. Hence the change in pH is not the cause for the anion effect.

Table 6.8: pH of 2-MBF suspension with ZnO in presence of various anions
[2-MBF] = 25 mg/L, [ZnO] = 80 mg/L, [Anion] =10 mg/L

Anion	pH
No anion	6.0
F^-	7.35
Cl^-	7.35
Br^-	7.34
I^-	7.35
CO_3^{2-}	9.33
HCO_3^-	7.53
SO_4^{2-}	7.48
NO_3^-	7.39
CH_3COO^-	7.33
$C_2O_4^{2-}$	7.75
PO_4^{3-}	7.86

6.3.14 Effect of oxidants

As in the case of AMS, ACP, and DMPC degradation study, the effect of some of the common oxidizing agents such as KIO_3, $K_2S_2O_8$ and H_2O_2 on the photocatalytic degradation of 2-MBF is investigated in detail and the results are shown in figures 6.32 and 6.33.

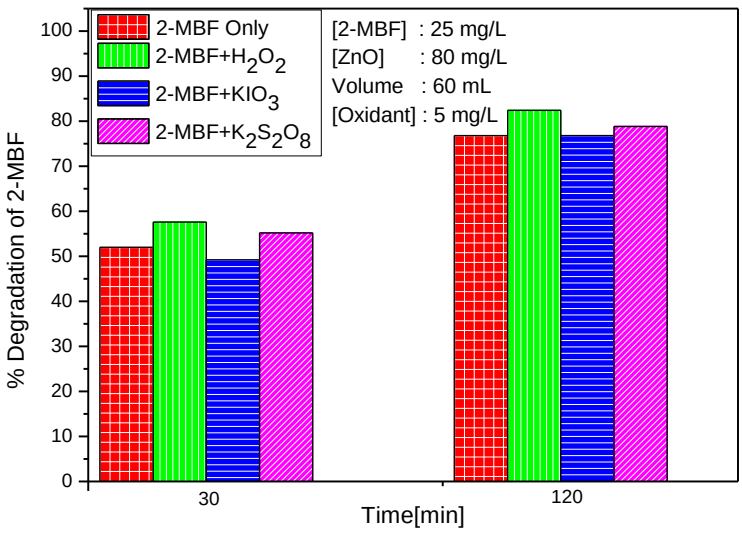

Fig. 6.32: Effect of oxidants on the photocatalytic degradation of 2-MBF at different reaction times.

At lower concentration of the oxidant (5 mg/L), after 30 min of irradiation, both H_2O_2 and $K_2S_2O_8$ enhance the degradation mildly. At higher reaction time of 120 min, both $K_2S_2O_8$ and H_2O_2 continue the mild enhancement while the initial 'no effect' by KIO_3 is sustained. However, the enhancement is not significant even in the case of H_2O_2 and $K_2S_2O_8$ and it may be more appropriately qualified as 'no effect'.

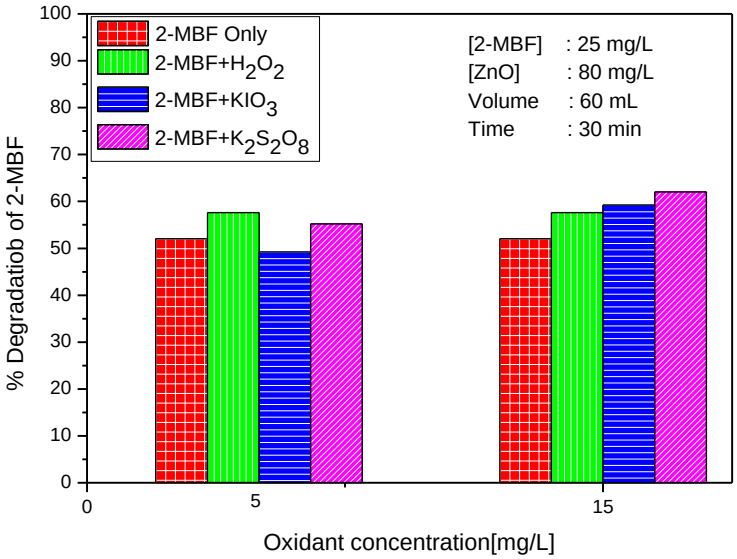

Fig. 6.33: Effect of oxidants at different concentration on the degradation of 2-MBF

At higher concentration (15 mg/L), all oxidants enhance the degradation, though only marginally. The degree of enhancement does not vary much with the concentration of the oxidant or with the reaction time as it happens in the case of salts/anions. In any case, investigation on the effect of oxidants are made at more concentrations and reaction times, to be consistent with the study of other pollutants reported in previous chapters. The results are shown in figures 6.34 - 6.36.

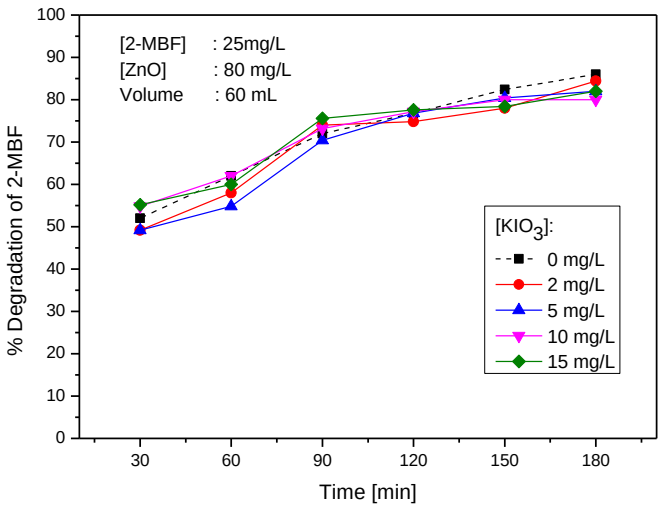

Fig. 6.34: Effect of concentration of KIO_3 and reaction time on the photocatalytic degradation of 2-MBF.

IO_3^- enhances the degradation only marginally at all concentrations and all reaction times.

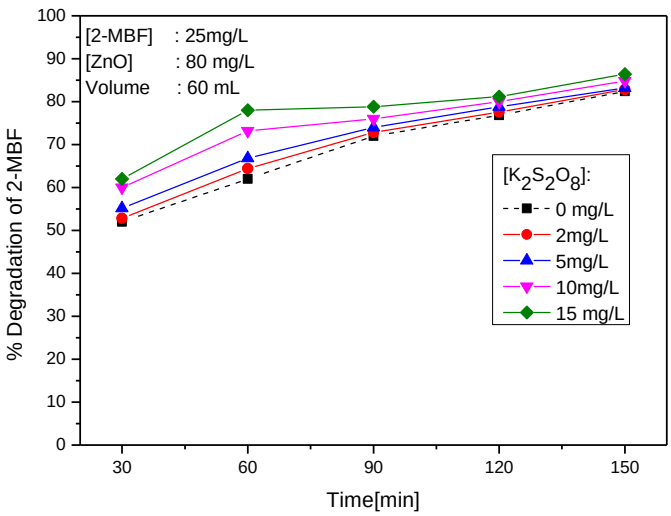

Fig. 6.35: Effect of concentration of $K_2S_2O_8$ and reaction time on the photocatalytic degradation of 2-MBF.

Figure 6.35 shows that $K_2S_2O_8$ enhances the 2-MBF degradation at all concentrations and reaction times. The degree of enhancement increases with increase in the concentration of the oxidant at the beginning of the reaction. Eventually, the enhancement at all concentrations stabilizes. The degree of enhancement also decreases with time of reaction.

The inconsistency in the effect of H_2O_2 on the photocatalytic degradation of organics is seen in the case of 2-MBF also (figure 6.36). The net effect in this case is mild enhancement. However, the degree of enhancement fluctuates with the concentration of H_2O_2 and time of reaction, thereby confirming the conflicting role of H_2O_2 as a generator and scavenger of the reactive $^{\bullet}OH$ radicals (details discussed in earlier chapters).

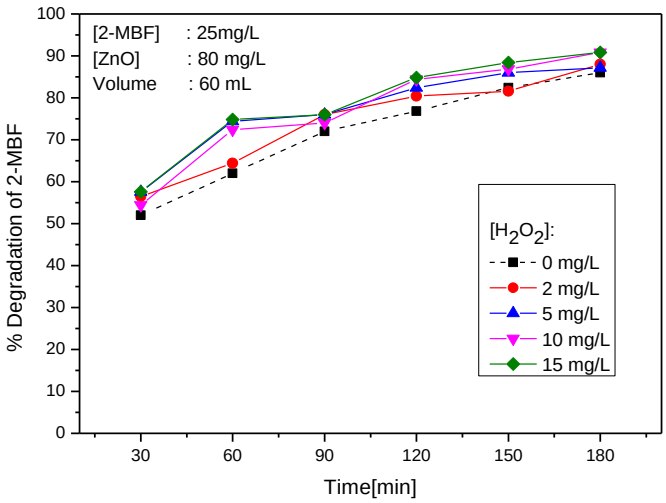

Fig. 6.36: Effect of concentration of H_2O_2 and reaction time on the photocatalytic degradation of 2-MBF

Since both H_2O_2 and $K_2S_2O_8$ are found to enhance the degradation of 2-MBF though only mildly, one typical combination of the two oxidants is

also tested and the results are plotted in figure 6.37. The trend is more or less same as that of individual components with only mild additive effect. Since the enhancement by the combination is also not significant to be evaluated in detail, no further study of the degradation is attempted.

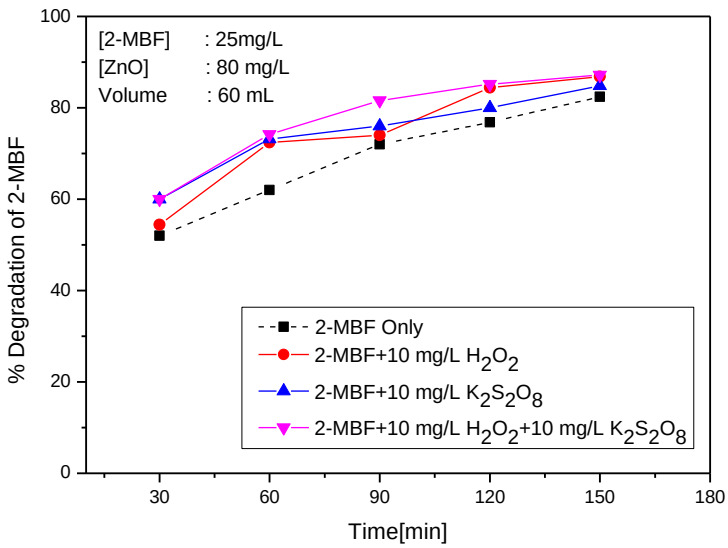

Fig. 6.37: Comparison of the effect of H_2O_2, $K_2S_2O_8$ and their combination on the photocatalytic degradation of 2-MBF.

6.3.15 Mineralization of 2-MBF

Solar photocatalysis using ZnO as catalyst is proven to be an effective method for the complete mineralization of trace amounts of organic pollutants such as AMS, ACP and DMPC in water as discussed in detail in previous chapters. The possibility of complete mineralization of 2-MBF in water is also investigated by carrying out the degradation of this pollutant for longer period and following the COD at regular intervals. The results are shown in figure 6.38.

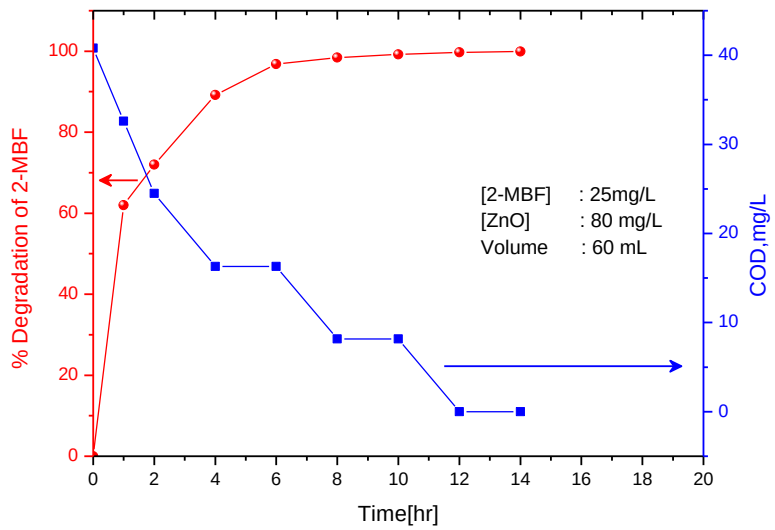

Fig. 6.38: Evidence for the complete mineralization of 2-MBF with ZnO under sunlight

The degradation is almost complete after 6-8 hr of irradiation. However, the complete mineralization (as seen from the COD) occurs only after 12 hr. Hence there may be more recalcitrant intermediates formed during the degradation, which may require extended periods of irradiation for mineralization. In any case, this study proves that solar photocatalysis using ZnO can be used for the mineralization of trace amounts of 2- MBF present in water.

6.3.16 Reuse of ZnO catalyst

As described in previous chapters, reusability of the photocatalyst is important for the efficient and economic application of this technology at industrial level. The reusability of the ZnO catalyst for 2-MBF degradation was investigated in the same manner as described in the case of AMS, ACP and DMPC degradation studies. The results are plotted in figure 6.39.

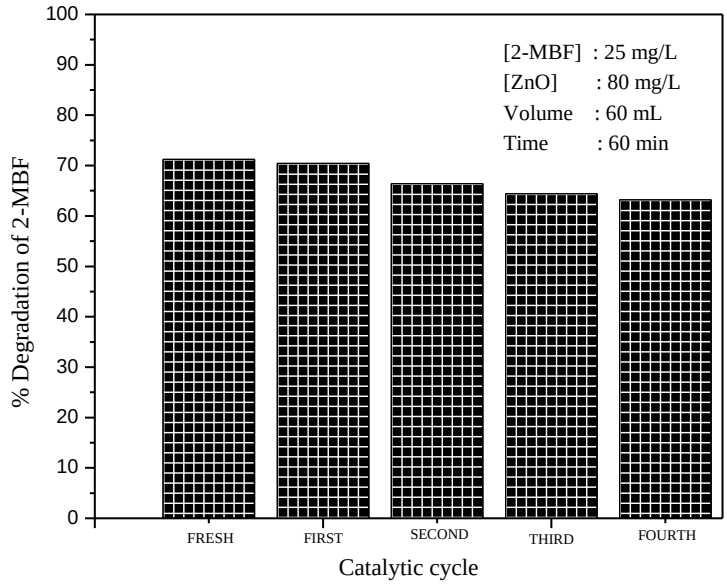

Fig. 6.39: Recycling of ZnO for the photocatalytic degradation of 2-MBF

The study clearly shows that the activity of the catalyst remains fairly same for the four recyclings as above. Slight decrease in the activity was observed from second recycle onwards. The marginal loss in catalytic activity may be due to several factors such as loss of catalyst during repeated filtration/separation, formation of surface hydroxide on the ZnO which results in decreased adsorption of substrate/intermediates, formation and adsorption of stubborn molecules, which may not get off the surface sites etc. The number of possible recyclings depends on the reaction conditions, chemistry of the pollutant and the intermediates, reactor size and geometry etc. However, the study gives a clear indication that by adopting proper separation/post treatment procedure, the catalyst can be effectively and economically reused for the photocatalytic degradation of 2-MBF in aqueous solution.

Comparison of the XRD, BET surface area, pore volume and pore size of the fresh and used ZnO catalyst is presented in figures 6.40 and 6.41and table 6.9.

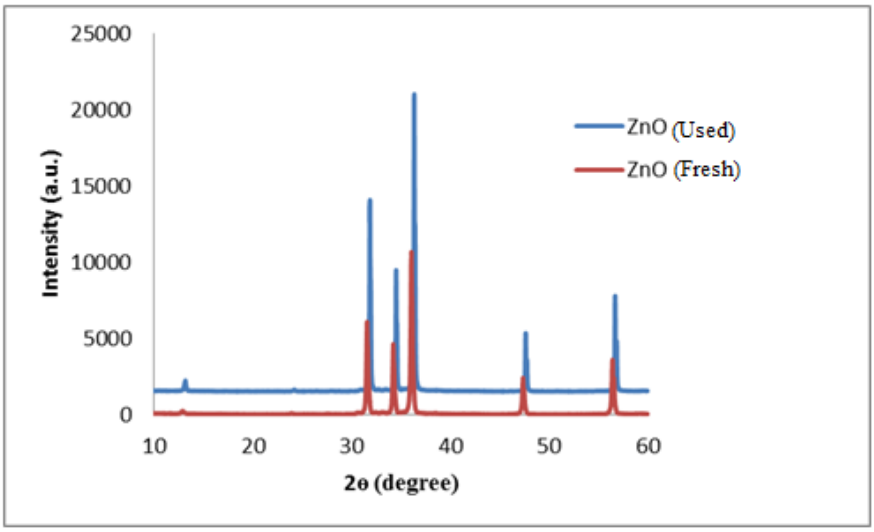

Fig. 6.40: Comparison of XRD of fresh and used ZnO catalyst

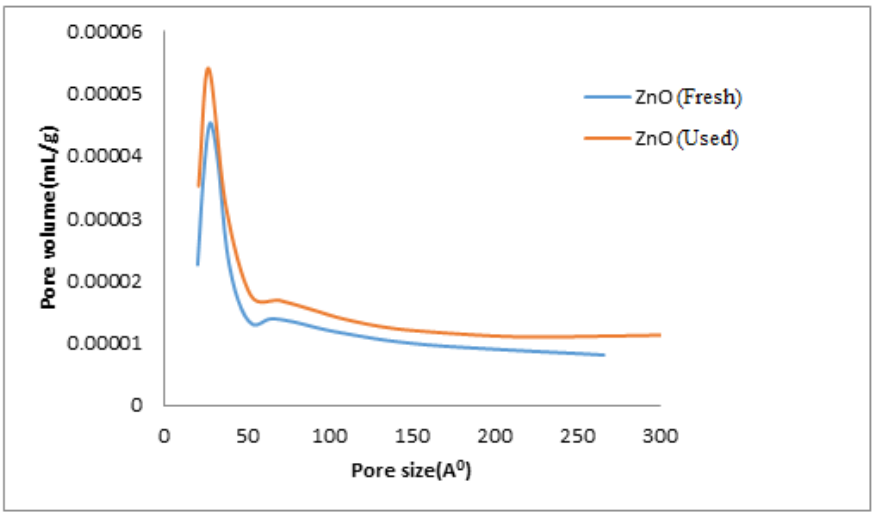

Fig. 6.41: Pore volume vs pore size curve for fresh and used ZnO catalyst

Table 6:9: Comparison of BET surface area, pore volume and pore size of fresh and used ZnO catalyst

Sample	BET Surface area (m^2/g)	Pore volume (cm^3/g)	Pore size (A^0)
Fresh ZnO	3.9745	0.012018	125.5911
Used ZnO	4.1672	0.016591	161.9875

6.4 Mechanism

The basic mechanism of the solar photocatalytic degradation and mineralization of 2-MBF in water is same as that for AMS, ACP and DMPC as discussed in Chapters 3, 4 and 5 respectively.

In the current study, phenol and acetophenone were identified as intermediates. Three other unidentified intermediates (A, B and C), are also formed in very small amounts periodically. Considering these, the possible steps involved in the mineralization can be represented as shown in figure 6.42. Details on the surface processes during irradiation, formation of reactive free radicals and possible interactions leading to the degradation of the pollutant molecules etc., are already discussed in previous chapters.

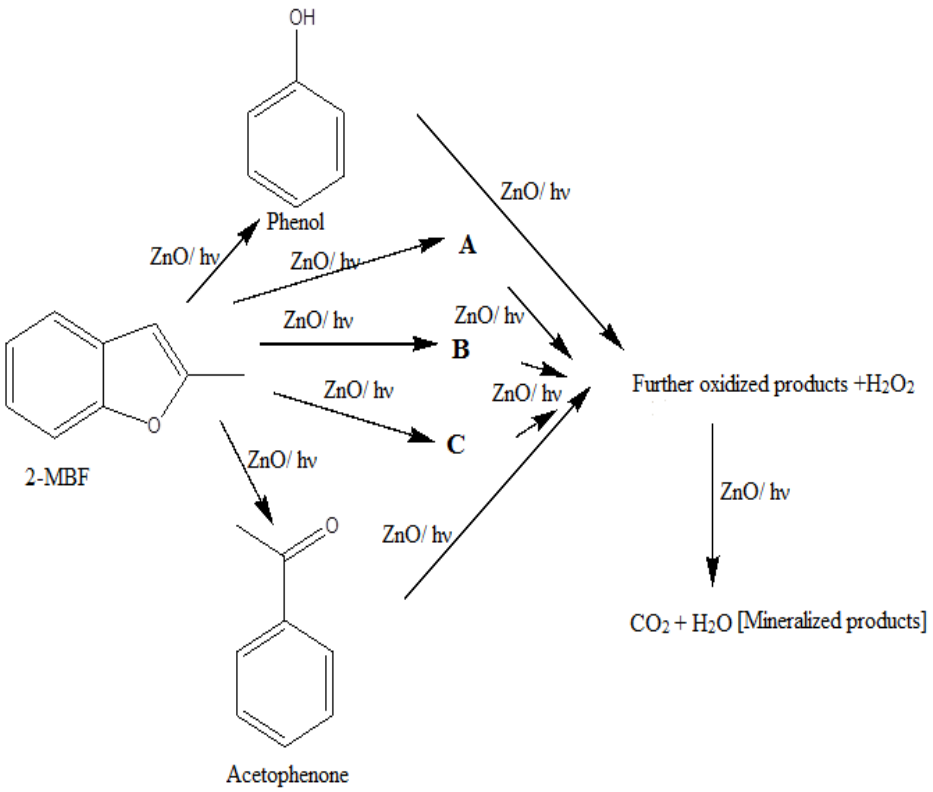

Fig. 6.42: Possible mechanism for the photocatalytic mineralization of 2-MBF

The mineralization of the pollutant as well as the intermediates is confirmed from the complete disappearance of COD.

6.5 Conclusions

Solar photocatalysis with ZnO as catalyst is investigated as an AOP for the degradation of trace amounts of 2-MBF in water. Various parameters affecting the degradation such as pH, pollutant concentration, catalyst loading, presence of salts and humic acid, externally added H_2O_2, oxidants etc., on the degradation were studied in detail. The role of dissolved oxygen in photocatalysis is confirmed by the inhibition of the

2-MBF degradation in deaerated system. Various intermediates formed during the degradation are identified. The complete mineralization of the pollutant was established by the reduction in COD value to zero on continuous irradiation. The recycling study of ZnO proves that the catalyst can be reused at least four times without any significant loss in its activity thereby showing the potential of this technology for industrial application.

.....ꕥ.....

Chapter 7

ZINC OXIDE MEDIATED SOLAR PHOTOCATALYTIC DEGRADATION OF AMS, ACP, DMPC AND 2-MBF IN SYNTHETIC AND REAL INDUSTRIAL WASTEWATERS

Contents

7.1 Introduction

Investigations on the solar photocatalytic degradation of four pollutants, i.e., AMS, ACP, DMPC and 2-MBF individually using ZnO as catalyst are discussed in Chapters 3, 4, 5 and 6 respectively. The study clearly shows that these pollutants can be successfully removed from water by this process. However, the real industrial waste water after the secondary treatment may contain more than one pollutant, often in trace quantities. The presence of one pollutant can affect the degradation efficiency of the other. Hence in order to scale up this technology for application at the industrial level, it is essential to study the degradation and the effect of various components on one another, in systems containing multiple pollutants. In this context, water containing traces of all the four pollutants is investigated to test the efficiency of ZnO mediated photocatalytic decontamination. The combination of these

pollutants in required quantities is prepared in distilled water as well as in real industrial effluent water matrix and the photocatalytic degradation is investigated. The efficiency is compared and the optimum parameters are identified. The mineralization of multiple pollutants in water offers more challenges and identification as well as optimization of critical parameters has to be done on a case to case basis.

7.2 Experimental details

7.2.1 Materials

AMS, ACP, DMPC, 2-MBF, ZnO and various reagents/chemicals used in the study were the same as reported in previous chapters.

7.2.2 Analytical procedure

Perkin Elmer Auto System XL Gas Chromatograph was used for the analysis of all the pollutants tested and the intermediates formed from them during the degradation. The detector, carrier gas and column are the same as reported in previous chapters. The calibration graph for the individual components are obtained by multiple level calibration method as described in Chapter 3. The advantage of the method is that all the components present in the sample can be simultaneously detected by a single injection of the sample [1.0 µL]. The gas chromatogram of a mixture [5 mg/L each] of AMS, ACP, DMPC and 2-MBF is shown in figure 7.1. By injecting varying concentrations of respective components, it is confirmed that the peak area of a particular component or its retention time is not affected significantly by other components in the sample. The instrument parameters are the same as those used for AMS analysis.

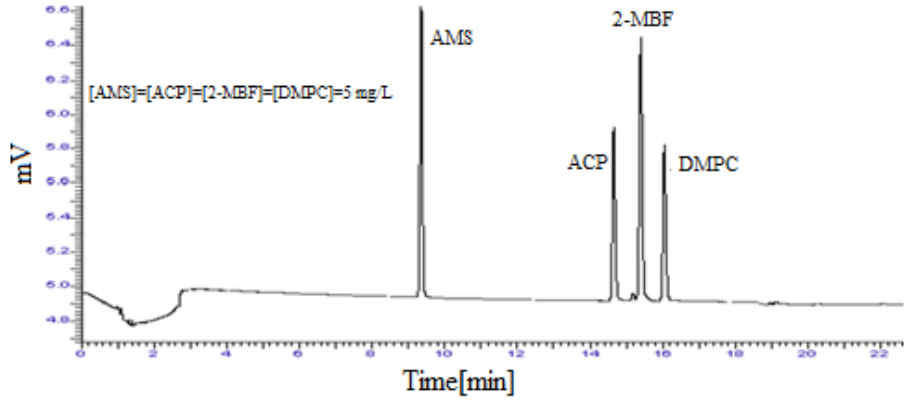

Fig. 7.1: Typical Gas chromatogram showing AMS, ACP, 2-MBF and DMPC

7.2.3 Other analyses

Various other analyses including COD analysis were done by the same procedures as described in Chapter 3.

7.2.4 Photocatalytic experimental setup

The experimental set up used in the study is same as that used in previous chapters.

7.3 Results and discussion

7.3.1 Degradation study of combination of two pollutants

The presence of multiple pollutants is known to affect the degradation of one another. When more than one pollutant is present in the system, there will be competition between the pollutants/intermediates for the available active surface sites on the catalyst. It is also possible that the pollutants or the intermediates may interact with one another or with the reactive free radicals and/or the surface species in different ways resulting in enhancement or inhibition of the degradation of the components.

Detailed investigation of the effect of each of the four pollutants on the degradation of the other at different concentrations and reaction times is carried out and the results are presented and discussed in this chapter. The objective was to test the possibility of using solar photocatalysis for the removal of these pollutants from water, inspired by the results presented in previous chapters. Detailed in-depth investigation of the degradation of multiple pollutants especially, the influence of components on the kinetics of degradation of one another, identity of the intermediates, variation in the mechanism of degradation, if any, etc., is beyond the scope of the current study. Hence the same will be taken up as another major research project.

Initially, the experiments were conducted with only two components. The degradation of various two component systems are plotted in figures 7.2-7.11.

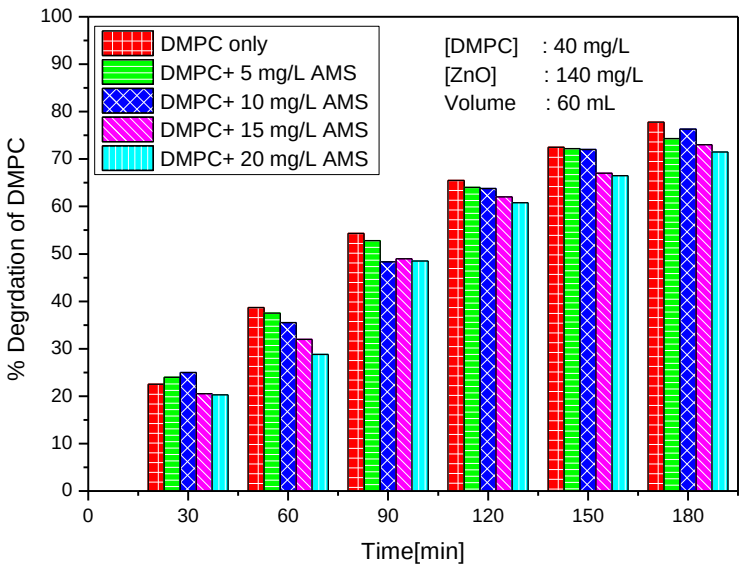

Fig. 7.2: Effect of AMS on the photocatalytic degradation of DMPC

AMS inhibits the degradation of DMPC slightly. The inhibition is negligible at lower concentrations [upto 10 mg/L] of AMS. Above 10 mg/L, the inhibition is slightly more. However, the overall effect of AMS is not much significant to affect the efficiency of degradation of DMPC. It will be more appropriate to conclude that the effect of AMS on the photocatalytic degradation of DMPC (40 mg/L) is negligible at least in the concentration range 5-20 mg/L (of AMS).

The effect of DMPC on the degradation of AMS is shown in figure 7.3.

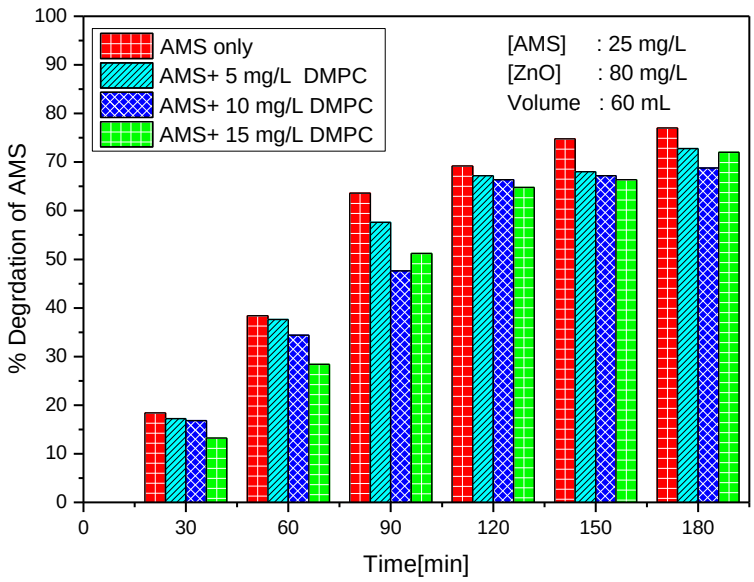

Fig. 7.3: Effect of DMPC on the photocatalytic degradation of AMS

In this case the inhibition of the degradation of the major component (AMS) by the minor component (DMPC) is slightly more compared to the data in figure 7.2. However, the effect is not significant even at higher

concentration or extended reaction time. Hence it may be inferred that the simultaneous presence of these two pollutants does not affect the degradation of one another significantly.

Similar plots for AMS and 2-MBF are shown in figures 7.4. and 7.5.

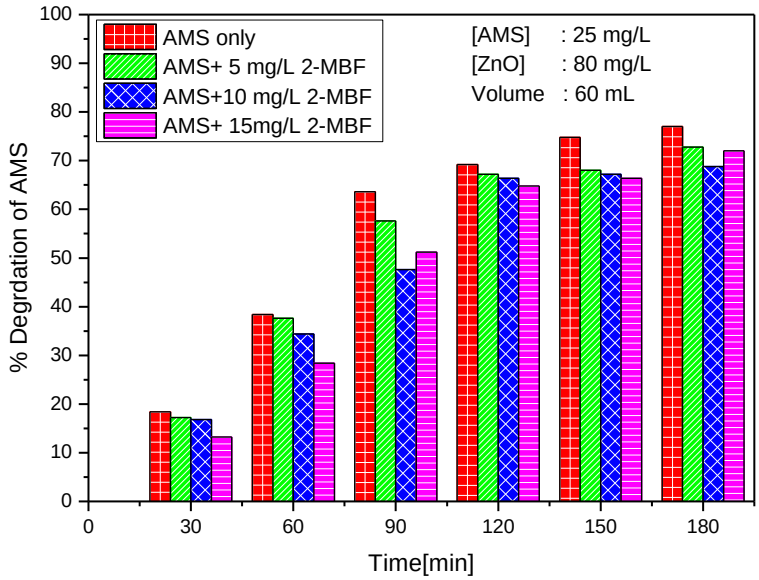

Fig. 7.4: Effect of 2-MBF on the photocatalytic degradation of AMS

2-MBF inhibits the degradation of AMS moderately. However, increase in concentration of 2-MBF or extended reaction time do not enhance the inhibition. Similarly moderate inhibition of the degradation of 2-MBF by AMS is observed as shown in figure 7.5.

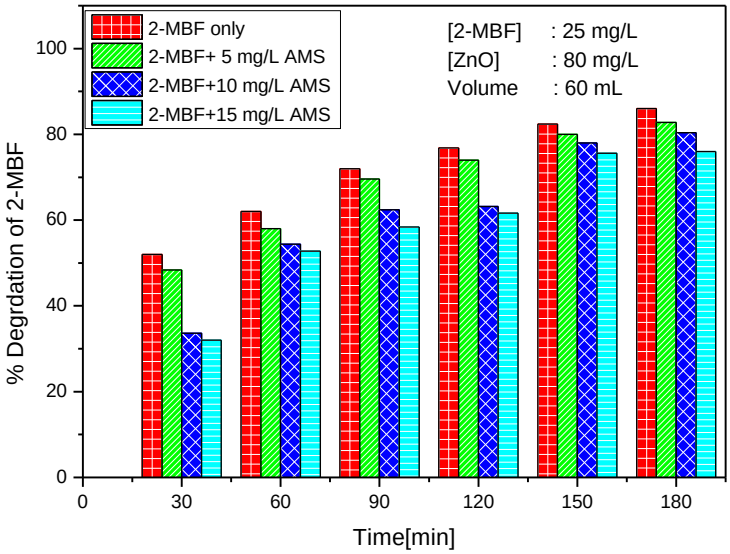

Fig. 7.5: Effect of AMS on the degradation of 2-MBF

In this case the inhibition is maximum in the early stage of the reaction when the concentration of both components is more. As the reaction progresses, the concentration of both components in relation to the availability of catalytic sites and reactive free radicals becomes lower. Hence the components can access reasonable number of active sites and ROS without much competition and consequently the inhibition is less.

Similar results are obtained in the case of degradation of 2-MBF in presence of ACP and vice versa (figures 7.6 and 7.7).

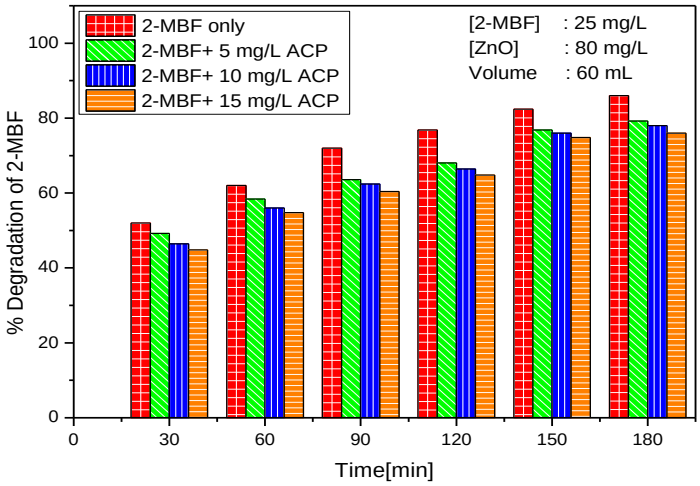

Fig. 7.6: Effect of ACP on the photocatalytic degradation of 2-MBF

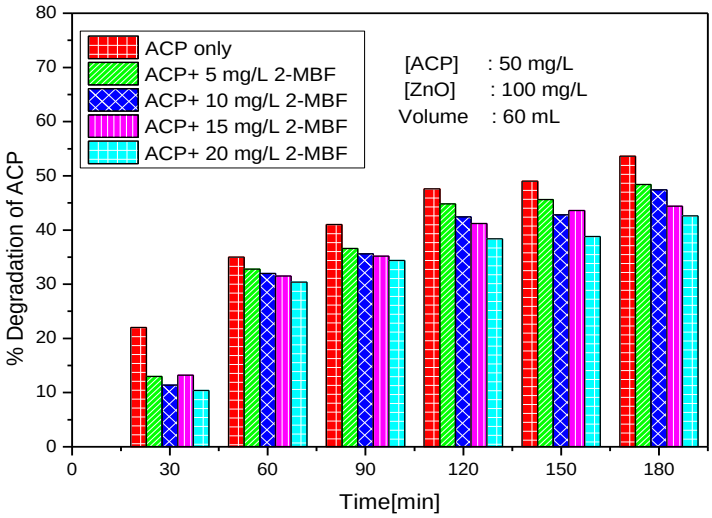

Fig.7.7: Effect of 2-MBF on the photocatalytic degradation of ACP.

The trend remains more or less the same as in other cases discussed above. The inhibition of the degradation of ACP is relatively more in the presence of 2-MBF in the beginning (figure 7.7). Hence it is possible that 2-MBF, which is more reactive compared to ACP competes and succeeds more effectively in adsorption at the surface sites. It is possible that they

may even displace ACP from at least some sites. With time, the concentration of both compounds decreases and the 2-MBF, which is more reactive will be degrading faster. Consequently, the number of sites available for ACP is more and hence the inhibition is less. In any case, both ACP and 2-MBF inhibit the degradation of each other. 2-MBF remains a relatively stronger inhibitor of the degradation of ACP compared to the inhibitive efficiency of the latter on the degradation of the former.

Similarly the effect of ACP and DMPC on the degradation of one another is experimentally verified and the results are shown in figure 7.8 and 7.9. In this case, ACP inhibits the degradation of DMPC in the beginning at all concentrations. However, with time the inhibition becomes weaker (figure 7.8).

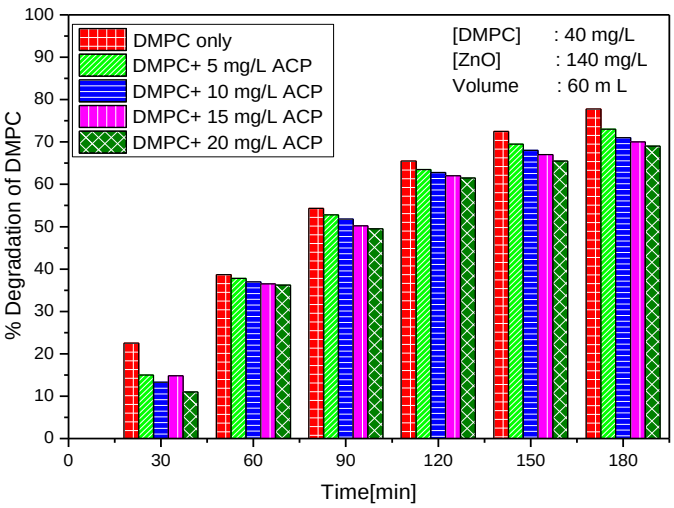

Fig. 7.8: Effect of ACP on the photocatalytic degradation of DMPC

DMPC has only very little effect at all concentrations on the degradation of ACP as seen in figure 7.9. However, the effect of either on

the degradation of the other is not significant enough to be of any consequence in the field application of photocatalysis for the removal of these pollutants from contaminated water.

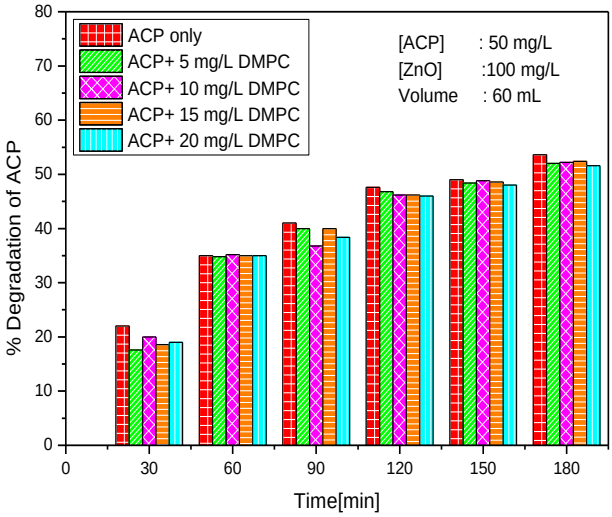

Fig. 7.9: Effect of DMPC on the photocatalytic degradation of ACP

In the case of DMPC/2-MBF the results are shown in figures 7.10 and 7.11.

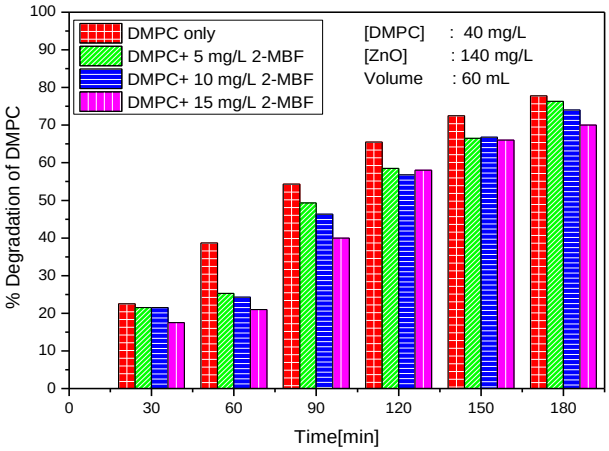

Fig. 7.10: Effect of 2-MBF on the photocatalytic degradation of DMPC

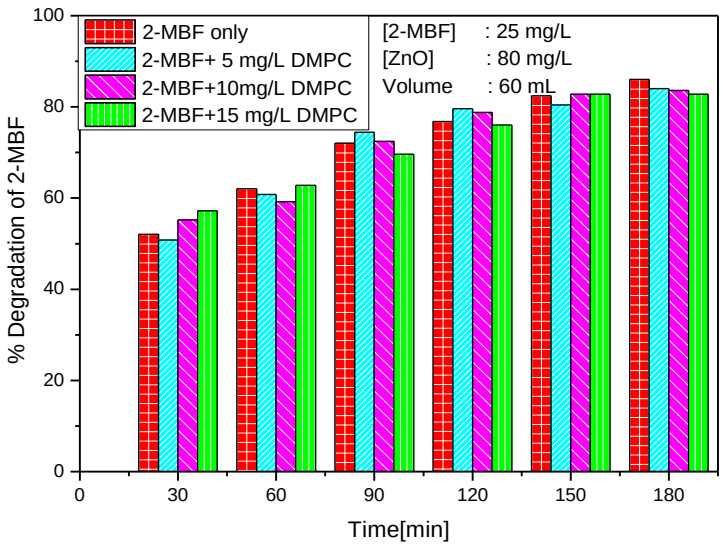

Fig. 7.11: Effect of DMPC on the degradation of 2-MBF

Similar to earlier cases, 2-MBF inhibits the degradation of DMPC. The extent of inhibition decreases with time (except at 30 and 60 min), which may be treated as relative concentration effect as discussed earlier. However, DMPC does not inhibit the degradation of 2-MBF and the effect is not significant. Hence, relatively 2-MBF may be getting better adsorbed on ZnO. This results in more frequent interaction of 2-MBF with the ROS compared to DMPC. The results in figures 7.10 and 7.11 support this inference.

The effect of AMS and ACP on the degradation of one another is reported in detail in Chapter 3 (section 3.3.7). The results showed that AMS is a strong inhibitor of the degradation of ACP, while the latter inhibits the degradation of the former only moderately.

This study clearly shows that in the case of the four pollutants investigated here, the presence of each pollutant affects the degradation of

the other only moderately in all cases. The effect becomes less significant with time, when the concentration of the minor component becomes much less compared to the other and there will be sufficient number of surface sites and ROS available in the system for the main component. However, waste water may contain many pollutants together at different concentrations. Hence it is important to study how the degradation of each pollutant is affected by others under different conditions. In this context, a preliminary investigation of the mutual effect of the above pollutants on the photocatalytic degradation behaviour of one another is carried out by taking equal concentrations [10 mg/L] of all the pollutants. The ZnO loading was 100 mg/L. The results at three different time periods of irradiation, i.e., 30, 90 and 180 min are plotted in figure 7.12.

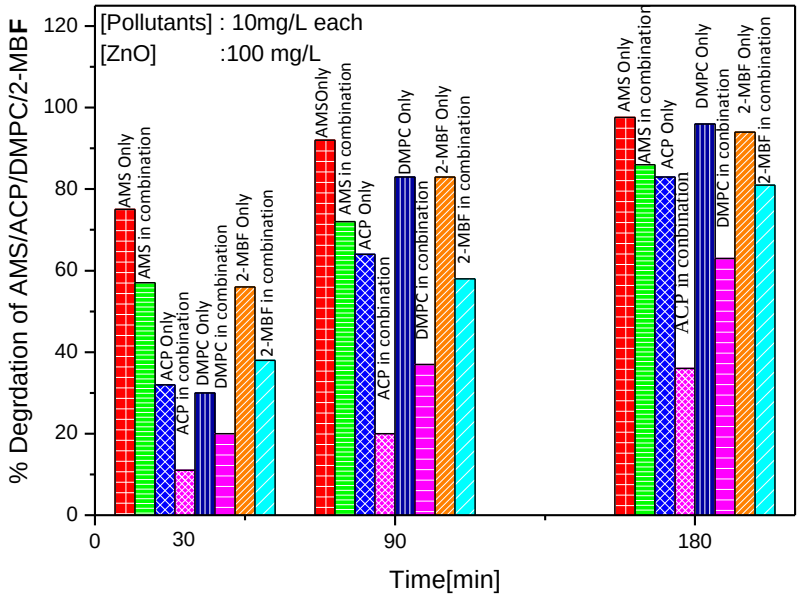

Fig. 7.12: Degradation of each pollutant in presence of the other three pollutants

The percentage degradation of every pollutant decreases considerably in presence of the other three pollutants. This is consistent with the moderate inhibition of each pollutant in presence of one another and may be treated as the cumulative effect of the inhibition by the other three pollutants. As observed in the studies reported in earlier chapters, maximum inhibition happens in the case of ACP (> 65%) and the least in the case of AMS (< 30%). The relative inhibition of the degradation of each pollutant in presence of the other three is computed and shown in table 7.1.

Table 7.1: Percentage inhibition of the degradation of individual components by others in the combination.

Time[min]	% Inhibition of degradation			
	AMS	**ACP**	**DMPC**	**2-MBF**
30	24	65.6	33.3	32.0
90	21.7	68.8	55.4	30.0
180	11.9	56.6	34.4	13.8

This inhibition, as explained earlier, may be due to the competition among the pollutants as well as the large number of intermediates formed from all of them for the available surface sites on the catalyst and for the reactive species on the surface as well as in the bulk.

7.3.2 Optimization of catalyst concentration for the combination of pollutants

The catalyst dosage optimized for individual pollutants was used in the above experiments. However, the optimum may not be the same when the system contains multiple pollutants. Hence the effect of catalyst dosage on the degradation of the combined pollutants is investigated by

varying the amount of ZnO from 50 to 300 mg/L and keeping other parameters identical. The results are shown in figure 7.13.

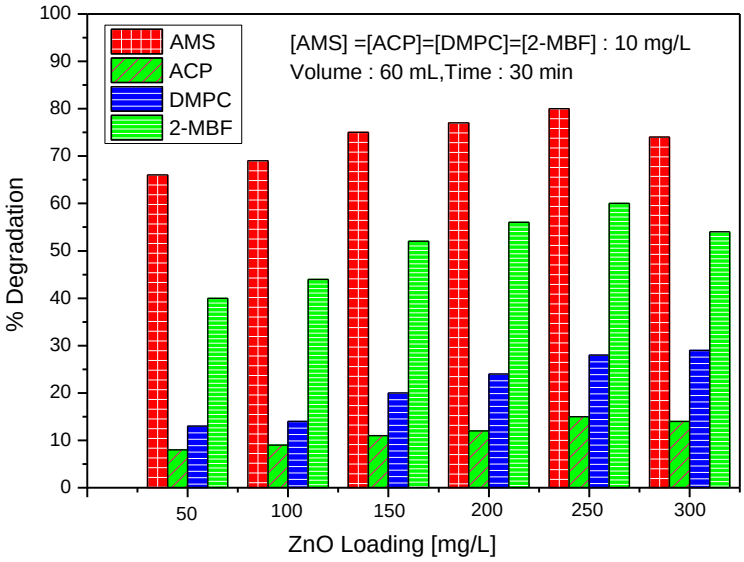

Fig. 7.13: Effect ZnO loading on the degradation of combined pollutants

The percentage degradation of all the pollutants increases with increase in catalyst loading upto 250 mg/L and slowly decreases thereafter. The increase in degradation with increase in catalyst loading is more in the case of AMS and 2-MBF, which are known to get better adsorbed on the catalyst. Hence the increase in degradation can be attributed to the increase in number of active surface sites for adsorption of those pollutants/intermediates. Other reasons for the catalyst dosage effect, as discussed earlier, such as scattering and reduced passage of light through the suspension at higher dosage, aggregation of the particles resulting in the decrease of active surface sites, deactivation of the activated catalyst by collision with ground state catalyst etc., may be

applicable in the case of combination of pollutants also. In the case of molecules like ACP and DMPC, whose adsorption over the ZnO is negligible, the increase in degradation may be due to the interaction of these molecules with the increased number of hydroxyl radicals and other reactive species generated with increased catalyst dosage.

The possibility of correlation between the relative adsorption of various contaminants and their degradation (when they are in combination) is further examined by measuring the adsorption of respective components from a solution containing all of them as well as from individual solutions. The results are shown in table 7.2.

Table 7.2: Adsorption of individual components from a solution of their combination as well as from respective individual solutions over ZnO

[AMS] = [ACP] = [DMPC] = [2-MBF] =5 mg/L, [ZnO] =250 mg/L, Volume= 60 mL

A: From the solution of the combination, **B**: From individual solutions

Time[hr]	% Adsorption over ZnO							
	AMS		ACP		DMPC		2-MBF	
	A	B	A	B	A	B	A	B
1	40.0	40.4	4.0	3.6	2.0	3.9	26.0	30.8
2	44.0	49.6	2.0	3.3	2.0	4.3	29.0	31.6
3	40.0	48.0	4.0	3.6	2.0	4.4	28.0	32.9

AMS and 2-MBF show good adsorption, whether present individually or in combination with other pollutants. ACP and DMPC are poorly adsorbed. The influence of individual components on the adsorption of other components in the combination is not significant. As shown earlier, the effect of the individual components on the degradation of other component in the combination also is not much. The results demonstrate that the lack of any

effect on the degradation of individual components by other components in the combination can be at least partly attributed to the lack of mutual effect on their adsorption. However, there may be other factors also as discussed in earlier chapters.

7.3.3 Optimization of combined concentration of the pollutants

Optimization of the concentration of any individual component in a combination of multiple pollutants is not practical or relevant since the actual composition of real industrial effluent water from different sources is never the same. Even from the same source, the concentration of individual components can always vary. In any case, a typical combination of pollutants at different but equal individual concentrations [5, 10, 15, 20 and 25 mg/L each] is tested to evaluate the relative photocatalytic degradation rate of the respective component. The results are plotted in figure 7.14.

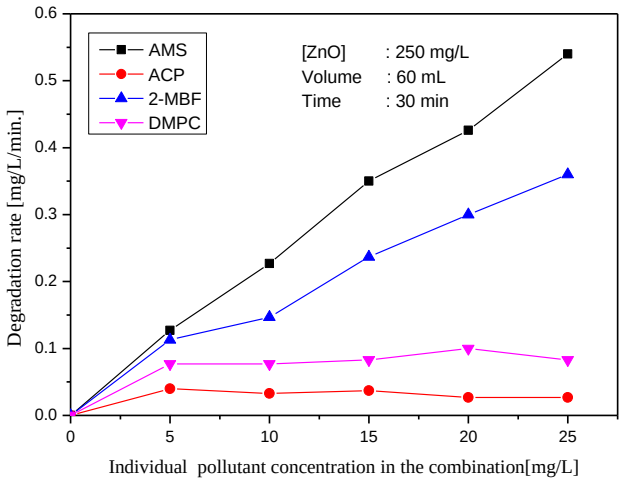

Fig. 7.14: Effect of concentration of the pollutants in the combination on the degradation rate of individual components

In the case of both AMS and 2-MBF, which get relatively better adsorbed on ZnO, the rate of degradation steadily increases with increased concentration. In the case of ACP and DMPC the rate increases very slowly with concentration initially and stabilizes later. Hence it is evident that in a competitive environment, those molecules which can get better adsorbed on the surface and are in close proximity to the reactive species will get degraded faster. Those molecules, which get only weakly adsorbed on the surface have access mainly to the limited ROS in the bulk. Hence increased concentration of such substrates may not be able to interact with corresponding number of reactive free radicals. This results in steady or even decreased rate of degradation with increase in concentration of those substrates. In the case of DMPC and ACP, the optimum concentration of each is 5 mg/L under the reaction conditions used here. However, in the case of AMS and 2-MBF, the rate goes on increasing even at 25 mg/L concentration of each. Hence in the case of contaminated water with multiple pollutants, optimization of the concentration of individual components may not be feasible and it will be more practical to optimize other relevant reaction parameters for the photocatalytic degradation of all the pollutants combined.

7.3.4 Mineralization of the pollutants in combination

As discussed in Chapters 3, 4, 5 and 6, it is evident that the molecules AMS, ACP, DMPC and 2-MBF, when present as sole pollutant in water, can be completely mineralized by ZnO photocatalysis under sunlight. In order to verify the effect of other components on the

mineralisation of the individual pollutants, the degradation (of the combined pollutants) is studied for longer duration and the COD of the reaction system is measured at periodic intervals. The results are given in figure 7.15.

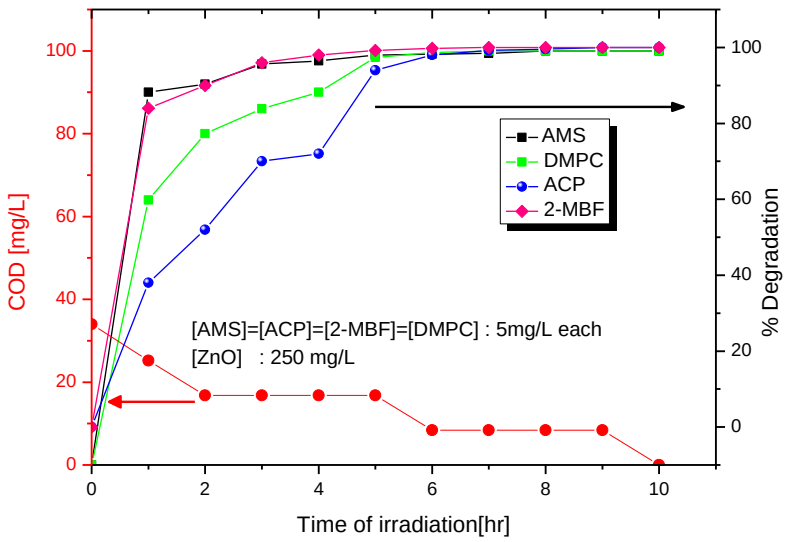

Fig. 7.15: Degradation of pollutants in combination and concurrent reduction in COD

The initial decrease in COD may be due to the mineralization of AMS and 2-MBF. Subsequent steady COD indicates the formation of more stable intermediates from the pollutants. Eventually, they also get mineralized in ~ 10 hr resulting in a COD of '0'. The gradual decrease in the concentration of the components and complete disappearance can be seen in the chromatogram shown in figure 7.16.

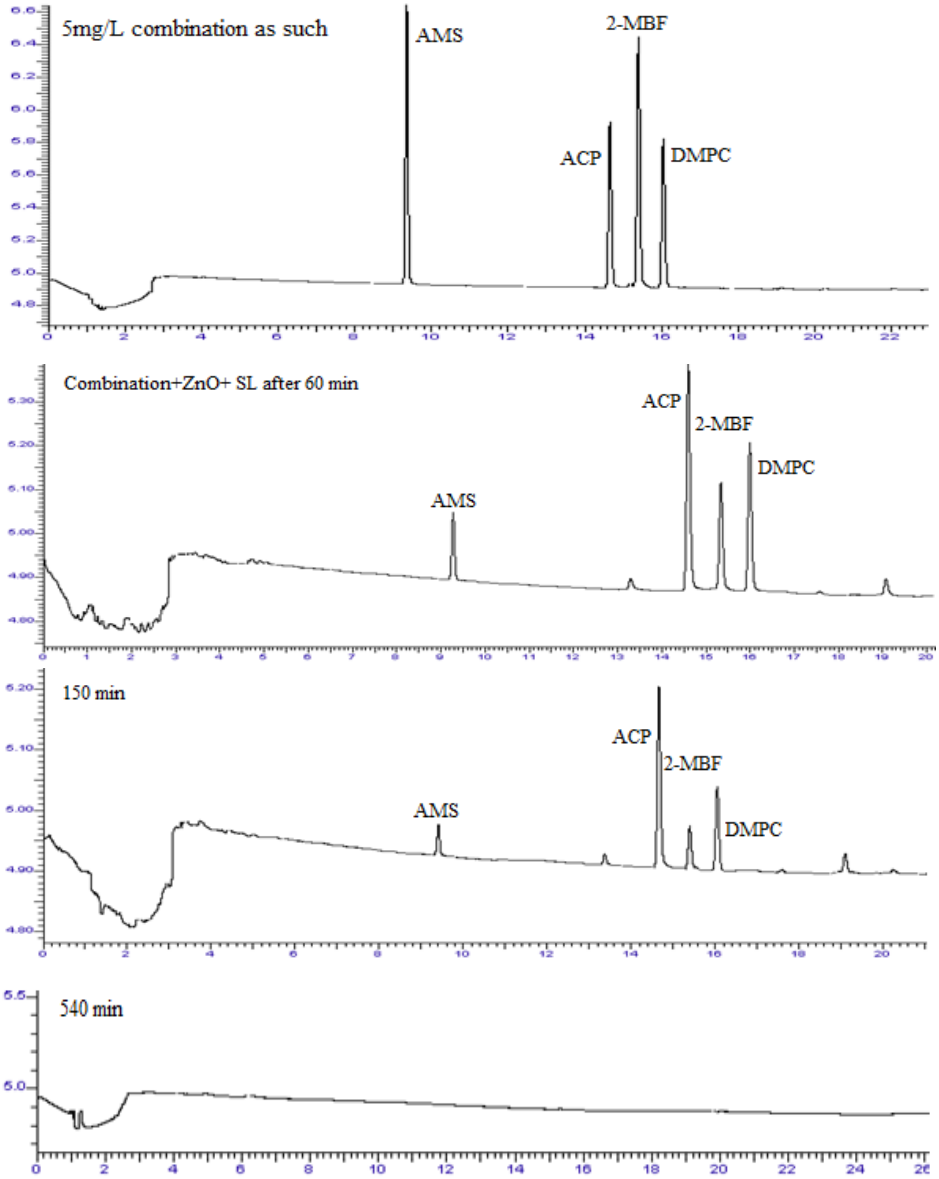

Fig. 7.16: Gas Chromatogram showing the degradation of pollutants

The faster degradation of AMS and 2-MBF is quite evident. All the peaks disappear after 9 hr of irradiation. This is consistent with the decrease and eventual disappearance of COD after 10 hr of prolonged irradiation.

The absence of any peak of the intermediates indicates that they are not accumulated in measurable quantities and may be getting further degraded and mineralized faster. This study confirms that ZnO mediated solar photocatalysis can be effectively used for the removal of both individual as well as combination of pollutants within a reasonable time interval.

7.3.5 Effect of pH

pH plays an important role in the photocatalytic degradation of pollutants in aqueous systems as already discussed in previous chapters. The effect of pH on the degradation of individual pollutants such as AMS, ACP, 2-MBF and DMPC is investigated in detail in Chapters 3, 4, 5 and 6 respectively. However, the effect may differ for individual pollutant in presence of other components. Hence a detailed study of the effect of pH on the degradation of each of the above four pollutants, when they are together, is undertaken. The results are shown in figure 7.17.

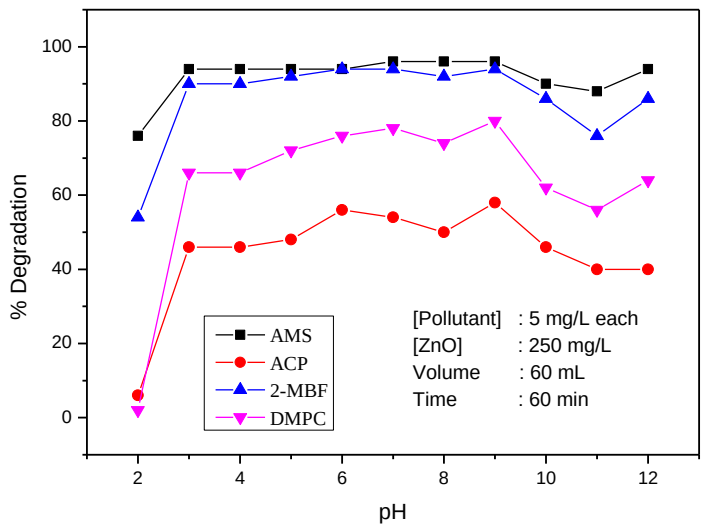

Fig. 7.17: Effect of pH on the degradation of individual components in the combination

The slow degradation observed in the case of all components at pH=2 may be due to the acidic and/or photo-corrosion of ZnO catalyst with corresponding decrease in the number of available active sites. This leads to a decrease in the adsorption and the reactive free radicals generated. Effect of pH variation on the degradation of all the pollutants follows almost the same trend. The percentage degradation increases initially with increase in pH upto ~3 and is stabilized thereafter till pH ~9. This is followed by moderate decrease in the degradation upto pH ~11 and slight increase thereafter. The decrease occurs at pH $\geq$ 9, which is very close to the point of zero charge of ZnO (~9.3). Above this pH, the surface is negatively charged and as explained earlier, the pollutants cannot be adsorbed or be in close proximity to the surface. Hence the interaction with the surface initiated ROS will be weaker and the degradation is less. However, at the alkaline pH, there will be more OH^- ions and correspondingly more $^{\bullet}OH$ radicals in the system leading to enhanced rate of degradation. Thus the negative effect arising from PZC of ZnO is compensated and there is good degradation even at alkaline pH. The study shows that combination with other pollutants does not influence 'the effect of pH on the degradation of individual components'.

7.3.6 Preliminary studies using real waste water from the industry as the medium

The above investigation on the photocatalytic degradation of the pollutants is made using synthetic 'polluted' water prepared by dissolving the components in required quantities in distilled water. However, real industrial waste water will contain many other contaminants like salts, humus materials, turbidity and other known and unknown materials.

These foreign contaminants can influence the efficiency of photocatalytic degradation of the target pollutants as demonstrated in earlier chapters. Hence for the scale up and subsequent commercialization, the efficiency of this technique has to be tested using real industrial effluent water as the medium. Accordingly, investigations on the degradation efficiency of the ZnO mediated solar photocatalysis for the degradation of the combination of pollutants in real industrial water matrix are made as follows.

1) The effluent water after secondary treatment from the phenol industry (referred earlier in this thesis) is collected and is divided into two parts. One part was used as such and the other part was filtered to remove the suspended solids, turbidity etc. Both samples were analysed for various parameters and the results are shown in table 7.3.

Table 7.3: Analysis of secondary effluent water

SL .No	Parameters	Values	
		Effluent water as such	Filtered effluent water
1	pH	8.25	8.20
2	Phenol	0.40 mg/L	0.40 mg/L
3	Phosphate	3 mg/L	3 mg/L
4	Sulphate	280 mg/L	280 mg/L
5	Chloride	10 mg/L	10 mg/L
6	TDS	638 mg/L	638 mg/L
7	COD	63 mg/L	56 mg/L
8	Turbidity	9.10 NTU	0.90 NTU
9	T SS	23.30 mg/L	NIL

TDS = Total Dissolved Solids, TSS = Total Suspended Solids
COD = Chemical Oxygen Demand

2) Required quantities of AMS, ACP, 2-MBF and DMPC are dissolved in both filtered and unfiltered water as well as in pure distilled water such that the concentration of each pollutant is 5 mg/L. The initial COD of the three solutions are determined.

3) The solar photocatalytic degradation study of the three suspensions is carried out with 250 mg/L of ZnO catalyst under identical conditions. The samples are drawn and analysed at regular intervals for the pollutant's concentration as well as for COD reduction to verify degradation and mineralization. The degradation of the pollutants under the above conditions is shown in figures 7.18 - 7.20.

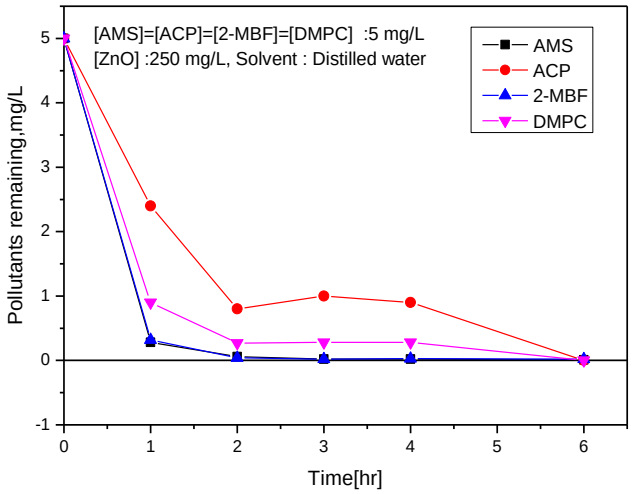

Fig. 7.18: Photocatalytic degradation of combination of pollutants in distilled water.

The results in the case of distilled water medium presented in figure 7.18 show that the degradation of all components is faster initially and is ~80% complete in ~2 hr. In the case of ACP, there is slight increase in the concentration after 2 hr of irradiation. This may also be due to the simultaneous formation of ACP as one of the intermediates during the photocatalytic degradation of AMS, DMPC and 2-MBF. At the same time, the degradation of ACP itself is relatively slow compared to that of the other molecules. Both these factors lead to the increase/stabilization in

the net concentration of ACP in the system for some time. As the degradation of the AMS and DMPC continues, their concentration in the system decreases and consequently the rate of formation of ACP also decreases. Once the concentration of other components has become lower, the degradation of ACP which was slower in the presence of those components, becomes faster. This may be the reason for the faster decrease in the concentration of ACP at the later stage of the reaction.

In the case of industrial waste water matrix, degradation efficiency is drastically reduced even after filtration (figures 7.19 and 7.20). Pollutants in filtered effluent water require ~20 hr for complete degradation (figure 7.19). The degradation in effluent water as such (no filtration) require 26 hr (figure 7.20).

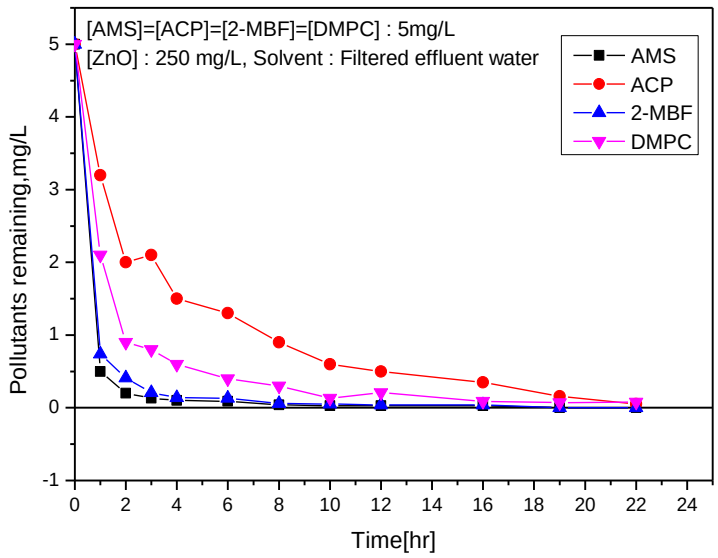

Fig. 7.19: Photocatalytic degradation of combination of pollutants in filtered effluent water.

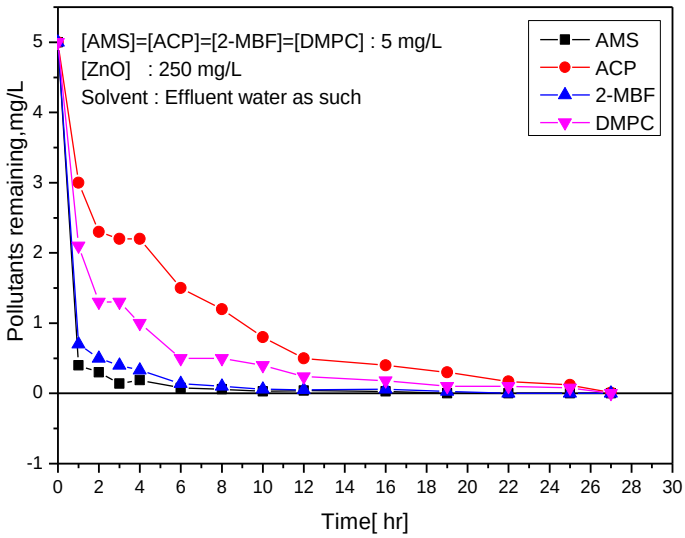

Fig. 7.20: Photocatalytic degradation of combination of pollutants in effluent water as such.

Thus it is seen that the degradation of pollutants is faster in distilled water thereby confirming that the dissolved and suspended impurities can inhibit the degradation. However, the inhibitory effect is mostly from dissolved impurities such as salts and organics and not from suspended particulate materials. This is evident from the more or less similar results obtained in the case of filtered and unfiltered effluent waters. In the case of distilled water, the degradation of all pollutants is complete in 6 hr. The time taken for complete degradation of the pollutants in filtered and unfiltered effluent waters is ~20 and ~26 hr respectively. The slow degradation in the case of natural industrial effluent gives time for the slow degrading components as well as the intermediates also to degrade and eventually mineralize in parallel. The time taken for complete mineralization as measured by the COD in the three types of water matrices is presented in figure 7.21.

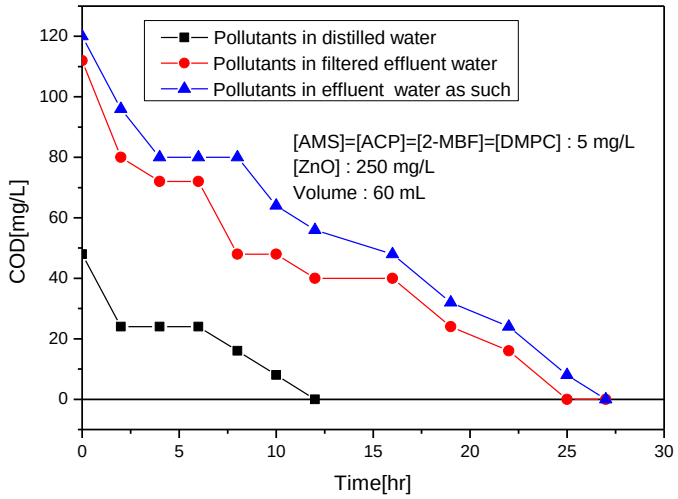

Fig. 7.21: Comparison of the mineralization of the combination of pollutants in distilled water, effluent water and filtered effluent water.

Comparative efficiency of degradation/mineralization of the pollutants in the three types of matrices in terms of the time taken is given in table 7.4

Table 7.4: Comparative efficiency of phtocatalytic degradation/mineralization of pollutants in different water matrices.

Matrix	Time(hr) taken for complete	
	Degradation	Mineralization
Distilled water	6 .0	12.0
Filtered effluent water	20.0	25.0
Unfiltered effluent water	26.0	27.0

7.3.7 Effect of miscellaneous contaminants present in real effluent water

Analysis of the industrial effluent water showed that it contains significant amounts of PO_4^{3-}, Cl^- and SO_4^{2-} ions (table 7.3). Of these Cl^- and SO_4^{2-} ions are known to inhibit/enhance the degradation of organic pollutants in water depending on the characteristics of the waste water

and the pollutants as well as the concentration of the anion and reaction time [143]. The effect of these anions on the degradation of the individual components is investigated in detail and reported in previous chapters. In any case, the effect of these three anions individually and in combination on the degradation is tested here using the combination of the four organics, i.e., AMS, ACP, 2-MBF and DMPC as the test pollutants. For convenience, the effect of the anions on individual pollutants is analysed (even though the pollutants are in combination). The anions are added to the solution of the four pollutants (5 mg/L each). The concentration of anions added is such that the net concentration will be the same as that present in industrial effluent water (see table 7.3). The effect of these anions individually as well as in combination on the degradation of respective individual pollutant (in the combination) is investigated and the results are presented in figures 7.22-7.25.

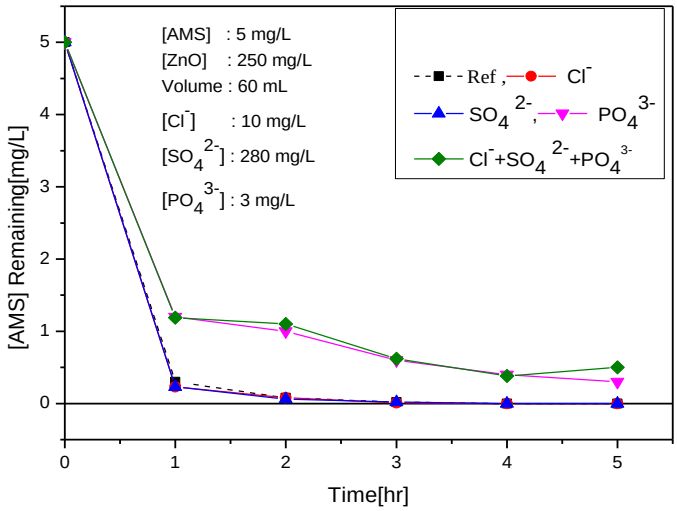

Fig.7.22: Effect of Cl^-, SO_4^{2-} and PO_4^{3-} individually and in combination on the degradation of AMS in the solution containing all the four pollutants.

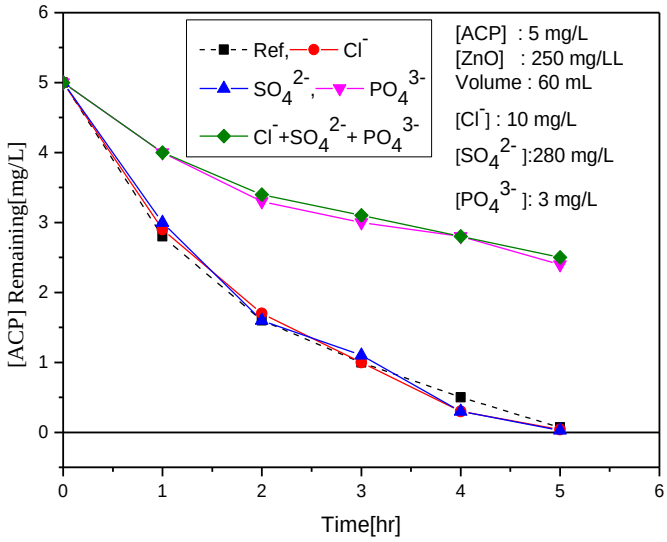

Fig. 7.23: Effect of Cl^-, SO_4^{2-} and PO_4^{3-} individually and in combination on the degradation of ACP in the solution containing all the four pollutants.

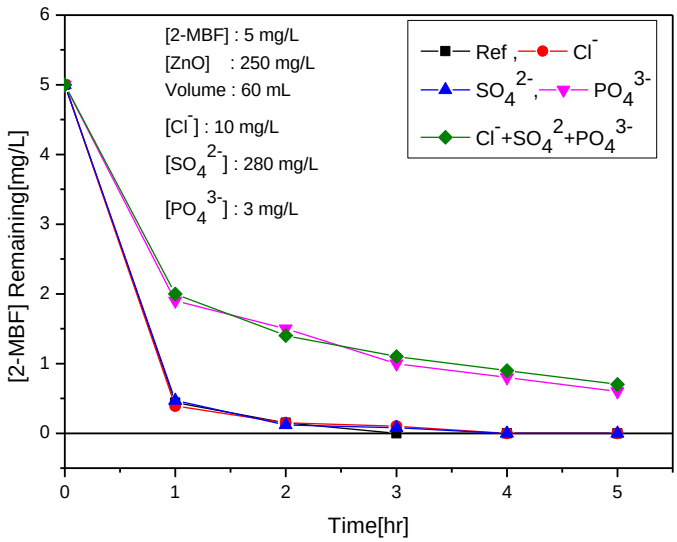

Fig. 7.24: Effect of Cl^-, SO_4^{2-} and PO_4^{3-} individually and in combination on the degradation of 2-MBF in the solution containing all the four pollutants.

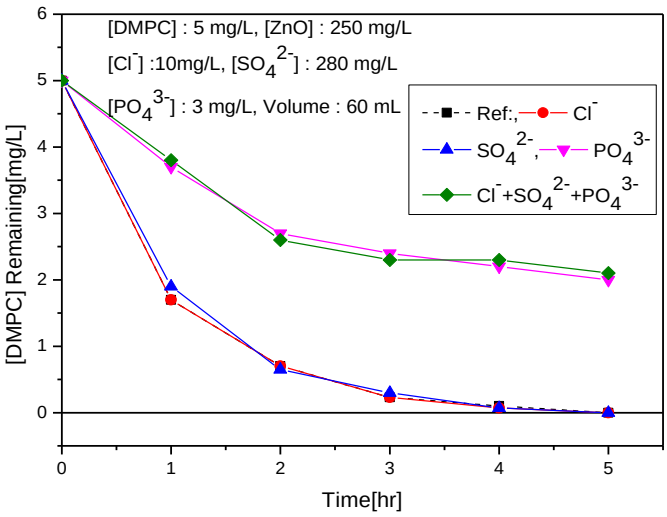

Fig. 7.25: Effect of Cl^-, SO_4^{2-} and PO_4^{3-} individually and in combination on the degradation of DMPC in the solution containing all the four pollutants.

The study clearly shows that the presence of both chloride and sulphate has no significant effect on the degradation of any of the four components in the combination of pollutants. However, the presence of phosphate individually as well as in combination with the other two anions inhibit the photocatalytic degradation of all the four pollutants significantly at all time intervals. Presence of Cl^- or SO_4^{2-} does not influence the inhibition by PO_4^{3-} in all cases. The extent of inhibition of the degradation of each pollutant (in the combination) in presence of the anions individually as well as in combination is presented in table 7.5.

Table 7.5: Effect of phosphate, chloride and sulphate individually and in combination on the degradation of each pollutant in the combination (of pollutants)

[Pollutant] = 5 mg/L each, **C** =10 mg/L of Cl^-, **P** = 3 mg/L of PO_4^{3-} and **S**=280 mg/L of SO_4^{2-} **C+S+P** =10 mg/L of Cl^- +280 mg/L of SO_4^{2-} +3 mg/L of PO_4^{3-}

Pollutant	% Change in degradation in presence of anions											
	1hr				2hr				3hr			
	C	P	S	C+S+P	C	P	S	C+S+P	C	P	S	C+S+P
AMS	+1.4	-18.0	+1.4	-17.8	0	-18.4	+0.4	-20.4	+0.2	-11.6	0	-12.0
ACP	-2.0	-24.0	-4.0	-24.0	-2.0	-34.0	0.0	-36.0	0.0	-40.0	-2.0	-42.0
2-MBF	+1.0	-29.0	- 0.6	-31.2	0.0	-27.0	+0.6	-25.0	-0.20	-20.0	-1.6	-22.0
DMPC	0	-40.0	-4.0	-42.0	0.0	-40.0	+1.0	-38.0	0.0	-43.4	-1.4	-41.4

(-) sign indicates inhibition; (+) sign indicates enhancement

The results confirm that the primary reason for the inhibition of the degradation of pollutants in industrial waste water matrix used here may be the presence of phosphate anion.

In real life effluent water, another factor which can affect the efficiency of photocatalysis is turbidity. In presence of anions, the effect may be different resulting in enhanced inhibition in many cases. Hence a typical anion PO_4^{3-} is chosen for studying the effect, '(turbidity + anion) combined' on the degradation of the combination of pollutants.

PO_4^{3-} is already proven to be strong inhibitor of most AOPs. Hence the decrease in the degradation of the pollutants in real effluent water may also be at least partially due to the presence of phosphate ion. This is reconfirmed by investigating the effect of PO_4^{3-} (3 mg/L) on the degradation of each of the four pollutants in the combination in distilled water. The results are presented in figure 7.26.

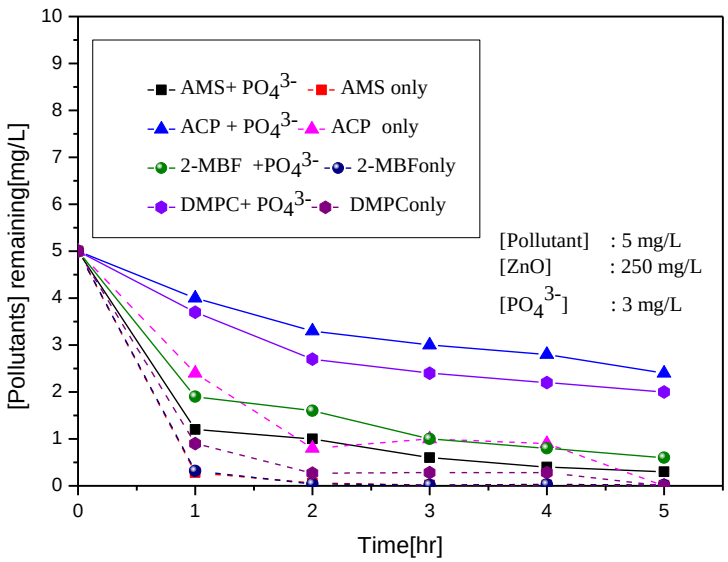

Fig. 7.26: Effect of PO_4^{3-} on the photocatalytic degradation of pollutants in distilled water

Earlier results (figures 7.19 and 7.20) showed that the degradation of the pollutants in effluent water as such is slightly lower, when compared to that in the filtered effluent water. This may be due to the presence of traces of suspended solids and consequent turbidity of the former. This turbidity reduces the amount of sunlight entering in and passing through the solution thereby affecting the efficiency of catalyst activation and subsequent generation of reactive species that can interact with the pollutants. In this context, the effect of turbidity on the degradation is tested by externally introducing turbidity in the reaction system prepared in distilled water. (The system is made turbid by adding calculated quantity of standard turbidity solution of 400 NTU prepared by mixing hydrazine sulphate and hexamethylenetetramine)[182].The results are presented in figure 7.27.

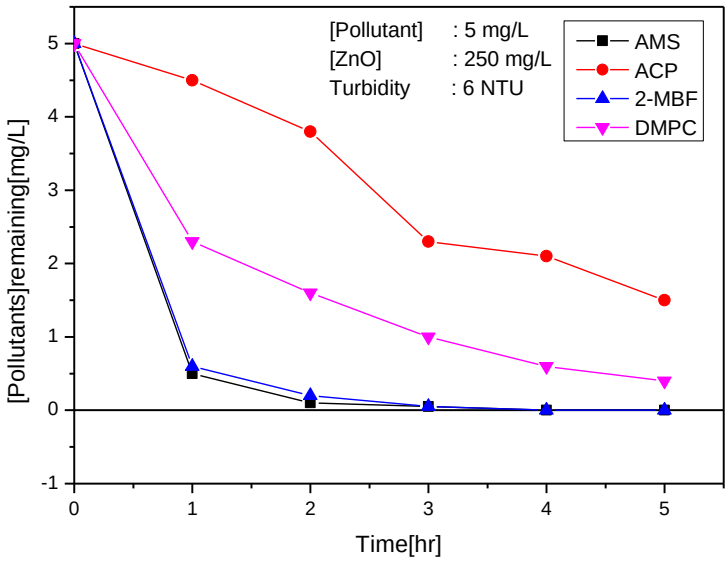

Fig. 7.27: Photocatalytic degradation of pollutants in distilled water with added turbidity (6 NTU)

Comparison of the data in figure 7.27 with those in figure 7.18 (with no added turbidity) clearly shows that turbidity inhibits the degradation of organic pollutants even when all other parameters are identical.

The effect of the two established inhibitors, i.e., turbidity and phosphate ion together on the photocatalytic degradation of the pollutants is tested by adding them to distilled water medium. The results are plotted in figure 7.28.

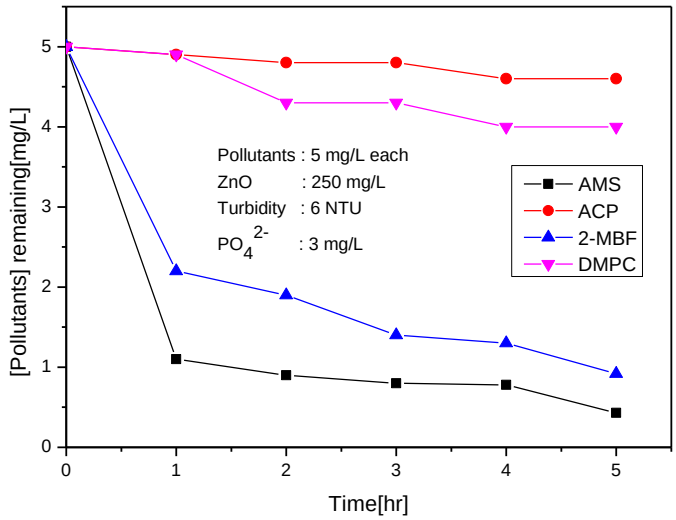

Fig. 7.28: Photocatalytic degradation of pollutants in distilled water in presence of externally added turbidity and PO_4^{3-}.

The degradation is severely inhibited in the combined presence of turbidity and phosphate ion in the reaction medium as can be seen when compared with the results in figure 7.18. The degree of inhibition in presence of PO_4^{3-} and turbidity individually and in combination is presented in table 7.6.

Table 7.6: Effect of turbidity and phosphate individually and in combination on the degradation of combination of pollutants.

[Pollutant]=5 mg/L each, **P** = 3 mg/L of PO_4^{3-} and no turbidity,
T= Turbidity of 6 NTU and no PO_4^{3-}

P+T=3 mg/L of PO_4^{3-} + Turbidity of 6 NTU

Pollutant	**% Change in degradation**								
	1 hr			**2 hr**			**3 hr**		
	P	**T**	**P+T**	**P**	**T**	**P+T**	**P**	**T**	**P+T**
AMS	-18.0	-4.0	-16.0	-18.4	-0.4	-16.4	-11.6	-0.6	-15.6
ACP	-24.0	-34.0	-42.0	-34.0	-44	-64.0	-40.0	-26.0	-76.0
2-MBF	-29.0	-6.0	-35.2	-27.0	-1.0	-35.0	-20.0	-0.6	-28.0
DMPC	-40.0	-12.0	-64.0	-40.0	-18.0	-72.0	-43.4	-15.4	-81.4

(-) sign indicates inhibition

In the case of AMS and 2-MBF, turbidity of 6 NTU (table 7.6 and figure 7.27) does not affect the degradation much. Degradation of ACP and DPMC, which do not get adsorbed on the surface and interact mostly with the ROS in the bulk, are the most affected. This may be partially due to the relatively poor degradation of these components even in distilled water. Consequently, even a small change will appear larger percentage-wise.

However, in the case of PO_4^{3-} ion, which is dissolved in water and can inhibit the photocatalytic efficiency of ZnO, the degradation of all the four pollutants is affected. Combination of turbidity and PO_4^{3-} ion produces additive effect on the degradation as shown in figure 7.28 and table 7.6. The percentage change in the case of ACP and DMPC appear very high since the reference level itself is very small and even minor changes will appear larger percentage-wise, as mentioned earlier.

This study is a clear indication that for successful field application of the solar photocatalytic technology, inhibiting factors such as the turbidity as well as phosphate ion should be removed from the secondary effluent before it is subjected to the process. Turbidity can be easily removed by filtration. Mild turbidity does not cause much inhibition of solar photocatalytic process, except the slight increase in the time needed for the degradation. The main source of phosphate in the effluent water in the present case is from the cumene section of the manufacturing unit, where solid phosphoric acid (SPA) is used as the catalyst. During the high temperature operation there is formation of phosphoric acid syrup, which will be collected and sent to the Effluent Treatment Plant (ETP) along with other liquid effluents. Hence if the entry of phosphate in the effluent

water is prevented, this technology can be effectively used for the complete mineralization of the pollutants in the secondary effluent from this chemical plant. In many industrial process effluents, the possibility of contamination by various anions from the process water and other sources cannot be ruled out. The effect of every contaminant needs to be worked out before eventually optimizing this process for commercial application.

7.3.8 Effect of oxidants

7.3.8.1 *Effect of H_2O_2*

The effect of H_2O_2 on the photocatalytic degradation of individual pollutants is discussed in previous chapters. The effect of added H_2O_2 on the photocatalytic degradation of individual components in the combination of pollutants is investigated with different concentrations of H_2O_2 and the results are shown in figures 7.29-7.32.

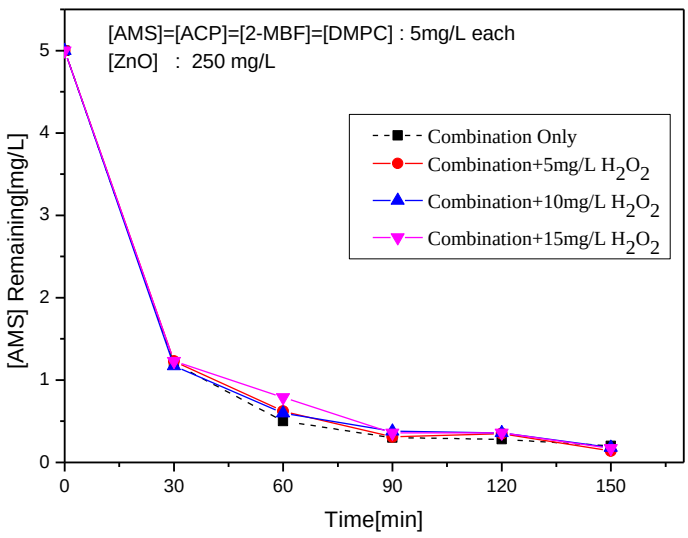

Fig. 7.29: Effect of H_2O_2 on the degradation of AMS in the combination of pollutants.

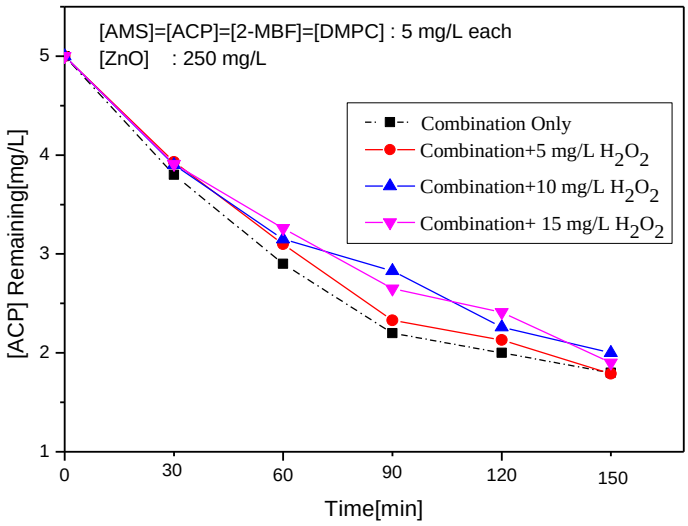

Fig. 7.30: Effect of H_2O_2 on the degradation of ACP in the combination of pollutants

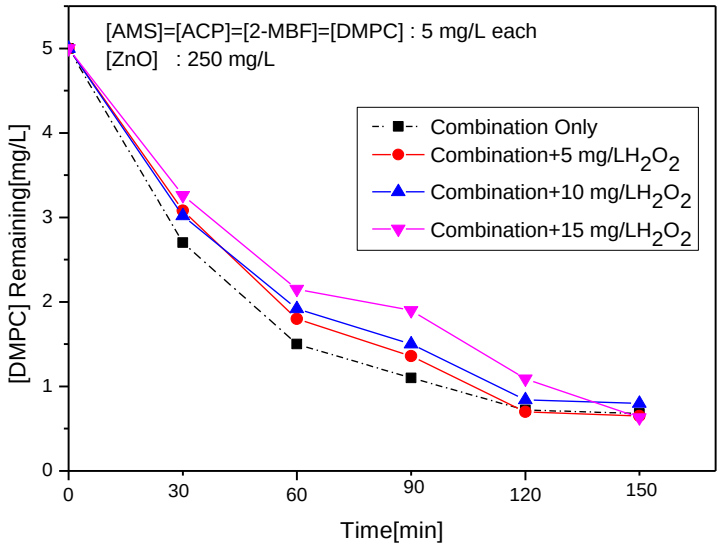

Fig. 7.31: Effect of H_2O_2 on the degradation of DMPC in the combination of pollutants

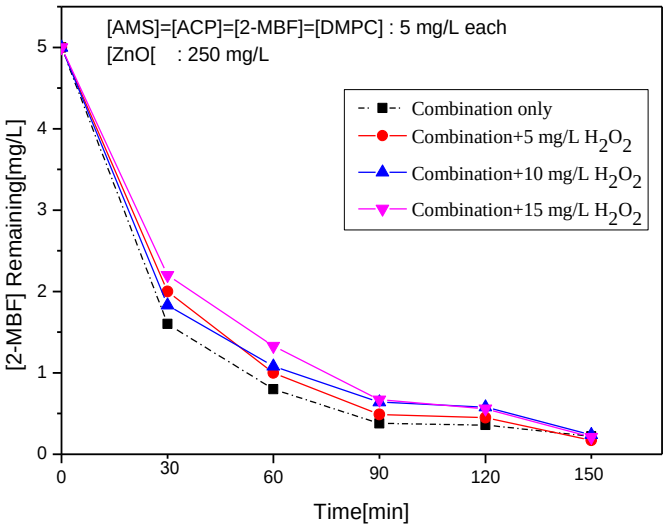

Fig. 7.32: Effect of H_2O_2 on the degradation of 2-MBF in the combination of pollutants

The study clearly shows that the addition of H_2O_2 at different concentrations inhibits the degradation of all the four pollutants initially. Eventually, the degradation is stabilized. The inhibition is not significant in the case of AMS. These results are consistent with the results on the effect of added H_2O_2 on the degradation of individual components, when each of them is the sole pollutant in the system. Possible causes and relevant mechanisms are discussed in respective chapters.

7.3.8.2 *Effect of persulphate*

The effect of the powerful oxidant persulphate on the photocatalytic degradation of individual pollutants AMS, ACP, 2-MBF and DMPC is already investigated and discussed in earlier chapters. The effect of persulphate at different concentrations on the photocatalytic degradation of individual pollutants in the combination is investigated and the results are presented in figures 7.33 -7.36.

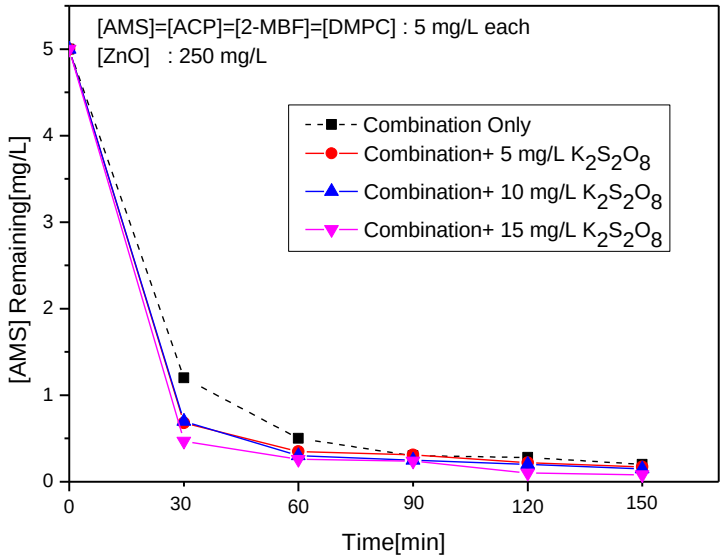

Fig. 7.33: Effect of $K_2S_2O_8$ on the degradation of AMS in the combination of pollutants

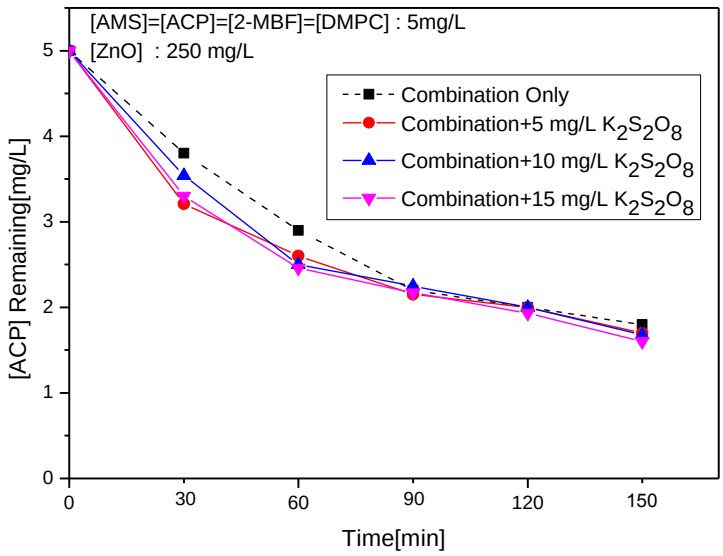

Fig. 7.34: Effect of $K_2S_2O_8$ on the degradation of ACP in the combination of pollutants

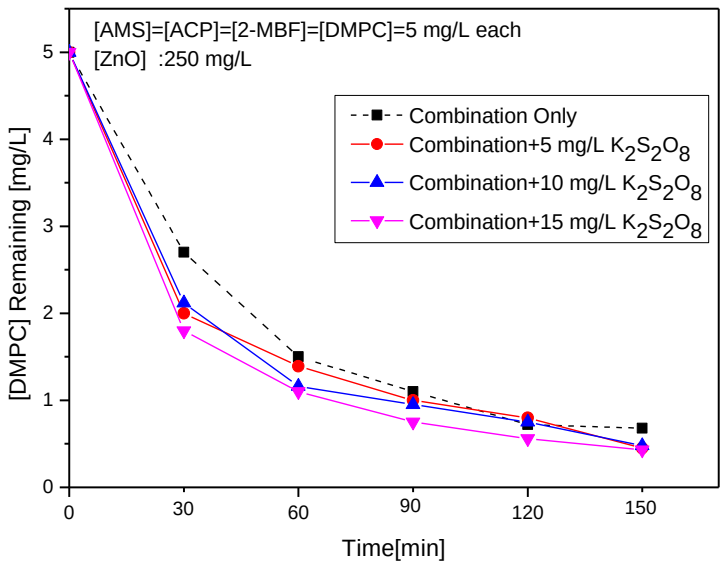

Fig. 7.35: Effect of $K_2S_2O_8$ on the degradation of DMPC in the combination of pollutants

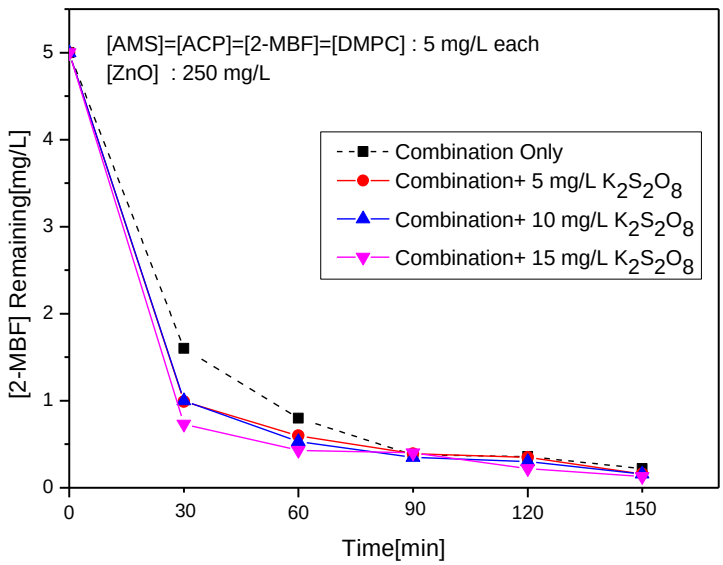

Fig. 7.36: Effect of $K_2S_2O_8$ on the degradation of 2-MBF in the combination of pollutants

The addition of persulphate enhances the degradation of individual pollutants at all concentrations. Eventually, the degradation is complete in all cases with or without persulphate. The mechanism of enhancement of photocatalytic degradation by persulphate is discussed in earlier chapters. The irradiation of aqueous solution of persulphate generates highly reactive $SO_4^{\bullet-}$ radical anion. These radicals can react with H_2O to produce $^{\bullet}OH$ radicals. Both $SO_4^{\bullet-}$ and $^{\bullet}OH$ are highly reactive and can interact with and degrade the pollutants. However, the consequent generation and accumulation of SO_4^{2-}, which acts as an inhibitor retards the acceleration and this explains the lack of enhancement towards later stages of the reaction.

7.4 General mechanism

The basic mechanism of solar photocatalytic degradation of organic pollutants and the possible steps involved in the mineralization of individual pollutants are already discussed in the previous chapters. The main difference in the case of combination of pollutants, when compared to the individual pollutants, is the competitive adsorption by the respective components and the abundance of multiple intermediates which can influence the process. This may complicate the reaction mechanism at the micro level, which needs to be investigated separately. However, eventually the COD becomes ’0’ indicating that irrespective of the presence of a number of components, all of them get mineralized under ZnO mediated solar photo catalysis.

7.5 Conclusions

Solar photocatalysis with ZnO as the catalyst is an effective AOP for the complete removal of even trace amounts of pollutants such as AMS, ACP, DMPC and 2-MBF from the effluent water in petrochemical industries. These compounds influence the degradation of one another only moderately and even their combination can be mineralized efficiently. This opens up the possibility of using the technology for the purification of real industrial waste water. The influence of various reaction parameters such as catalyst dosage, concentration of pollutants, pH, presence of salts, oxidants etc., is the same irrespective of whether the pollutant is present individually or in combination. The study also reveals that the effective removal/mineralization of these pollutants from water is affected by turbidity. Filtration to remove suspended particles, followed by removal of salts/anions by appropriate technology such as complexation with suitable chelating agents (not done here) will enhance the efficiency of the solar photocatalysis for the mineralization of toxic and hazardous organic pollutants. It is important that every type of effluent is scientifically analysed for its characteristics and the contaminants. Accordingly, appropriate modifications have to be made in the technique, so that the pollutants can be effectively and efficiently mineralized.

.....ꕥ.....

Chapter 8

SUMMARY AND CONCLUSION

Conventional secondary treatment methods are found to be ineffective for the removal of trace amounts of recalcitrant organic pollutants from industrial wastewaters. Many of these trace pollutants adversely affect our ecosystem and environment in the long run, as many of them have bio-accumulation potential. Industry is one of the largest consumers of water and the treated water after conventional treatment cannot be reused often due to the presence of these trace contaminants. Hence an efficient tertiary treatment technique is necessary for the removal of these contaminants so that large quantities of industrial wastewater can be reused. Unfortunately, many of the tertiary treatment techniques such as ultrafiltration, microfiltration, reverse osmosis adsorption etc., are expensive and not economically viable at industrial level. Advanced Oxidation Process [AOP], which involves the generation and utilization of reactive free radicals, mainly hydroxyl radical ($^{\bullet}OH$), is emerging as a viable technology for the removal of recalcitrant pollutants from industrial waste water. The present study is an investigation on the possibility of using semiconductor oxide mediated solar photocatalysis for the removal of traces of Alpha methylstyrene (AMS), Acetophenone (ACP), Dimethyl phenylcarbenol (DMPC) and 2-Methyl benzofuran

(2-MBF) from water, both individually and in combination. These are the major pollutants present in the effluent discharge from phenol manufacturing industry.

Zinc oxide (ZnO) is used as the semiconductor oxide photocatalyst. It was characterized by standard methods such as SEM, TEM, XRD, adsorption, BET etc., and the pollutants/intermediates are analysed by Gas chromatography, LC/MS and spectrophotometry. Analysis of H_2O_2 was done by standard iodometric method. The effect of various reaction parameters on the degradation of individual pollutants is investigated in detail and optimum conditions are identified. Effect of anions/oxidants on the degradation efficiency of the pollutants is also investigated. The possibility of reuse of the catalyst in multiple operation is also verified.

Major findings and conclusions of the study are:

1) ZnO mediated solar photocatalysis is an effective AOP for the complete degradation /mineralization of all the four pollutants individually as well as in combination.
2) The degradation of all the four pollutants follows first order kinetics, at least in the concentration range tested here.
3) The concentration of H_2O_2 formed during the photocatalytic degradation follows an oscillatory pattern indicating its concurrent formation and decomposition.
4) The photocatalytic degradation is affected by parameters such as pH, initial concentration of substrate, catalyst loading, presence of natural contaminants such as humic acid, anions/salts etc.

5) The anions, phosphate and iodide, are strong inhibitors of the degradation at all concentrations and reaction times, for all the four pollutant molecules studied. The effect of other anions does not follow any consistent pattern and it depends on the concentration of the anions, reaction time, nature of the pollutant molecule/intermediates and various other interactions.

6) Major intermediates formed during the degradation of the pollutants are detected by GC, LC/MS and colorimetry. ACP is identified as one of the main intermediates formed from the degradation of AMS, DMPC and 2-MBF. Trace amount of phenol is also formed during the photocatalytic degradation of ACP, DMPC and 2-MBF. Hydroxy acetophenone is the major intermediate of ACP degradation. All the pollutants and intermediates formed from them are completely degraded/ mineralized as is confirmed by the reduction in COD value to 'zero' on prolonged irradiation.

7) Persulphate, which is a common oxidising agent, enhances the photocatalytic degradation of all the four pollutants moderately. However, the effect of another oxidant H_2O_2 is dependent on concentration and the effect varies from 'mild enhancement' to 'no effect'. The reasons for the poor enhancement by these otherwise powerful oxidants are analysed.

8) The essential role of oxygen in the photocatalytic degradation of all pollutants is confirmed by the inhibition of their degradation in systems deaerated with nitrogen.

9) The catalyst ZnO can be reused in all cases at least four times without any significant loss in its activity. Even those used catalysts with decreased activity can be restored to their original efficiency by thermal treatment in presence of air.

10) Investigation on the photocatalytic degradation of the combination of the four pollutants in equal concentration shows that every component inhibits the degradation of the other.

11) The degradation study of equal concentrations of all the four pollutants in distilled water as well as in real industrial effluent water matrix shows that the degradation/mineralization of individual pollutants is slower in the latter. This is proven to be due to the presence of turbidity as well as phosphate ion in the effluent water.

12) The study clearly shows that ZnO mediated solar photocatalysis can be effectively used for the decontamination of industrial wastewater containing trace amounts of these four pollutants (AMS, ACP, DMPC and 2-MBF) individually as well as in combination provided the phosphate ion and turbidity are removed by suitable techniques. The use of sunlight as the energy source and the potential for reuse of the ZnO catalyst for multiple application make the technique economically also attractive.

13) The study thus opens up the possibility of using solar photocatalysis for the irreversible removal of various types of organic pollutants from water, thereby making the water reusable in the industry. Sunlight as the energy source, reuse of

the catalyst and potential recycling of the treated water are the specific attractions of this process, especially from the environmental and economical angles.

The study clearly shows that solar photocatalysis can be used as an effective, environment-friendly and economical technology for the complete removal of toxic and hazardous organic pollutants from water. Identification and optimization of relevant reaction parameters is the most important prerequisite for this.

.....ꕥ.....

References

[1] http://www. eoearth.org/article/Human population explosion (accessed September 3, 2012).

[2] S. Baruah, J. Dutta, Nanotechnology applications in pollution sensing and degradation in agriculture: a review, Environ. Chem. Lett. 7 (2009) 1-14.

[3] A. Sugunan, J. Dutta, Pollution treatment remediation and sensing. In: Nanotechnology, K. Harald, Ed. Wiley-VCH: Weinheim. 3 (2008).

[4] (UN), U. N., International decade for action water for Life, 2005-2015: Water Scarcity. (2010) (accessed August 18, 2012).

[5] http://www.who.int/infectious-diseasereport/pages/textonly.html (accessed July 26, 2012).

[6] S. Baruah, R. Kitsomboonloha, R. M. T. Z. Myint, J. Dutta, Nanoparticle applications for environmental control and remediation. In: Nanoparticles: Synthesis, characterization and applications, R. S Chaughule, R.V. Ramanujan, R, Eds. American scientific publishers, Valencia, California, USA. (2009)195-216.

[7] Water quality in India- Status and trends (1999-2001) CPCB, Govenment of India.

[8] D. Dore, G. Peiyuan, A. S. Nette, J. An, Water in China, issues for responsible investors (2010)

[9] D. Mantzavinos, E. Psillakis, Enhancement of biodegradability of industrial wastewaters by chemical oxidation pre-treatment, J Chem Technol Biotechnol.79 (2004) 431-454.

[10] K. L. Walid, Z. Al-Qodah, Combined advanced oxidation and biological treatment processes for the removal of pesticides from aqueous solutions, J.Hazard.Mater. B137 (2006) 489-497.

[11] W. H. Glaze, J. W. Kang, D. H. Chapin, The chemistry of water treatment processes involving ozone, hydrogen peroxide and ultraviolet radiation, Ozone Science & Engineering. 9 (1987) 335-352.

[12] A. L. Estrada, Y. Y. Li, A.Wang, Biodegradability enhancement of wastewater containing cefalexin by means of the electro-Fenton oxidation process, J. Hazard. Mater. 227-228 (2012) 41-48.

[13] R. Munter, Advanced Oxidation Processes-Current status and prospects, Proc. Estonian Acad. Sci. Chem. 50 (2001) 59-80.

[14] T. Oppenlander, Photochemical purification of water and air, advanced oxidation processes (AOPs): Principles, reaction mechanisms, reactor concepts, Wiley-VCH. (2003).

[15] A. Goi, Advanced oxidation processes for water purification and soil remediation, Thesis on chemistry and chemical engineering.

[16] J. Kochany, J. R. Bolton, Mechanism of photodegradation of aqueous organic pollutants. Measurement of the primary rate constants for reaction of •OH radicals with benzene and some halobenzenes using an EPR spin-trapping method following the photolysis of H_2O_2, Environ. Sci. Technol. 26 (1992) 262-265.

[17] J. M. Poyatos, M. M. Muñio, M. C. Almecija, J. C. Torres, E. Hontoria, F. Osorio, Advanced oxidation processes for wastewater treatment: State of the art, Water Air Soil Pollut. 205 (2010) 187-204.

[18] M. Fox, Photocatalytic oxidation of organic substances. In: Kluwer (ed.) Photocatalysis and environment: Trends and applications. New York Academic Publishers. (1988) 445-467.

[19] O. Legrini, E. Oliveros, A. M. Braun, Photochemical processes for water treatment, Chem. Rev. 93 (1993) 671-698.

[20] M. I. Litter, Introduction to photochemical advanced oxidation processes for water treatment, Hdb Env Chem 2M. (2005) 325-366.

[21] G. R. Peyton, Oxidative treatment methods for removal of organic compounds from drinking water supplies. In: Significance and treatment of volatile organic compounds in water supplies; N. M. Ram, R. F. Christman, K. P. Cantor, Eds.; Lewis Publ.: Chelsea. MI (1990) 313-362.

[22] E. Neyens, J. Baeyen, A review of classic Fenton's peroxidation as an advanced oxidation technique, J.Hazard.Mater.B98 (2003) 33-58.

[23] M. Niaounakis and C.P. Halvadakis, Olive processing waste management-Literature review and patent survey, 2nd Ed, (2006) Elsevier, Amsterdam.

[24] J. E. F. Moraes, F. H. Quina, C. A. O. Nascimento, D. N. Silva, O. C. Filho, Treatment of saline waste water contaminated with hydrocarbons by photo-Fenton process, Envion.Sci.Technol.38 (2004) 1183-1187.

[25] M. P. G. De. S. Lucas, Application of advanced oxidation processes to waste water Treatment, Thesis, University of Tras-os-Montes and Atto Douro, Oct (2009).

[26] M. Muruganandham, N. Sobana, M. Swaminathan, Solar assisted photocatalytic and photochemical degradation of Reactive Black 5, J. Hazard. Mater. B137 (2006) 1371-1376.

[27] R. A. Doong, R. A. Maithreepala, S. M. Chang, Heterogeneous and homogeneous photocatalytic degradation of chlorophenols in aqueous titanium dioxide and ferrous ion, Water Sci Technol. 42 (2000) 253-260.

[28] J. Saien, A. R. Soleymani, Degradation and mineralization of direct blue 71 in a circulating up flow reactor by UV TiO_2 process and employing a new method in kinetic study, J. Hazard. Mater. 144 (2007) 506-512.

[29] J. M. Herrmann, Photocatalysis fundamentals revisited to avoid several misconceptions, Appl. Catal. B: Environ. 99 (2010) 461-468.

[30] C. Kittle, Introduction to solid state physics, Wiley Eastern Limited, New Delhi (1976).

[31] R. Ullah, J. Dutta, Photocatalytic degradation of organic dye with manganese-doped ZnO nanoparticles. J. Hazard. Mater. 156 (2008) 194-200.

[32] A. Punnoose, K. Dodge, J. W. Rasmussen, J. Chess, D. Wingett, C. Anders, Cytotoxicity of ZnO nanoparticles can be tailored by modifying their surface structure: A green chemistry approach for safer nanomaterials, ACS Sustainable Chem. Eng. 2 (2014) 1666-1673.

[33] R. Comparelli, E. Fanizza, M. L. Curri, P. D. Cozzoli, G. Mascolo, A. Agostiano, UV-induced photocatalytic degradation of azo dyes by organic-capped ZnO nanocrystals immobilized onto substrates, Appl. Catal. B: Environ. 60 (2005) 1-11.

[34] K. Kabra, R. Chaudhary, R. L. Sawhney, Treatment of hazardous organic and inorganic compounds through aqueous-phase photocatalysis: A review, Ind. Eng. Chem. Res. 43 (2004) 7683-7696.

[35] S. Ahmed, M. G. Rasul, W. N. Martens, R. Brown, M. A. Hashib, Heterogeneous photocatalytic degradation of phenols in wastewater: A review on current status and developments, Desalination. 261 (2010) 3-18.

[36] S. Devipriya, S. Yesodharan, Photocatalytic degradation of pesticide contaminants in water, Sol. Energy Mater. Sol. Cells. 86 (2005) 309-348.

[37] M. R. Hoffmann, S. T. Martin, W. Choi, D. W. Bahnemann, Environmental applications of semiconductor photocatalysis, Chem. Rev.95 (1995) 69-96.

[38] M. N. Chong, B. Jin, C. W. K. Chow, C. Saint, New developments in photocatalytic water treatment technology: A review, Water Res. 44 (2010) 297-302.

[39] H. Gulyas, Solar heterogeneous photocatalytic oxidation for water and wastewater treatment: Problems and challenges, J. Adv. Chem. Eng. 4 (2014) 2-11.

[40] K. M. Lee, C.W. Lai, K. S. Ngai, J. C. Juan, Recent developments of zinc oxide based photocatalyst in water treatment technology: A review, Water Res. 88(2015) 428-448.

[41] B. O. Ugwuishiwu1, I. P. Owoh, I. J. Udom, Solar energy application in waste treatment - A review, Nigerian Journal of Technology. 35 (2016) 432-440

[42] P. Magalhães, L. Andrade, O. C. Nunes, A. Mendes, Titaniumdioxide photocatalysis: Fundamentals and application on photoinactivation, Rev.Adv.Mater.Sci.51 (2017) 91-129.

[43] X. Yan, Y. Li, T. Xia, Black Titanium dioxide nanomaterials in photocatalysis, International Journal of Photoenergy (2017) 1-16

[44] M. Qamar, A. Muneer, Comparative photocatalytic activity of titanium dioxide and zinc oxide by investigating the degradation of vanillin, Desalination. 249 (2009) 535-540.

[45] S. Baruah, M. Jaisai, R. Imani1, M. M. Nazhad, J. Dutta, Photocatalytic paper using zinc oxide nanorods, Sci. Technol. Adv. Mater. 11 (2010) 055002

[46] B. N. Patil, D. B. Naik, V. S. Shrivasthava, Treatment of textile dying and printing wastewater by semiconductor photocatalysis, Journal of Applied Sciences in Environmental Sanitation. 5 (2010) 309-316.

[47] S. Dhanavel, E. A. K. Nivethaa, V. Narayanan, A. Stephen, Photocatalytic activity of Chitosan/ZnO nanocomposite for degrading methylene blue, Int. J.Chem Tech Res.6 (2014) 1880-1882.

[48] R. Sharma, L. C. Heda, S. C. Ameta, S. Sharma, Use of Zinc Oxide as Photocatalyst for Photodegradation of copper soap derived from Azadirecta Indica (Neem) Oil, Research Journal of Pharmaceutical, Biological and Chemical Sciences. 4 (2013) 537.

[49] M. S. Mashkour, A. F. AL-Kaim, L. M. Ahmed, F. H. Hussein, Zinc oxide assisted photocatalytic decolorization of reactive red 2 dye, Int. J. Chem. Sci. 9 (2011) 969-979.

[50] M. Nirmala, M. G. Nair, K. Rekha, A. Anukaliani, S. K. Samdarshi, R. G. Nair, Photocatalytic activity of ZnO nanopowders synthesized by DC thermal plasma, African J. of Basic & Appl. Sci.2 (2010) 161-166.

[51] P. Jayamadhava, A. Sudhakara, S. Ramesha, G. Nataraja, Synthesis of ZnO nano particle as an alternative catalyst for Photocatalytic degradation of brilliant red azo dye, American Journal of Environmental Protection. 3 (2014) 318-322.

[52] N. P. Mohabansi, V. B. Patil1, N. Yenkie, A comparative study on photodegradation of Methylene Blue dye effluent by Advanced Oxidation process by using TiO_2/ZnO photocatalyst, Rasayan J. Chem. 4 (2011) 814-819.

[53] R. He, R. K. Hocking, T. Tsuzuki, Local structure and photocatalytic property of mechanochemical synthesized ZnO doped with transition metal oxides, Journal of the Australian Ceramic Society. 49 (2013) 70-75.

[54] H. J. Kim, C. S. Kim, Synthesis and characterization of ZnO/fly ash composite with highly photocatalytic activity using a hydrothermal process, Digest Journal of Nanomaterials and Biostructures. 9 (2014) 997-1006.

[55] V. Borker, R. Karmali, K. Rane, Comparison of degradation of methylene blue dye by ZnO, N doped ZnO and iron ore rejects, Eur. Chem. Bull. 3 (2014) 520-529.

[56] H. Fu, T. Xu, S. Zhu, Y. Zhu, Photocorrosion inhibition and enhancement of photocatalytic activity for ZnO via hybridization with C60, Environ. Sci. Technol. 42 (2008) 8064-8069.

[57] Y. Lv, C. Pan, X. Ma, R. Zong, X. Bai,Y. Zhu, Production of visible activity and UV performance enhancement of ZnO photocatalyst via vacuum deoxidation, Appl. Catal. B: Environ. 138-139 (2013) 26-32.

[58] F. A. Cataño, H. Gomez, E. A. Dalchiele, R.E. Marotti, Morphological and structural control of electro-deposited ZnO thin films and its influence on the photocatalytic degradation of Methyl Orange dye, Int. J. Electrochem. Sci. 9 (2014) 534-548.

[59] J. Zhang1, S. J. Deng1, S. Y. Liu, J. M. Chen, B. Q. Han, Y. Wang, Y. D. Wang, Preparation and photocatalytic activity of Nd doped ZnO nanoparticles, Materials Technology: Advanced Performance Materials. 29 (2014) 262-266

[60] M. T. Ghaneian, M. Tabatabaee, P. Morovati, M. H. Ehrampoush, A. Dehghani, Photocatalytic degradation of Humic Acid by Ag/ZnO nanoparticles under UVC irradiation from aqueous solutions, Journal of Community Health Research. 3 (2014) 153-161

[61] S. Hiremath, C. Vidya, M. A. L. Antonyraj, M. N. Chandraprabha, R. Shrinidhi, R. Manjunath, Padmanabha, H. Agrawal, Photocatalytic degradation of Rhodamine B using bio synthesized ZnO, International Review of Applied Biotechnology and Biochemistry. 2 (2014) 207-213.

[62] C. Tian, Qi Zhang, A. Wu, M. Jiang, Z. Liang, B. Jiang, H. Fu, Cost-effective large-scale synthesis of ZnO photocatalyst with excellent performance for dye photodegradation, Chem. Commun. 48 (2012) 2858-2860.

[63] R. M. Mohamed, M. A. Barakat, Enhancement of Photocatalytic Activity of ZnO/SiO_2 by nano sized Pt for photocatalytic degradation of phenol in wastewater, International Journal of Photo energy. (2012) 1-8.

[64] K.Yogendra, S. Naik, K. M. Mahadevan, N. Madhusudhana, A comparative study of photocatalytic activities of two different synthesized ZnO composites against Coralene Red F3BS dye in presence of natural solar light, International Journal of Environmental Sciences and Research. 1 (2011) 11-15.

[65] M. Sudha, M. Rajarajan, Deactivation of photocatalytically active ZnO nanoparticle by surface capping with poly vinyl pyrrolidone, IOSR Journal of Applied Chemistry. 3 (2013) 45-53.

[66] N. Karthikeyan, L. Prettencia, V. Narayanan, A. Stephen, Synthesis and characterization of coupled ZnO/Ag/CuO nanomaterials for photocatalytic degradation of organic dye under UV irradiation, International Journal of Innovative Research in Science & Engineering ISSN (Online) 2347-3207.

[67] M. Shanthi, V. Kuzhalosai, Photocatalytic degradation of an azo dye, Acid Red 27, in aqueous solution using nano ZnO, Indian J Chem, 51A (2012) 428-434.

[68] M. Muneer, B. Abbad, A. A. H. Kadhum, A. B. Mohamad, M. S. Takriff, K. Sopian, Solar photocatalytic degradation of environmental pollutants using ZnO prepared sol-gel: 2, 4-Dichlorophenol as Case Study, Int. J. of Thermal & Environmental Engineering. 1 (2010) 37-42.

[69] C. W. Tang, Study of photocatalytic degradation of Methyl Orange on different morphologies of ZnO catalysts, Modern Research in Catalysis. 2 (2013)19-24.

[70] M. Tabatabaee, S. A. Mirrahimi, Photodegradation of dye pollutant on Ag/ZnO nanocatalyst under UV-irradiation, Orient. J.Chem.27 (2011) 65-70.

[71] R. Y. Hong, J. H. Li, L. L. Chen, D. Q. Liu, H. Z. Li, Y. Zheng, J. Ding, Synthesis, surface modification and photocatalytic property of ZnO nanoparticles, Powder Technology. 189 (2009) 426-432.

[72] N. Elamin, A. Elsanousi, Synthesis of ZnO nanostructures and their photocatalytic activity, International Journal of Advance Industrial Engineering. 1 (2012) 6-7.

[73] M. Kulkarni, P. Thakur, Photocatalytic degradation and mineralization of reactive textile azo dye using semiconductor metal oxide nano particles, International Journal of Engineering Research and General Science. 2 (2014) 245-254.

[74] Y. Abdollahi, A. H. Abdullah, Photodegradation of m-cresol by Zinc Oxide under visible-light irradiation, International Journal of Chemistry. 3 (2011) 31-43.

[75] K. M. Parida, S. S. Dash, D. P. Das, Physico-chemical characterization and photocatalytic activity of zinc oxide prepared by various methods, Journal of Colloid and Interface Science. 298 (2006) 787-793.

[76] Y. J. Lee , N. K. Park, G. B. Han, S. O. Ryu, T. J. Lee, C. H. Chang, The preparation and desulfurization of nano-size ZnO by a matrix-assisted method for the removal of low concentration of sulfur compounds, Current Applied Physics. 8 (2008) 746-751.

[77] N. Daneshvar, S. Aber, M. S. S. Dorraji, A. R. Khataee, M. H. Rasoulifard, Preparation and investigation of photocatalytic properties of ZnO nanocrystals: Effect of operational parameters and kinetic study, World Academy of Science, Engineering and Technology. 29 (2007) 267-272.

[78] Swati, R. C. Meena, UV irradiation assisted photocatalytic decolorization of Direct Red 23, International Journal of Scientific and Research Publications.3 (2013) 1-7.

[79] W. Sun, J. Li , G. Mele, Z. Zhang, F.Zhang, Enhanced photocatalytic degradation of Rhodamine B by surface modification of ZnO with copper (II) porphyrin under both UV-vis and visible light irradiation, J. Mol.Catal. A: Chem. (2012) 1-7

[80] P. Banerjee, S. Chakrabarti, S. Maitra, B. K. Dutta, Zinc oxide nano-particles- Sonochemical synthesis, characterization and application for photo-remediation of heavy metal, Ultrasonics Sonochemistry. 19 (2012) 85-93.

[81] A. Giwa, P. O. Nkeonye, K. A. Bello, E. G. Kolawole, A. M. F. Oliveira Campos, Solar photocatalytic degradation of reactive Yellow 81 and reactive Violet 1 in aqueous solution containing semiconductor oxides, International Journal of Applied Science and Technology. 2 (2012) 90-105.

[82] S. K. Kansal, M. Chopra, Photocatalytic degradation of 2, 6-Dichlorophenol in aqueous phase using Titania as a photocatalyst, Engineering. 4 (2012) 416-420.

[83] V. Mangalampalli, P. Sharma, V. D. Kumari, M. Subrahmanyam, TiO_2 supported over porous silica photocatalysts for pesticide degradation using solar light: Part 2. Silica prepared using acrylic acid emulsion, J. Hazard. Mater. 175 (2010) 1101-1105.

[84] G. S. Pozan, A. Kambur, Removal of 4-chlorophenol from wastewater: Preparation, characterization and photocatalytic activity of alkaline earth oxide doped TiO_2, Appl. Catal. B: Environ. 129 (2013) 409-415.

[85] M. Qamar, M. Saquib, M. Muneer, Photocatalytic degradation of two selected dye derivatives, chromotrope 2B and amido black 10B, in aqueous suspensions of titanium dioxide, Dyes and Pigments. 65 (2005) 1-9.

[86] Aarthi, G. Madras, Photocatalytic degradation of Rhodamine dyes with nano-TiO_2, Ind. Eng. Chem. Res. 46 (2007) 7-14.

[87] T. Kogure, Y. Bando, J. Electron Microsc. 47 (1993) 7903.

[88] A. B. M. A. Ashrafi, A. Ueta, A. Avramescu, H. Kumano, I. Suemune, Y. W. Ok T. Y. Seong, Growth and characterization of hypothetical zinc-blende ZnO films on GaAs (001) substrates with ZnS buffer layers, Appl. Phys. Lett. 76 (2000) 550

[89] S. K. Kim, S. Y. Seong, C. R. Cho, Structural reconstruction of hexagonal to cubic ZnO films on Pt/Ti/SiO_2 /Si substrate by annealing, Appl. Phys. Lett. 82 (2003) 562.

[90] C. H. Bates, W. B. White, R. Roy, New high-pressure polymorph of Zinc oxide, Science. 137 (1962) 993.

[91] H.W. Engels, H. J. Weidenhaupt, M. Abele, M. Pieroth, W. Hofmann, in: Ullmann's encyclopedia of industrial chemistry, sixth ed. (Electronic release: 2001**)**.

[92] H. Heine, H.G.Volz, J. Kischkewitz, P. Woditsch, A. Westhaus, W.D. Griebler, M. de Liederkerke, in: Ullmann's encyclopedia of industrial chemistry, sixth ed. (Electronic release: 2001).

[93] C. H. Yan, J. Zhang, L. D. Sun, Zinc Oxide nanostructures in: H.S. Nalwa (Ed.), Encyclopedia of Nanoscience and Nanotechnology, American Science Publishers. 10 (2004) 767.

[94] A. Becheri, M. Durr, P. L. Nostr, P. Balglioni, Synthesis and characterization of zinc oxide nanoparticles: application to textiles as UV-absorbers, J Nanopart Res. 10 (2008) 679.

[95] R. H. Wang, J. H. Xin, X. M. Tao, UV-blocking property of dumbbell-shaped ZnO crystallites on cotton fabrics, Inorg. Chem. 44 (2005) 3926.

[96] A. C. Dodd, A. J. McKinley, M. Saunders, T. Tsuzuki, Effect of particle size on the photocatalytic activity of nanoparticulate Zinc Oxide, J Nanopart Res. 8 (2006) 43.

[97] B. Innes, T. Tsuzuki, H. Dawkins, J. Dunlop, G. Trotter, M. Nearn, P. G. McCormick, Nanotechnology and the Cosmetic chemist, Nutracos Cosmet. 1 (2002) 7.

[98] J. Scognamiglio, L. Jones C. S. Letizia, A. M. Api, Fragrance material review on 2-phenyl-2-propanol, Food and Chemical Toxicology. 50 (2012) S130-S133.

[99] C. S. Jimenez, J. W. D. Leeuw, Chemical structure of a soil humic acid as revealed by analytical pyrolysis.103-112.

[100] I. Obernosterer, G. J. Herndl, Differences in the optical and biological reactivity of the humic and non humic dissolved organic carbon component in two contrasting coastal marine environments, Limnol. Oceanogr. 45 (2000) 1120-1129.

[101] Standard methods for the examination of water and waste water, [APHA] sixteenth edition. (1985) 445-446.

[102] U. I. Gaya, A. H. Abdullah, Heterogeneous photocatalytic degradation of organic contaminants over titanium dioxide: a review of fundamentals, progress and problems, J. Photochem. Photobiol. C: Photochem. Rev. 9 (2008) 1-12.

[103] D. Ollis, P. Pichat, N. Serpone, TiO_2photocatalysis-25 years, Appl. Catal. B: Environ. 99 (2015) 377-387.

[104] M. A. Rauf, S. S. Ashraf, Fundamental principles and application of heterogeneous photocatalytic degradation of dyes in solution, Chem. Eng. J.151 (2009) 10-18.

[105] P. Pichat, Photocatalysis and water purification: From fundamentals to recent applications, Wiley-VCH Verlag GmbH and Co. (2013).

[106] R. W. Matthews, Photo oxidation of organic material in aqueous suspensions of titanium dioxide, Water Res. 20 (2015) 569-578.

[107] H. Yahiro, T. Miyamoto, N. Watanabe, H. Yamaura, Photocatalytic partial oxidation of α Methylstyrene over TiO_2supported on zeolites, Catal. Today.120 (2007) 158-162.

[108] O. Beaune, A. Finiels, P. Geneste, P. Graffin, J. L. Olive, A. Saaedan, Zeolite effect on the oxidation of hydrocarbons with irradiated TiO_2 semiconductor, J.Chem. Soc. Chem. Commun. (1992) 1649-1650.

[109] H. Nitadori, T. Takashahi, A. Inagaki, M. Akita, Enhanced photocatalytic activity of AMS oligomerization through effective metal to ligand charge transfer localization on the bridging ligand, Inorg. Chem. 51 (2012) 51-62.

[110] C. S. Turchi, D. F. Ollis, Photocatalytic degradation of organic water contaminants: mechanisms involving hydroxyl radical attack, J. Catal. 122 (1990) 178-192.

[111] B. Neppolian, H. C. Choi, S. Sakthivel, B. Aurobindo, B. Murugesan, Solar/UV induced photocatalytic degradation of three commercial textile dyes, J. Hazard. Mater. 89 (2002) 303-317.

[112] S. Anandan, A. Vinu, N. Venkatachalam, B. Arabindoo,V. Murugesan, Photocatalytic activity of ZnO impregnated H β and mechanical mix of ZnO/H β in the degradation of monocrtophos in aqueous solution, Journal of Molecular Catalysis A: Chemical.256 (2006) 312-320.

[113] S. G. Anju, S. Yesodharan, E. P. Yesodharan, Zinc oxide mediated sonophotocatalytic degradation of phenol in water, Chem. Eng. J. (189-190) (2012) 84-93.

[114] S. Rabindranathan, S. Devipriya, S. Yesodharan, Photocatalytic degradation of phosphamidon on semiconductor oxides, J. Hazard. Mater. 102 (2003) 217-229.

[115] H. C. Yatmaz, A. Akyol, M. Bayramoglu, Kinetics of photocatalytic degradation of an azo reactive dye in aqueous ZnO suspension, Ind. Eng. Chem. Res. 43 (2004) 6035-6039.

[116] K. E. Oshea, I. Garcia, M. Aguilar, Titanium dioxide photocatalytic degradation of dimethyl and diethyl methyl phosphonate: effect of catalyst and environmental factors, Res. Chem. Intermed. 23 (1997) 325-339

[117] S. Zhou, A. K. Ray, Kinetic studies for photocatalytic degradation of Eosin B on a thin film of Titanium dioxide, Ind. Eng. Chem. Res. 42 (2003) 6020-6033.

[118] E. Evgenidou, K. Fytianos, I. Poulios, Semiconductor sensitized photodegradation of dichlorvos in water using TiO_2 and ZnO as catalysts, Appl. Catal B: Environ. 59 (2005) 81-89.

[119] M. Mrowetz, E. Selli, Photocatalytic degradation of Formic and Benzoic Acids and Hydrogen peroxide evolution in TiO_2 and ZnO water suspensions, J. Photochem. Photobiol. A: Chem. 180 (2006)15-22.

[120] W. Y. Wang, Y. Ku, Effect of solution pH on the adsorption and photocatalytic reaction behaviors of dyes using TiO_2 and Nafion-coated TiO_2. Colloid and Surfaces A: Physicochem. Eng. Aspects. 302 (2007) 261-268.

[121] M. N. Chong, B. Jin, C. W. K. Chow, C. Saint, Recent Developments in Photocatalytic Water Treatment Technology: A Review. Water Res. 44 (2010) 2997-3027.

[122] N. Daneshvar, D. Salari, A. R. Khataee, Photocatalytic degradation of azo dye acid red 14 in water on ZnO as an alternative catalyst to TiO_2, J. Photochem. Photobiol. A: Chem. 162 (2004) 317-322.

[123] J. Poulios, I. Tsachpinins, Photodegradation of textile reactive black 5 in the presence of semiconducting oxides, J Chem Technol Biotechnol. 74 (1999) 39-357.

[124] C. Karunakaran, R. Dhanalashmi, Semiconductor catalyzed degradation of phenol by sunlight, Energy Materials and Solar Cells 92 (2008) 1315-1321.

[125] Y. Xu, C. H. Langford, Variation of Langmuir adsorption constant determined for TiO_2 photocatalysed degradation of acetophenone under different light intensity, J. Photochem. Photobiol. A: Chem. 133 (2000) 67-71.

[126] S. Joseph, K. P. Jyothi, S. P. Devipriya, S. Yesodharan, E. P. Yesodharan, Influence of reaction intermediates on the oscillation in the concentration of insitu formed hydrogen peroxide during the photocatalytic degradation of phenol pollutant in water on semiconductor oxides, Res. J.Recent Sci. 2 (2013) 82-89.

[127] K. P. Jyothi, S. Yesodharan, E. P. Yesodharan, Ultrasound, Ultraviolet light and combination assisted semiconductor catalyzed degradation of organic pollutants in water: oscillation in the concentration of H_2O_2 formed insitu, Ultrasonics Sonochemistry 21 (2014) 1782-1796.

[128] S. Malato, J. Blanco, M. I. Maldonado, P. Fernandez-Ibanez, A. Campos, Optimizing solar photocatalytic mineralization pesticides by adding inorganic oxidizing species: application to recycling of pesticide containers, Appl. Catal.B: Environ. 28 (2000) 163-174.

[129] B. Jenny, P. Pichat, Determination of the actual photocatalytic rate of H_2O_2 decomposition over suspended titania: fitting to the Langmuir-Hinshelwood form, Langmuir. 7 (1991) 947-954.

[130] D. D. Dionysiou, M. T. Suidan, I. Baudin, J. M. Baudin, Effect of H_2O_2 on the destruction of organic contaminants-synergism and inhibition in a continuous mode photocatalytic reactor, Appl. Catal. B. 50 (2004) 259-269.

[131] J. R. Harbour, J. Tromp, M. L. Hair, Photogeneration of hydrogen peroxide in aqueous TiO_2 dispersions, Can. J. Chem. 63 (1985) 204-208.

[132] P. Mac Carthy, The principles of humic substances. Soil Science. 166 (2001)

[133] P. S. Kopplin, N. Hertkorn, H. R. Schulten, A. Kettrup, Structural changes in a dissolved soil humic acid during photochemical degradation processes under O_2 and N_2 atmosphere, Environ. Sci. Technol. 32 (1998) 2531-2541.

[134] J. S. Gaffney, N. A. Marley, S. B. Clark, Humic and Fulvic acids and Organic Colloidal Material in the Environment. In: Humic and fulvic acids: isolation, structure, and environmental role, Amer. Chemical. Soc. Washington. (1996) 2-16.

[135] B. M. Bartschat, S.E. Cabaniss, F. M. M. Morel, Oligo electrolyte model for cation binding by humic substances, Environ. Sci. Technol. 26 (1992) 284-294.

[136] H. S. Shin, S. W. Rhee, B. H. Lee, C. H. Moon, Metal binding sites and partial structures of soil fulvic and humic acids compared: Aided by Eu(III) luminescence spectroscopy and DEPT/QUAT C-13 NMR pulse techniques, Org. Geochem. 24 (1996) 523-529.

[137] C. T. Chiou, R. L. Malcolm, T. I. Brinton, D. E. Kile, Water solubility enhancement of some organic pollutants and pesticides by dissolved humic and fulvic-acids, Environ. Sci. Technol. 20 (1986) 502-508.

[138] S. Tanaka, K. Oba, M. Fukushima, K. Nakayasu, K. Hasebe, Water solubility enhancement of pyrene in the presence of humic substances, Analytica Chemica Acta. 337 (1997) 351-357.

[139] M. Fukushima, K. Tatsumi, K. Morimoto, Influence of iron (III) and humic acid on the photodegradation of pentachlorophenol, Environ. Toxicol. Chem. 19 (2000) 1711-1716.

[140] I. K. Konstantinou, Y. Deligiannakis, Effect of fumic acids and fulvic acids on the photocatalytic degradation of N diethyl-m-toluamide (DEET) using TiO_2suspension and simulated sunlight in functions of natural organic matter in changing environment, in: J. Xu, J. Wu, Y. He (Eds.), Functions of Natural Organic Matters in Changing Environment, Springer, Netherlands. 8217 (2013) 633-636.

[141] C. H. Liao, M. D. Gurol, Chemical oxidation by photolytic decomposition of H_2O_2, Environ. Sci. Technol. 29 (1995) 3007-3014.

[142] T. Hirakawa, T. Daimon, M. Kitazawa, N. Ohguri, C. Koga, N. Negishi, S.Matsuzawa, Y. Nosaka, An approach to estimating photocatalytic activity of TiO_2 suspension by monitoring dissolved oxygen and superoxide ion on decomposing organic compounds, J. Photochem. Photobiol. A: Chem. 190 (2007) 58-68.

[143] K. P. Jyothi, S. Yesodharan, E. P. Yesodharan, Contaminant salts as enhancers of sonocatalytic degradation of organic water pollutants: Effect of concentration, reaction time and adsorption on the efficiency of enhancement and the fate of concurrently formedH_2O_2, Journal of Environmental Chemical Engineering. doi.org/10.1016/j.jece.2016.12.053.

[144] H. P. Boehm, Acidic and basic properties of hydroxylated metal oxide surfaces, Discuss Faraday Soc. 52 (1971) 264-275.

[145] L. Amalric, C. Guillard, E. Blanc-Brude, P. Pichat, Correlation between the photocatalytic degradability over TiO_2 in water of meta and para substituted methoxybenzenes and their electron density, hydrophobicity and polarizability properties, Wat. Res. 30 (1996) 1137-1142.

[146] C. Guillard, E. Puzenat, H. Lachheb, A. Houas, J. M. Herrmann, Why inorganic salts decrease the TiO_2 photocatalytic efficiency, Int. J. Photoenergy. 7 (2005) 1-9.

[147] Tauber, G. Mark, H. P. Schuchmann, C. von Sonntag, Sonolysis of tert-butyl alcohol in aqueous solution, J. Chem. Soc., Perkin Trans. 2 (1999) 1129-1135.

[148] C. Minero, V. Maurino, E. Pelizzetti, D. Vione, An empirical, quantitative approach to predict the reactivity of some substituted aromatic compounds towards reactive radical species (Cl_2 –•, Br_2 –•, •NO_2, SO_3 –•, SO_4 –•) in aqueous solution, Environ. Sci. Pollut. Res. (2006) 1-3.

[149] P. Calza, E. Pelizzetti, Photocatalytic transformation of organic compounds in the presence of inorganic ions, Pure Appl. Chem. 73 (2001)1839-1848.

[150] R. G. Zepp, J. Hiogne, H. Bader, Nitrate induced photo oxidation of organic chemicals in water, Environ. Sci. Technol. 21 (1987) 443-450.

[151] M. Karaca, M. Kıransan, S. Karaca, A. Khataee, A. Karimi, Sonocatalytic removal of naproxen by synthesized zinc oxide nanoparticles on montmorillonite, Ultrasonics Sonochemistry 31 (2016) 250–256.

[152] S. T. Martin, A. T. Lee, M. R. Hoffmann, Chemical mechanism of inorganic oxidants in the TiO_2/UV process: Increased rates of degradation of chlorinated hydrocarbons, Environ. Sci. Technol. 29 (1995) 2587-2573.

[153] G.V. Buxton, C. L, Greensoock, W. P. Helman, A. B. Ross, J. Physic, Chem, Ref.data.17 (198 8)573

[154] K. J. Laidler, Chemical kinetics, 3rd ed. Harper Collins, New York. (1987)

[155] M. V. P. Sharma, V. D. Kumari, M. Subrahmanyam, TiO_2 supported over porous silica photocatalysts for pesticide degradation using solar light: part 2. Silica gel prepared using acrylic acid emulsion, J. Hazard. Mater. 175 (2010) 1101-1105.

[156] M. Tasbihi, C.R. Ngah, N. Aziz, A. Mansor, A. Z. Abdulla, L. K. Teong, A. R. Mohamed, Lifetime and regeneration studies of various supported TiO_2 photocatalysts for the degradation of phenol under UV-C light in a batch reactor, Ind. Eng. Chem. Res. 46 (2007) 9006-9014.

[157] W. S. Jenks, in: P. Pichat (Ed.), Photocatalysis and water purification: From fundamentals to recent applications, Wiley-VCH Verlag GmbH and Co. (2013) 25-51.

[158] Poulios, A. Avranas, E. Rekliti, A. Zouboulis, Photocatalytic oxidation of Auramine O in the presence of semiconducting oxides, J Chem Technol Biotechnol. 75 (2000) 205-212.

[159] J. Yu, W. Wang, B. Cheng, B-L Su, Enhancement of photocatalytic activity of mesoporous TiO_2 powders by hydrothermal surface fluorination treatment, J. Phys. Chem. C. 113 (2009) 6743-6750.

[160] Y. Liu, L. Sun, J. Wu, T. Fang, R. Cai, A. Wei, Preparation and photocatalytic activity of ZnO/Fe_2O_3 nanotube composites, Mater. Sci. Eng. B. 194 (2015) 9-13.

[161] Y. Nosaka, A. Nosaka, in: P. Pichat (Ed.), Photocatalysis and water purification, First Ed., Wiley-VCH Verlag GmbH and Co. (2013) 1-24.

[162] D. Ollis, P. Pichat and N. Serpone, TiO_2 photocatalysis-25 years, Appl. Catal. B: Environ. 99 (2010) 377-387.

[163] E. Amereh, S. Afshar, Photodegradation of acetophenone and toluene in water by nano-TiO_2 powder supported on NaX zeolite, Materials Chemistry and Physics. 120 (2010) 356-360.

[164] Y. Z. Wen, X. Z. Jiang, Pulsed corona discharge-induced reactions of acetophenone in water, Plasma Chemistry and Plasma Processing. 21 (2001) 345-354.

[165] S. Kohtani, M. Mori, E. Yoshioka, H. Miyabe, Photohydrogenation of acetophenone using coumarin dye-sensitized titanium dioxide under visible light irradiation, Catalysts. 5 (2015) 1417-1424.

[166] R. J. Tayade, H. C. Bajaj, R.V. Jasra, Photocatalytic removal of organic contaminants from water exploiting tuned band gap photocatalysts, Desalination. 275 (2011) 160-165.

[167] S. Sakthivel, B. Neppolean, M. V. Shankar, B. Arabindoo, M. Palanichamy V. Murugesan, Solar photocatalytic degradation of azo dye: comparison of photocatalytic efficiency of ZnO and TiO_2, Solar Energy Materials and Solar Cells. 77 (2003) 65-82.

[168] S. M. Lam, J. C. Sin, A. Z. Abdullah, A. R. Mohamad, Degradation of wastewater containing organic dyes photocatalysed by ZnO: a review, Desalination and Water treatment. 41 (2012) 131-169.

[169] M. Fujihira, Y. Satoh, T. Osa, Heterogeneous photocatalytic oxidation of aromatic compounds on TiO_2, Nature. 293 (1981) 206-208.

[170] J. M. Herrmann, Heterogeneous photocatalysis: fundamentals and applications to the removal of various types of aqueous pollutants Catalysis Today. 53 (1999)115.

[171] M. M. Mahlambi, C. J. Ngila, B. B. Mamba**,** Recent developments in environmental photocatalytic degradation of organic pollutants: The case of titanium dioxide nanoparticles-A review, Journal of Nanomaterials. (2015) 1-29.

[172] X. Liu, G. Lu, Y. Guo, Yun Guo, Y.Wang, X. Wang, Catalytic transfer hydrogenolysis of 2-phenyl-2-propanol over palladium supported on activated carbon, Journal of Molecular Catalysis A: Chemical. 252 (2006) 176-180.

[173] N. Serpone and E. Pelizzetti (eds.), Photocatalysis, fundamentals and applications, Wiley Interscience, New York. (1989)

[174] M. Schiavello (ed.), Photocatalysis and environment. Trends and applications, Kluwer Acad. Pub., Dordrecht. (1988)

[175] H. A. Al-Ekabi and D. Ollis (eds.), Photocatalytic purification and treatment of water and air, Elsevier Science Pub. B. V., Amsterdam. (1993).

[176] D. W. Bahnemann, J. Cunningham, M. A. Fox, E. Pelizzetti, P. Pichat, N. Serpone, Aquatic surface photochemistry (R. G. Zeep, G. R. Helz, and D. G. Crosby, eds.), F. L. Lewis Publishers, Boca Raton. (1994) 261.

[177] S. Malato, J. Blanco, A. R. Fernandez-Alba, A. Agüera, Solar photocatalytic mineralization of commercial pesticides: acrinathrin, Chemosphere. 40 (2000) 403.

[178] Y. Wang, Solar photocatalytic degradation of eight commercial dyes in TiO_2 suspension, Wat. Res. 34 (2000) 990-994.

[179] C. Guillard, J. Disdier, J. M. Herrmann, C. Lehaut, T. Chopin, S. Malato, J. Blanco, Comparison of various titania samples of industrial origin in the solar photocatalytic detoxification of water containing 4-chlorophenol, Catalysis Today. 54 (1999) 217-228.

[180] N. Daneshvar, D. Salary, M. A. Behnasuady, Decomposition of anionic sodium dodecylbenzene sulphonate by UV/TiO_2 and UV/H_2O_2 processes-A comparison of reaction rate, Iran. J. Chem. & Chem. Eng. 21 (2002) 55-62.

[181] M. A. Fox, M. T. Dulag, Heterogeneous photocatalysis, Chem. Rev. 93 (1993) 341-357.

[182] Standard methods for the examination of water and waste water, (APHA) sixteenth edition. (1985) 135.

.....ꕥ.....

ANNEXURES

Annexure 1

List of Abbreviations and Symbols

µm	Micro meter
2-MBF	2-methylbenzofuran
4-CP	4-chlorophenol
ACP	Acetophenone
AMS	Alpha methyl styrene
AMSC	AMS column
AOP	Advanced Oxidation Process
BET	Brunauer-Emmett Teller
CAC	Crude Acetone Column
CB	Conduction Band
CHP	Cumenehydroperoxide
CNS	Central Nervous System
COD	Chemical Oxygen Demand
DAP	Diammonium Phosphate
DMPC	Dimethyl phenylcarbenol
DNET	Direct Neutralization and Effluent Treatment
DOC	Dissolved Organic Carbon
EDS	Energy Dispersive Spectroscopy
ETP	Effluent Treatment Plant
eV	Electron Volt
FAC	Finished Acetone Column
FAPs	Fly Ash Particles
FAS	Ferrous Ammonium Sulphate
FE-SEM	Field Emission Scanning Electron Microscopy
FT-IR	Fourier Transform Infrared Spectroscopy

GAC	Granulated Activated Carbon
GC	Gas Chromatography
GRAS	Generally Recognized as Safe
H_2O_2	Hydrogen Peroxide
HA	Humic acid
HAAs	Haloaceticacids
HACP	Hydroxy acetophenone
L-H	Langmuir-Hinshelwood
MB	Methylene Blue
MEA	Mono Ethanol Amine
MEO	Mesityl oxide
MO	Methyl Orange
NHE	Normal Hydrogen Electrode
nm	Nano Meter
NTU	Nephelometric Turbidity Unit
O_3	Ozone
OEC	Oil Extraction Column
PAD	Photo Assisted Deposition
PCBs	Polychlorinated biphenyls
PL	Photoluminescence Spectroscopy
ppb	Parts per billion
ppm	Parts per million
PRU	Propylene Recovery Unit
PTR	Phenol Treating Reactor
PVP	Poly Vinyl Pyrrolidone
PZC	Point of Zero Charge
REET	Raw Effluent Equalization Tank
RhB	Rhodamine B
ROS	Reactive Oxygen Species
SEM	Scanning Electron Microscope

SPA	Solid Phosphoric Acid
TC	Tar Column
TEM	Transmission Electron Microscopy
TF/UF	Trickling Filter Underflow
THMs	Trihalomethanes
Q-TOF	Quadrupole Time of Flight
TPA	Terephthalic acid
TSS	Total Suspended Solids
UV	Ultra violet
VB	Valence Band
VPC	Vapour Phase Calibration
WHO	World Health Organization
XRD	X-ray Diffraction

.....ꕥ.....